



**Inhibition of Extracellular Vesicle Release Enhances Cancer
Chemotherapy and Inhibition of Outer Membrane Vesicle Release
Sensitises Bacteria to Antibiotic and Bacteriophage Therapy**

Presented By

Uchini Shamilka Kosgodage BSc (Hons) PgCert LIBMS

Thesis submitted in partial fulfilment of the requirement

for the degree of

DOCTOR OF PHILOSOPHY (PhD)

Director of Studies: Prof. Jameel M. Inal

Second supervisor: Dr. Chris Bax

External Supervisor: Dr. Sigrun Lange (University of Westminster)

Cellular and Molecular Immunology Research Centre (CMIRC)

Faculty of Life Sciences, School of Human Sciences, London Metropolitan University

May 2019

Table of Contents

Acknowledgements.....	1
Abstract.....	3
Publications.....	5
Conference and Public Presentations.....	6
Abbreviations.....	7
1.0 Introduction.....	10
1.1 Emerging Role of Extracellular Vesicles in Malignancy.....	10
1.1.1 Extracellular Vesicles (EVs) as Mediators of Signal Transduction.....	10
1.1.2 EVs are Key Drivers of Tumorigenesis and Metastasis.....	11
1.2 Mechanism of Secretion of Microvesicles.....	12
1.2.1 Physiological and Exogenous Stimulation of Microvesiculation	12
1.2.2 Enzymes that catalyse EV biogenesis and release	13
1.2.2.1 Acid Sphingomyelinase (A-SMase).....	13
1.2.2.2 Rho- Kinase.....	13
1.2.2.3 Flippase and Floppase.....	13
1.2.2.4 Scramblase.....	13
1.2.2.5 Peptidylarginine Deiminases (PADs) and Tumorigenesis	14
1.3 Apoptosis.....	14
1.4 EVs and Cancer.....	15
1.4.1 The release of EVs	15
1.4.1.1 EVs are conveyors of intercellular communication	15
1.4.1.2 Vesicular Mediated Unconventional Protein Export	16
1.4.2 EVs in Malignancy and Tumour Metastasis	16
1.4.2.1 Angiogenesis.....	17
1.4.2.2 Immune surveillance Evasion	17
1.4.2.2.1 EVs and evasion from the Immune System.....	17
1.4.2.3 EVs induce Multi-drug Resistance	17
1.4.2.3.1 Role of p53 and P-glycoprotein (P-gp) in Cancer drug Resistance.....	18
1.5 EV Inhibition and Cancer Immunotherapy.....	19
1.5.1 Pharmacological Mitotic Inhibitors	20

1.5.1.1Taxanes.....	20
1.5.1.2Anti-metabolites.....	20
1.5.1.3Anthracyclines	21
1.6 Bacterial Outer-membrane Vesicles (OMVs).....	22
1.6.1Bacterial OMVs and Bacteriophage Infection	23
1.7 EVs and Viral Infection.....	24
1.8 Cannabidiol (CBD) and the Biology of EVs.....	25
1.9 Reagents used as Potential Inhibitors in the Study.....	26
1.10 Gold Standards of Detection and Quantification of EVs.....	28
1.10.1Flow Cytometry	28
1.10.2Nanoparticle Tracking Analysis.....	29
1.10.3Fluorescence Microscopy	29
1.10 Overall Aim.....	30
2.0 Materials & Methods.....	32
2.1 Cell lines.....	32
MCF-7 cells.....	32
PC3 cells.....	32
HEPG2 cells.....	32
MDA-MB-231 cells.....	33
LN18 and LN229 cells.....	33
2.2 Cell Growth Medium (CGM).....	35
2.3 Methods.....	35
2.3.1Maintaining cell lines.....	35
2.3.2Cryopreservation of cells	35
2.3.3Defrosting of cryopreserved cells	35
2.4 Biochemical Methods.....	36
2.4.1Isolation of EVs from conditioned medium.....	36
2.4.2Detection of PS-Positive EVs	36
2.4.3Immunostaining of Cells.....	36
2.4.4PKH labelling of PC3 cells and PC3-derived EVs	37
2.4.5Protein Quantification.....	37

2.5	Flow Cytometry.....	37
2.5.1	Guava ViaCount Assay.....	37
2.6	Image Flow Cytometry [NucleoCounter® NC-3000™ (Chemometec)].....	38
2.6.1	Viability Assay.....	38
2.6.2	Annexin V apoptosis Assay	38
2.6.3	Cell Vitality Assay.....	38
2.6.4	Mitochondrial Membrane Potential Assay	38
2.7	Nanoparticle Tracking Analysis.....	39
2.8	Fluorescent Microscopy.....	39
2.9	Western Blot (WB) and Mass Spectrometry Analysis.....	39
2.9.1	Preparation of cell lysates for Western blot analysis	39
2.9.2	Sample preparation for SDS-Polyacrylamide Gel Electrophoresis (SDS-PAGE).....	39
2.9.3	SDS-PAGE Protein Molecular Weight Standards	40
2.9.4	SDS-Polyacrylamide Gel Electrophoresis	40
2.9.5	Western Blotting Analysis	40
2.9.6	Immunochemical Protein Detection using the ECL System.....	40
2.10	Liquid Chromatography-Mass Spectrometry (LC-MS/MS).....	41
2.11	Microbiology Techniques.....	41
2.11.1	Preparation of Agar Plates	41
2.11.2	Preparation of Müller Hinton Broth.....	42
2.12	Transmission Electron Microscopy.....	42
2.13	Statistical Data Analysis.....	42
3.0	Pharmacological Inhibition of Microvesicle Biogenesis and Release.....	44
3.1	Introduction.....	44
3.2	Methods.....	44
3.2.1	Determining the PC3 Growth Rate	44
3.2.2	Revisiting EV Isolation Techniques	45
3.2.3	EV inhibitors.....	45
3.2.3.1	Optimum concentration of BzATP to stimulate EV release	45
3.2.3.2	Effect of potential EV inhibitors on Microvesiculation.....	45
3.2.4	Nicotine plays a role in EV Inhibition	46

3.3 Results.....	47
3.3.1Growth rate of PC3 cells.....	47
3.3.2Immunostaining	48
3.3.2.1Immunostaining of PC3 cells.....	48
3.3.2.2PKH labelling of PC3-cells and PC3- derived EVs.....	49
3.3.3EV Isolation.....	50
3.3.3.1Optimisation of the Centrifugation Speed Resulting in a higher yield of EVs	51
3.3.3.2Optimisation of the Duration of Centrifugation Resulting in a higher yield of Microvesicles.....	51
3.3.4EV Inhibitors.....	53
3.3.4.1Pharmacological Stimulation of EV release	53
3.3.4.2Cl-amidine and Bis-I are more potent inhibitors of EV release.....	55
3.3.4.3D-Pantethine and Cl-amidine inhibit EV release most effectively compared to other candidate EV inhibitors.....	57
3.3.4.4Nicotine dose-dependently inhibits the release of EVs from PC3 cells.....	61
3.4 Discussion.....	64
4.0 Effect of Inhibiting Extracellular Vesicle Release on Chemotherapeutic Drug-induced Apoptosis.....	67
4.1 Introduction.....	67
4.2 Methods.....	67
4.2.1Effect of Nicotine on drug Induced Apoptosis in PC3 Cells	67
4.2.2Effect of combinatory EV inhibition withNicotine and Cl-amidine on 5-FU treated MCF-7 cells.....	67
4.2.3Effect of synergistic EV inhibition with Bisindolylmaleimide-I and Cl-amidine on PC3 cell apoptosis.....	68
4.2.3.1Apoptosis study using Bisindolylmaleimide-I and 5-FU.....	68
4.2.3.2Preparing 5-FU-EVs	68
4.2.3.3Effect of Bisin-I activity on PC3 Cell Survival	69
4.2.4Effect of Chloramidine activity on DOX treated PC3 cells.....	69
4.2.4.1Identification of the optimum DOX concentration	69
4.2.4.2Annexin V assay of PC3-EVs and encapsulation of DOX in EVs	69
4.2.4.3Effect of Cl-amidine on EV release in PC3 cells.....	69
4.2.4.4Fluorescent Microscopy Analysis of DOX transfer via PC3-EVs.....	69

4.2.4.5HPLC analysis of DOX internalisation in PC3.....	70
4.2.4.6Fluorescence Spectrometry analysis of the effect of EV inhibition on Sensitisation to Chemotherapy.....	70
4.3 Results.....	71
4.3.1Bisindolylmaleimide- I Augments 5-FU Efficacy against PC3 Cells.....	71
4.3.2Nicotine increases Anti-tumour Drug Effectiveness.....	73
4.3.3Synergistic Effect of Inhibitors Promotes Cumulative Apoptosis in MCF7 Cells	77
4.3.4Bis- I and Cl-amidine shed light for Novel Cancer Immunotherapy	81
4.3.5Pre-treatment with Bis-I abolish EV release Increasing the Cytotoxicity of Anti-cancer Drug-EVs.....	85
4.3.6Optimisation of DOX Concentration to be Used in Apoptosis Studies	92
4.3.7PC3-cell derived, annexin-V positive EV Drug Encapsulation	94
4.3.8Cl-amidine significantly inhibits EV release in PC3 cells	94
4.3.9Fluorescence Microscopy analysis of Anti-cancer Drug transfer via EVs	94
4.3.10HPLC analysis confirms the importance of EV inhibition on the increased Effect of Anti-cancer Drug.....	102
4.3.11Fluorescence Spectrometry Analysis further confirms that EV inhibition Increases the Effectiveness of Anti-tumour Therapy	102
4.4 Discussion.....	105
5.0 Cannabidiol (CBD) is a Novel Inhibitor of Extracellular Vesicle Biogenesis and Release in Cancer Cells.....	109
5.1 Introduction.....	109
5.2 Methods.....	110
5.2.1 Cell viability assays.....	110
5.2.3 Effects on EV biogenesis using Cannabidiol (CBD) and Cl-amidine.....	110
5.2.4 Effect of Temozolomide (TMZ) on Glioblastoma cell lines.....	111
5.2.5 Effect of CBD on TMZ treatment in LN18 and LN229 cells.....	111
5.3 Results	112
5.3.1 CBD inhibits EV release in PC3 cells.....	112
5.3.2 Effect of CBD on EV release in HEPG2 cells.....	114
5.3.3 Effect of CBD on EV release in MDAMB231 cells.....	116
5.3.4 Optimum concentration of TMZ to treat Glioblastoma cell lines.....	118
5.3.5 Effect of CBD and TMZ treatment on the viability of GBM cells.....	119

5.3.4 Optimum concentration of TMZ to treat Glioblastoma Multiforme (GBM) cell lines.....	120
5.3.6 Effect of EV inhibition on TMZ-treated LN229 GBM cells.....	121
5.3.7 Effect of EV inhibition on TMZ-treated LN18 GBM cells.....	122
5.3.8 Size exclusion analysis of vesicle release in GBM cell lines.....	123
5.3.7 Effect of EV inhibition on TMZ-treated LN18 GBM cells.....	124
5.3.8 Comparison of Size Exclusion Vesicle release in GBM cell lines.....	125
5.4 Discussion.....	126
6.0 Isolation of Bacterial Outer Membrane Vesicles	130
6.1 Introduction.....	130
6.2 Materials & Methods	131
6.2.1 Maintenance of <i>E. coli</i> cultures.....	131
6.2.2 Preparation of Outer Membrane Vesicles (OMVs).....	131
6.2.2.1 Centrifugation Method.....	131
6.2.2.2 Ultrafiltration Method	132
6.2.3 Immunoprecipitation (IP).....	132
6.2.3.1 Materials and Reagents	133
6.2.3.2 IP Protocol.....	133
6.2.4 Western blot analysis of citrullinated/deiminated proteins from <i>E. coli</i> and <i>E. coli</i> -derived OMVs.....	134
6.2.5 Mass Spectrometry analysis of citrullinated/deiminated proteins from <i>E. coli</i> and <i>E. coli</i> -derived OMVs.....	134
6.2.6 Effect of pharmacological EV Inhibitors on <i>E. coli</i> -OMV Release.....	135
6.2.7 Effect of pharmacological PAD inhibitors on <i>E. coli</i> -OMV Release.....	135
6.2.8 Effect of pharmacological EV and PAD inhibitors on <i>S. aureus</i> - OMV Release.....	135
6.3 Results.....	135
6.3.1 Isolation of Bacterial OMVs.....	135
6.3.2 Phylogenetic reconstruction of <i>E.coli</i> - PAD sequences.....	138
6.3.3 Detection of PAD enzymes and citrullinated/deiminated proteins in <i>E. coli</i> via Western blot Analysis.....	138
6.3.3 Detection of PAD enzymes and citrullinated/deiminated proteins in <i>E.coli</i> and observation of transfer in <i>E.coli</i> -OMVs.....	141
6.3.4 Immunoprecipitation and Protein Identification.....	142

6.3.5 LC-MS/MS analysis of citrullinated proteins in <i>E. coli</i> and <i>E. coli</i> -OMVs	6.3.5.1 Common deiminated proteins identified in <i>E. coli</i> -F95, <i>E. coli</i> -PAD4 and OMVs-F95.....	143
6.3.5.2 Unique deiminated proteins identified in <i>E. coli</i> -F95		143
6.3.5. Identification of deiminated proteins from <i>E. coli</i> and <i>E. coli</i> -OMVs by Immunoprecipitation.....		147
6.3.6 Massspectrophotometry analysis of immune-precipitated proteins from <i>E. coli</i> and <i>E. coli</i> -OMVs.....		147
6.3.7 Effect of EV inhibitors on OMV Inhibition.....		148
6.3.8 Effect of PAD inhibitors on OMV Biogenesis and Release.....		148
.....		150
6.3.9 Effect of inhibitors on <i>S. aureus</i> -OMV Biogenesis and Release.....		152
6.4 Discussion.....		153
7.0 Effect of Inhibiting OMV Release on Antibiotic Activity and Phage Therapy		159
7.1 Introduction.....		159
7.1.1 Colistin.....		159
7.1.2 Vancomycin.....		160
7.1.3 OMV inhibition and Phage Therapy.....		160
7.1.4 Phage Therapy.....		161
7.1.5 Lambda Phage.....		161
7.2 Methods.....		162
7.2.1 Disc Diffusion Method.....		162
7.2.2 Effect of OMV inhibitors on MIC of Colistin.....		162
7.2.3 Isolation and Propagation of Lambda Phage.....		163
7.2.4 Effect of phage concentration on OMV Release.....		163
7.2.4.1 Effect of incubation time on OMV Release		164
7.2.5 Effect of addition of OMVs on Phage Therapy.....		164
7.2.6 Transmission Electron Microscopy imaging of Lambda phage and phage-OMV Interaction.....		165
7.3 Results.....		165
7.3.1 OMV inhibitors enhance the effect of antibiotic activity against <i>E. coli</i>		165
7.3.2 Effect of OMV Inhibitors on MIC value of Colistin against <i>E. coli</i>		167
7.3.3 OMV inhibitors enhances the effect of antibiotic activity against <i>S. aureus</i>		167

7.3.4 Effect of OMV Inhibitors on MIC value of Vancomycin against <i>S. aureus</i>	171
7.3.5 Propagation of Lambda phage	171
7.3.6 Effect of phage concentration on OMV Release.....	172
7.3.7 Effect of phage-OMV incubation time on the release of OMVs.....	174
7.3.8 Pharmacological inhibition of PAD significantly improves therapeutic usage (in phage therapy) of Lambda Phage.....	175
7.3.9 Electron Microscopy Imaging confirms the likelihood of a phage-OMV Interaction during Bacterial Infections.....	177
7.4 Discussion.....	179
8.0 Discussion.....	184
8.1 Identification of novel EV inhibitors and their effect on EV Biogenesis and Release	185
8.2 Combinatory effect of Protein Kinase C and PAD inhibition together with Nicotine treatment augments the effectiveness of Chemotherapy.....	187
8.3 CBD-mediated EV inhibition: A novel implication of its Activity	189
8.4 OMV isolation and the identification of PAD- mediated citrullination/deimination in <i>E. coli</i>	190
8.5 OMV inhibition enhances Gram-positive and Gram-negative bacterial Antibiotic Sensitivity and increases Susceptibility to Bacteriophage Therapy	192
8.6 Summary and Concluding Remarks	194
9.0 Appendix.....	199
9.1 Complete Proteomic Analysis of <i>E.coli</i> and <i>E.coli</i> -derived OMVs.....	199
9.1.2 Complete proteomic Analysis of unique <i>E.coli</i> -OMV proteins.....	219
9.2 Materials.....	221
9.2.1 Reagents & Solutions.....	221
9.2.2 Equipment.....	223
9.2.3 Antibodies.....	223
9.3 Experimental Solutions	224
9.3.1 Mammalian cell freeze medium.....	224
9.3.2 RIPA Lysis Buffer pH 7.4.....	224
9.4.1 Sample Buffer (10x).....	224
9.4.2 Running Buffer.....	224
9.4.3 TBS buffer (10x).....	224
9.4.4 Blocking buffer.....	224

9.4.5 Transfer Buffer (10X).....	225
9.4.6 Transfer Buffer (1X).....	225
10.0 References.....	226

Table of Figures

Figure 1: Microscopic Images of cells used in the study.....	34
Figure 3.1 PC3 growth curve.....	47
Figure 3.2 Immunostaining of PC3 cells. PC3 cells were stained with FITC-labelled antibodies	48
Figure 3.3 PKH labelling of PC3 cells and PC3-derived EVs.....	49
Figure 3.4 25,000 g maximises EV isolation. A,.....	50
Figure 3.5: Centrifugation at 60 min was considered to be ideal for EV isolation.....	52
Figure 3.6: Stimulation of PC3 cells with 300 μ M of BzATP for 30 min increased microvesiculation.....	54
Figure 3.7: Bisindolylmaleimide-I and Chloramidine are more potent inhibitors of EVs.....	56
Figure 3.8 D-Pantethine and Cl-amidine are the most potent EV inhibitors.....	57
Figure 3.9 Nanosight tracking Analysis (NTA) plots of the reagents used.....	60
Figure 3.10 Nicotine is a strong EV inhibitor.....	62
Figure 3.11 Effect of Nicotine on EV release.....	63
Figure 4.1 1 μ M of 5-FU was the optimum concentration for Apoptosis Assays.....	72
Figure 4.2 Pre-treatment with 25 μ M nicotine increased 5-FU effect on PC3.....	74
Figure 4.3 Multiplex assays demonstrating VitaBright-48 TM staining following Nicotine pre- treatment.....	76
Figure 4.4 Combination of EV Inhibitors causes 5-FU retaining ability and causes cumulative apoptosis in MCF7.....	78
Figure 4.5 Multiplex assays demonstrating VitaBright-48 TM staining following Cl-amidine- Nicotine pre-treatment/priming.....	80
Figure 4.6 Combination of Inhibitors increases PC3 cell apoptosis.....	82
Figure 4.7 Multiplex assays demonstrating VitaBright-48 TM staining following Cl-amidine- Bisindolylmaleimide-I pre-treatment/priming.....	84
Figure 4.8 Schematic representation of the synergistic effect of EV inhibitor and chemotherapy.....	85
Figure 4.9 Presence of Bis-I abolishes EV release enhancing the Chemotherapeutic Cytotoxicity	86
Figure 4.10: Multiplex assays demonstrating Annexin-V staining following Bisindolylmaleimide-I pre-treatment/priming.....	87
Figure 4.11 5 μ g/ml of DOX was the optimum concentration to treat PC3 cells.....	88
Figure 4.12: Apoptosis of PC3 cells post-treatment with different concentrations of DOX.....	91

Figure 4.13: Flow cytometry confirmation of drugs encapsulated in EVs.....	93
Figure 4.14 EV release in the presence of DOX and pan-PAD inhibitor, Cl-amidine.....	95
Figure 4.15 Fluorescent microscopy analysis of Cl-amidine pre-treatment sensitising PC3 cells to DOX-EVs.....	96
Figure 4.16 HPLC chromatograms of the effect of EV inhibition on DOX retention in PC3 cells	100
Figure 4.17 Cl-amidine pre-treatment increases sensitisation of PC3 cells toDoxorubicin.....	101
Figure 4.18 Absorbance of DOX by PC3 cells and PC3-EVs analysed by fluorescent spectroscopy.....	103
Figure 4.19 Fluorescence intensity of PC3 cells and supernatant analysed by fluorescence spectroscopy.....	104
Figure 5.1 Effect of CBD on PC3-derived EV release.....	112
Figure 5.2 Effect of CBD on HEPG2-derived EV release.....	114
Figure 5.3 Effect of CBD on MDAMB231-derived EV release.....	116
Figure 5.4 GBM cells LN18 and LN229 tolerate similar TMZ concentration.....	118
Figure 5.5 Glioblastoma cell viability is minimally affected following CBD and TMZ treatment	119
Figure 5.6 CBD modulated vesicle release is increased compared to TMZ treatment in LN229	121
Figure 5.7 CBD modulated vesicle release is decreased compared to the TMZ treatment in LN18.....	124
Figure 5.8 LN18-derived EV release is significantly lower than TMZ-sensitive LN229.....	125
Figure 6.1 Ultrafiltration method of OMV isolation.....	132
Figure 6.2.1: Size distribution of vesicles using ultrafiltration.....	136
Figure 6.2.2: Size distribution of vesicles using centrifugation.....	137
Figure 6.3 Neighbour joining tree and Multiple Sequence Alignment (MAP) showing phylogenetic clustering of <i>E.coli</i> - PAD.....	140
Figure 6.4 Western blotting of deiminated proteins in <i>E.coli</i> and OMVs.....	141
Figure 6.5 Immunoprecipitated deiminated proteins (F95) and PAD4 from <i>E. coli</i> and OMVs	142
Figure 6.6 Deiminated proteins identified in <i>E.coli</i> -OMV-F95 sample.....	146
Figure 6.7 Effect of inhibitors on OMV inhibition.....	149
Figure 6.8 Effect of PAD inhibitors on OMV biogenesis and release in <i>E. coli</i>	150
Figure 6.9 Effect of inhibitors on <i>S.aureus</i> OMV biogenesis and release.....	151

Figure 6.10 Formulaic representation of the effect OMV inhibition could have on antibiotic and phage therapy.....	157
Figure 7.2: MIC of Colistin.....	163
Figure 7.3. Using OMV inhibitors increase the antibiotic activity against <i>E. coli</i>	166
Figure 7.4 OMV inhibitors reduce the MIC value of Colistin.....	168
Figure 7.5 Using OMV inhibitors increase the antibiotic activity against <i>S. aureus</i>	169
Figure 7.6 OMV inhibitors reduce the MIC value of Vancomycin.....	170
Figure 7.7 Lambda phage propagated at 10^{-3} concentration.....	171
Figure 7.8 Effect of phage concentration on OMV release.....	173
Figure 7.9 Effect of Incubation time on OMV release.....	174
.....	176
Figure 7.10 Effect of PAD inhibition on OMV release and its impact on Phage activity.....	176
Figure 7.11 Negative stain TEM micrographs of OMVs after incubation with lambda phage.....	177
Figure 7.12 Schematic representation of the effect Cl-am- mediated OMV inhibition on phage therapy.....	178
Figure 7.13. Identification of common inhibitors of EVs and OMVs.....	198

Table of Tables

Table 1. Chemical structures of the potential inhibitors used in the study.....	28
Table 2: Deiminated proteins identified in <i>E. coli</i> and <i>E. coli</i> -OMVs.....	143
Table 3: Deiminated proteins identified in <i>E. coli</i> -F95 sample.....	143
Table 4: Deiminated proteins identified in <i>E. coli</i> -PAD4 sample.....	145
Table 5: Comparative analysis of the Effect of different inhibitors on EV and OMV release.....	197
Table 4: Total proteomics data of <i>E.coli</i> and <i>E. coli</i> -derived OMVs.....	218
Table 6: Total proteomics data of proteins isolated from <i>E.coli</i> and <i>E.coli</i> -derived OMVs.....	220

Acknowledgements

First and foremost, I praise the Lord for blessing me with courage, good health and wellbeing towards completion of my PhD.

A very special gratitude is offered to Prof. Jameel Inal, the director of my studies, firstly for the opportunity to undertake research under his guidance and supervision and secondly for all the support he has offered me throughout the course of my studies. I would not have succeeded without his encouragement, advice and all opportunities I've encountered during the past few years. He was truly a mentor who has provided me with the strength and motivation that was necessary during this period. His experience and enthusiasm in research have enabled me to persevere in producing high quality novel research findings which has been successfully published in international peer reviewed journals. I would also like to thank my second supervisor Dr. Chris Bax for his support during the course of research.

My sincere appreciation is offered to my external supervisor, Dr. Sigrun Lange for her continuous expert guidance and advice towards the completion of my projects and thesis. She very kindly offered me the opportunity to gain the skills in western blotting and other related techniques in her laboratory which was essential towards the success of the research project. She has actively engaged in preparing manuscripts for my first author publications and given me the valuable opportunity to be the owner of a set of publications which is highly uncommon to a young researcher at this stage. Dr. Lange has been a truly inspirational role model who has supported me in many special ways. Her passion for science and innovation has encouraged me to strive for success through hard work. I am privileged to have completed my studies under the wings of such a great supervisory team.

My special thanks go to Dr. Paul Matewele for his support in completing the microbiology aspect of my research. He has been very helpful in providing me with the knowledge of different techniques and continuously steering me towards success. The support I have received from Dr. Brigitte Awamaria is immeasurable. I would like to offer my eternal gratitude for her wholehearted support and encouragement received over the years which has been a blessing towards completion. I am much obliged to the advice and support offered to me by Dr. Sheelagh Heugh, Dr. Kenneth White, Prof. Chris Palmer, Dr. Garry McLean and all members of staff during my stay at London Metropolitan University.

I would also like to thank all the members of CMIRC including, Dr. Dan Stratton, Dr. Smaireh Jorfi, Dr. Ahmad Zia Haidery, Dr. Ephraim Ansa- Addo, Dr. Sharad Kholia and Dr. Ryan Grant for the continuous support and encouragement. Special thanks are offered to my colleagues in

the research lab for their support and friendship. I wish you all the best in all future endeavours. The technical staff at Science Centre has played a special role towards completion of the experiments.

My appreciation is offered to the staff at St. John's Immuno-dermatology and Dermatopathology laboratories, St. Thomas' Hospital, London for their guidance and encouragement during the past two years. I have been very kindly granted leave at short notice in order to successfully complete my research. I have been fortunate to have been working with such an understanding team.

I have been blessed with the most loving and caring family. My heartfelt gratefulness is offered to my devoted parents, sister and the entire family for their love, support and blessings which have been my driving force and the true inspiration towards completion of my PhD. My success would have not been possible without your eternal reassurance. I am a better researcher and most importantly a successful human being because of you all.

Finally, I would like to dedicate this thesis to my beloved family who has walked with me every step of the way towards my success and welfare.

Abstract

Extracellular vesicle (EV) release from tumour cells plays an important role in cancer drug resistance. It is essential that chemotherapeutic drugs are retained within target cells for increased efficacy in inducing apoptosis and as microvesiculation influences drug retention, this study has focused on modulating microvesiculation. Based on EV biogenesis pathways, a range of potential inhibitors were tested on PC3, prostate cancer and MCF7, breast cancer cells. Flow cytometry (FCM), nanoparticle tracking analysis (NTA) and fluorescent microscopy were used for the investigation. All inhibitors tested were shown to inhibit EV release with minimal effect on the cell viability. Peptidyl Arginine Deiminase (PAD) inhibitor, Chloramidine (Cl-amidine, Cl-am) and Protein Kinase C inhibitor, Bisindolylmaleimide-I (Bis-I) exhibited extensive EV inhibition in PC3 and MCF-7 cells. This effect was further tested using an Annexin-V-based apoptosis assay and VB-48 vitality assay through image FCM. There was a significant increase in 5-fluorouracil (5-FU) activity in the presence of the inhibitors which was more apparent when a combination of inhibitors was applied. The hypothesis was further tested using a second, chemotherapeutic drug, Doxorubicin (Dox) on PC3 cells. Pre-treatment of PC3 cells with Cl-am prior to chemotherapy, exhibited increased activity of Dox and increased drug retention was shown by fluorescent microscopy, HPLC, FCM and fluorescence spectrophotometry. Overall the findings demonstrated the implication of EV inhibitors in improving chemotherapy while at the same time reducing its side effects.

Cannabidiol (CBD) has been well known for its psychotherapeutic function and has also been used in some cancers, including in Glioblastoma multiforme (GBM), although the exact pathways that could explain its clear mode of action have not been revealed. This study presents CBD as a potent inhibitor of EVs for the first time. Its potential role has here been examined in many types of cancer including, prostate, liver, breast and GBM across the study. Successful EV inhibition was shown to elicit a favourable response in Temozolomide (TMZ)-mediated therapy against GBM cells, which sensitized some GBM cells to TMZ-mediated chemotherapy.

Outer membrane vesicles (OMVs) are released by bacterial cells upon activation. Isolation and characterisation of these vesicles was carried out using differential centrifugation, ultrafiltration and nanoparticle tracking analysis. The presence of an arginine deiminase enzyme, corresponding to mammalian Peptidyl Arginine Deiminase (PAD), was confirmed in *E. coli* samples and its deiminating activity on various target proteins was shown in this study for the first time. Identification of PAD and PAD-mediated citrullinated/deiminated proteins was identified using immunoprecipitation and Western blotting techniques. The same range of EV

inhibitors as used for cancer cells, along with the PAD inhibitors, was used to investigate the effect on OMV biogenesis from Gram-negative, *E.coli* and Gram-positive *S. aureus*. EV inhibitors Bisindolylmaleimide-I, EGTA, Imipramine, Pantethine and Y27632 inhibited OMV release significantly. The role of EV inhibitors on antibiotic therapy was then further explored. The disc diffusion method and Minimum Inhibitory Concentration (MIC) was used to determine whether OMV inhibition affected antibiotic activity. *E. coli* samples were treated with OMV inhibitors and a range of antibiotics including colistin, erythromycin, rifampicin, kanamycin and vancomycin to identify an optimal OMV inhibitor. The OMV inhibitors had a selective response to antibiotics which facilitated the choice for the most sensitive antibiotic to use in further studies to examine the effect of OMV inhibition in lowering minimum inhibitory concentration. .

These findings, together with previous studies on the association of OMVs with bacteriophage particles, prompted an investigation of the role of OMV inhibition on phage therapy. *E. coli* samples were treated with lambda phage with/without pre-treatment of Cl-am. Bacterial titres were calculated after each experiment. Electron microscopy was used to visualise the formation of phage-*E.coli*-OMVs which confirmed the outcome of the experiments.

The increase of cancer cells with resistance to chemotherapy has increased over time which has added immense pressure on scientists to discover novel therapies within short periods. EVs play a major role in transferring a drug-resistance phenotype to drug-sensitive cells via cellular cargo. This also interferes with its negative role of drug efflux which together drive cancer metastasis. Increasing the dosage of chemotherapy or introducing novel therapeutic agents has hitherto not minimised this effect successfully. Therefore, EV inhibition, as introduced in this study, may have a positive influence in developing novel effective anti-cancer therapies.

The use of OMV inhibition to sensitize bacterial cells to antibiotics is a novel idea which may become an effective solution to combat antibiotic resistance and permit the treatment of such diseases through effective phage therapy. Overall, the research ideas presented in the current study will benefit the implementation of new therapeutic strategies for cancer metastasis and bacterial colonisation, minimising multi drug resistance.

Publications

- **Kosgodage, U.S., Matewele, P., Mastroianni, G., Brotherton, D., Awamaria, B., Nicholas, A.P., Lange, S., and Inal, J.M. (2019)** Inhibition of Bacterial Membrane Vesicle Release, via Conserved Peptidylarginine Deiminase Pathways, Sensitises Gram-negative and Gram-positive Bacteria to Antibiotic Treatment. - Submitted
- **Kosgodage, U.S., Onganer P.U., Maclathcy A., Mould R., Nunn A.V., Guy G.W., Kraev N., Chatterton N., Thomas E. L., Inal J.M. Bell J.D., and Lange S. (2019)** Cannabidiol Affects Extracellular Vesicle Release, miR21 and miR126, and Reduces Prohibitin Protein in Glioblastoma Multiforme Cells. *Translational Oncology*,12(3), 513-522
- **Kosgodage, U.S., Onganer P.U., Maclathcy A., Kraev N., Chatterton N., Nicholas A.P., Inal J.M. and Lange S. (2018)**.Peptidylarginine Deiminases Post-Translationally Deiminate Prohibitin and Modulate Extracellular Vesicle Release and MicroRNAs in Glioblastoma Multiforme. *Int J Mol Sci.*, 28;20(1)
- **Kosgodage, U. S., Mould, R., Henley, A. B., Nunn, A. V., Guy, G. W., Thomas, E. L., Inal J.M., Bell J.D., and Lange, S. (2018)**. Cannabidiol (CBD) Is a Novel Inhibitor for Exosome and Microvesicle (EV) Release in Cancer. *Frontiers in Pharmacology*, 9, 889.
- **Kosgodage, U.S., Trindade, R.P., Thompson, P.R., Inal, J.M., and Lange, S. (2017)** **Chloramidine/Bisindolylmaleimide-I-Mediated** Inhibition of Exosome and Microvesicle Release and Enhanced Efficacy of Cancer Chemotherapy. *Int. J. Mol. Sci.* 2017, 18, 1007
- **Lange, S., Gallagher, M., Kholia, S., Kosgodage, U. S., Hristova, M., Hardy, J., and Inal, J. M. (2017)**. Peptidylarginine Deiminases—Roles in Cancer and Neurodegeneration and Possible Avenues for Therapeutic Intervention *via Modulation* of Exosome and Microvesicle (EV) Release? *International Journal of Molecular Sciences*. 18(6), 1196
- **Lange S., Kholia S., Kosgodage U.S., and Inal J.M. (2017)** **Treatment of Prostate Cancer Using Deimination** Antagonists and Microvesicle Technology. In: Protein Deimination in Human Health and Disease, Volume II (Bhattacharya, S.; Nicholas, A. (Eds.), Chapter 22. Springer; 2nd ed. 2017 edition (10th Nov 2017). ISBN-13: 978-3319582436; ISBN-10: 3319582437.
- **Moore C., Kosgodage U., Lange S. and Inal J.M. (2017)** The emerging role of exosome and microvesicle- (EEV-) based cancer therapeutics and immunotherapy. *Int J Cancer* 2017 Mar 1. Epub 2017 Mar 1.

- **Inal J.M., Kosgodage U., Azam S., Stratton D., Antwi-Baffour S. and Lange S. (2013)** Blood/plasma secretome and microvesicles. *BiochimBiophysActa* 2013 Nov 13; 1834(11):2317-25. Epub 2013 Apr 13.

Conference and Public Presentations

- **Kosgodage U., Lange S. and Inal J.M. (2018)** Chloramidine/Bisindolylmaleimide-I mediated inhibition of Exosome and Microvesicle release Enhanced Efficacy of Cancer Chemotherapy. - Presented at the Horizon Symposium, London Metropolitan University (March 2018)
- **Kosgodage U. (2017)** Exploration of Novel Inhibitors of Extracellular Vesicle biogenesis and Release- Presented to Dukes Team (Collaboration of University of North Carolina, USA and University of Ruhuna, Sri Lanka) ,September 2017, Sri lanka
- **Kosgodage U., Lange S. and Inal J.M. (2017)** Exploration of Novel Inhibitors of EV Biogenesis and Release: An Influential Constituent of Effective Chemotherapy. Presented at the PhD Symposium, April 2017, London Metropolitan University
- **Kosgodage U., Lange S. and Inal J.M. (2016)** Inhibitors of microvesicle release with the potential to enhance effectivity of cancer chemotherapy.Presented at the International Society for Extracellular Vesicles 3rd to 5th May 2016, Rotterdam, Netherlands.
- **Kosgodage U., Lange S. and Inal J.M. (2016)** Non-phagocytic epithelial cells take up microvesicles by macropinocytosis. Presented at the International Society for Extracellular Veseicles 3rd to 5th May 2016, Rotterdam, Netherlands.
- **Obioha P. and Kosgodage U. (2016)** Molecular Identification as a Bridge between Food Microbiology and Cancer Immunotherapy. Presented at the Research Horizon, March 2016, London Metropolitan University, UK.

Abbreviations

ASMase	Acid sphingomyelinase
ATP	Adenosine Tri-phosphate
BCA	Bicinchoninic acid assay
Bis-I	Bisindolylmaleimide-I
BSA	Bovine serum albumin
BzATP	3'-O-(4-benzoylbenzoyl)-ATP
CBD	Cannabidiol
Cl-amidine, Cl-am	Chloramidine
Cyto D	Cytochalasin D
Dex	Dendritic cell-derived EVs
DMSO	Dimethylsulfoxide
DOX	Doxorubicin
DPBS	Dulbecco's Phosphate Buffer Saline
<i>E.coli</i>	<i>Escherichia coli</i>
EGTA	Ethylene glycol-bis(β -aminoethyl ether)-N,N,N',N'- tetraacetic acid
EGF	Epidermal growth factor
ELISA	Enzyme linked Immunosorbent Assay
EV	Extracellular Vesicles
EV	Exosomes- Microvesicles
EXO	Exosomes
FACS	Fluorescence-activated cell sorting
FBS	Fetal Bovine Serum
FSC	Forward scatter
GBM	Glioblastoma
HPLC	High-performance liquid chromatography
HEPES	4-(2-hydroxyethyl)-1-piperazineethanesulfonic acid
IP	Immunoprecipitation
LC-MS/MS	Liquid chromatography-mass spectrometry

MAP	Multiple sequence alignment
MDR	Multi-drug resistance
MHC	Major Histocompatibility complex
MMP	Matrix metalloproteinases
MVs	Microvesicles
NTA	Nanoparticle tracking analysis
OMV	Outer membrane vesicles
PAD	Peptidylarginine deiminase
PBS	Phosphate buffer saline
PC	Phosphatidylcholine
PE	Phosphatidylethanolamine
PFA	Paraformaldehyde
P-gp	P-glycoprotein
PI	Propidium iodide
PoncS	Ponceau S staining
ROCK	Rho-associated kinase
RPMI	Roswell Park Memorial Institute
<i>S.aureus</i>	<i>Staphylococcus aureus</i>
SSC	Side scatter
TMZ	Temozolomide
TNF	Tumour necrosis factor
5-FU	5-Fluorouracil

Chapter 1: Introduction

1.0 Introduction

1.1 Emerging Role of Extracellular Vesicles in Malignancy

1.1.1 Extracellular Vesicles (EVs) as Mediators of Signal Transduction

Intercellular signalling is an intricate process of ligand-receptor interaction which may or not involve cell contact. It involves the uptake and transfer of secretory molecules such as growth factors (Okoye et al., 2009, Antebi et al., 2017). Of the many pathways of cellular-cross talking, the short-range paracrine is common. Much intercellular signaling stimulates biochemical changes within the cell which results in proliferation, differentiation and ultimately apoptosis. There is a particular interest in how cells and their respective signaling pathways (whose molecular interactions have largely been deciphered) perceive and process extracellular signals (Antebi et al., 2017).

These cell surface interactions triggering signal transduction and ultimately changes in gene expression impose stresses at every stage (Tanase et al., 2012). One of the more recent challenges to emerge in cell biology is communication which also does not require the direct contact of cells but is organised through the release of particular signalling factors embedded in membranous structures, namely, extracellular vesicles (EVs) (Plotnikov et al., 2017). Extracellular vesicles (EVs) are plasma membrane bound structures that are released ubiquitously by all types of cells and are considered to be key mediators of cell-to-cell communication (Balaj et al., 2011). Generally known as the 'secretome' (Inal et al., 2013), these small vesicles that are formed as a consequence of external stimuli such as stress, have come to the fore in recent years in helping us to further understand signal transduction. The capacity of these vesicles to package an assortment of macromolecules, including various nucleic acids, lipid and proteins, facilitates the compound shuttling between cells. This has logically led to research into the EV-mediated transmission of pathological stimuli to healthy cells and it has now become clear that EVs are directly involved in disease progression (Kalra et al., 2016). The EV field has grown extensively in recent years, with research focusing on the mechanism of EV modulated inter-cellular shuttling. Many research findings are evident of its crucial role of enhancing the pathology of various diseases.

EVs comprise exosomes (EXOs) that range in size from 40 nm to 100 nm, released through exocytosis and microvesicles (MVs) larger in size (100 nm to 1000 nm) that bud off directly from the plasma membrane. These shed particles collectively known as EVs in this study carry lipid and protein characteristic of their parental cells and are vehicles for membrane and cytoplasmic components (Gangoda et al., 2015). The composition of EVs depends on the cell of origin and once released these vesicles mediate intercellular communication between

neighbouring and distant cells. They are responsible for conferring new properties on recipient cells after the acquisition of new receptors, enzymes or even genetic material from the vesicles (They et al., 2009). This is evident in the lateral trafficking and vertical transfer of cellular cargo to distant cells via EVs.

1.1.2 EVs are Key Drivers of Tumorigenesis and Metastasis

EVs from cancer cells, stem cells and blood cells have been used in vital research with a diagnostic approach in different pathologies. They have been mainly used as target therapy against many cancers and cardiovascular disease (Dörsam et al., 2018, Danielson and Das, 2014). Tumour cell-released EVs have been shown to promote a tumour-supporting environment in non-malignant tissue and, thus, benefit metastasis. Cancer cells excessively secrete EVs as a response to high intracellular stress levels, making the EVs a target to develop novel chemotherapies. However, dendritic cell-derived EVs (Dex) (Segura et al., 2005) are involved in the host immune response to the tumour whilst also increasing the proliferation and cytolytic activity of natural killer (NK cells) (Viaud et al., 2009). Cancer cells continually undergo stress due to hypoxia, starvation and chemotherapy and this result in a massive release of EVs. It is well known that tumours shape their microenvironment by EV-driven intercellular messaging that leads to increased proliferation, angiogenesis, suppression of the host's immune defence and initiation of pre-metastatic niches (Szczepanski et al., 2011, Miller and Grunewald, 2015). EVs can also carry so-called tumour-associated antigens (TAAs), costimulatory molecules and major histocompatibility complexes (MHC) components mediating a stimulatory effect on immune cells (Altevogt et al., 2014). It is also apparent that tumour-derived EVs are directly involved in immunomodulation that alters between immunoactivation and immunosuppression during metastasis (Barros et al., 2018).

A recent phase II clinical trial applying IFN- γ -Dex loaded with MHC class I- and class II-restricted cancer antigens as immunotherapy of NSCLC patients after chemotherapy showed that the expression of MHC class II on Dex correlated with the expression of the NK cell activating NKp30 ligand BCL2-associated athanogene 6 (BAG6) (Binici et al., 2013). The chaperone BAG6 plays a role in a multitude of cellular processes and was identified as ligand of the activating NK cell receptor NKp30 (Pogge von Strandmann et al., 2007). NK cells are required for the interaction of DCs and HSP70 to induce a CTL response and anti-metastatic effect *in vivo* (Granucci et al., 2004, Ciocca and Calderwood, 2005). This double-edged sword effect of EVs has made it more concerning to develop novel therapeutic strategies to overcome its negative effects but use its special attributes in preventing disease progression.

1.2 Mechanism of Secretion of Microvesicles

1.2.1 Physiological and Exogenous Stimulation of Microvesiculation

Cellular modifications directly affect the membrane asymmetry that drives vesiculation. In the resting stage, Phosphatidylserine (PS) and Phosphatidylethanolamine (PE) are expressed in the inner membrane leaflet while Phosphatidylcholine (PC) and sphingomyelin are enriched in the outer membrane leaflet (Zargarian et al., 2017). Furthermore, scramblase and floppase, ATP-dependent enzymes remain inactive. By contrast, flippase, an ATP-dependent translocase actively catalyses the internalisation of PS and PE (Birge et al., 2016, Hankins et al., 2015). Therefore, aminophospholipids are expressed in the outer membrane. Increased levels of intracellular calcium up-regulate scramblase and floppase activity and concomitantly inactivate flippase activity leading to the PS exposure on the outer leaflet of the lipid bilayer. This transverse migration of anionic phospholipids promotes MV release (Beer and Wehman, 2017, Muthusamy et al., 2009, Takeda et al., 2014).

During programmed cell death, apoptotic bodies are formed as a result of Rho-kinase enzyme dependent cytoskeletal reorganisation (Street and Bryan, 2011, Povea-Cabello et al., 2017). This facilitates calcium influx which results in PS exposure on the outer membrane. Similarly, Angiotensin II, homocysteine, thrombin, collagen, cholesterol, pro-inflammatory cytokines, sublytic concentrations of complement membrane attack complex (C5b-9) and sheer stress are known to stimulate MV biogenesis and release (Antwi-Baffour et al., 2015). Following on with the theme of pore formation and increases in intracellular calcium a larger portion of the vWf-adherent platelet membranes (approximately 21%) was released as MVs subsequent to platelet stimulation with the non-physiological agonist calcium ionophore A23187 (Harrison P., 2014).

Peptidylarginine Deiminases (PADs) have been closely associated with many pathologies, including neurodegeneration(Lange et al., 2017b, Tu et al., 2016, Moscarello et al., 2013b, Muth A. and Thompson P.R. Development of the Protein Arginine Deiminase (PAD) Inhibitors. In: Nicholas A., 2017), rheumatoid arthritis (Damgaard et al., 2016, Basu et al., 2011, Auger et al., 2010) and recently cancer(Funayama et al., 2017, Horibata et al., 2017, Lange et al., 2017b, Cedervall et al., 2017, Mohanan et al., 2012, Kholia et al., 2015). Many studies have been performed on the clinical relevance of PAD inhibition in preventing carcinogenesis. Our laboratory at CMIRC first showed that inhibition of PAD expression through chloramidine (Cl-amidine) decreased EV release which suggested that PADscan directlyinfluence EVbiogenesis(Kholia et al., 2015). Adding to these previous findings, our recent research from the same group who reported the therapeutic significance of Cl-am- mediated inhibition of EV release in prostate cancer (Kosgodage et al., 2017)thus is encouraging the use of EV inhibition as a novel therapeutic approach against cancer.

1.2.2 Enzymes that catalyse EV biogenesis and release

1.2.2.1 Acid Sphingomyelinase (A-SMase)

Membrane blebbing is initiated by the activation of ATP receptor-P2X7 preceded by the externalisation of PS, loss of lipid asymmetry and formation of membrane protrusions. Sphingomyelin (SM), a phospholipid abundant in the outer leaflet of the PM has a high affinity for cholesterol (Ayers et al., 2015). A-SMase and other sphingomyelinases catalyse the hydrolysis of SM which in turn increases the efflux of cholesterol and increased membrane fluidity. This destabilises the plasma membrane asymmetry and facilitates microvesiculation (Bianco et al., 2009).

1.2.2.2 Rho- Kinase

The Rho-GTPase-dependent signalling pathway triggers the activation of its downstream targets, Rho Kinase ROCK-I and ROCK-II. ROCK-I and ROCK-II are responsible for actin cytoskeletal remodelling and actomyosin contraction respectively. Activated ROCK phosphorylates Lim-Kinase (LIMK), its downstream target stimulates its kinase activity enabling it to phosphorylate Ser3 on cofilin, which prevents cofilin from severing actin filaments and prolongs the extension of actin fibres (Li et al., 2012). This hyper phosphorylation of cofilin is essential for EV formation together with ROCK and LIMK activation. Moreover Rho-Kinase plays a major role in targeting other signalling pathways in addition to ROCK that lead to EV biogenesis and release.

1.2.2.3 Flippase and Floppase

These enzymes are ATP-dependent lipid transporters that help maintain the lipid asymmetry of the plasma membrane. They require the energy input to transfer phospholipids against a concentration gradient. When the cell is at rest flippase actively translocates PE and PS from the outer leaflet to the inner leaflet while floppase is inactive. Oxidative stress usually leads to an influx of calcium increasing the intracellular concentration. This in turn inactivates flippase and concomitantly activates floppase. This flip-flop transition ultimately leads to the release of EVs (Bianco et al., 2009).

1.2.2.4 Scramblase

Scramblase is a calcium dependent enzyme that is activated in the presence of high concentration of cytosolic Ca²⁺ due to physiological changes in the cells such as platelet activation and neurotransmitter release (Suzuki et al., 2013). This allows PS externalisation resulting in the release of EVs. The PS exposure on the outer leaflet is a classic characteristic of

an apoptotic cell which acts as an 'eat me' signal allowing phagocytosis of post-apoptotic bodies.

1.2.2.5 Peptidylarginine Deiminases(PADs) and Tumorigenesis

PADs are a family of 5 calcium-dependent enzymes designated as PADs 1-4 and PAD 6. They catalyse the citrullination/deimination of arginine residues to citrulline in proteins. Post-translational modifications of proteins, including citrullination/deimination have become novel therapeutic targets in cancer. Autoantibodies that are generated by deimination due to PAD2, PAD3 and PAD4 activation have also been shown to play an important roles in autoimmune diseases, including in joint damage in rheumatoid arthritis patients (Seaman et al., 2016) and are also implicated in Multiple sclerosis (Moscarello et al., 2013a). Furthermore, pan-PAD inhibition was shown to prevent neuronal damage following spinal cord injury (Lange et al., 2011) following hypoxic ischemic insult (HI) (Lange et al., 2014) which further emphasises its relevance as a novel therapeutic agent in neuro-inflammation and also highlights deiminated proteins as potential biomarkers. The role for PAD-inhibition to sensitise cancer cells to chemotherapy has been shown by our group (Kosgodage et al., 2017, Kholia et al., 2015). In humans, the PAD genes are localised to a well-organized gene cluster at 1p36.13, which is also the cluster region for the tumour suppressor gene RUNX3 (Ellsworth et al., 2008). PAD4 is a well characterised isozyme that is widely expressed in immune cells as well as tumour cells, localising to cytoplasmic granules and the nucleus(Kholia et al., 2015) . PAD4 acts as a transcriptional co-regulator for tumour suppressor gene, p53. It is also known as a co-mediator of gene transcription and epigenetic transfer with histone deacetylase 2 (HDAC2) (Li et al., 2010) to regulate the p53 activity during apoptosis. PAD4 co-localises with cytokeratins deimination of which makes them more resistant to caspase-mediated cleavage therefore inhibiting apoptosis of tumour cells. Similarly, its association with epidermal growth factor (EGF) mediated gene activity activates the proto-oncogene c-fos promoting carcinogenesis (Wang et al., 2012). As both PAD activation and EV biogenesis are calcium-dependent processes their synergistic effect in oncogenesis and cancer metastasis are of great interest.

1.3 Apoptosis

Programmed cell death occurs via an energy-dependent proteolytic cascade that results in morphological and biochemical changes in a cell in preparation for lysis. Our understanding of the process has led to a specific targeting of apoptosis with a view to developing effective treatment. Apoptosis comprises three mechanisms, intrinsic, extrinsic and the perforin-granzyme pathway (Elmore, 2007). Involvement of death receptors of the tumour necrosis factor (TNF) family initiates this pathway resulting in the activation of caspases- 3 and 8 which as a consequence undergo DNA degradation and rapid cell death. Mitochondrial depolarisation

releases cytochrome C that activates the intrinsic pathway leading to the activation of Apaf-1 as well as procaspase-9, forming an “apoptosome” (Hill et al., 2004). Bcl-2 proteins control the intrinsic pathway eventually resulting in nuclear fragmentation and cell shrinkage. Some of the members of the Bcl-2 family, Bax, Bad and Bak are pro-apoptotic while other members such as Bcl-XL, Mcl-1 and Bcl-2 act as anti-apoptotic proteins. Bcl-2 may also play a role in non-haematological tumours, and inappropriate expression has been observed in solid tumours such as prostate, breast, and small cell and non-small cell lung cancers (Das, 2015, Anagnostou et al., 2010). This pathway has been the target for chemotherapy over the years. Overall disruption in pro-/anti-apoptotic stability directly regulates the cell survival during chemotherapy which in turn determines its effectivity as a powerful onco-therapeutic agent. Furthermore, DNA has been a more suitable target for chemotherapy and its methylation is associated with transcriptional inhibition. Caspase-8 (CASP8) is silenced owing to gene deletion or promoter methylation, especially in paediatric tumours and their cell lines (Teitz et al., 2000, Olsson and Zhivotovsky, 2011). The loss of this expression is associated with the amplification of the MYCN oncogene facilitating carcinogenesis.

A hall mark for oncogenesis is to evade this major barrier against cancer which is vital for tumour development. P53 mutations act as the main anti-apoptotic mechanism driven by cancer cells. This is regulated by inhibition of p53 activation. This is more apparent in viral infections in which onco-proteins, E6 and E7 (Indran et al., 2011) produced by Human papilloma Virus (HPV) binds and inactivates p53 causing cell death arrest. Also, the excessive secretion of anti-apoptotic proteins such as Bcl-XL allows rapid cell division aiding carcinogenesis. Likewise some rapidly developing tumour cells are programmed to secrete low levels of pro-apoptotic proteins to minimise cell death contributing to its aggressiveness in the system (Pistritto et al., 2016). Classical and novel cancer immunotherapy targets these evading mechanisms adopted by cancer cells during their infection.

1.4 EVs and Cancer

1.4.1 The release of EVs

Exosomes and Microvesicles (EVs) are released by cells upon physiological and pathological stimulation and play a distinctive role in all cellular activities. These ubiquitously released particles serve as bioactive effectors in maintaining many cellular processes including homeostasis, thrombosis, inflammation, angiogenesis and pathogenesis.

1.4.1.1 EVs are conveyors of intercellular communication

EVs carry cellular cargo within them that is specific to the cell of origin. This can be transferred to and induce phenotypic changes in recipient cells. Koppler and co-workers described

neutrophil-derived EVs that can mediate inflammation while the release of matrix metalloproteases (MMPs) through tumour-derived EVs promotes metastasis (Kim et al., 2007). They are also involved in signal transduction pathways where fusion or endocytosis of EVs with neighbouring cells can directly alter cellular properties (Andre et al., 2004, Jorfi et al., 2015). EVs harbour membrane proteins and other nuclear matter such as microRNAs and long ncRNAs, and are involved in non-selective transfer between cells via fusion or that are ligand-receptor mediated. The phagocytosis of EVs by antigen presenting cells increases the internalisation of molecular information that can be used to trigger signalling cascades (Kovar et al., 2006). EV-cellular interaction can occur locally, regionally or systemically and can result in the emission of chemoattractants, growth factors, chemokines and cytokines that may modulate cancer metastasis, inflammation or be involved in the development of infectious diseases.

1.4.1.2 Vesicular Mediated Unconventional Protein Export

Conventional protein secretion involves the signal-peptide dependent protein translocation from ER to the Golgi apparatus which is mediated by intracellular transport vesicles. However, the proteins that lack a signal peptide can still be secreted via self-sustained protein translocation between membranes, via ABC transporters, vesicular pathways and Golgi bypass for trafficking to the plasma membrane. Cytoplasmic proteins such as interleukin 1 β (IL1 β) (Kovar et al., 2006) are transported across membranes via autophagosome-like vesicles (Andreola et al., 2002). Golgi bypass involves the release of proteins to the extracellular space through the shedding of EVs which is adopted by proteins of the galectin family. Vesiculation is an important mechanism for non-conventional protein secretion (Malhotra, 2013, Nickel, 2005).

1.4.2 EVs in Malignancy and Tumour Metastasis

Microvesiculation modulates tumour formation and metastasis. The activation of mutant oncogenes such as KRAS, EGFR and loss of tumor suppressor genes stimulate EV biogenesis and release (van Doormaal et al., 2009). Elevated production of EVs has been associated with prostate cancer cultures that have been correlated to the increased oncogenic activity of protein kinase B. It has also been shown that inhibition of diaphanous related formin 3 (DRF3) (Di Vizio et al., 2009), an actin regulating protein resulted in increased membrane shedding which is suggestive that DRF3 acting as an EV inhibitor. DRF3 expression is lost during metastasis which suggests a link between EV biogenesis, oncogenesis and metastasis. Similarly, EVs have been shown to play a dynamic role in tumorigenesis. Transfer of oncogenes from tumour cells to adjacent cells initiates cancer progression. Pro-angiogenic properties of EVs further increases the malignancy. EVs safeguard the cancer cells from immuno-hijackers such as Natural Killer T-cells therefore facilitating metastasis (Griffioen, 2008). Microvesiculation in the event of drug

treatment reduces its intracellular concentration thus making the tumour cells more resistant to various chemotherapeutics.

1.4.2.1 Angiogenesis

Tumour growth and survival depends on angiogenesis. EVs carry pro-angiogenic factors such as VEGF, FGF-2 and proteases that can be transferred to neighbouring cells inducing metastatic potential in them (Pluchino et al., 2012). EV-associated EGFR activates the VEGF-VEGFR pathway in endothelial cells that in turn promotes angiogenesis. EVs are enriched in sphingomyelins which is known to be a primary factor regulating angiogenesis. Furthermore, Tissue factor (TF) (Valenti et al., 2006) expressing EVs lead to fibrin deposition and formation of niches for tumour cell proliferation that contributes to metastasis.

1.4.2.2 Immune surveillance Evasion

Microvesiculation enhances the cancer cell's ability to protect itself from the immune system and to promote carcinogenesis accordingly.

1.4.2.2.1 EVs and evasion from the Immune System

Secretions of complement-enriched EVs prevent complement mediated lysis of cancer cells. Van Doormaal and colleagues (van Doormaal et al., 2009) discussed 'complement resistance' as a mechanism to escape from C5b-9, MAC (membrane attack complex) induced lysis. It has also been shown that EVs can liberate complement inhibitor CD46 promoting the inactivation of C4b and C3b. Microvesicles bearing PS also have the capacity to inhibit complement by binding protein S in plasma which has a high affinity for the soluble complement inhibitory protein, C4 binding protein (C4bp)(Stratton et al., 2015). Microvesicles also aid the release of immune-modulatory molecules which safeguard the cancer cells from any immune complex attacks. EVs bearing Fas ligand (Andreola et al., 2002) CD95L induce T-cell apoptosis and weaken the immune system. Similarly, the exposure of latent membrane protein-1 (LMP-1) inhibits the leucocyte proliferation that further attenuates the immune system mediated tumour cell lysis. Incorporation of EVs into monocyte membranes impairs differentiation to antigen presenting cells (Andre et al., 2004) which in turn increases tumour survival. Cancer cells can fuse with non-cancer cells through integrin rich EVs. Therefore, transfer of lipids and membrane proteins can expedite the chance of survival through immune cell editing.

1.4.2.3 EVs induce Multi-drug Resistance

Multidrug resistance (MDR) is a major obstacle for effective chemotherapy. Microvesicles enhance the anti-tumoural drug resistance by active efflux of the anti-cancer drug via

vesiculation that decreases the intracellular viable concentration needed for apoptosis. In the presence of calpeptin (calpain inhibitor) the EV release was inhibited which in turn increased the effect of docetaxel and methotrexate in inducing apoptosis of prostate cancer cells, PC3(Jorfi et al., 2015) . It is also clear that drug resistance is transferred from drug-resistant tumour cells to drug-sensitive tumour cells via vesicles. Microvesicle surface molecules (adhesion molecules) are proposed to be associated with tissue selectivity in the transfer of P-gp in malignant breast cells (Pokharel et al., 2014). P-glycoprotein (P-gp) and MRP1 are members of the ATP Binding Cassette (ABC) superfamily of transporting molecules and have shown detrimental effects on MDR allowing cancer cell survival. In the presence of inhibitors of P-gp and MRP-1, the effect was reversed which suggests that such mechanisms are essential to prevent cancer recurrence (Gong et al., 2012) .

As a consequence of their detrimental effect on cancer metastasis, EVs have become a target for cancer therapeutics. In particular, the inhibition of EV release has been considered to increase the effectivity of chemotherapy with minimum side effects (Moore et al., 2017, Kosgodage et al., 2017).

1.4.2.3.1 Role of p53 and P-glycoprotein (P-gp) in Cancer drug Resistance

Tumour suppressor gene, p53 is either mutated or inactivated in cancer and has shown a marked involvement in drug resistance. Alkylating agents used in oncotherapy operate through DNA damage so the sensitivity of p53 affects the sensitivity of tumours for such therapy if p53-mediated apoptosis occurs readily in these cells (Hientz et al., 2017). Chemoresistance with p53 is most commonly reported in studies related to ovarian cancers (Brachova et al., 2013). Its also been shown that p53+ tumours have an increased survival rate compared to p53- tumours which suggests that increases in genomic instability due to p53 abnormalities tends to evolve resistance to anti-cancer drugs (Darrah et al., 2012). This coupled with high expression of bcl-2 diminishes the susceptibility to apoptosis leading to a systemic accumulation of cancer cells.

Wild type p53 suppresses the expression of drug resistance genes, MDR-1 and MRP-1 and it has been shown that mutant p53 upregulates the expression of MDR-1 (the gene product is P-gp) but not MRP-1(multi-drug resistant associated protein-I) which are both drug efflux pumps in cancer (Breen et al., 2007, Sampath et al., 2001). It is just as likely that these genes could be up-regulated by the “gain-of-function” activity of mutant p53 (Sigal and Rotter, 2000). The deletion analysis in a human colon carcinoma cell line revealed the involvement of only mutant p53 with promoter, Ets-1 site that was essential for its activation in MDR-1 but not the wildtype p53(Sampath et al., 2001). Interestingly it is shown that loss of p53-mediated repression increases the expression of both MDR-1 and MRP-1 which would be problematic for successful oncotherapy.

Similar studies elicit the correlation between MYCN activation and the upregulation of the MDR-1 gene that affects curability with chemotherapy in human neuroblastomas. This concomitantly increases MYCN and MDR1 transcripts levels, consistent with chemoresistance phenotype and active P-gp (Blanc et al., 2003). IGR-N-91 neuroblastoma cells enriched with the MYCN transcription factor bind to two E-box motifs localized within the MDR1 promoter (Blanc et al., 2003). This data is comparable to the above study in terms that both mutant p53 and MYCN genes do not affect the upregulation of MRP-1.

P-gp acts as a transmembrane drive which eliminates drugs from the cell membrane and cytoplasm. It has further been proposed that P-gp acts like a hydrophobic vacuum cleaner or "floppase," transporting drugs from the inner leaflet of the plasma membrane lipid bilayer to the outer leaflet or to the external medium (Homolya et al., 2011). Lysosomal fractionation has been used to demonstrate the role of P-gp in MDR. P-gp substrate doxorubicin (DOX) was used in this study of the mechanism used by the tumour cells to provoke resistance. It was shown that p-gp substrates that are ionizable at lysosomal pH (pH 5) (Yamagishi et al., 2013) were sequestered and trapped in lysosomes affecting their ability to target apoptosis in cells and thus increasing the survival span of circulating tumour cells.

These research findings reveal the consequence of p53 mutation and P-gp activation through MDR-1 translation in developing MDR. This has led to further investigations in using alternative therapeutic agents either individual or in combination to combat cancer cell survival.

1.5 EV Inhibition and Cancer Immunotherapy

EVs have been identified as potent cancer biomarkers and different therapeutic approaches have been used to target the adverse effect of these vesicles on oncogenesis. EVs have also become a major topic of interest with regard drug delivery. They have been used widely in targeted therapy for many diseases such as cancer (Tian et al., 2014), cerebral occlusions (Armstrong et al., 2017) and neurodegenerative diseases (Croese and Furlan, 2018, Ciregia et al., 2017). Conventional chemotherapy targets the DNA damage of the cancer cells that leads to apoptosis. This approach has been widely used though not without adverse effects on healthy cells. Also the increases in MDR through mutations have allowed the chemotherapeutic agents to fail successively, irrespective of their mode of action (Alfarouk et al., 2015). This has alarmed the need of complimentary therapy to combat this issue and halt the cancer cell survival. The majority of cancer researchers focus on successful cancer drug delivery. In the past decade the use of nanocarriers to drive target therapy have pioneered the research field. Using EVs provides multiple advantages including their biocompatibility, stability, low immunogenicity and target delivery (Shen et al., 2018).

Nevertheless, therapeutic applications of EVs as drug delivery systems have not been without challenges. This has limited the use of this strategy due to a lack of methods for scalable EV isolation and efficient drug loading (Saari et al., 2015). Furthermore, in order to achieve targeted drug delivery, their intrinsic cell targeting properties should be tuned through EV engineering (Barkalina et al., 2015). Expulsion of chemotherapeutic drug due to EV release can decrease its intact time with the cancer cells making them less susceptible to chemotherapy. In the same way, anti-cancer drugs delivered to cells via biological nano-carriers such as stem-cell-derived vesicles can also be expelled from the cells during this release (Qi et al., 2017). This in return leaves the cells with a non-effective dose of chemotherapy, insufficient for cell cytotoxicity but that induces MDR in cancer cells (Singh et al., 2017). There have been previous studies bringing together ideas on improvement of chemotherapy through EV inhibition using different types of cancers (Roseblade et al., 2015, Menck et al., 2017, Kholia et al., 2015, Jorfi et al., 2015). A recent review has discussed pharmacological inhibitors that are connected with different pathways of inhibition of EV release and uptake in renal diseases (Karpman et al., 2017). However, there is no such study related to EV- driven chemotherapy. This was a great driver for part of the research presented in this thesis. It has not only resulted in studying most of the pathways of EVbiogenesis and release using multiple cancer cell-lines of different origin but has also worked through into introducing novel inhibitors.

1.5.1 Pharmacological Mitotic Inhibitors

1.5.1.1 Taxanes

The taxanes are a class of chemotherapeutic agent that increase microtubule polymerisation and maintain its stability (by inhibiting its depolymerisation through binding to the β -tubulin); as a result they inhibit cell division. Paclitaxel and Docetaxel are abundantly used taxanes against tumours which are reported to be well tolerated with minimum side effects in breast cancer patients (Crown et al., 2004). Microtubule stabilisation is ensured by centrosomal impairment, induction of abnormal spindles and suppression of spindle microtubule dynamics (Xie et al., 2016). Taxanes are known to be more effective against prostate cancer. Taxane binding to microtubules halts the movement of androgen receptors therefore inhibiting their activity. This has been shown to be more active against androgen dependent prostate cancer (Martin and Kyprianou, 2015).

1.5.1.2 Anti-metabolites

An antimetabolite is any agent that interferes with the normal cell metabolism. 5-Fluorouracil (5-FU) has been known to be effective against a wide range of solid tumours including gastrointestinal related carcinomas. *In vivo*, 5-FU is converted to the active metabolite 5-

fluorouracil (5-FU) is converted to fluorouridylic acid (F-Uridylic acid) and fluoroxyuridine monophosphate (F-UMP); replacing uracil, F-UMP incorporates into RNA and inhibits RNA processing, thereby inhibiting cell growth (Jacob et al., 2001). Another active metabolite irreversibly inhibits thymidylate synthase, resulting in the depletion of thymidine triphosphate (TTP) preventing *in vivo* DNA synthesis (Gottesman, 2002). Previous studies have shown that 5-FU can be used in conjunction with radiotherapy merely to enhance its cytotoxicity, effectively abrogating metastasis (Swanson et al., 2006). Additionally a novel antimetabolite, zebularine has shown promise inducing apoptosis and arresting cellular growth in various pancreatic cancer cell lines (Valenzuela et al., 2014). However, resistance to these anti-metabolites remains a problem, emphasising the absolute need of either discovering new antimetabolites or of developing alternative therapies that will improve a patient's overall survival. This increased resistance to 5-FU has been reported extensively in the field in relation to prostate, colorectal and breast cancers. Similar to most cytotoxic anticancer agents, anti-metabolites are toxic to normal cells, especially those in the bone marrow and gastrointestinal tract (Scholar, 2007). Therefore, it is crucial that only a minimal dose of the drug is used to treat cancers in order to prevent undesirable toxicity to healthy cells. This research has opened up novel ideas to achieve this through coupling of anti-cancer drugs with EV inhibition.

1.5.1.3 Anthracyclines

Anthracyclines are a class of drugs that are produced by certain types of *Streptomyces* bacteria such as *Streptomyces peucetius* var. *caesius*. They are used in chemotherapy, and therefore termed antitumour antibiotics which include daunorubicin, doxorubicin, epirubicin, aclarubicin and mitoxantrone (Rabbani et al., 2005). The use of anthracyclines in combination has proven to be more effective in chemotherapy than as single agents and appears to have improved therapeutic efficacy and to reduce toxicities (Bachur, 2002). The types of malignancies that are treated with the various anthracyclines range from acute myelogenous leukemia to lymphoma to solid tumors of the breast, lung, gastrointestinal tract, and genitourinary system (Vejjongsang and Yeh, 2014). These anticancer agents work by damaging DNA and by generation of free radicals.

The anthracyclines are believed to exert their cytotoxic effects through a variety of mechanisms; Topoisomerase II (Top II) plays a key role during DNA synthesis, nicking and resealing the DNA helix so that it does not become tangled during replication (Liu et al., 2009). The anthracyclines prevent the resealing step from occurring by intercalating into and inhibiting the DNA–topoisomerase II complex after the nicking phase. This results in a large number of DNA fragments, eventually prompting the cancer cell to undergo apoptosis (Bardal et al., 2011).

As a secondary mechanism, anthracyclines produce free radicals, and these free radicals in turn damage cell membranes, proteins, and lipids (Bhattacharyya et al., 2014). The generation of free

radicals is also believed to mediate an important toxicity associated with this class which can lead to cardiomyopathy (Bardal et al., 2011).

Cancer cells are known to build up resistance to anthracyclines due to drug efflux through P-glycoprotein (Pgp-170) or multidrug-resistant (MDR) gene (Pasquier et al., 2011), altered topoisomerase II levels, mutations in topoisomerase II (Wang et al., 2014), increased glutathione (a free radical scavenger) (Rivera and Gomez, 2010), increased glutathione peroxidase activity and decreased concentration of glucose-6-phosphate (G6P) dehydrogenase (Wagner et al., 2005). It is thus crucial to develop a mechanism to combat the resistance and make the tumour cells more susceptible to the cytotoxicity of these drugs.

This study has used DOX to examine the effect of EV inhibition. Also known as Adriamycin, it is a prodrug with an active metabolite (Zhao et al., 2015). The anthracyclines are eliminated through hepatic metabolism, through a variety of routes. Its widespread use in cancer treatment is not without side effects, especially cardiotoxicity (Volkova and Russell, 2011). Dose adjustments should be considered in patients with significant hepatic impairment and cardiac instabilities and it is vital that the cancer patients are treated with the minimum, yet effective dose of the drug. This study will look at how EV inhibition will allow the use of a minimum operative dose of doxorubicin in an attempt to reduce drug resistance.

1.6 Bacterial Outer-membrane Vesicles (OMVs)

Outer membrane vesicles (OMVs) are predominantly produced by Gram-negative bacteria by direct budding of the outer membrane under stress conditions (Kulp and Kuehn, 2010). Bacterial OMVs were first reported with respect to *E. coli* in the 1960s (Pérez-Cruz et al., 2015). However recent studies have emphasised the production of OMVs by Gram-positive bacteria such as *Staphylococcus aureus* (Brown et al., 2015). OMV release is a conserved phenomenon, but there are considerable differences in composition and activity of OMVs between species, between strains, and even between the same strains under different external pressures (O'Donoghue and Krachler, 2016). Different mechanisms of OMV biogenesis have been discussed in the literature. Initial publications have mentioned that bacterial membrane blebbing has occurred as a consequence of cell lysis where the OMVs contain cellular debris (McCaig et al., 2013). However latter publications have strongly suggested that OMV biogenesis rather than being a byproduct of cell lysis is a deliberate process which gives rise to vesicles following dissociation of the bacterial outer-membrane from the peptidoglycan cell wall in the absence of anchoring (Schwechheimer and Kuehn, 2015, Kulp and Kuehn, 2010). Therefore, the vesicles contain functional bacterial cargo and not 'cellular debris' as previously suggested. Nevertheless, the mechanism of OMV biogenesis through the peptidoglycan cell wall in such bacteria is still not well known. OMVs from these microorganisms range from 20 nm to 400 nm in diameter

(Schrempf et al., 2011). This variability in the size of vesicles suggests that although vesiculogenesis may be a universal phenomenon, different bacteria utilise different regulatory mechanisms to synthesise these vesicles (Toyofuku et al., 2017). Bacterial OMVs contain enzymes and other biologically active proteins which get transferred to neighbouring cells bringing about many changes in the recipient cells. OMVs can deliver virulence factors and control the host immune system during pathogenesis (Katsir and Bahar, 2017) They may also aid in nutrient acquisition (Schwechheimer and Kuehn, 2015), be involved in ecological niche protection (Jain and Pillai, 2017) and provide structural support in biofilm formation (Jain and Pillai, 2017). Recently, OMVs have been discovered to have therapeutic potential through vaccines, adjuvants or as drug delivery vehicles (Jain and Pillai, 2017) not only in the presence of bacterial infections but against viral replication (Acevedo et al., 2014). Therefore, as with extracellular vesicles (EVs) in eukaryotes, bacterial OMVs are useful as mediators in intercellular communication. The discovery of this broad spectrum of usability has allowed OMVs to continue their transition from ‘cellular rubbish’ (akin to an early description platelet MVs as ‘platelet dust’(Wolf, 1967)) to an important means of intercellular communication between bacteria and eukaryotic cells (Olsen and Amano, 2015)

There are many studies that have discussed the involvement of OMVs in directing antibiotic resistance (AR) and reduced phage titre directing phage therapy. A recent comparative proteomic analysis on OMVs by Park and colleagues resulted in more drug-binding proteins (efflux proteins) in the biofilm compared to planktonic growth of *Pseudomonas aeruginosa* (Park et al., 2014). Similarly, Fulsundar reported that OMVs act as carriers of AR genes which are laterally transferred to recipient cells causing phenotypic transformation leading to insensitivity to treatment in *Acinetobacter baylyi* (Fulsundar et al., 2014b). Likewise, β -Lactamase-harboured OMVs from *Bacteroides thetaiotaomicron* protected *Salmonella Typhimurium* and *Bifidobacterium breve* from an otherwise lethal dose of cefotaxime (Stentz et al., 2015). This was an insight into how enteric and commensal bacteria in the colon are protected by β -lactam antibiotics. Furthermore, bacterial defence mechanism was conserved, if not augmented through hypervesiculation. This was examined in a wild-type *E.coli* treated with antimicrobial-peptides. Vesicle-mediated protection was also observed for a human pathogen, enterotoxigenic *E. coli* (ETEC), challenged with polymyxin B (Manning and Kuehn, 2011).

1.6.1 Bacterial OMVs and Bacteriophage Infection

Efficacious adsorption of virus particles to a bacterial surface receptor initiates a successful phage invasion. These receptors are typically protein or polysaccharide (lipopolysaccharide) and must be in a permissive spatial distribution which makes it readily accessible. Interestingly, it has been shown that OMVs interfere with phage invasion in many ways. The culprit mostly affects the adsorption phase as highlighted by Manning and co-workers (Manning and Kuehn,

2011). The T4 phage is obstructed by *E.coli*-OMVs in this instance which acts as a decoy to prevent infection.

However original research carried out recently has highlighted the beneficial role of OMVs in phage attack. Bacteriophage largely impact Horizontal gene transfer (HGT). This work used *Bacillus subtilis* and its lytic phage SPP1 to demonstrate that SPP1 resistant cells regaining the sensitivity through co-infection with SPP1-sensitive cells. This acquisition of sensitivity is believed to be mediated via OMVs through HGT of the sensitivity gene to the resistant cells (Tzipilevich et al., 2017).

The latter however is possible if the adsorption of phage takes place. Many studies support the phenomenon that OMVs obstruct this surface assimilation of phage to initiate the infection. Therefore, it is important that this defence mechanism adopted by bacterial cells is overcome to provide effective phage therapy. In this research, pharmacological OMV inhibition is reported for the first time with an insight into the inhibitory pathways of OMV biogenesis and release. This has extended to its beneficial role in preventing antibiotic resistance and ameliorating the use of minimum effective antibiotic dose with pronounced changes in both Gram-negative and Gram-positive bacterial cells.

The research presented in this thesis further elaborates into the role of OMVs during bacteriophage infection. The implication of OMV inhibition on phage therapy has been investigated using *E.coli* and lambda phage. Also, the putative effect of Cl-amidine has been further investigated as a preventative measure of OMV release that can impact phage assembly during infection.

1.7 EVs and Viral Infection

Numerous studies have also looked into EV association with viruses. Captivatingly it has been shown that these vesicles have many characteristics in common with enveloped viruses more commonly retroviruses (Meckes and Raab-Traub, 2011). Retaining similar characteristics that include biophysical properties, biogenesis and uptake by cells (Nolte-t Hoen et al., 2016) has enabled the virus-EV relationship to thrive during infection. Recent discoveries have further explained its mode of action through vesicle-mediated intercellular transfer of functional cellular proteins, RNAs, and mRNAs which have revealed additional similarities between viruses and EVs. Interestingly, many virally infected cells secrete microvesicles that differ in content from their virion counterparts but may contain various viral proteins and RNAs.

A group has looked into the viral-vesicle relationship in herpes simplex virus-infected HOG-cells. HSV-1 virions were detected from vesicles isolated from these infected cells. Furthermore virus-containing vesicles were endocytosed into CHO-K1 cells and were able to

actively infect these otherwise nonpermissive cells (Bello-Morales et al., 2018). In conclusion it was also revealed that co-infected CHO cells with viral vesicles were not completely neutralised by anti-HSV-1 antibodies which excitingly suggested that immune shielding was acquired by the virus from its vesicle coating. A similar study on Epstein-Barr virus further confirmed this mechanism of host immune system circumvention. Internalization of fluorescently labelled exosomes derived from EBV-uninfected and EBV-infected B cells of type I and type III latency into EBV-negative epithelial cells was observed (Nanbo et al., 2013). This resulted in significant phenotypic changes in the recipient cells which suggested that this tumorigenic herpesvirus also utilizes exosomes as a mechanism of cell-to-cell communication through the transfer of signaling competent proteins and functional microRNAs to uninfected cells (Teow et al., 2017, Keryer-Bibens et al., 2006, Ruiss et al., 2011). The vesicle-mediated high virus virulence is now central to research and recently interested a group to evaluate the possibility of a similar rapport in enteric-viral infections in humans. This has led into the discovery of ‘vesicle-cloaked virus clusters’ driving the faecal-oral transmission of norovirus and Rotavirus enhancing both the multiplicity of infection (MOI) and disease severity between hosts. The research was conducted in pigs’ stool samples. There was a significant fraction of vesicle-containing Rotaviruses in the stool rotavirus pool and it was confirmed that virus coated in vesicles are more infectious than free stool Rotaviruses *in-vitro* (Santiana et al., 2018). It suggests that viral-vesicle clusters are considered the optimal agents for spreading infections as opposed to freely circulating virus particles. Therefore, target therapy should focus on preventing EV-virus cluster formation as a means of controlling inter-organismal viral evasion.

1.8 Cannabidiol (CBD) and the Biology of EVs

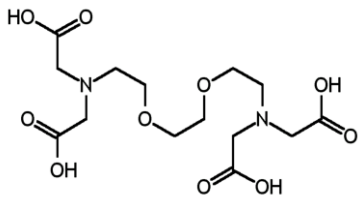
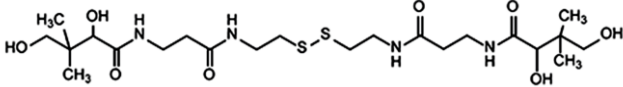
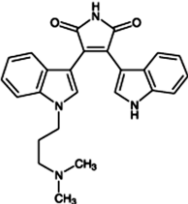
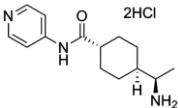
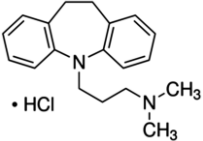
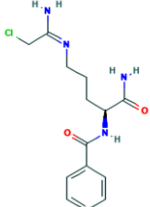
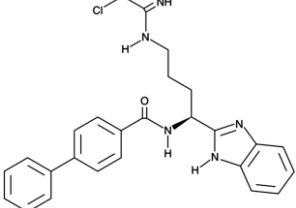
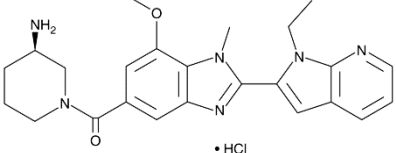
CBD, a phytocannabinoid derived from *Cannabis sativa*, is anxiolytic (Blessing et al., 2015) and has analgesic, anti-inflammatory, anti-neoplastic and chemo-preventive properties (Pisanti et al., 2017, Fernandez-Ruiz et al., 2011). CBD has been shown to have a plethora of molecular targets, including the classical endocannabinoid system, while effects that do not involve the classical cannabinoid system are also gaining increased attention (Ibeas Bih et al., 2015, Pisanti et al., 2017). Recent findings have managed to extend the role of CBD in preventing behavioural, electrophysiological, and neuropathological effects in epilepsy. Results conducted on an intrahippocampal pilocarpine epilepsy model managed to introduce anticonvulsant and neuroprotective characteristic of CBD (Do Val-da Silva et al., 2017, Tang and Fang, 2017). Known anti-cancerous effects of cannabinoids include inhibition of tumour proliferation, angiogenesis and induction of tumour cell death (McAllister et al., 2005, McAllister et al., 2015, Velasco et al., 2016, Solinas et al., 2013, Dumitru et al., 2018).

Critically, CBD has been shown to be effective in various EV-linked pathologies (Chiurchiù et al., 2018), and seems to modulate mitochondrial function, including ATP, ROS and proton leak, as well as uptake and release of calcium (Ibeas Bih et al., 2015, Rimmerman et al., 2013, Ryan et al., 2009). These observations may be relevant as mitochondria are key in modulating calcium signaling (Liu et al., 2001). As described previously, calcium signalling is crucial for EV release (Hay, 2007). Furthermore, altered calcium signalling and mitochondrial function are hallmarks of many cancers (Chattopadhyay and Roy, 2017, Vyas et al., 2016, Lynam-Lennon et al., 2014).

This study has undoubtedly led to the discovery of a novel role of CBD (Kosgodage et al., 2018). Its function as an EV inhibitor has here been explored in five different cancer cell lines. Its inhibitory role has further been confirmed in the presence of the standard anti-cancer drug, temozolomide in glioblastoma (Kosgodage et al., 2018) which indicates EV-mediated effects for effective cancer therapy.

1.9 Reagents used as Potential Inhibitors in the Study

A range of reagents have been used to investigate the potential of inhibiting both the release of EV and bacterial OMV release. CBD, AMF30a and GSK199 were not water soluble and were dissolved in DMSO to prepare working solutions. Nicotine was a ready to use liquid. The rest of the reagents were water soluble including, BB-Cl-amidine and Cl-amidine. The abundance of non-polar groups in the chemical structure contributes to the hydrophobicity of some reagents while the presence of polar groups makes the reagents hydrophilic as seen with EGTA. The chemical structures, hydrophobicity and the net charge of all inhibitors were taken into account during data analysis (Table 1).

Potential Inhibitor	Chemical Structure	Hydrophobicity	Net charge
EGTA (Nowak et.al., 2018)		Less	0
D-Pantethine (PubChem 2019)		More	0
Bisindolymaleimide-I (PubChem 2019)		Less	0
Y27632 (Leonel et.al., 2017)		More	0
Imipramine (Browman & Fox 2007)		More	0
Chloramidine (Luo et al., 2006)		More	0
BB-Chloramidine (Knight et al., 2014)		More	0
GSK199 (Lewis et al., 2015)		More	0

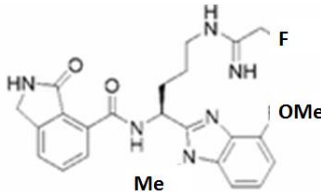
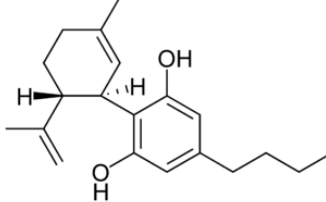
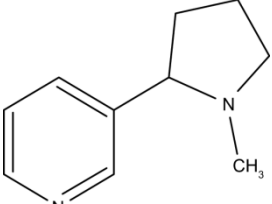
AMF30a (Muth et al., 2017)	<p style="text-align: center;">AMF30a PAD2 specific, reversible</p> 	More	0
Cannabidiol (Istvan & Lumir 2016)		More	0
Nicotine (Pubchem 2019)		More	0

Table 1. Chemical structures of the potential inhibitors used in the study. These reagents were used in different experiments to investigate the effect on EV and OMV inhibition. Their hydrophobicity and the net charge have been taken into consideration during results analysis.

1.10 Gold Standards of Detection and Quantification of EVs

High throughput analytical platforms have been developed to analyse EVs. Researchers in the EV field have utilised various methods to characterise and quantify EVs (Rupert et al., 2017). Flow cytometry has been the classic approach (Morales-Kastresana et al., 2017) amongst them, but recently more sophisticated techniques such as Nanoparticle Tracking Analysis (NTA), based on brownian motion of particles in fluids, have been introduced for high accuracy and verification of results.

1.10.1 Flow Cytometry

Flow cytometry has been used to analyse the physical and chemical properties of EVs in the fluid phase (Akers et al., 2016), especially using high resolution flow cytometers. The forward scatter correlates to its particle size while side scatter reflects the granularity. These measurements along with fluorescent intensity can be measured as EVs pass through the laser beams resulting in the FACS plot. Phosphatidylserine (PS) exposure on EVs can be detected using FITC, PE or alexa fluor conjugates of Annexin-V and using this method it is possible to analyse large numbers from a single isolate. The experiments carried out in this study have used a Guava EasyCyte flow cytometer (Guava Technologies, UK) which has allowed multiple antigen detection using FSC-Hlog and SSC-Hlog settings that allowed, where

necessary, accurate quantification of the whole sample. Cytograms consisting of dot plot and histograms have been used for data analysis (Reggeti and Bienzle, 2011).

1.10.2 Nanoparticle Tracking Analysis

The EV field has shown interest in using a better method than flow cytometry to quantify EVs (Malvern, 2015 News Medical, Wang et al., 2010, Gardiner, 2011). This sophisticated technique has become increasingly prevalent among researchers and has allowed accurate analysis of particles according to size, based on Brownian motion. The Nanosight LM-10 has mainly been used to analyse size distribution and quantify EVs in this study, while the NS300 model was also used for analysis of the GBM data. The Nanosight has allowed the rapid and accurate analysis of the data samples utilising the properties of both light scattering and Brownian motion in order to obtain the size distribution and concentration measurement of particles in a liquid suspension (Malvern, 2015 News Medical). Minimal sample preparation and increased sensitivity has made it more viable for EV studies than traditional methods (Dragovic et al., 2011).

1.10.3 Fluorescence Microscopy

High resolution fluorescence microscopy analysis which involves single object studies has supported research findings in many studies. Its significance in performing morphology studies has encouraged more laboratories to include this identification tool in their investigations. Single object studies have the general advantage of uncovering heterogeneity that may be hidden during the ensemble averaging which is common in any bulk conventional biochemical analysis (Ter-Ovanesyan et al., 2017). The implementation of single object analysis in the study of extracellular vesicles (EVs) may therefore be used to characterize specific properties of vesicle subsets which would otherwise be undetectable (Carpintero-Fernández et al., 2017, Reátegui et al., 2018).

1.10 Overall Aim

Phase I

The identification of a suitable inhibitor or a combination of inhibitors of EV release from cancer cells. Findings from cancer cells were further applied to identify potential strong OMV inhibitors using *E.coli* and *S. aureus*.

Phase II

PC3 and MCF-7 cells treatment with anti-cancer drugs, 5-FU in the presence and absence of the chosen inhibitors from phase I as well as Peptidyl Arginine Deiminase (PAD) inhibitor and the measurement of resulting apoptosis. Additionally, assessment of the effect of EV inhibition in DOX-treated PC3 cells.

Phase III

Assessments of the effects of OMV inhibitors on Minimum Inhibitory Concentration (MIC) of antibiotics. This data was then utilised to conduct further experiments related to antibiotic resistance and phage therapy

Phase IV

Assessment of vesicle-mediated drug delivery using DOX encapsulated in PC3 cell-derived EVs.

Chapter 2: Materials and Methods

2.0 Materials & Methods

2.1 Cell lines

EVs were isolated from PC3 cells (Human prostate cancer cells). PC3, MCF-7 cells (Human breast cancer), HEPG2, MDA-MB-231, LN18 and LN229 cell lines were used in EV inhibition and apoptosis experiments.

MCF-7 cells (ECACC; Ref No. 86012803)

MCF-7 is based on the acronym Michigan Cancer Foundation -7 in Detroit where it was established. It is a breast cancer cell line that was first isolated in 1970 from a pleural effusion of a 69-year old Caucasian woman following a radical mastectomy of her left breast for malignant adenocarcinoma.

These cells retain mammary epithelial characteristics. They are able to process oestrogen (ER) via ER receptors and are sensitive to cytokeratin. The cells are adherent and grow in monolayers forming domes.

PC3 cells (ATCC® CRL-1435™)

The PC3 cell line was established in 1979 from bone metastasis (grade IV) of prostate cancer in a 62-year-old Caucasian male (Cunningham and You, 2015). The cells do not respond to androgens, glucocorticoids or fibroblast growth factors but are influenced by epidermal growth factors (Tai et al., 2011). PC3 cells are androgen receptor (AR) and prostate specific antigen (PSA) and prostate-specific membrane antigen (PSMA) negative and express characteristics similar to Prostatic small cell neuroendocrine carcinoma (SCNC) (Tai et al., 2011). Electron microscopy reveals the similarity between epithelial neoplasms and PC3 cells such as the presence of numerous microvilli, junctional complexes, abnormal nuclei and nucleoli, abnormal mitochondria, annulated lamellae, and lipid bodies (Kong et al., 2011).

HEPG2 cells (Received as a kind gift from Dr K. White, London Metropolitan University)

Liver cancer cells were first isolated from a 15 year old male Caucasian with a well-differentiated hepatocellular carcinoma. These cells are epithelial in morphology and secrete plasma proteins such as albumin, transferrin and plasminogen (Mersch-Sundermann et al., 2004).

These cells have been widely used in research relating to hepatotoxicity and drug metabolism. They are able to activate and detoxify xenobiotics and therefore reflect the metabolism of xenobiotics in the human body better than other metabolically incompetent cells used in conventional in vitro assays (Donato et al., 2015). Cell lines are characterized by their unlimited life span, stable phenotype, high availability, and easy handling (Bokhari et al., 2007). However,

their major limitation is the lower expression of some metabolic activities compared with hepatocytes.

MDA-MB-231 cells(Received as a kind gift from Dr. T. Kalber, UCL)

This is a human Caucasian breast adenocarcinoma cell line established from pleural effusion. It has previously been used to study the changes in the morphological pattern and gene expression of cells when grown in the presence of sera positive for anti-carbonic anhydrase I (CA I) autoantibodies, the effects of normothermic conditioned microwave irradiation on cultured cells using an irradiation system and the transendothelial migration rates of the cells under different shear stress levels (Chavez et al., 2010). They are of epithelial origin and are adherent cells.

MDA-MB-231 is a highly aggressive, invasive and poorly differentiated triple-negative breast cancer (TNBC) cell line as it lacks oestrogen receptor (ER) and progesterone receptor (PR) expression, as well as HER2 (human epidermal growth factor receptor 2) amplification. Invasiveness of the cell line is modulated by proteolytic degradation of the extracellular matrix (Holliday and Speirs, 2011).

As a result of lacking ER and PR expression and HER2 amplification, the cell line was initially classed as a 'basal' breast cancer cell line. However, it is now recognised as belonging to the claudin-low molecular subtype as it exhibits down-regulation of claudin-3 and claudin-4, low expression of the Ki-67 proliferation marker, enrichment for markers associated with the epithelial-mesenchymal transition and the expression of features associated with mammary cancer stem cells (CSCs), such as the CD44⁺CD24⁻/low phenotype (Dai et al., 2017, Subik et al., 2010, Sun et al., 2017).

In 3D culture, the cell line displays endothelial-like morphology and is distinguished by its invasive phenotype, having stellate projections that often bridge multiple cell colonies (Syed et al., 2017)(Figure 1, D).

LN18 and LN229 cells (ATCC® CRL-2610™ and ATCC® CRL-2611™)

Glioblastoma (GBM), the most malignant intrinsic glial brain tumour, hardly colonizes outside the central nervous system (CNS). It seems to need the unique composition of the cranial microenvironment for growth and invasion as the incidence of extracranial metastasis of GBM is as low as 0.5 % (De Vleeschouwer and Bergers, 2017). On the basis of histopathological features, GBM are divided into two major groups, astrocytomas (morphologically resembles normal and reactive astrocytes) and oligodendrogliomas (similar to oligodendrocyte lineage)(Zong et al., 2012). GBM is a grade IV and an aggressive tumour and prevailing target therapy consists of radiotherapy in conjunction with TMZ-mediated chemotherapy. Two GBM cell lines have been used in the present study.

The LN-18 cell line was established in 1976 from the cells of the right temporal lobe glioma in a 65 year old white male. The cells are poorly differentiated and negative for glial fibrillary acidic proteins and S-100 protein(Wybranska et al., 2013). They exhibit mutated p53 and possible homozygous deletions in the p16 and p14ARF tumor suppressor genes, and have a wild-type PTEN gene (Sesen et al., 2015).

Overexpression of Bcl-2 protects these cells from Fas ligand-induced cell death. This cell line is frequently used in apoptosis studies and is considered to be TMZ resistant (Happold et al., 2012).LN-18 cells grow in vitro as bipolar or stellate cells with pleomorphic nuclei, having a doubling time of about 72 h and a plating efficiency of 3%(Klein et al., 2012).

Similarly, LN229 which is also used in apoptosis experiments is used in the current study. They were first isolated from brain/right frontal parieto-occipital cortex tissue of a 60 year old white, female (Hong et al., 2012). The cells exhibit mutated p53 (TP53) and possible homozygous deletions in the p16 and p14ARF tumor suppressor genes. They have a wild-type PTEN gene (Ren et al., 2010). LN229 is well known as a TMZ-sensitive cell line as well as to Belinostat exposure , a cytostatic agent used in GBM (Kusaczuk et al., 2016).

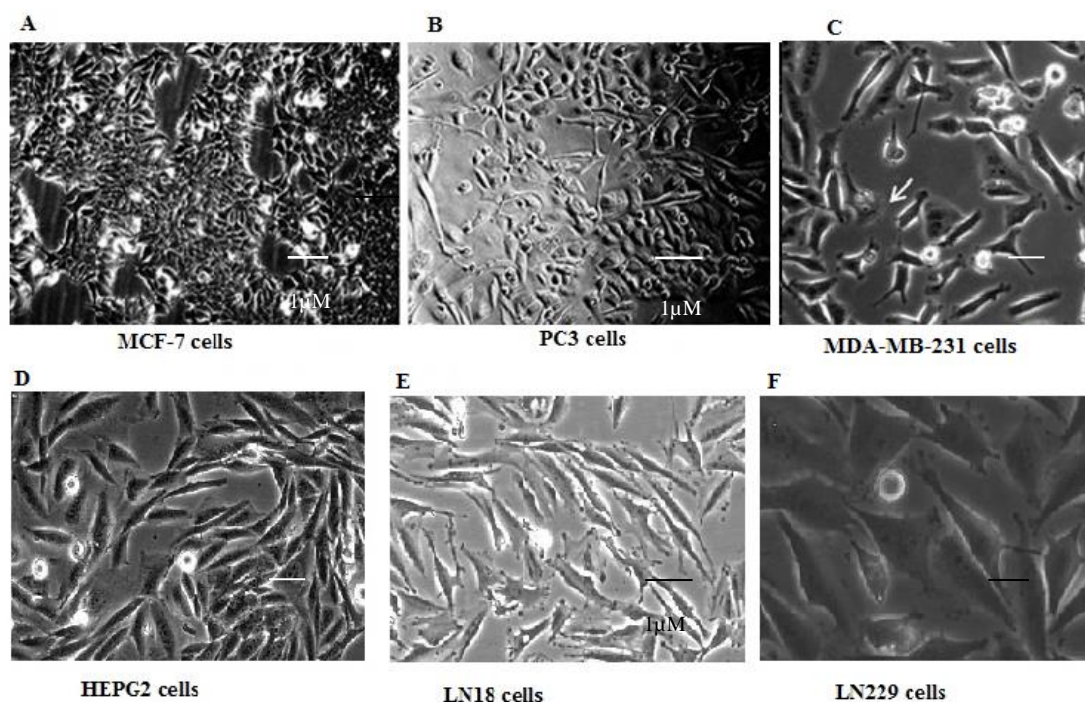


Figure 1: Microscopic Images of cells used in the study.A, MCF-7 are adherent cells that form domes in monolayers. B, PC3 elongated adherent cells.C, MDA-MB-231 cells, spindle-shaped that are adherent.D, HEPG2, adherent cells. E-F, glioblastoma cell lines, LN18 (TMZ-resistant) and LN229 (TMZ-sensitive). The cells are morphologically epithelial and are adherent.

2.2 Cell Growth Medium (CGM)

To make complete growth medium, RPMI 1640 medium with phenol red, containing 2.05mM glutamine and sodium pyruvate was supplemented with 10% FBS (v/v) and 1% Penicillin / Streptomycin in 500 ml volumes and stored at 4 °C.

2.3 Methods

2.3.1 Maintaining cell lines

Adherent cell lines, PC3, MCF-7, HEPG2, MDA-MB-231, LN18 and LN229 were maintained at 37 °C with 5% CO₂, in suitable growth media. Both PC3 and MDA-MB-231 cell lines were grown using RPMI supplemented with 10% FBS while MCF-7, HEPG2, LN18 and LN229 were grown in DMEM supplemented with 10% FBS. These cells were split depending on confluence every 3 to 5 days. Cells were washed twice by changing GM with DPBS and 0.25% (v/v) trypsin/EDTA was added. After 10-15min incubation at 37°C with 5% CO₂, the flask was observed under the microscope and if the cells were detached and floating, growth medium was added to inactivate the trypsin. The trypsin solution was removed by centrifugation at 200 g for 5 min followed by one wash in DPBS for PC3 and centrifuged at 120 g for 5 min followed by one wash in DPBS for all other cell lines. Cell pellets were resuspended in the appropriate GM volume and seeded in the desired dilution into new culture flasks. Exponentially growing cells with a viability of 95% or higher were used in every experiment. The number of cells and viability was determined before the start of every experiment using the haemocytometer and viability assays on Guava viacount (Guava Technologies, UK) and NucleoCounter® NC-3000™ (Chemometec) at different occasions.

2.3.2 Cryopreservation of cells

To prepare frozen stocks for long term storage, cells grown to almost 100% confluency were detached using trypsin/EDTA, washed twice (200 g, 5 min for PC3 and 120g, 5min for all other cell lines) with DPBS and cell number determined using Guava Viacount and NucleoCounter® NC-3000™ as mentioned in section 3.10. Cells were carefully resuspended in freezing mix (growth medium + 10% DMSO), transferred into cryo-vials (Greiner) at 1×10^7 cells/ml in 1 ml volumes and immediately placed on ice. The cryo-vials were frozen at -80 °C in polystyrene boxes, which ensure a temperature decrease of 1 °C per minute. For long-term storage the deep frozen cryo-vials were kept in liquid nitrogen.

2.3.3 Defrosting of cryopreserved cells

To defrost cells, cryo-vials were removed from liquid nitrogen and immediately thawed in a water-bath at 37°C. After cleaning the lid with 70% ethanol the contents were transferred to a

15 ml centrifuge tube containing 9 ml of complete growth medium, prewarmed to 37°C and cells were pelleted by centrifugation at the appropriate speed (200 g, 5 min for PC3 and 120 g, 5 min for MCF-7). To remove DMSO, the medium was discarded, and the cell pellet resuspended in fresh growth medium. The cells were then placed into tissue culture flasks and incubated at 37 °C with 5% CO₂.

2.4 Biochemical Methods

2.4.1 Isolation of EVs from conditioned medium

EVs were isolated from the supernatant of the cell culture medium that consisted of serum-free EV-free RPMI which was centrifuged once at 200 g for 5 min (PC3) to remove the cells. The supernatant was then centrifuged once at 4,000 g for 60 min at 4°C to remove cell debris. The resultant supernatant was centrifuged at 25,000 g for 1h at 4 °C. The isolated EV pellet (which also contains exosomes as clumps, were not separated by sonication(Grant et al., 2011)was resuspended in sterile-filtered (0.22µM) DPBS and centrifuged again at 25,000 g for 1h at 4 °C to remove proteins such as albumin possibly bound to the EV membrane surface. The EV pellet was resuspended in sterile-filtered (0.22 µm pore size) DPBS and quantified on a Guava EasyCyte flow cytometer using ExpressPlus software (Guava Technologies), Nanosight LM10 or else a BCA protein quantification was performed. Isolated EVs were then used immediately or stored at -80 °C for experiments. For EV associated experiments serum free medium (RPMI) was used after ultracentrifugation at 75000 g for 24 h to obtain a medium of minimal contamination with vesicles.

2.4.2 Detection of PS-Positive EVs

Twenty microlitres of EVs (2×10^6 EVs/ml) were resuspended in 5µl Annexin V-FITC and 50 µl Annexin V binding buffer (FITC was added or not (control)). The sample was then incubated at room temperature (RT) for 1.5h with shaking. Fifty microlitres of Ann V binding buffer was added and centrifuged at 13,000 g for 1h to pellet EVs. Samples were analysed immediately as directed by the manufacturer using the flow cytometer (Guava EasyCyte, GuavaTechnologies).

2.4.3 Immunostaining of Cells

PC3 cells were labelled with FITC-labelled anti-CD9, anti-CD29, anti-CD58 and anti-CD71. FITC- IgG1 was used as the control for specific binding. Cells were washed three times (200 g for 5 min) with serum-free RPMI prior to experiments and once in DPBS for 5 min at 200 g. Cell count was determined using the Guava Viacount assay. Cells were fixed with 4% paraformaldehyde for 1 0min at RT. Fixed cells were washed 2x with PBS at 400 g for 5 min. Cells were equally distributed into 1.5 ml microfuge tubes and pre-incubated with 3% BSA/PBS for 45 min at RT. The cell mixture was then treated with 5 µl of the FITC-conjugated antibody

for 1h at 4 °C. Stained cells were washed 3 times with PBS and observed using a NucleoCounter® NC-3000™ (Chemometec).

2.4.4 PKH labelling of PC3 cells and PC3-derived EVs

PC3 cells were detached with trypsin and washed twice with DPBS at 200 g and a cell pellet obtained. 100 µl of diluent was added to the cell pellet. PKH dye + diluent mixture was made by adding 40 µl of the dye to 200 µl of the diluent. The cell suspension and dye solutions were mixed and incubated at RT for 15 min in the dark. 100 µl of BSA solution was added to the reaction mixture and washed thrice at 200 g with DPBS. The washed cells were mounted on a glass slide and analysed by fluorescent microscopy.

The same protocol was used to label isolated EVs but the incubation time was extended to 30 min in dark and the washing centrifugation was carried out at 25,000 g.

2.4.5 Protein Quantification

The concentration of a protein solution was determined using the BCA Protein Assay Kit (Pierce, Thermo Scientific, UK). It uses a combination of the biuret reaction (reduction of Cu²⁺ ions to Cu⁺ ions by proteins in an alkaline medium) and the colorimetric detection of the Cu⁺ cations by a bicinchoninic acid-containing colour reagent. Following the manufacturer's instructions (Pierce BCA Protein Assay Kit, Thermo Scientific) standards were prepared. The assay was performed in a 96-well microtitre plate and 25 µl of protein samples were added to 200 µl of a working solution consisting of a mixture of kit reagent A and reagent B (ratio 50:1 respectively). The plate was incubated for 30 min at 37°C, followed by 10 min incubation at RT to cool the samples. A540 readings were taken on a FLUOstar Omega microplate reader. Protein concentrations of the unknown samples were determined by interpolation on a standard curve using the Beer Lambert law.

2.5 Flow Cytometry

The Guava EasyCyte flow cytometer allows complex biological studies such as cell counting and viability testing, cell activation marker analysis and other complex molecular analyses to be performed simultaneously. ViaCount assay (counting cells and determining viability) and ExpressPlus assay (microvesicle analysis) were used in this study.

2.5.1 Guava ViaCount Assay

Cell number and viability were determined using the ViaCount assay, which distinguishes between viable and non-viable cells based on the differential permeability of two DNA-binding dyes in the Guava ViaCount reagent. The nuclear dye only stains nucleated cells, while the viability dye brightly stains necrotic or apoptotic cells. This exclusive combination of dyes enables the Guava ViaCount assay to distinguish between viable, apoptotic and dead cells.

2.6 Image Flow Cytometry [NucleoCounter® NC-3000™ (Chemometec)]

2.6.1 Viability Assay

The Via1-Cassette™ was used to determine the viacount. A sample of the cell suspension was drawn directly into the Via1-Cassette™. The live and dead cell count was distinguishable through the presence of two different dyes, staining the entire cell population and the non-viable cells respectively. The image of the Viability and Cell Count Assay was created through plot manager. All cells were stained with Acridine Orange (AO) represented by green cells. Nonviable cells are stained with DAPI, represented by blue cells.

2.6.2 Annexin V apoptosis Assay

Externalisation of phosphatidylserine (PS) occurs in early apoptosis which is easily detected through Annexin V staining. Cells were stained with Hoechst 33342, Propidium Iodide (PI) and Annexin V-FITC. Hoechst 33342 stains the total cell population, while Annexin V stains apoptotic and necrotic cells. Scatter plots and histograms created through Plot Manager provided the images which were easily analysed. Early apoptotic cells exclude PI, while late stage apoptotic and necrotic cells stain positive for both Annexin V and PI.

2.6.3 Cell Vitality Assay

Reduced Glutathione (GSH) is involved in many cellular processes such as cell signalling and proliferation. The reduction in GSH is a marker for early apoptosis. The vitality assay provides easy determination of the level of thiols, such as reduced glutathione (GSH). The VB-48 assay was performed according to the manufacturer's protocol and scatter plots and histograms created through Plot Manager. By comparing the VB-48™ intensity of treated cells and control cells the fraction of cells with low vitality (e.g. necrotic or apoptotic cells) could be determined. Quadrants and polygons were used to define specific areas of apoptosis within the cell populations in the samples.

2.6.4 Mitochondrial Membrane Potential Assay

Apoptosis leads to many mitochondrial changes in a cell. One of them is loss of membrane potential (Ψ). The assay uses tetraethylbenzimidazolylcarbocyanine iodide (JC-1), a cationic, lipophilic dye that accumulates in energized mitochondria to measure the mitochondrial membrane potential. JC-1 at low concentrations (normal cells) is predominantly a monomer that yields green fluorescence with emission of 530-545 nm (depolarisation). At high concentrations the dye aggregates yielding a red to orange coloured emission of 590- 605 nm (hyperpolarisation). This is seen in apoptotic and necrotic cells. An optional dead cell dye, 7-AAD, is also included for discrimination between apoptotic cells and dead cells. Flow cytometric analysis of JC-1 fluorescence is best performed using two-dimensional green versus red fluorescence plots, where the ratio of green to red fluorescence allows comparative

measurements of membrane potential between cell populations which has given a better insight into determining the most effective concentration of doxorubicin (DOX) with minimal effect on healthy cell viability.

2.7 Nanoparticle Tracking Analysis

Samples were diluted 1:50 using sterile-filtered DPBS and the minimum concentration of samples was set at 5×10^7 particles/ml. The settings at the capturing stage screen and camera gain were 8 and 13 respectively and at the process stage, screen gain and detection threshold were set at 9 and 3 respectively.

2.8 Fluorescent Microscopy

For fluorescence microscopy analysis, adherent cell samples placed into 12-well plates containing 18 mm coverslips were cultured on coverslips at 37 °C with 5% CO₂ for 24 h. Cells were then gently washed twice with PBS and fixed with 4% paraformaldehyde at 37 °C for 10 min and mounted on microscope slides with DAPI-VECTASHIELD medium (Vector Laboratories Inc. Burlingame, CA) for fixed cells and mounting medium (Agar Scientific, Essex, UK) for fixed MVs. Coverslips were mounted on microscope slides and images were collected using a fluorescence microscope (1X81 motorized inverted fluorescence microscope, Olympus Corporation). The images were processed using Image J software. This technique was used for PKH labelling of cells, EVs and to visualise drug transfer via EVs.

2.9 Western Blot (WB) and Mass Spectrometry Analysis

2.9.1 Preparation of cell lysates for Western blot analysis

The bacterial cells were sedimented by centrifugation at 4,000 g for 10 min at RT before lysis. OMVs were subjected to a centrifugation of 25,000 g at 4°C prior to lysis. The pellets were washed once by careful resuspension in SM buffer by centrifugation. After that, cells were counted using a flow cytometer for cells and NTA for vesicles to give a protein concentration equivalent to 2×10^5 cells/10 µl. Bacterial cell and vesicle lysis was performed by resuspension of the pellet in B-PER® Bacterial Protein Extraction Reagent from Thermo Scientific containing Lysozyme and DNase adhering to manufacturer's protocol (User Guide: B-PER Bacterial Protein Extraction Reagent). The total protein concentration was determined of the resultant supernatant (**section 2.5.5**) and then subjected to sodium dodecyl sulphate polyacrylamide gel electrophoresis (SDS-PAGE) analysis.

2.9.2 Sample preparation for SDS-Polyacrylamide Gel Electrophoresis (SDS-PAGE)

Sodium dodecyl sulphate (SDS) sample buffer (2X) was added to samples in a ratio of 1:1 followed by boiling at 95°C for 4 min.

2.9.3 SDS-PAGE Protein Molecular Weight Standards

As a protein molecular weight standard, pre-stained Protein-marker I (BioRad) was used. Prestained markers, ranging from 10 to 250 kDa were used when analysing gels by Western blot using the enhanced chemiluminescence (ECL) detection system. Markers were applied by loading 7 µl into wells.

2.9.4 SDS-Polyacrylamide Gel Electrophoresis

To separate proteins which were denatured by SDS according to their molecular masses, SDS-PAGE was performed as described (Laemmli, 1970) using the Mini PROTEAN III Electrophoresis System (Bio-Rad UK). Ready made TGX gels, 4-20% were used (BioRad UK).

To perform electrophoresis, the gel was placed into the electrode assembly device inside a clamping frame in the tank of the Mini PROTEAN III system. Electrophoresis running buffer was added to the inner and outer chambers of the tank and the plastic comb was carefully removed. Wells were washed with the running buffer to remove any free unpolymerized acrylamide/bisacrylamide. *E.coli* and *E.coli*-derived OMV samples (total protein concentration added varied according to the sample) were loaded into the wells of the stacking gel using loading pipette tips. Electrophoretic separation was performed at 160 V, 3A and 13W for 1h until the bromophenol blue front of the SDS sample buffer reached the end of the resolving gel. Gels were transferred onto nitrocellulose membrane for Western blotting analysis.

2.9.5 Western Blotting Analysis

Proteins separated by SDS-PAGE were transferred to a Hybond C nitrocellulose membrane for further analysis using a semidry transfer device (Bio-Rad Sartoblot system). A Hybond C nitrocellulose membrane and two pieces of blotting paper (Whatman 3 MM, BioRad) were cut to the size of the separating gel. Blotting paper, nitrocellulose membrane and the sandwich-blotting cassette were equilibrated in Sartoblot buffer. One piece of blotting paper was placed on the cathode plate, and the nitrocellulose membrane was placed on top of the blotting paper. The gel was removed from between the sandwich-blotting cassette and placed on top of the membrane, and a second blotting paper was also placed on top of the gel. Having removed air bubbles, the anode plate, also dampened with the Sartoblot buffer was used to complete the sandwich. Electroblothing was carried out at 15V for 1 h.

2.9.6 Immunochemical Protein Detection using the ECL System

Western blotting was performed as described above using hybond C nitrocellulose membrane (Amersham Biosciences). The membrane was incubated in blocking buffer for 1 h at RT on a shaker. Following blocking, the membrane was rinsed with PBS-T (PBS with 1% v/v Tween20) and incubated overnight at 4°C on a shaker with the primary antibody at the desired dilution. Three 10 min washing steps with PBS-T were performed and the membrane was incubated with

isotype matched HRP-conjugated secondary antibody in the desired dilution for 1 h at room temperature on a shaker. After three 10 min washes with PBS-T, visualization was performed using ECL system (Amersham Pharmacia). The ECL solutions (reagent A and B) were mixed at equal volumes and the membrane was incubated with the mixture for 2 min at RT and chemiluminescence detected using the UVP ChemiDoc-It system (UVP systems, UK).

2.10 Liquid Chromatography-Mass Spectrometry (LC-MS/MS)

Proteomics experiments were performed using mass spectrometry as reported (Rajeeve et al., 2014, Casado et al., 2013). In brief, *E.coli* protein complexes were digested into peptides using the protease inhibitor trypsin. Peptides were desalted using C18+carbon top tips (Glygen Corporation, TT2MC18.96) and eluted with 70% acetonitrile (ACN) in 0.1% formic acid.

Dried peptides were dissolved in 0.1% TFA and analysed by nanoflow liquid chromatography (ultimate 3000 RSL nano instrument) coupled on-line to a tandem mass spectrometer (Q Exactive plus, Thermo Fisher Scientific). Gradient elution was from 3% to 35% buffer B in 120 min at a flow rate 250nL/min with buffer A being used to balance the mobile phase (buffer A was 0.1% formic acid in water and B was 0.1% formic acid in ACN). The mass spectrometer was controlled by Xcalibur software (version 4.0) and operated in the positive mode. The spray voltage was 1.95 kV and the capillary temperature was set to 255°C. The Q-Exactive plus was operated in data dependent mode with one survey MS scan followed by 15 MS/MS scans. The full scans were acquired in the mass analyser at 375- 1500m/z with the resolution of 70 000, and the MS/MS scans were obtained with a resolution of 17 500.

MS raw files were converted into Mascot Generic Format using Mascot Distiller (version 2.5.1) and searched against the SwissProt database (release December 2015) restricted to *E. coli* entries using the Mascot search daemon (version 2.5.0). Allowed mass windows were 10 ppm and 25 mmu for parent and fragment mass to charge values, respectively. Variable modifications included in searches were oxidation of methionine, pyro-glu (N-term) and phosphorylation of serine, threonine and tyrosine.

The mascot result (DAT) files were extracted into excel files for further normalisation and statistical analysis.

2.11 Microbiology Techniques

2.11.1 Preparation of Agar Plates

Twenty five grams of Müller Hinton Agar was dissolved in 500 ml of distilled water and shaken well. The medium was autoclaved for 15 min at 121 °C, and then allowed to cool. Plates were prepared in a laminar flow cabinet. Initially plates were labelled with the type of medium and date. The medium was thoroughly mixed by shaking the bottle prior to pouring and then poured

into plates and left to solidify for a maximum of 1h. These were then taped up firmly with autoclave tape and incubated overnight.

After 24 h the plates were checked for any growth. If growth was seen these were autoclaved and the rest of the plates placed in the fridge after thorough sealing to use for future experiments.

2.11.2 Preparation of Müller Hinton Broth

Eleven grams of Müller Hinton powder was dissolved in 100ml of distilled water and shaken well until the contents were fully dissolved. The medium was autoclaved for 15 min at 121 °C (15 psi), and then allowed to cool before using in experiments.

2.12 Transmission Electron Microscopy

In advance, 400 mesh copper grids with carbon films deposited on them were cleaned via glow discharge for 1.5 min on a PELCO easiGlow™ Glow Discharge Cleaning System, Ted Pella. Samples were prepared by applying 10 µL to the grid (OMVs, 10-3 lambda phage and the phage-OMV mixture as three different samples) and incubated for 2 min. The grids were then washed 5 × with 50 µl of 1% aqueous uranyl acetate. The last drop was left to incubate on the grid for 1.5 min before being wicked off by torn filter paper. Grids were left to dry for 5 min before being viewed. Micrographs were taken with a JEOL JEM 1230 transmission electron microscope operated at 80 kV at a range of magnification mainly around a magnification of 80,000 to 100,000. Digital images were recorded on a Morada CCD camera and processed via iTEM both from EMSIS.

2.13 Statistical Data Analysis

Statistical analysis for all data presented was performed by the unpaired t-test for repeated measures using GraphPad Prism version 8.0 for Windows (GraphPad Software, San Diego, USA). Statistical correlations between data values were also determined using GraphPad Prism software. Differences giving a value of $P < 0.05$ with confidence interval of 95% were considered statistically significant.

Chapter3: Pharmacological Inhibition of Microvesicle Biogenesis and Release

3.0 Pharmacological Inhibition of Microvesicle Biogenesis and Release

3.1 Introduction

The metastatic prostate cancer PC3 cells are adherent cells that grow rapidly in the presence of suitable growth conditions. It was essential from the outset to determine the growth rate of these cells. Revisiting the EV isolation protocols, many of which had been established at the Cellular and Molecular Immunology Research Centre (CMIRC) was essential to adhere to the latest advances in the EV field. As a result, experiments to isolate EVs (exosomes and microvesicles) from PC3 cells were carried out altering the speed and the duration of centrifugation.

Much recent research on EVs has focused on taking into account their release from cancer cells and the possible influence of their biogenesis on the effectivity of cancer therapy. To optimise the effectiveness of chemotherapy, it is essential that the drug is retained within the target cell for the optimum duration. This is directly influenced by microvesiculation, so it is important that EV release is halted to ensure minimum expulsion of the drug. To this aim it is crucial that effective EV inhibitors are used in experiments to investigate the efficiency of anti-cancer drugs. Therefore, a set of experiments was designed to study the effect on cells stimulated to release EVs with (2'(3')-O-(4-Benzoylbenzoyl) adenosine-5'-triphosphate tri(triethylammonium) salt (BzATP). BzATP is an agonist of purinergic receptor P2X7. Triggering of P2X7 by BzATP induces phosphatidylserine (PS) externalization and membrane blebbing, increasing EV release (MacKenzie et al., 2001).

Nicotine has previously been used as an EV inhibitor by CMIRC (Grant et al., 2011) so it was interesting to revisit the idea with some modifications. The substance is a naturally occurring alkaloid in organic plants such as aubergine and tomatoes. Interestingly high abundance in the tobacco plant makes its presence and involvement more apparent in carcinogenesis (Sanner and Grimsrud, 2015b). Cigarette smoke promotes cancer cell survival and metastasis in many tumours such as breast, lung and colon. Since nicotine is a naturally occurring product and present in vegetables it cannot be harmful when consumed in lower quantities. The detrimental effect of cigarette smoke is not only due to nicotine but a contribution of more than 5,000 chemicals (Talhout et al., 2011). As a result it was interesting to know whether nicotine can play a role in cancer immunotherapy if used in minute concentrations.

3.2 Methods

3.2.1 Determining the PC3 Growth Rate

PC3 cells were maintained as described earlier (**section 2.4.1**). Cells were seeded in triplicate at 3.8×10^5 /well in a 12-well microtitre plate in the presence of 1.5 ml of complete growth

medium/well. The day of setting up the experiment was taken as day 0 and the cell viability was checked from day 3 to day 7 using the Guava Viacount assay as described before (**section 2.6.1**).

3.2.2 Revisiting EV Isolation Techniques

PC3 cells were maintained as described in 2.4.1. 24 h before the experiment, the cells were maintained in serum-free RPMI 1640 at 37°C in 5% CO₂. Cells were seeded in triplicate at 3.8×10^5 /well in a 12-well microtitre plate in the presence of 1.5 ml of serum-free RPMI/well and incubated for 48 h. EVs were isolated as described in 3.5.1 with the exception of centrifuging the samples initially at different speeds (5000 g, 10,000 g, 15,000 g, 20,000 g and 25,000g) for 2 h after the first step of 4,000 g centrifugation for 1h. The experiment was repeated twice and the second experiment with a different range of speeds (5,000 g to 15,000 g) was carried out. Furthermore, a third experiment was designed to evaluate the optimum duration of centrifugation. PC3 cells were maintained as described in 3.4.1. 24 h before the experiment, the cells were maintained in serum-free RPMI 1640 at 37°C in 5% CO₂. Cells were seeded in triplicate at 3.8×10^5 /well in a 12-well microtitre plate in the presence of 1.5 ml of serum-free RPMI/well and incubated for 48 h. EVs were isolated as described in 2.5.1 with the exception of centrifuging the samples initially at 4,000 g for 1h followed by centrifugation at 13,000g for 30min, 60min, 90min and 120 min respectively. EV count was determined via Guava ExpressPlus.

3.2.3 EV inhibitors

3.2.3.1 Optimum concentration of BzATP to stimulate EV release

The adherent prostate cancer cells, PC3 were maintained in complete growth medium containing RPMI and 10% Fetal Bovine Serum. Then 24 h before the experiment the cells were maintained in serum-free RPMI 1640 at 37°C in 5% CO₂. Cells were washed and resuspended in pre-warmed serum-free RPMI and seeded in triplicate at 3.8×10^5 cells/well in a 12-well microtitre plate. The cells were treated with 100 µM and 300 µM of BzATP and incubated for 30 min and 60 min respectively. Cell viability and EV production was determined using Guava Viacount and Guava ExpressPlus respectively.

3.2.3.2 Effect of potential EV inhibitors on Microvesiculation

Cells were pre-treated as stated before and washed and resuspended in pre-warmed serum-free RPMI and seeded in triplicate at 3.8×10^5 cells/well in a 12-well microtitre plate. EGTA (1.5mM), Bisindolylmaleimide-I (10 µM), Imipramine (25 µM), Y27632(1 µM), D-pantethine (1 mM) and Chloramidine (50 µM) were added separately and incubated for 1 h at 37°C in 5% CO₂. At the end of the first incubation, the cells were washed and 300 µM EV stimulator, BzATP was added and further incubated for 30 mins at 37°C in 5% CO₂. The experiment was

repeated thrice and the EV count was determined using the Guava EasyCyte flow cytometer (Guava Technologies, UK) which was further confirmed by using NTA analysis (Nanosight LM10). Annexin V staining was performed to confirm the MV release. Guava ViaCount was used to investigate the effect of using these reagents on cell viability.

3.2.4 Nicotine plays a role in EV Inhibition

Cells were pre-treated as stated before and washed and resuspended in pre-warmed serum-free RPMI and seeded in triplicate at 3.8×10^5 cells/well in a 12-well microtitre plate. The cells were treated with different concentrations of nicotine. Cell viability and EV concentration was determined using Viacount on the NucleoCounter® NC-3000™ (Chemometec) and the BCA assay respectively where EV protein concentration was calculated using the Beer- Lambert's law. The results were also confirmed by performing nanosight tracking analysis (NTA).

3.3 Results

3.3.1 Growth rate of PC3 cells

It was essential to carry out the growth curve to obtain an idea about the doubling time and the point where natural death starts occurring in the experimental set-up (**Figure 3.1**). In this way the duration to be used for cytotoxicity experiments was determined. Furthermore, it was important to visualise whether EVs derived from PC3 cells carry the parent cells' characteristics. Therefore, immunostaining of PC3 cells was performed using CD markers and visualised on the NucleoCounter® NC-3000™ (Chemometec) as shown in (**Figure 3.2**). Furthermore, PKH labelling of PC3 cells and PC3-derived EVs was visualised using fluorescent microscopy (**Figure 3.3**).

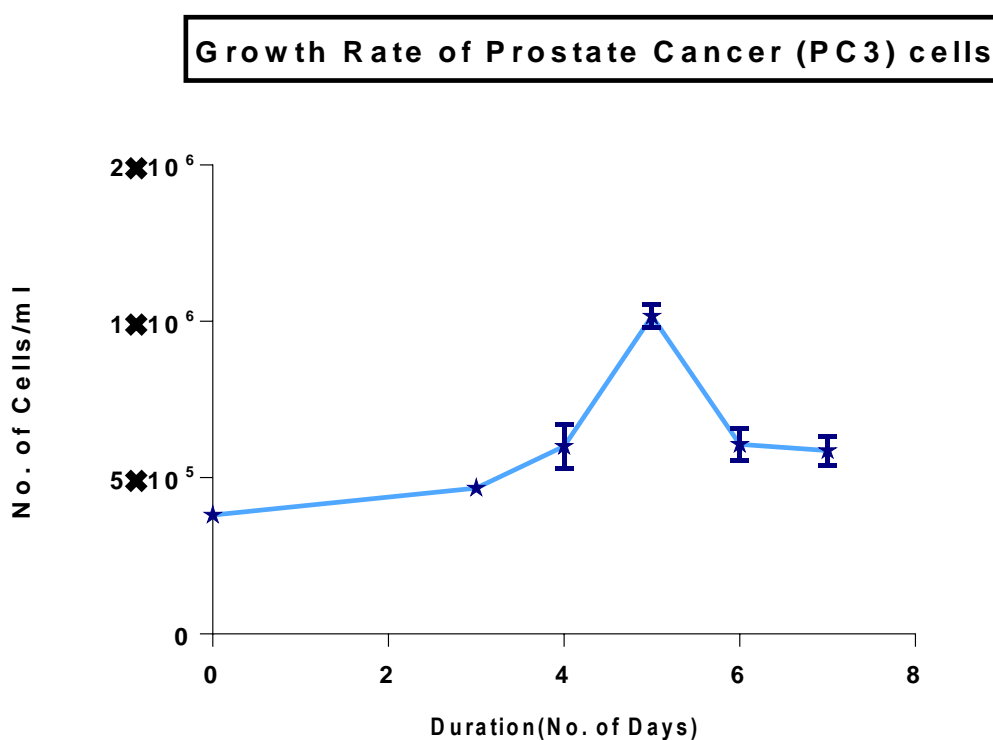


Figure 3.1 PC3 growth curve.The lag phase was between days 3 to 4 followed by a rapid increase in growth. The highest growth was recorded at day 5 which eventually declined by day 7. The doubling time was 23.19 h.

3.3.2 Immunostaining

3.3.2.1 Immunostaining of PC3 cells

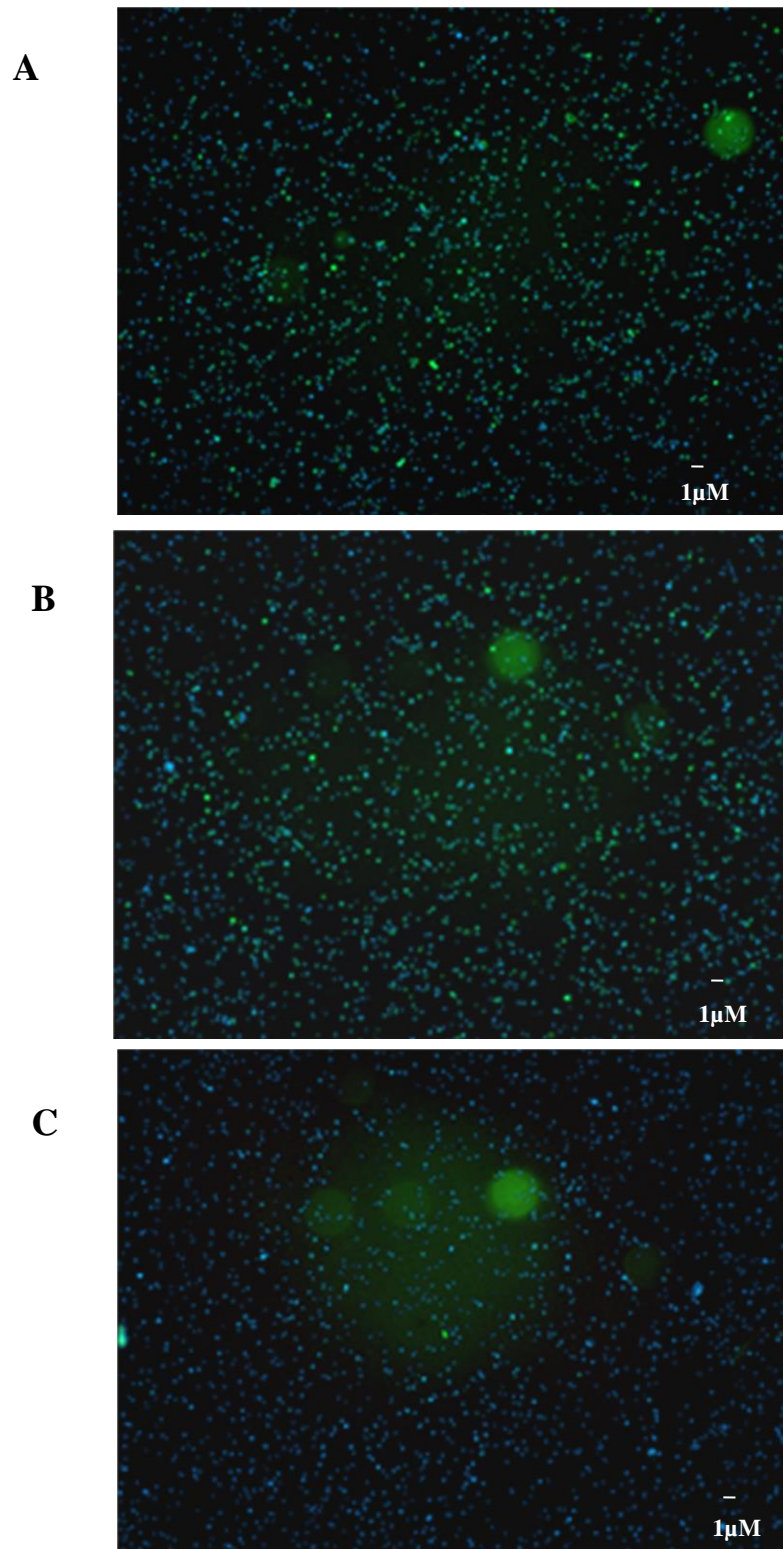
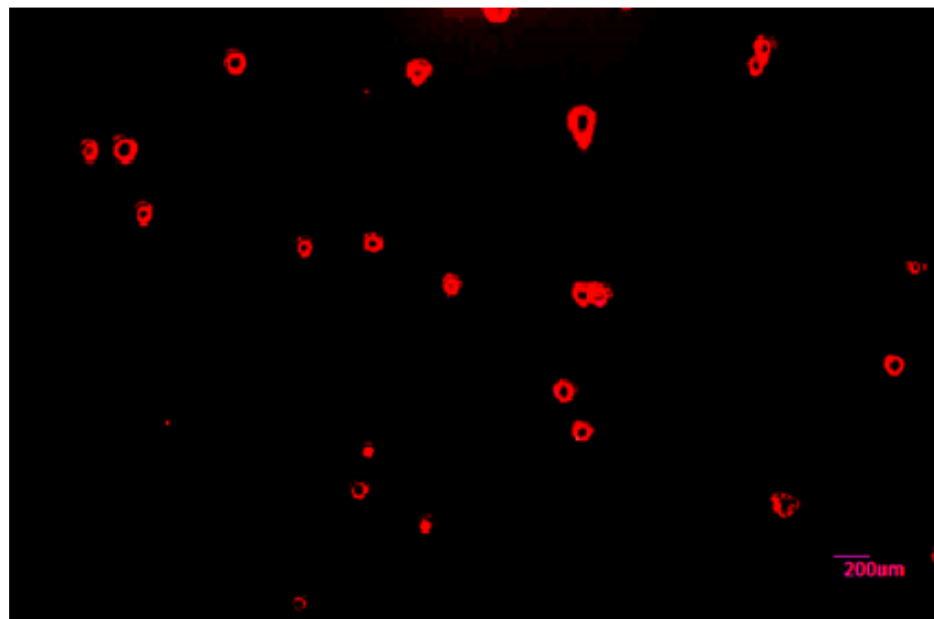


Figure 3.2 Immunostaining of PC3 cells. PC3 cells were stained with FITC-labelled antibodies. **A**, PC3 cells show expression of CD58 and in **B** of CD29. Nuclei are counter-stained blue using DAPI.

3.3.2.2 PKH labelling of PC3-cells and PC3- derived EVs

A



B

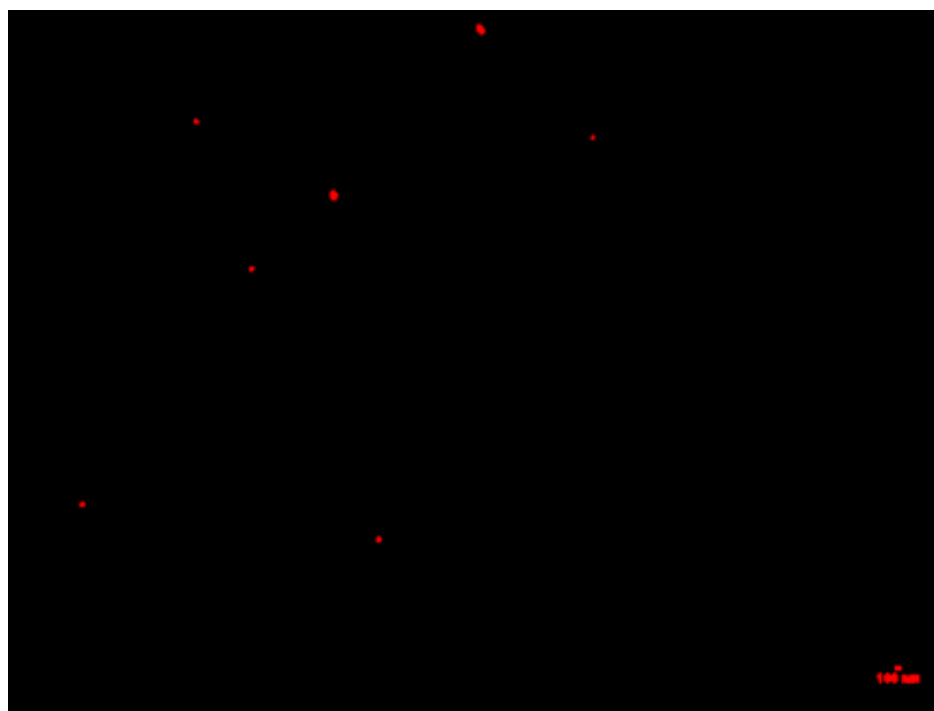
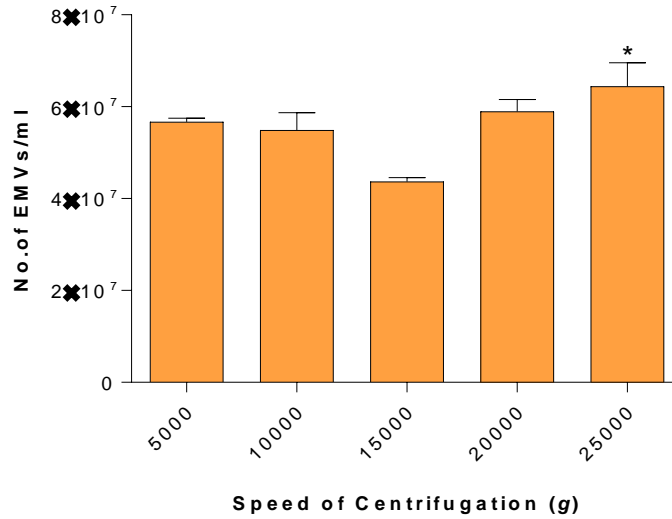


Figure 3.3 PKH labelling of PC3 cells and PC3-derived EVs. **A**, PKH26- labelled PC3 cells. **B**, PKH26- labelled PC3-EVs.

3.3.3 EV Isolation

A Effect of Centrifugation Speed on the Isolation of PC3 cell-derived EMVs



B Effect of Centrifugation Speed on the Isolation of PC3 cell-derived MVs

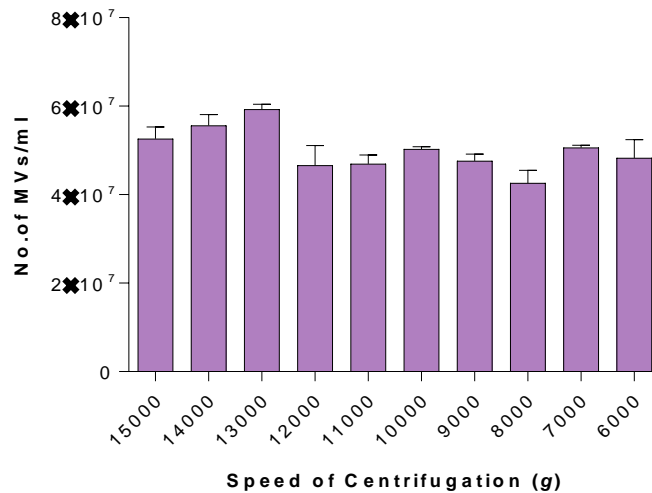


Figure 3.4 25,000 g maximises EV isolation. **A**, The initial experiment was designed to compare the different speeds of centrifugation. The samples were centrifuged at different speeds for 1h and the above data was obtained. 25,000 g resulted in the highest EV count ($p= 0.0163$). **B**, Centrifugation at lower speeds facilitated the isolation of MVs. However as the study focuses on the total EV population 25,000 g was used in future experiments. The experiment was repeated three times and the data presented are mean \pm SEM of the results.

3.3.3.1 Optimisation of the Centrifugation Speed Resulting in a higher yield of EVs

Revisiting the isolation techniques was essential to understand the protocols used in the EV field. The range of centrifugal force used in (Figure 3.4A) was utilised to match those generally used among EV researchers and 25,000 g which was previously used in our lab as well as many other labs for isolation. 25,000 g resulted in the highest EV count (43.02% greater compared to the lowest EV release at 15,000g, $p=0.0163$) which suggested that such EV isolations need to be carried out at lower speeds. To further investigate the optimum speed for MV isolation the experiment was repeated at a broad range of lower centrifugation speeds. **Figure 3.4B** depicts that 13,000 g results in a maximal MV count. However, 25,000 g was used throughout this study as it focuses on the total population of EVs.

EV isolation has been carried out for various durations by researchers and it was evident that spinning cell culture supernatants for long periods yielded a lower percentage of vesicles. Since spinning for 120 min was the standard in our lab, it was essential to revisit this parameter of our protocols as well. **Figure 3.5** represents the data from this experiment.

3.3.3.2 Optimisation of the Duration of Centrifugation Results in a higher yield of Microvesicles

Centrifugation maintained at 13,000 g for 90min resulted in higher EV counts although it was even significantly raised after 60min of centrifugation at 80.84% ($p=0.0001$) of the maximum yield obtained after 90 min. Spinning for 120mins resulted in an EV count 52.41 % ($p<0.0001$) lower than at 60 min and 56.11% ($p<0.0001$) lower compared to 90min. This further supported that centrifugation for prolonged durations lowers the yield obtained. Therefore, all EV isolations in this study were performed at 13,000 g for 60 min (**Figure 3.5**).

Effect of Centrifugation Time on the Isolation of PC3 cell-derived EMVs

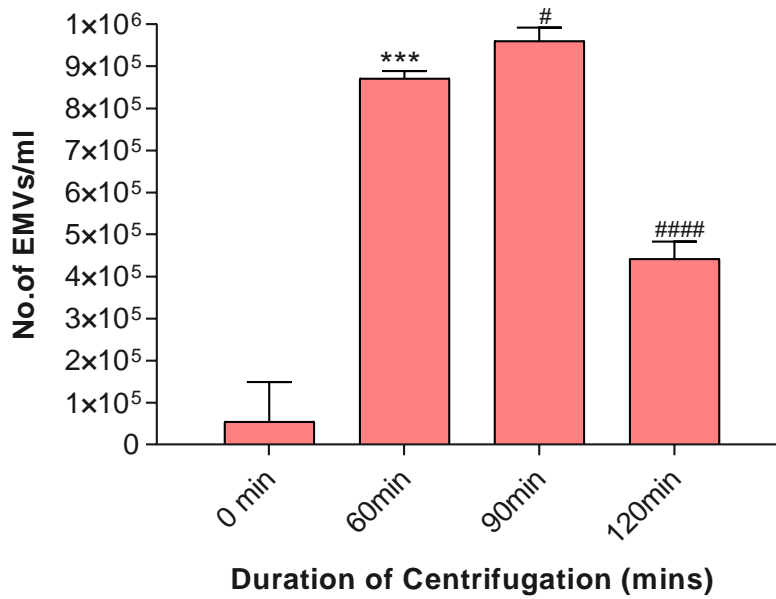
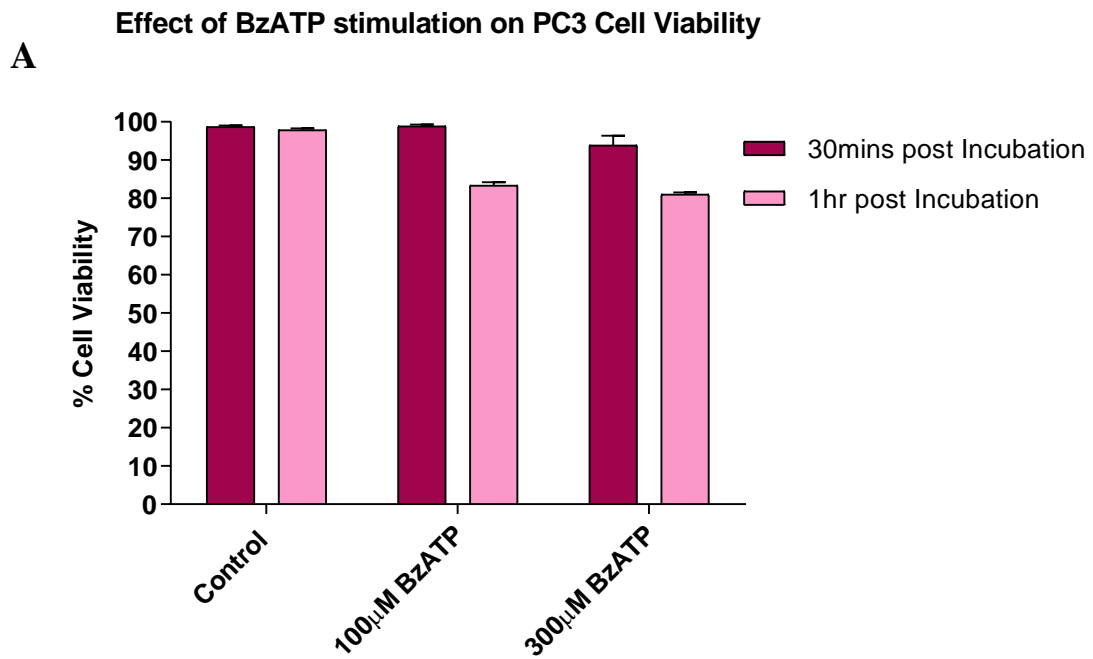


Figure 3.5 Centrifugation at 60min was considered to be ideal for EV isolation. The EV count was significantly higher at 90 min of centrifugation compared to 60 min ($p=0.0131$). Standard centrifugation duration of 120min resulted in a lower EVcount to that obtained at 60min ($p<0.0001$). * = significance to control (0 min) and # = significance compared to 60min. Experiments were carried out thrice and the data presented are mean \pm SEM of the results.

3.3.4 EV Inhibitors

3.3.4.1 Pharmacological Stimulation of EV release

Using an EV stimulator was deemed important to increase the release of EVs in order to be able to observe any inhibition of MV release. However, it was crucial to choose the optimum concentration of BzATP that should not directly affect the cell viability as it should not interact with the drug treatments in future cytotoxicity assays. It was evident that using 300 μ M for 30 min was ideal. From this work represented in **Figure 3.6A** it was clear that using 300 μ M of BzATP did not adversely affect the viability of PC3 cells, even after 1h incubation. Compared to untreated PC3 cells, the levels of released EVs increased in a dose-dependent manner. The EV count was 68.75% higher upon stimulation for 1h. Treatment with 100 μ M for 30 min was significantly higher than the untreated control by 74.07% ($p<0.0001$). However after treating with 300 μ M BzATP for 30min the EV count was 83.89% higher than the untreated control ($p<0.0001$) which was also 37.88% ($p<0.0001$) higher than for cells treated with 100 μ M (**Figure 3.6B**).



B Effect of BzATP stimulation on PC3-cell derived EMVs

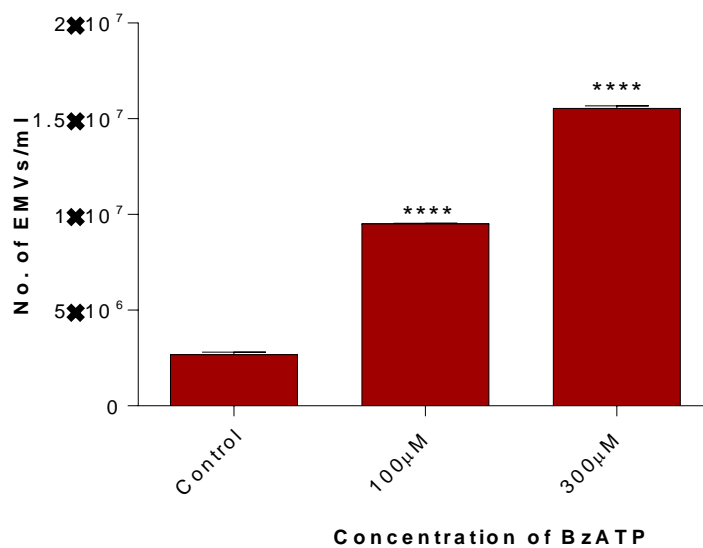


Figure 3.6 Stimulation of PC3 cells with 300 µM of BzATP for 30min increased microvesiculation. **A**, % Cell viability was reduced when the cells were treated with BzATP for 60 min as opposed to 30 min. Therefore 30min was considered to be the standard duration of stimulation. **B**, EV count was significantly higher (**** $p < 0.0001$) in the presence of 300 µM.

3.3.4.2 Cl-amidine and Bis-I are more potent inhibitors of EV release

Before testing pharmacological agents for their capacity to inhibit EV release, it was important to ensure that they did not in their own right adversely affect cell viability. To this aim, the ViaCount assay (using two DNA-binding dyes, one nuclear the other a viability dye) (**Figure 3.7A**) showed that the viability of cells in the presence of each reagent was 80% or above with the exception of pantethine which resulted in 25% viability. The presence of 50 μ M Chloramidine (Cl-am) and 10 μ M Bisindolylmaleimide-I (Bis-I) resulted in the maximal EV inhibition resulting in 95% and 96.2% reduction respectively (**Figure 3.7B**). However, all the reagents used resulted in a clear inhibition. This is suggestive of their involvement in different pathways of EV biogenesis that can be used as individually or in combination to develop strong EV inhibitors.

Nanosight results (**Figure 3.7 and 3.8**) further confirm the flow cytometry (FCM) results. The presence of 50 μ M Cl-am and 1mM Pantethine resulted in the maximal EV inhibition (98% and 99.2% respectively). However, all the reagents used resulted in a clear inhibition. This further suggests the importance of using them to improve the cytotoxic effect of drug treatment, in the case of cancer therapy.

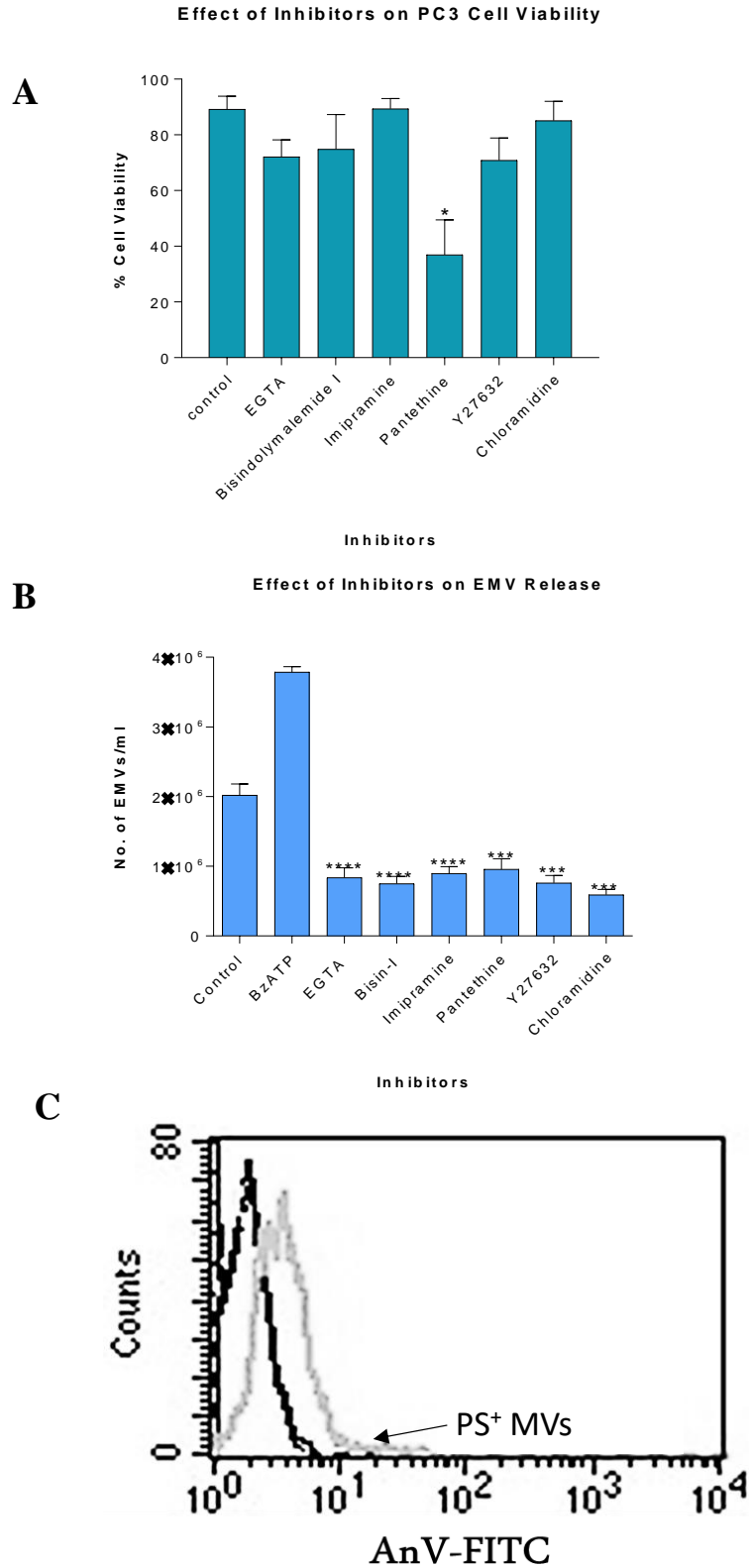


Figure 3.7 Bisindolylmaleimide-I and Chloramidine are more potent inhibitors of EVs. **A**, The viability assay clearly demonstrated that the reagents used in this experiment had no detrimental effect on the cell viability. **B**, The flow cytometry values obtained were compared to the control and a significant inhibitor of EV release (** $p < 0.001$, **** $p < 0.0001$) was seen with respect to all the reagents used in the experiment. **C**, Annexin V staining confirmed that the majority of vesicles identified and counted in the study were MVs.

3.3.4.3 D-Pantethine and Cl-amidine inhibit EV release most effectively compared to other candidate EV inhibitors

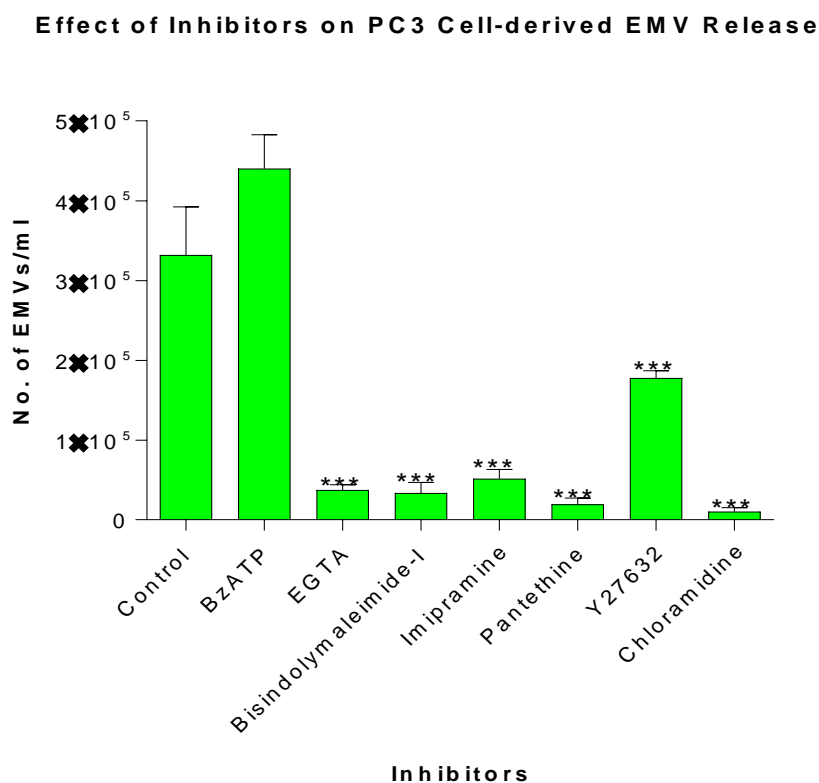
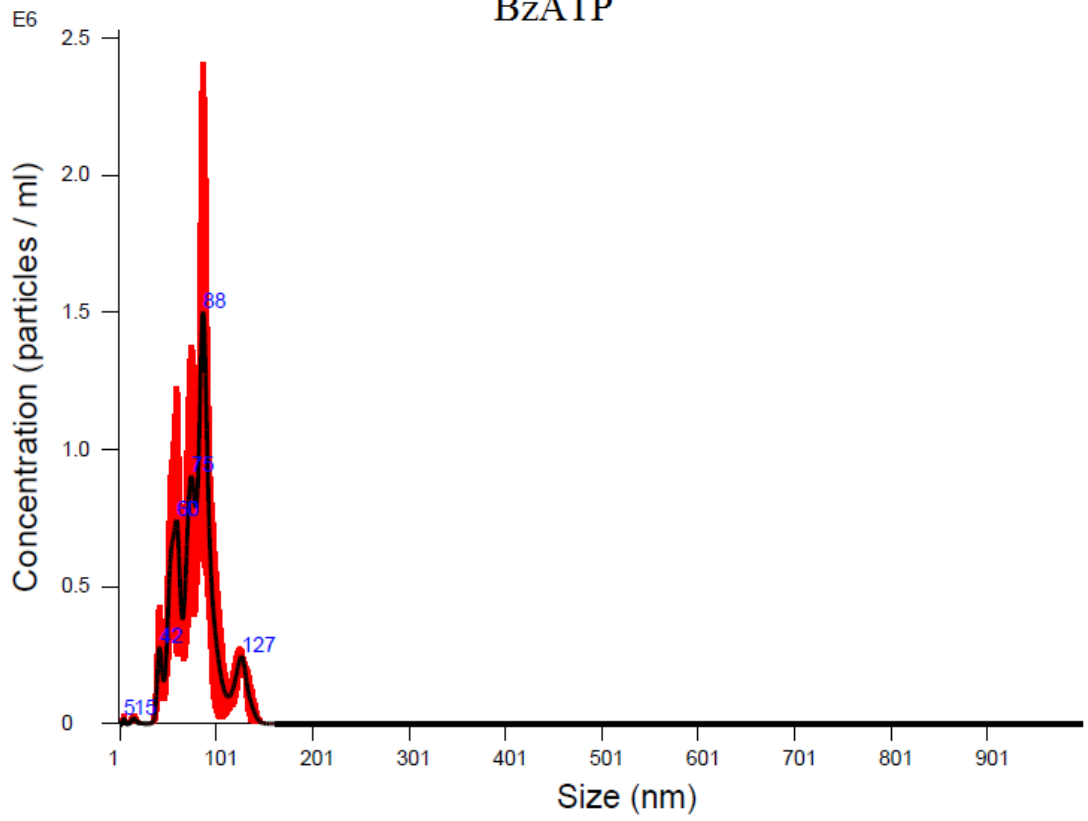
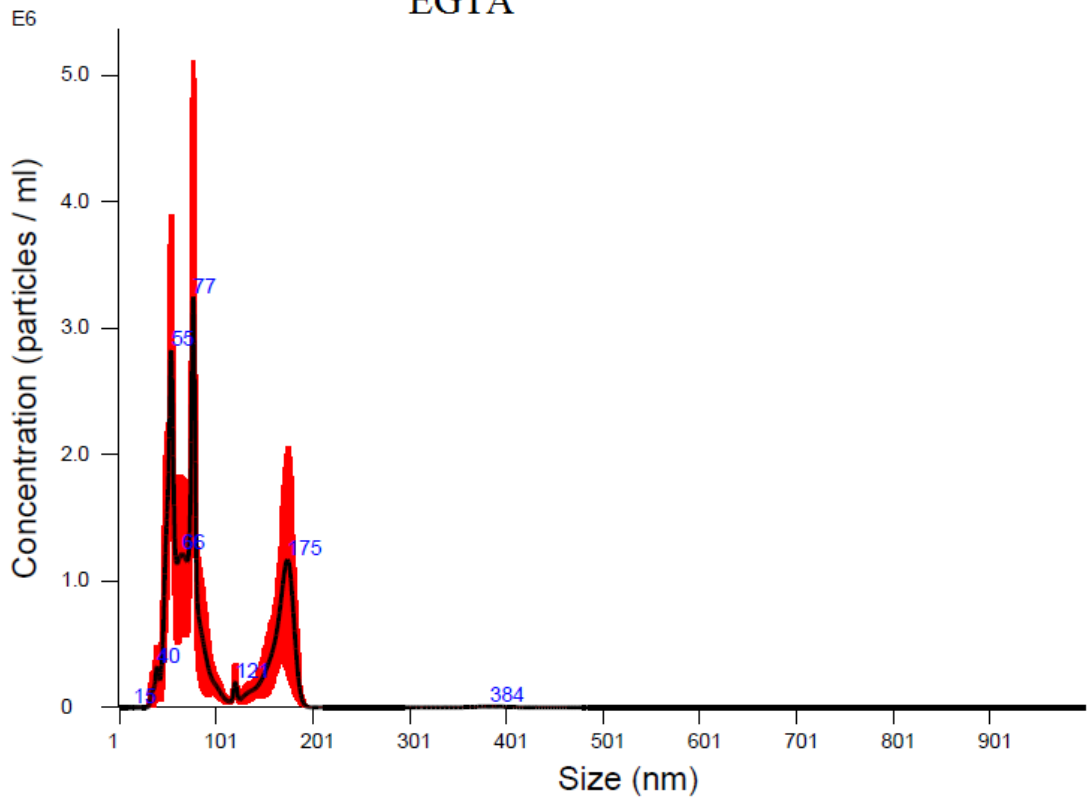


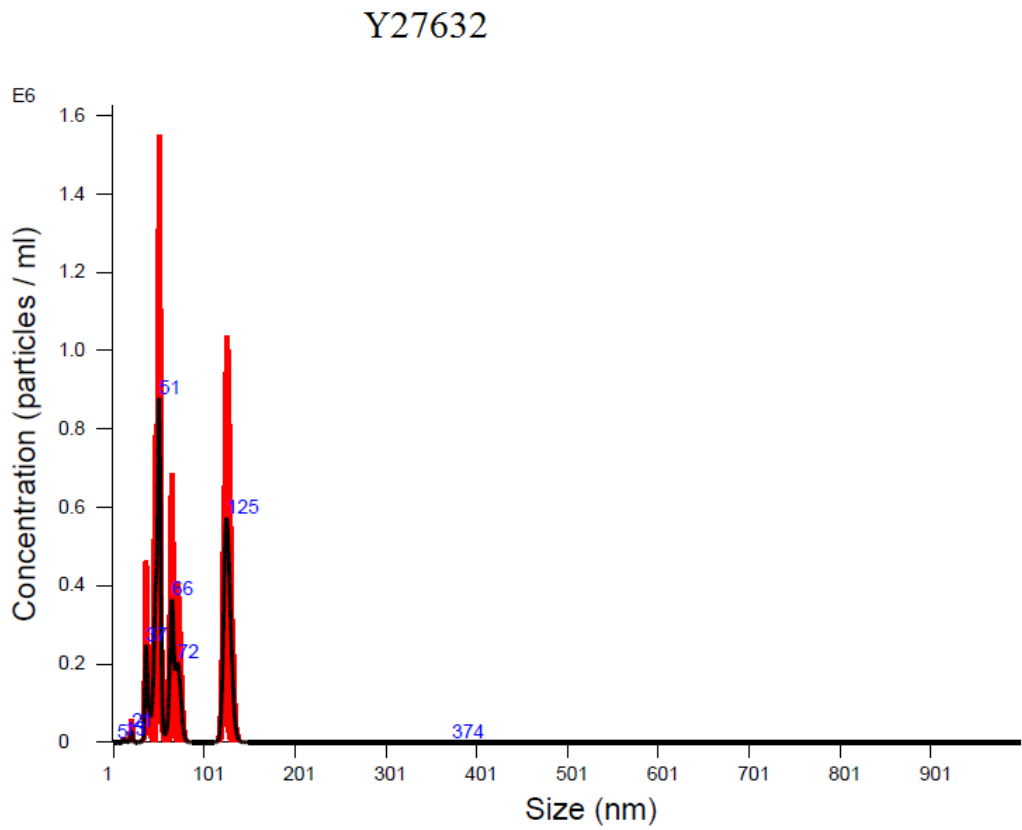
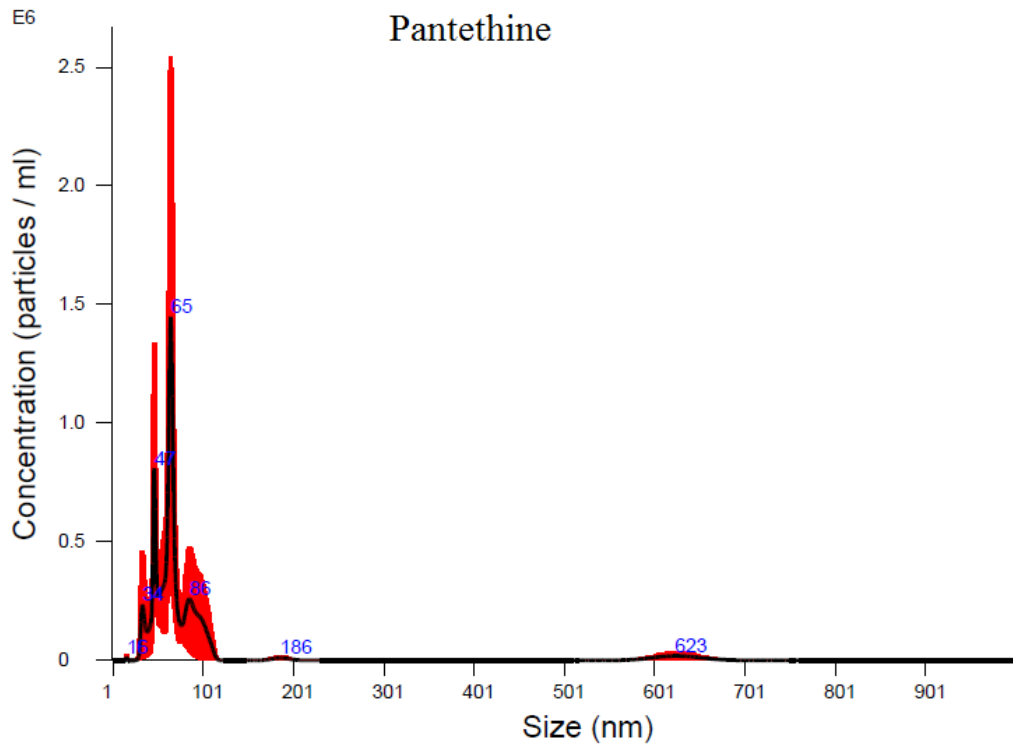
Figure 3.8 D-Pantethine and Cl-amidine are the most potent EV inhibitors. The concentration values of EVs released obtained by nanosight tracking analysis for D-Pantethine and Chloramidine were compared to the control and a significant inhibition of EV release (***) ($p < 0.001$) was seen with respect to all the reagents used in the experiment. There was however significant reduction in EV concentration in the presence of all other inhibitors used in the experiment. EGTA (34%) and Bisindolylmaleimide-I (3%) were less inhibiting than Chloramidine but was more potent compared to Y27632 by 88% ($p = 0.0009$). Y27632 reduced the EV concentration by 28% compared to the untreated control. The experiment was repeated three times and the data presented are mean \pm SEM of the results.

BzATP



EGTA





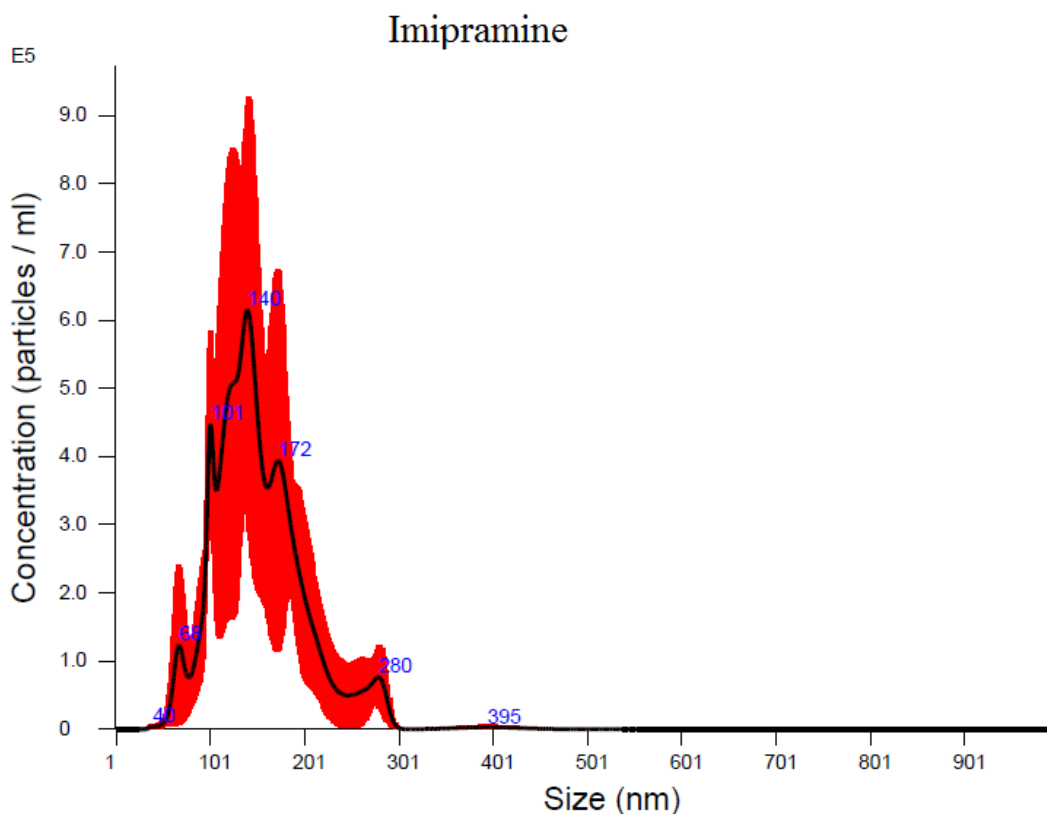
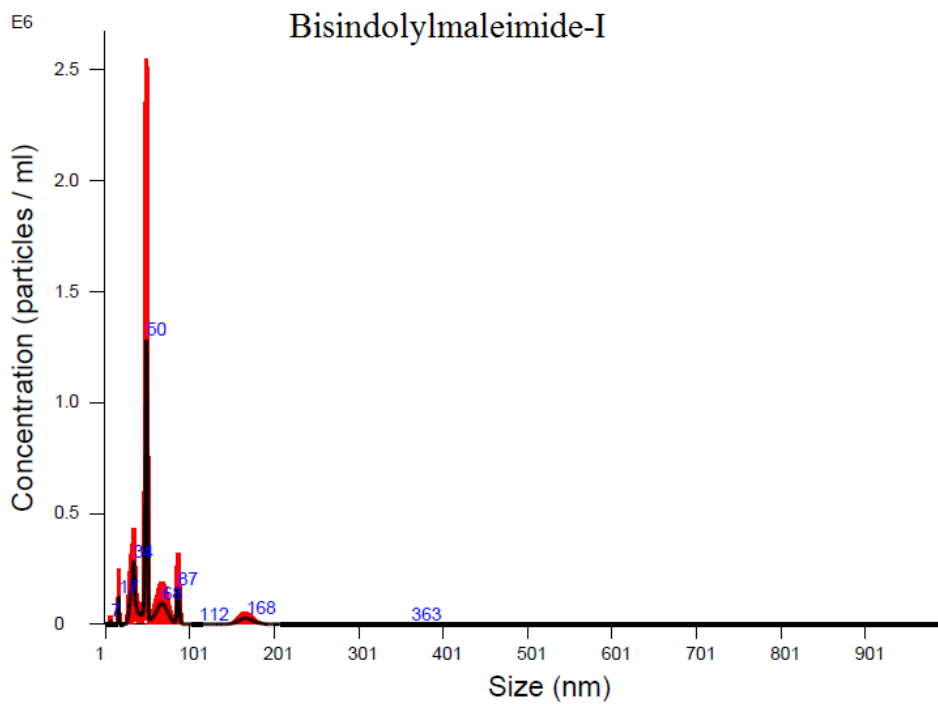


Figure 3.9 Nanosight tracking Analysis (NTA) plots of the reagents used. The concentration of the particles that ranged in size between 100 nm-500 nm was taken into account. The particles outside this size range were not included to avoid misrepresentation of results such as smaller particles corresponding to exosomes and larger particles to EV aggregates or apoptotic bodies.

3.3.4.4 Nicotine dose-dependently inhibits the release of EVs from PC3 cells

Previously at CMIRC a small clinical study of 39 volunteers (Grant et al., 2011), showed smokers to have significantly lower plasma EV levels than non-smokers. This was confirmed in another small study which also looked at changes in miRNA signatures (Badrnya et al., 2014). Following on it was found that nicotine could inhibit EV release from THP-1 pro-monocytic leukaemic cells significantly at concentrations of 50 and 100 μM .

Carrying on from the study, it was interesting to see whether the results obtained were reproducible. **Figures 3.10 and 3.11** summarise the results from the experiment. The EV protein concentration with respect to nicotine was calculated using the BCA assay (**Figures 3.10B and 3.10C**). EV inhibition was seen throughout the experiment in the presence of nicotine. The highest concentration of nicotine used in the study resulted in a 24.21% reduction in cell viability. Cells treated with 50 μM nicotine in the presence of BzATP strongly inhibited EV release by 63.79% ($p=0.0001$) compared to the control and 75.45% ($p<0.0001$) in the presence of BzATP alone. Since there was no significance in results between 25 μM and 100 μM , the lowest concentrations (25 μM and 50 μM) were used to treat the recipient cells in future apoptosis studies.

Nanosight Tracking Analysis of the nicotine experiment resulted in similar findings (**Figure 3.11A**). 10 μM to 75 μM caused significant EV inhibition when compared to both the untreated control and the EV stimulator. The least inhibition was in the presence of 10 μM with only 29.37 % reduction ($p<0.0001$) compared to control and 43.89 % ($p=0.0236$) compared to stimulation. Nicotine treatment at 75 μM resulted in the highest significant inhibition being 79.72 % ($p<0.0001$) compared to control and 83.89% ($p<0.0001$) compared to BzATP with no detrimental effect on cell viability (**Figures 3.11A and 3.11B**).

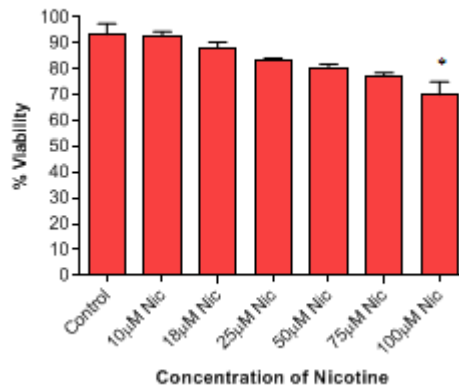
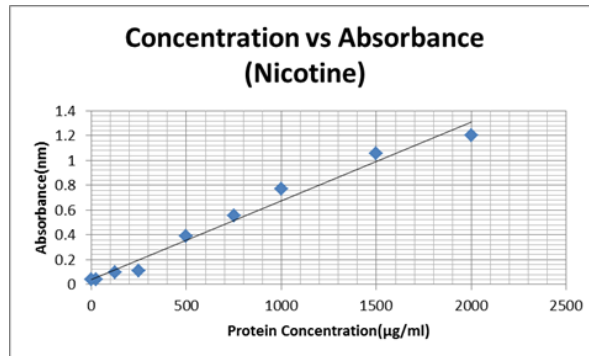
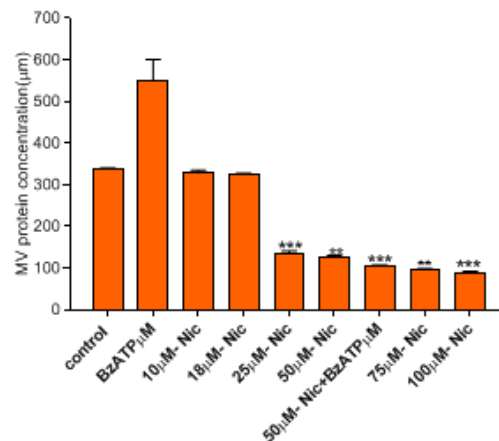
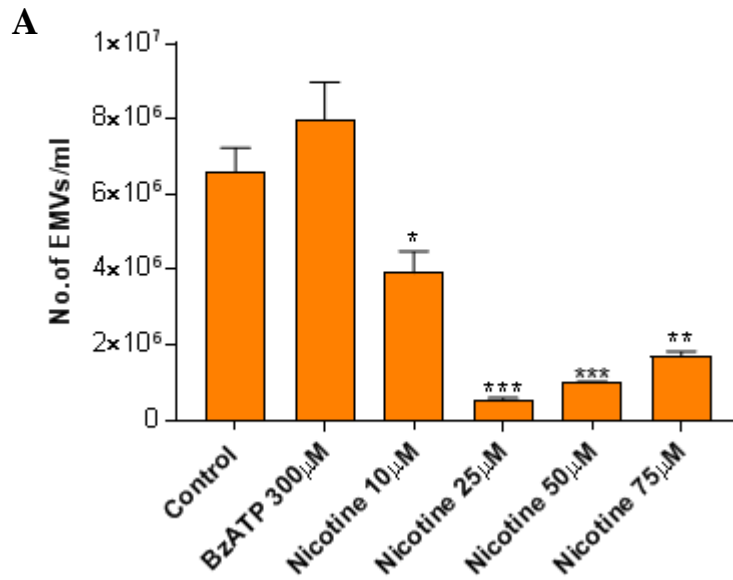
A**Viability of PC3 cells in the Presence of Nicotine****B****Concentration vs Absorbance (Nicotine)****C****Effect of Nicotine on EV Protein Content**

Figure 3.10 Nicotine is a strong EV inhibitor. A, Nicotine at lower concentrations doesn't affect the cell viability. B-C, EV stimulation was apparent in the presence of BzATP. 25µM to 100µM of nicotine portrayed significant inhibition of EV protein concentration. 100µM reduced the EV protein concentration by 78.60% which was significantly higher than using 50µM which only reduced by 54.98% ($p=0.0046$). Cells were at least 78% viable in the presence of all variables of Nicotine. The average of three independent experiments carried out in triplicates has been considered.

Effect of Nicotine on EV Inhibition



Effect of Nicotine on PC3 Cell Viability

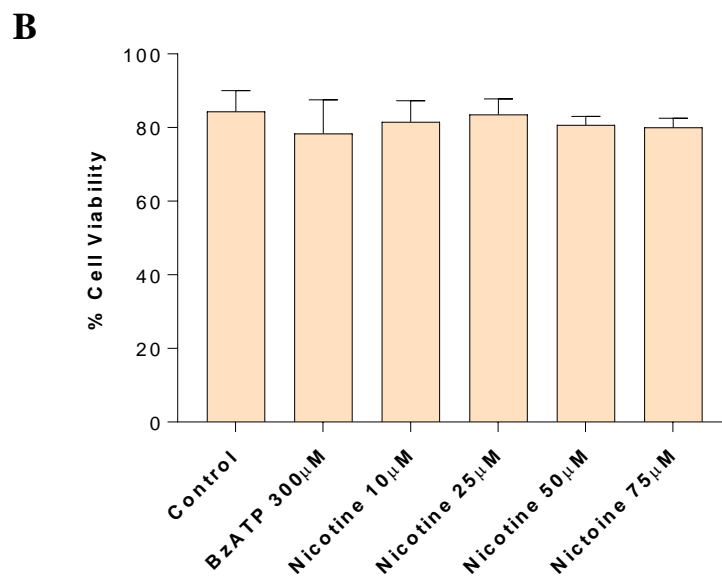


Figure 3.11 Effect of Nicotine on EV release.A, Nicotine demonstrates strong inhibitory activity against EV secretion. 10 µM, 25 µM and 75 µM showed significant inhibition ($p < 0.0001$). However, 25 µM resulted in the maximum inhibition of 91.6% ($p = 0.0007$). **B**, Nicotine doesn't seem to affect the healthy cells as it resulted in at least 80% viability.

3.4 Discussion

The doubling time of PC3 cells was shown to be 23.19h (**Figure 3.1**) which was useful to plan subsequent experiments involving apoptosis assays. The standard for EV isolation was established as 13,000 g for 1h (**Figures 3.4A, 3.4B and 3.5**). This resulted in a higher yield of less contaminated EVs. PC3 cells upon stimulation with 300 μ M of BzATP for 30min generated a high EV count which was apparent through flow cytometry and NTA results (**Figures 3.7 and 3.8**).

All the reagents used in the later stage of the experiment resulted in clear EV inhibition (**Figures 3.7, 3.8, and 3.9**). EGTA is a calcium chelator that mops up intracellular Ca^{2+} (Xiong et al., 2012) leading to a decrease in intracellular calcium concentration which prevents EV release. Activation of Protein Kinase C (PKC) allows the exposure of phosphatidylserine (PS) in the outer membrane driving EV release. Bis-I is a PKC inhibitor which prevents the activation and the externalisation of PS (Smith and Hoshi, 2011) thereby inhibiting the EV release. On activation of the ATP receptor P2X₇, EV shedding is associated with rapid activation of A-SMase which moves to the outer leaflet of the plasma membrane. Imipramine is an inhibitor of A-SMase thus inhibiting EV release. D-pantethine is a dimer of a pantothenic acid linked by a disulphide cystamine. It blocks the translocation of phosphatidylserine (El-Assaad et al., 2014). This non-externalisation of PS inhibits microvesiculation. It has been shown to reduce vesicle formation in mice infected with malaria compared to that of non-pantethine treated but interestingly there was no effect on vesicle formation in mice that were not infected with malaria (Watanabe et al., 2007). Y27632 inhibits Rho-associated, coiled-coil containing protein kinase (ROCK), which influences the redistribution of actin-cytoskeletal changes and regulates the apoptosis induced EV release (Li et al., 2012). Inhibition by Y27632 prevents the activation of Rho A which in turn abrogates EV biogenesis. PAD2 and PAD4 expression levels and the deimination of cytoskeletal actin are increased during microvesiculation (Kholia et al., 2015). Pharmacological inhibition of PAD enzyme activity using Cl-am significantly reduced EV release.

Cl-amidine, Bisindolylmaleimide-I and D-pantethine resulted in maximum inhibition of EV release as determined by flow cytometry and nanosight tracking analysis respectively (**Figures 3.7B and Figure 3.8**). However D-pantethine affected the cell viability which was confirmed to be 25% suggesting there can be a detrimental effect on neighbouring healthy prostate cells (**Figure 3.7A**). Although pantethine is unknown to have toxic effects (Brunetti et al., 2014), its high lipid solubility compared to other reagents used in the study could explain the low cell viability. There is an increased tendency to penetrate healthy cells and create an adverse effect. Similarly, the more potent inhibitors showed increased hydrophobic properties meaning that

they can easily penetrate the cell membrane compared to hydrophilic reagents (**Table 1**). Therefore the results were suggestive of potential use of both chloramidine and bisindolylmaleimide-I either individually or in conjunction to inhibit EV release in recipient cells to directly minimise drug efflux. The minimal effect on cell viability and the high rate of inhibition makes it more suitable for these reagents to be used either alongside the classic inhibitors or as novel EV inhibitors in future experiments.

Nicotine has been shown to reduce the EV count previously (Grant et al., 2011). Experiments presented in **3.2.3.4** were designed to establish the optimum concentration of nicotine that can be used on recipient cells to inhibit microvesiculation. The presence of 25 μM and 50 μM nicotine resulted in maximum inhibition (**Figure 3.9B and Figure 3.9C**) with minimal effect on cell viability (**Figure 3.9A**). This supports Grant et al. 2011's findings that 50 μM nicotine inhibits EV release (Grant et al., 2011). Opinions can be raised against this phenomenon as it is well known that cigarette smoke is carcinogenic developing lung cancer. Nicotine is known to be a promoter of cancer (Sanner and Grimsrud, 2015a) but other elements of tobacco increase the tumorigenicity of cigarette smoke. Nicotine content per cigarette on average is 1.2 mg; the smoker will absorb around 0.1 mg of nicotine from it which can increase addiction to cigarette smoke. The concentrations used in the study (25 μM = 0.0045 mg/ml and 50 μM = 0.0081 mg/ml) represent smaller quantities compared to the average nicotine content of a cigarette. Therefore it is arguable that the effect nicotine has on promoting metastasis under experimental settings is minimal compared to the inhalation of a high quantity of nicotine. Nanosight enumeration of EVs released further proves that nicotine is a strong EV inhibitor.

Also, there has been research carried out to understand the effect of nicotine on cell viability. A study conducted by Silva and colleagues compared the effect of cigarette smoke condensate and nicotine on cell viability in gingival wound healing. Here, the results clearly state that nicotine does not alter the cell viability in gingival mesenchymal cells (Silva et al. 2012). In contrast, another group reported that nicotine did affect the cell growth and migration of cementoblasts. It further clarified that nicotine induced inflammatory cytokines and ROS by cementoblasts (Chen et al. 2015). Therefore, there are mixed thoughts on the effect of cell viability. However, our findings have clearly shown that although it is not detrimental, using nicotine can affect the cell viability. There was a progressive decrease in cell viability with the use of different concentrations of nicotine which plateaued around 80%. The nicotine used in the experiment had 99.7% purity according to the manufacturer's data sheet. Treatment of recipient cancer cells with nicotine at desired concentrations may directly retain the cancer drug within the intracellular environment effectively targeting cancer cell apoptosis. Therefore, further research on its use is strongly encouraged in prostate cancer apoptosis studies.

Chapter 4: Effect of Inhibiting Extracellular Vesicle Release on Chemotherapeutic Drug-Induced Apoptosis

4.0 Effect of Inhibiting Extracellular Vesicle Release on Chemotherapeutic Drug-induced Apoptosis

4.1 Introduction

Reagents which were analysed and evaluated as potential EV inhibitors in the previous chapter were utilised herein to investigate their role in enhancing drug efficacy. Apoptosis studies in the presence of a single inhibitor were performed initially, and carrying on, the effect of combination therapy with inhibitors was analysed. In both studies, Bis-I, Nicotine and Chloramidine were used as the EV inhibitors. The aim of the experiments was to detect the influence of EV inhibitors on the activity of the anti-cancer drug, 5-FU and Doxorubicin (Dox) in targeting prostate cancer cells and breast cancer.

Apoptosis was analysed using the NucleoCounter® NC-3000™ (Chemometec) and different assays (Annexin V and VB-48 vitality) were utilised. The initial stages of the study were performed by direct addition of the 5-FU into cells that were either pre-treated with inhibitor/inhibitors or not. However the later phase of the chapter moves away from this direct addition of the anti-cancer drug towards the treatment of cells with EVs carrying the drug. This was performed again with or without the pre-treatment of cells with Bis-I and the apoptosis was determined using an Annexin V and VB-48 vitality assay for externalisation of PS.

The apoptosis of DOX-treated cells was analysed using Flow cytometry (Annexin V and mitochondrial membrane potential assay), fluorescent microscopy, fluorescent spectrophotometry and HPLC. Cl-amidine, a pan-PAD inhibitor was used in this study to examine its effect of EV inhibition and PC3 sensitisation to DOX.

4.2 Methods

4.2.1 Effect of Nicotine on drug Induced Apoptosis in PC3 Cells

The cells were maintained as before and were seeded in triplicate at 3.8×10^5 cells/well in a 12-well microtitre plate with pre-warmed RPMI 1640. They were pre-treated with 25 μ M and 50 μ M nicotine for 24 h and 1 μ M 5-FU then being added or just treated with 1 μ M 5-FU as shown in **(Figure 4.1)**. The control well was not treated with either nicotine or 5-FU. It was then incubated for 72 h at 37°C in 5% CO₂. After 24, 48 and 72 h, upon addition of chemotherapeutic drug, a VB48 Vitality assay was performed using the NucleoCounter® NC-3000™ (Chemometec).

4.2.2 Effect of combinatory EV inhibition with Nicotine and Cl-amidine on 5-FU treated MCF-7 cells

In order to confirm that nicotine acts as a pan-inhibitor of EVs, a similar experiment was carried out on MCF-7 cells. The adherent cells were maintained as before, seeded in triplicate at 3.8

$\times 10^5$ cells/well in a 12-well microtitre plate with pre-warmed RPMI 1640. They were either pre-treated with 25 μ M and 50 μ M nicotine and 50 μ M chloramidine for 24 h and 1 μ M 5-FU then added or just treated with 1 μ M 5-FU as shown in **(Figure 4.3)**. The control well was not treated with either of the inhibitors or 5-FU. It was then incubated for 72 h at 37°C in 5% CO₂. After 24, 48 and 72 h, upon addition of chemotherapeutic drug, a VB48 Vitality assay was performed using the NucleoCounter® NC-3000™ (Chemometec).

4.2.3 Effect of synergistic EV inhibition with Bisindolylmaleimide-I and Cl-amidine on PC3 cell apoptosis

The synergistic effect of two or more EV inhibitors can increase the anti-cancer drug efficacy. A combination of 10 μ M Bis-I and 50 μ M Chloramidine was used to test the hypothesis. PC3 cells were maintained as before and seeded in triplicate at 3.8×10^5 cells/well in a 12-well microtitre plate with pre-warmed RPMI 1640. They were either pre-treated with 10 μ M, 50 μ M chloramidine or the combination of inhibitors for 24 h and 1 μ M 5-FU was added (or the cells were just treated with 1 μ M 5-FU-EVs as shown in **Figure 4.5**). The control well was not treated with either of the inhibitors or 5-FU. It was then incubated for 72 h at 37°C in 5% CO₂. After 24, 48 and 72 h, upon addition of chemotherapeutic drug, a VB48 Vitality assay was performed using the NucleoCounter® NC-3000™ (Chemometec).

4.2.3.1 Apoptosis study using Bisindolylmaleimide-I and 5-FU

PC3 cells were maintained as described in 2.4.1. Cells were seeded in triplicate at 3.8×10^5 cells/well in a 12-well microtitre plate in the presence of 1.5 ml of RPMI 1640/well. The cells were treated with different concentrations of 5-FU as shown in **Figure 4.7A**. The remaining wells were pre-treated with Bis-I and one set was washed after 24 h of pre-treatment and the other set left unwashed. The cells were then treated with 1 μ M of 5-FU. EVs were isolated after 24 h post treatment as described in **section 2.5.1**. EV concentration was determined using a BCA assay as described in **section 2.5.4** to ascertain the EV protein content. The control well had cells that were neither pre-treated with Bis-I nor with 5-FU. The experiment was repeated thrice and the average of the results was plotted using GraphPadPrism 7.0 (**Figure 4.7A and B**).

4.2.3.2 Preparing 5-FU-EVs

A T75 flask of PC3 cells was maintained with RPMI 1640 for 24 h. The cells were then washed and 1 μ M 5-FU added and incubated for a further 24 h. EVs were isolated according to the protocol described in **section 2.5.1** and EV proteins were quantified using a BCA assay (**section 2.5.4**).

4.2.3.3 Effect of Bisin-I activity on PC3 Cell Survival

A second set of cells was maintained as before and seeded in triplicate at 3.8×10^5 cells/well in a 12-well microtitre plate in the presence of 1.5 ml of RPMI 1640/well. Two of the experiment subjects were pre-treated with Bis-I for 24 h and 1 μ M 5-FU bearing EVs isolated previously were added with/without washing. After 24, 48 and 72 h upon addition of drug EVs, an Annexin V apoptosis assay was performed using the NucleoCounter® NC-3000™ (Chemometec). The average of two experiments was used to graphically illustrate the results.

4.2.4 Effect of Chloramidine activity on DOX treated PC3 cells

4.2.4.1 Identification of the optimum DOX concentration

A range of DOX concentrations were tested to determine the effect on cell viability. PC3 cells were grown at a concentration of 3.8×10^5 cells/well in a 12-well microtitre plate for 24 h. The cells were washed twice with PBS and a mitochondrial membrane potential assay was performed according to manufacturer's instructions (JC-1 - Mitochondrial Membrane Potential Assay Kit [ab113850]). The cells were subjected to flow cytometry analysis at the end of the incubation time and the results recorded as illustrated in **Figures 4.10 and 4.11**).

4.2.4.2 Annexin V assay of PC3-EVs and encapsulation of DOX in EVs

EVs were isolated from PC3 cells as stated (**section 2.5.1**) and quantified using a nanosight LM10 (**section 2.8**). An Annexin V assay was performed as described earlier (**section 2.5.2**). DOX encapsulation of EVs was performed as previously described (**section 4.2.4.2**). EVs were treated with 5 μ g/ml DOX for 24 h at 37°C and analysed using a Guava flow cytometer. The results are summarised in **Figure 4.12**.

4.2.4.3 Effect of Cl-amidine on EV release in PC3 cells

PC3 cells were maintained for 24 h as before and seeded in triplicate at 3.8×10^5 cells/well in a 12-well microtitre plate with pre-warmed RPMI 1640. The cells were incubated for 24 h and washed with DPBS post-incubation. Cells were treated with either 50 μ M Cl-am, 5 μ M DOX, 50 μ M Cl-amidine and 5 μ M DOX or left untreated (**Figure 4.13**). The cells were then incubated for 1h at 37°C. The EVs were isolated from the supernatant post-incubation according to protocol in **section 2.5.1** and quantified using the nanosight LM10 (**section 2.8**).

4.2.4.4 Fluorescent Microscopy Analysis of DOX transfer via PC3-EVs

PC3 cells were maintained as mentioned before. The cells were washed and incubated in two T25 flasks at a density of 5×10^6 cells/flask for 24 h at 37°C. Cells were washed with DPBS at the end of the incubation period. One flask was treated with 50 μ M Cl-am for 1h at 37°C. At the

end of the second incubation, equal numbers of pre-prepared DOX-EVs were added to both flasks and incubated at 37°C for 4h and 24h respectively. The proportion of DOX stained cells were quantified using fluorescent microscopy as described in **section 2.9**, the data for which is presented in **Figure 4.14**.

4.2.4.5 HPLC analysis of DOX internalisation in PC3

PC3 cells were grown in three T75 flasks at a density of 8×10^6 cells/flask for 24h. The cells were washed with DPBS. One flask was pre-treated with Cl-am for 1h. The cells were washed at the end of the incubation. This flask together with another was treated with 50 µg/ml DOX, while the remaining flask was left untreated. The cells were incubated for 24 h at 37°C. The supernatants were collected from all 3 flasks and EVs were isolated as described elsewhere (**section 2.5.1**). Both cell and EV extractions were prepared by treating with 1× RIPA buffer for 15 min. Proteins were then precipitated with 400 µl of acetonitrile (ACN), followed by centrifugation at 3000 rpm using Lab med centrifuge at room temperature for 15 min. The supernatant was filtered through a 0.45 µm filter. Proteins were quantified as before (**section 2.5.5**).

Dionex D3 was used as the HPLC system consisting of a pump with a column from Merck C18 (4.6 mm × 100 mm). A UV-detector with data processor (Chromeleon software) was used to produce specific high resolution chromatographs of the drug. UV detection for Doxorubicin was set at 232 nm. The mobile phase of water: acetonitrile (30:70, pH 3.0, adjusted with 85 % phosphoric acid) was delivered at a flow rate of 1.0 ml/min and ambient temperature. The mobile phase was delivered by gradient method at ACN gradient of 15 % at 0 min, 25 % at 5 min, 40 % at 10 min, 70 % at 15 min and 100 % at 20 min. Peak identity was confirmed by retention time (RT) of DOX at 2.4-2.6 min.

The standard stock solution of DOX (1.0mg/mL) was prepared in acetonitrile. The working standard solution (10 µg/ml) was prepared by diluting the stock solution in the mobile phase (30:70, ACN: water) with ph adjusted to 3.0. A serial calibration line of sample concentrations of 1, 2.5, 5, 12.5, 25, 50 µg/ml of DOX was prepared by diluting definite aliquots of working standard mobile phase. The results obtained were as shown in **Figure 4.15 and 4.16**.

4.2.4.6 Fluorescence Spectrometry analysis of the effect of EV inhibition on Sensitisation to Chemotherapy

PC3 cells were prepared as described in **section 4.2.5.3**. One set of cells was pre-treated with 50 µM Cl-am for 1h at 37°C and the other left untreated. Both sets of cells were then treated with 5 µg/ml of DOX for 24 h and EVs were isolated post-incubation. The cells and EVs were

subjected to absorption spectrum analysis at 480nm and fluorescence intensity analysis at 485-590nm. The results are summarised in **Figure 4.17 and 4.18**.

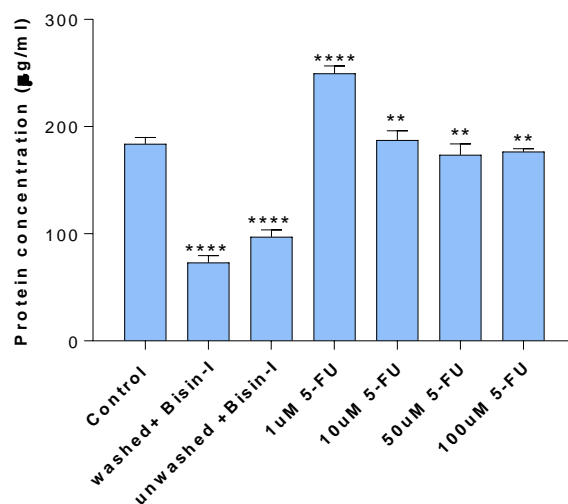
4.3 Results

4.3.1 Bisindolylmaleimide- I Augments 5-FU Efficacy against PC3 Cells

A range of different concentrations of Bis-I and 5-FU on the cell viability and EV protein analysis were tested. Protein concentration upon pre-treatment with Bis-I was lowered by 62.19% ($p=0.0093$) under washed conditions and by 52.39% ($p=0.0052$) without washing following treatment with Bis-I. This reduction in protein concentration was not only significant compared to the control but significant compared to treatment with 1 μ M 5-FU alone, which was reduced by 72.72% ($p<0.0001$) in washed and by 64.28% ($p=0.0018$) in unwashed conditions. 5-FU treatment was carried out only for 1h. This further justifies that Bis-I abrogates EV release (**Figure 4.1A**). However, washing cells after pre-treatment with the inhibitor reduced the death cell count by 11.43% compared to unwashed conditions (**Figure 4.1B**). Using high concentration of the drug was not encouraging therefore 1 μ M was used as the optimum 5-FU concentration in future experiments.

Effect of different concentrations of 5-FU on EMV Protein analysis

A



Effect of different concentrations of 5-FU on Cell Viability

B

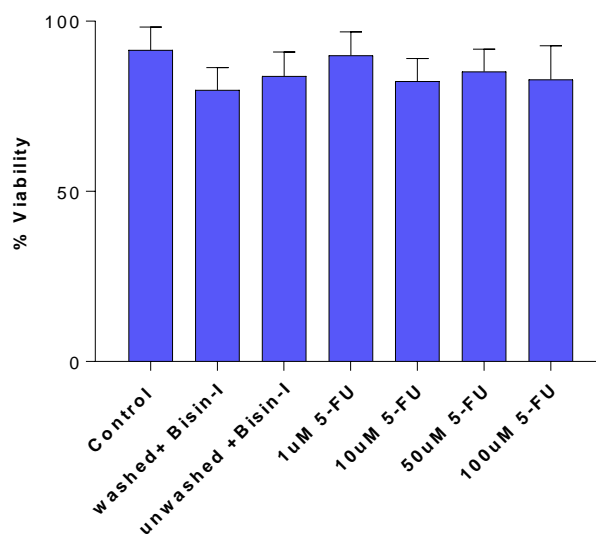


Figure 4.1 1µM of 5-FU was the optimum concentration for Apoptosis Assays. **A**, The optimum concentration of 5-FU to be used for the experiments was 1µM where protein concentration was significantly higher compared to 10µM by 19.42% ($p=0.0594$), to 50µM by 37.19% ($p=0.0124$) and to 100µM by 26.03% ($p=0.0068$). 5-FU alone increased the protein concentration by 26.8% ($p=0.0283$) compared to the untreated control. There was a prominent reduction of protein concentration in the presence of bisindolylmaleimide-I. Although not significant, protein concentration was reduced by 21.43% when cells were washed following Bisindolylmaleimide-I treatment compared to the unwashed condition ($p=0.0619$). Protein concentration after washing was however significantly reduced compared to 5-FU treatment alone by 72.72% ($p<0.0001$) and by 62.71% ($p=0.0093$) to the untreated control. **B**, There was no detrimental effect on cell viability following treatment with 5-FU and Bisindolymaleimide-I.

4.3.2 Nicotine increases Anti-tumour Drug Effectiveness

The effect of different concentrations of Nicotine was examined. Both 25 μM and 50 μM nicotine treated cells indicated that inhibition of EVs increases the drug efficacy compared to treatment with anti-cancer drug (even not in combination) (**Figure 4.2**). There was a reduction of viable cells by 37.56% ($p=0.0001$) on day 1 in the presence of 25 μM which was further reduced by 47.31% ($p<0.0001$) compared to 5-FU treatment by day 3. Similarly, pre-treatment with 50 μM reached the maximum apoptosis of 30.13 % ($p<0.0001$) compared to sole 5-FU treatment. The trend in the results was maintained throughout the 72 h duration but the cell viability on day 3 was lower even in the control sample by 38.09% ($p<0.0001$) suggesting that natural cell death occurs after few days.

Presence of 25 μM nicotine with 1 μM 5-FU resulted in the maximum PI (+ve) dead cells compared to the untreated both 2 4h and 72 h post incubation. However, pre-treatment of cells with both 25 μM and 50 μM showed a significant increase in apoptosis compared to untreated, even in the presence of the drug ($p<0.0001$) (**Figure 4.3**).

Apoptosis of PC3 cells in the presence of Nicotine + 5-FU

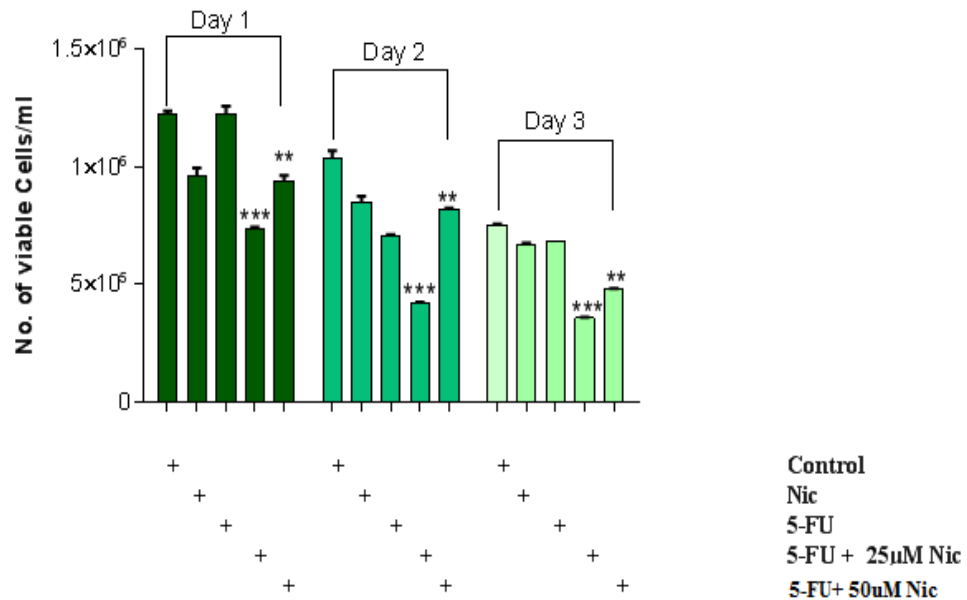
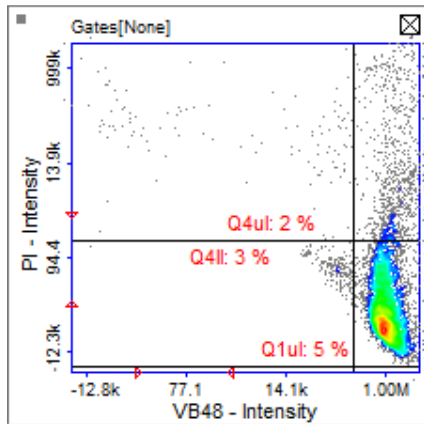


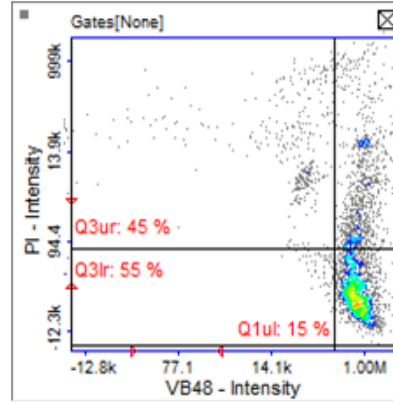
Figure 4.2 Pre-treatment with 25µM nicotine increased 5-FU effect on PC3. % Cell viability was lowest in the presence of 25 µM nicotine. There was 45% decrease in cell viability between day 1 and day 2 in the presence of 25µM ($p=0.0302$). This was only less than 12% by day 3 ($p=0.0445$). However, effect of 50µM treatment was more prominent between day 2 and day 3. The apoptosis was increased by 41.6% ($p<0.0001$) compared to day 1 and day 2 which was only 16.61% ($p=0.0087$). These results suggest that 50µM pre-treatment might be more effective in apoptosis studies carried out for longer periods. However, both conditions of nicotine pre-treatment increased the sensitisation of PC3 cells to 5-FU from day 1. This was less sensitive in the presence of 50µM by 24.72% compared to the presence of 25µM nicotine even on day 1. Data presented are mean \pm SEM of three independent experiments performed in triplicate. *** $p<0.007$; ** $p<0.01$; were considered statistically significant compared to the control.

A: Control

24h post-treatment

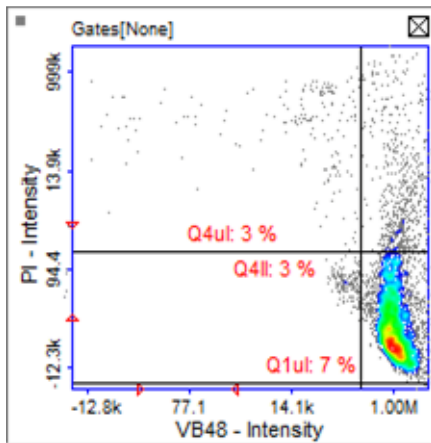


72h post-treatment

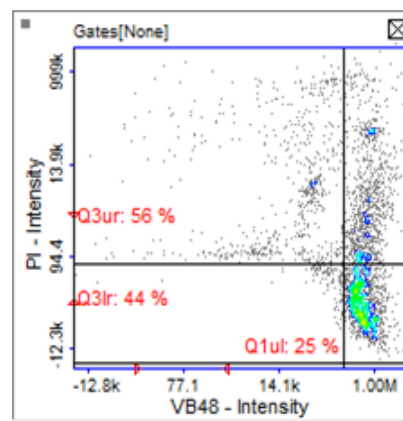


B: Nicotine

24h post-treatment

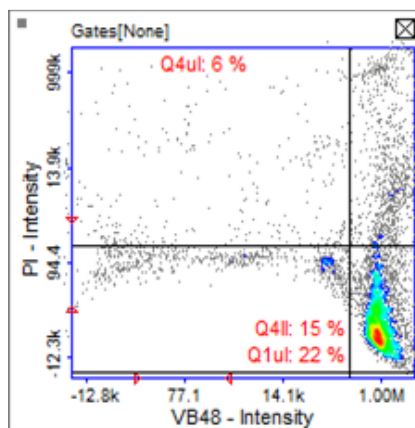


72h post-treatment

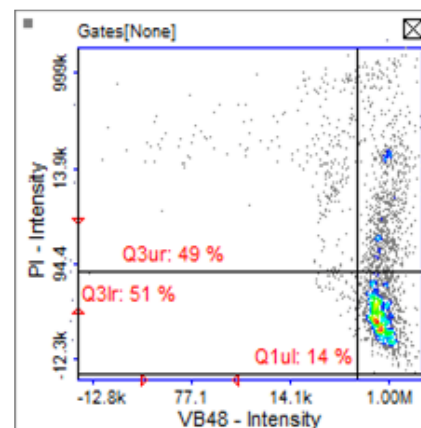


C: 5-FU

24h post-treatment

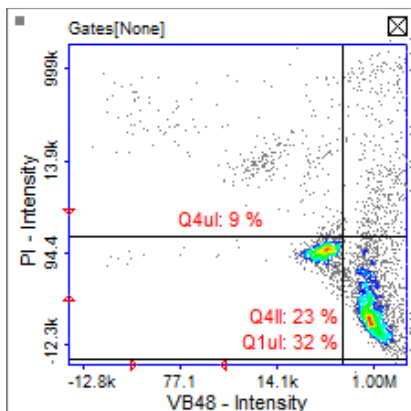


72h post-treatment

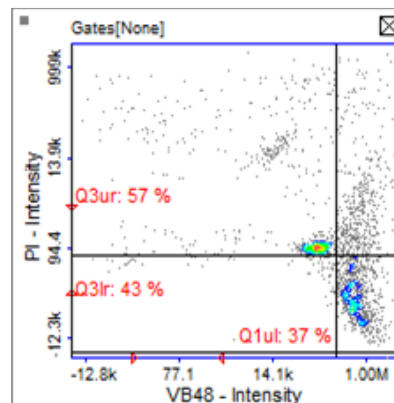


D: 25 μ M Nicotine + 5-FU

24h post-treatment

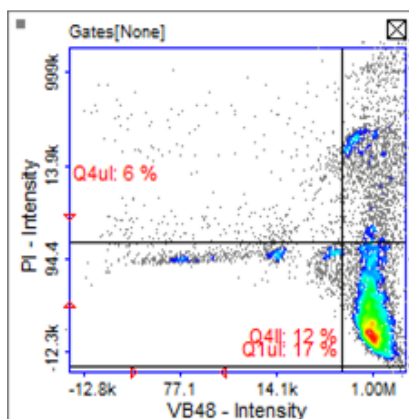


72h post-treatment



E: 50 μ M Nicotine + 5-FU

24h post-treatment



72h post-treatment

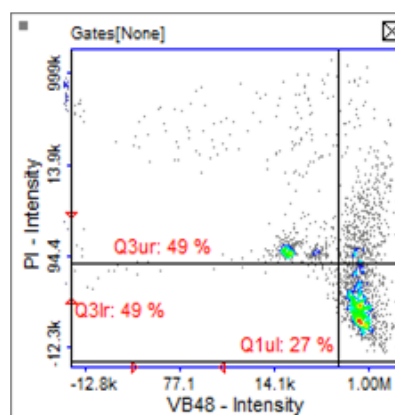


Figure 4.3 Multiplex assays demonstrating VitaBright-48™ staining following Nicotine pre-treatment. PC3 cells were treated with 25 and 50 μ M Nicotine and 1 μ M 5-FU as shown in A-E. The cells were treated with nicotine and 5-FU for 24h. Cells were stained with VB-48™, Acridine Orange (AO) and Propidium Iodide (PI) and analysed using the Vitality Assay and a NucleoCounter® NC-3000™. Scatter plots and histograms were obtained from the NucleoView™ NC-3000™ software. Polygons and markers in the displayed plots were used to separate the various cell populations. Plots show VitaBright-48™ intensity versus PI intensity. Nonviable cells were gated out based on propidium iodide uptake. Plots show VitaBright-48™ intensity versus PI intensity. Nonviable cells were gated out based on SYTOX green uptake. 25 μ M was 24.72% more effective resulting in less VB-48+ve cells compared to 50 μ M pre-treatment even on day 1 ($p=0.0013$). However, both 25 μ M and 50 μ M Nicotine treatment increased 5-FU sensitivity of the cells at least by 20% ($p=0.0001$ and $p=0.0023$).

4.3.3 Synergistic Effect of Inhibitors Promotes Cumulative Apoptosis in MCF7 Cells

A combined use of inhibitors was deemed the most potent way of enhancing the apoptotic potential of 5-FU on MCF7 cells. Both Cl-amidine and nicotine inhibited EV release. Cl-amidine pretreatment reduced the cell viability by 89.21% ($p<0.0001$) compared to 5-FU alone. However pre-treatment with 50 μ M nicotine was less inhibiting than 25 μ M by 10.97%, even on day 1. Apoptosis with 25 μ M was however significantly higher compared to 5-FU alone which was 64.71% ($p<0.0001$) but reduced by 69.43% ($p<0.0001$) compared to Cl-am pre-treatment on day 1. This was however further reduced to 51.08% ($p=0.0010$) by day 3. Combination pre-treatment resulted in the maximum apoptosis throughout the study which was 90.11% ($p<0.0001$) on day 1 and 95.83% ($p<0.0001$) on day 3 compared to 5-FU alone (**Figure 4.4 and 4.5**). The results indicate the synergistic effect of the EV inhibitors in minimising the drug efflux therefore increasing their bioavailability. EV results suggest that the effect of nicotine is not limited to prostate cancer cells but apparent even in other cell lines which together with the data presented in **Figure 3.10B** suggest that it could be used as an EV inhibitor that improves chemotherapeutic efficacy. The trend in the results was maintained throughout the 72-h duration. With the cell viability on day 3 being lowered by 49.18% ($p<0.0001$) even in the absence of inhibitors and the drug, this suggested that natural cell death occurred after a few days.

Apoptosis of MCF-7 cells in the presence of Nicotine + Chloramidine + 5-FU

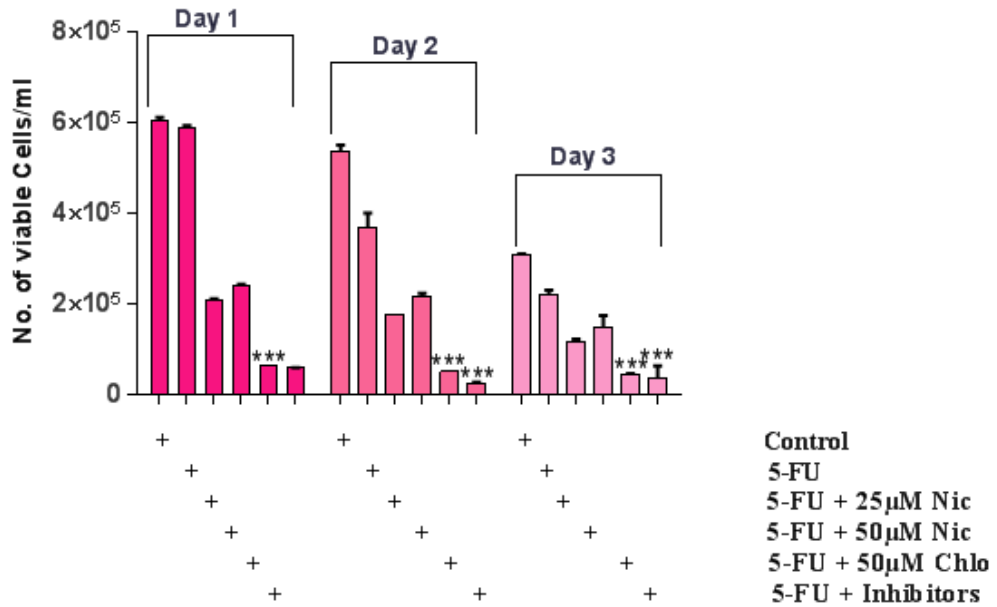
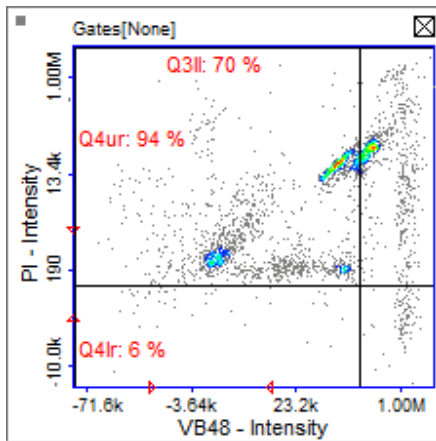


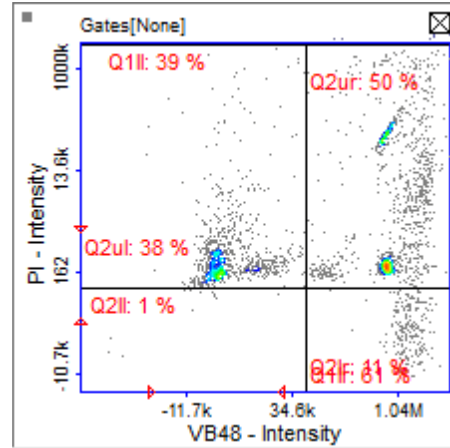
Figure 4.4 Combination of EVinhibitors causes 5-FU retaining ability and causes cumulative apoptosis in MCF7. % Cell viability was significantly lower in the presence of the inhibitors. Pre-treatment with Cl-am and 50µM Nicotine together resulted in the maximum apoptosis throughout the study, 90.11% ($p < 0.0001$) on day 1 and 95.83% ($p < 0.0001$) on day 3 compared to 5-FU alone. The natural cell death occurred by day 3 which was reduced by 49.18% in the absence of drug and inhibitors. Chloramidine alone was more potent than even the most sensitive, 25µM nicotine pre-treatment by 69.43% ($p < 0.0001$) even on day 1 suggesting that Chloramidine is more potent as an inhibitor compared to nicotine. Data presented are mean \pm SEM of three independent experiments performed in triplicate.

A: 25 μ M Nicotine + 5-FU

24h post-treatment

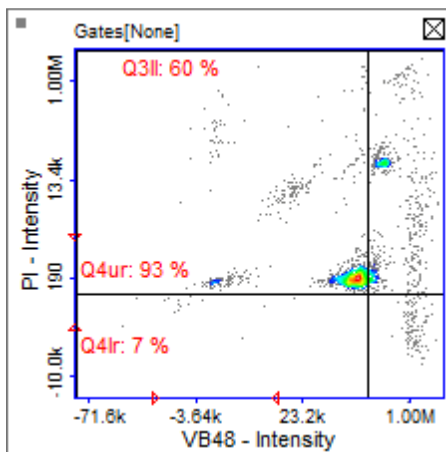


72h post-treatment

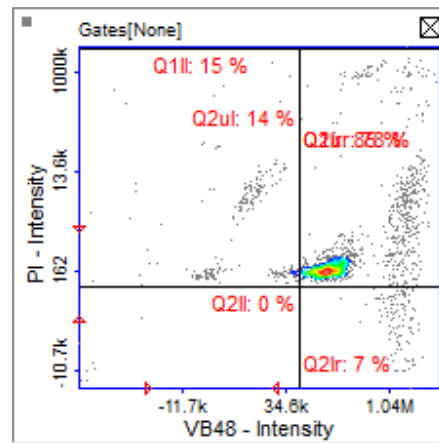


B: 50 μ M Nicotine + 5-FU

24h post-treatment

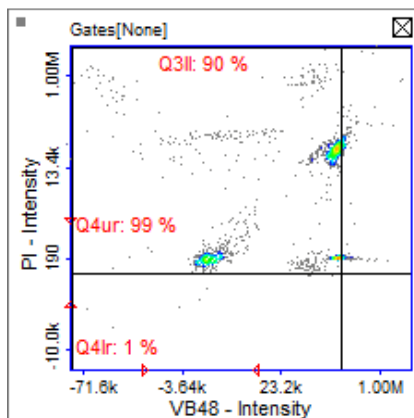


72h post-treatment

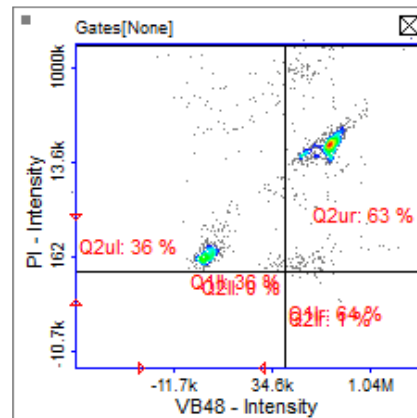


C: 50 μ M Chloramidine + 5-FU

24h post-treatment

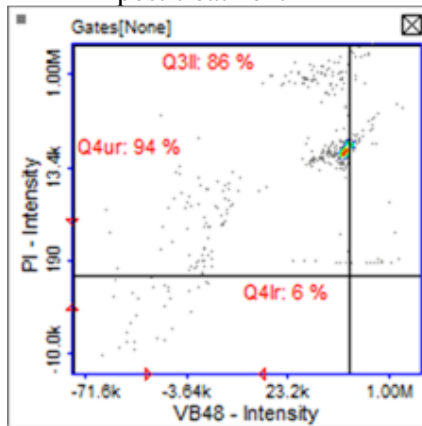


72h post-treatment

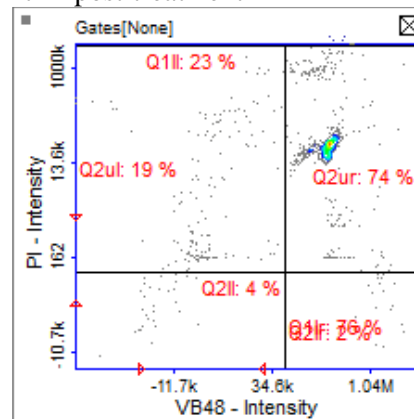


D: 5-FU + Inhibitors

24h post-treatment

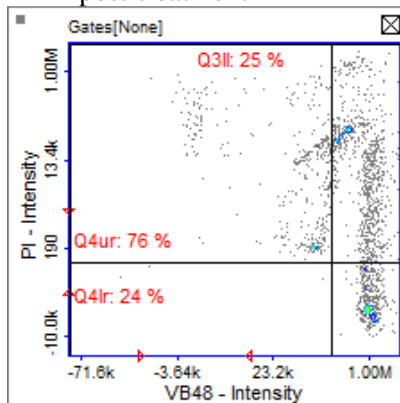


72h post-treatment

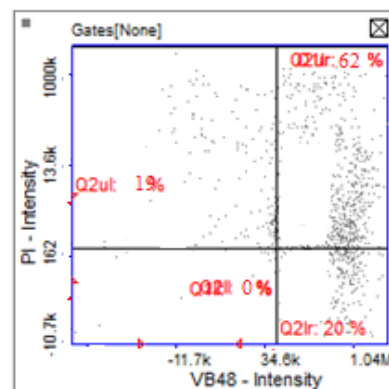


E: 5-FU

24h post-treatment

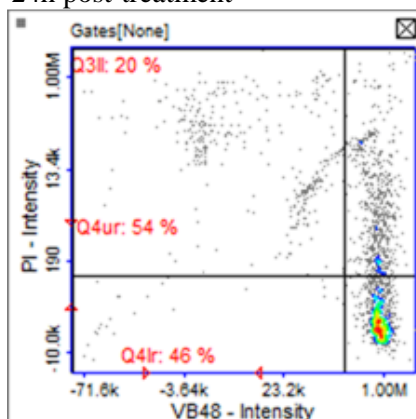


72h post-treatment



F: Control

24h post-treatment



72h post-treatment

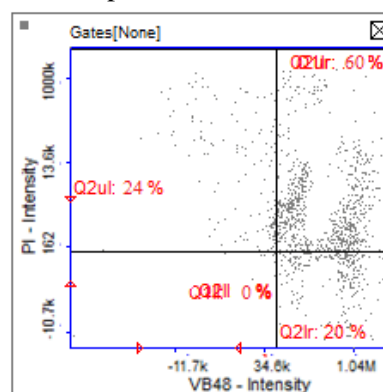


Figure 4.5 Multiplex assays demonstrating VitaBright-48™ staining following Cl-amidine-Nicotine pre-treatment/priming. MCF-7 cells were treated with 25µM and 50 µM Nicotine, 50µM chloramidine and 1µM 5-FU as shown in A-F. The cells were treated with for 24h, 48h and 72h. Cells were stained with VB-48™, Acridine Orange (AO) and Propidium Iodide (PI) and analysed using the Vitality Assay and a NucleoCounter® NC-3000™. Scatter plots and histograms were obtained from the NucleoView™ NC-3000™ software. Polygons and markers in the displayed plots were used to separate the various cell populations. Plots show VitaBright-48™ intensity versus PI intensity. Nonviable cells were gated out based on propidium iodide uptake. Plots show VitaBright-48™ intensity versus PI intensity. Nonviable cells were gated out based on SYTOX green uptake. Chloramidine treatment was 69.43% more effective resulting in less VB-48+ve, and more PI+ve cells compared to even most sensitive, 25µM nicotine pre-treatment even on day 1 ($p < 0.0001$). However combinatory pre-treatment resulted in the maximum % apoptosis by 90.11% ($p < 0.0001$) compared to 5-FU alone.

4.3.4 Bis- I and Cl-amidine shed light for Novel Cancer Immunotherapy

The outcome of the apoptotic study using Bis-I and Cl-amidine justifies the effectiveness of using a combination of inhibitors to enhance the anti-neoplastic effect of pharmacological reagents. As portrayed in **Figure 4.6 and 4.7** there was a significant decrease in live cells in the presence of Cl-am by 87.15% ($p<0.0001$) on day 1 and 81.05% ($p<0.0001$) on day 3 compared to 5-FU alone. The combination treatment was even more effective even on day 3 by 88.18% ($p<0.0001$) compared to 5-FU alone. However, Bis-I was less potent in inhibiting EV release compared to Cl-amidine (52.40%, $p=0.0001$) and combination (70.32%, $p<0.0001$) even on day 3 (**Figure 4.6**). The trend in the results was maintained throughout the 72 h duration but the cell viability on day 3 was significantly lower even in the absence of inhibitors and the drug by 18.11% ($p=0.0050$) suggesting that natural cell death occurs after a few days. Comparing these results with those presented in **Figure 4.4** suggest that Cl-amidine can be used as a pan -inhibitor. The data presented suggests that the presence of inhibitors may improve the activity of 5-FU by inhibiting its elimination from the intracellular space as manifest by the increase of percentage of dead cells even after 24 h compared to the untreated control cells (**Figure 4.7**). Overall these results indicated the importance of having a combination of EV inhibitors which strongly increases the efficiency of the chemotherapy compared to the presence of a single EV inhibitor.

Apoptosis of PC3 cells in the presence of combination of Inhibitors + 5-FU

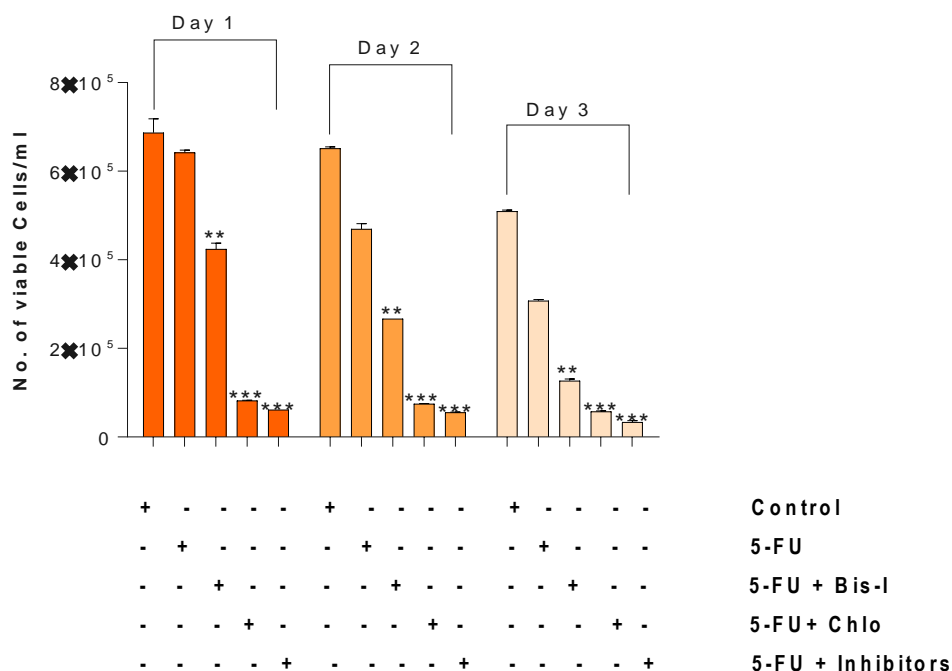
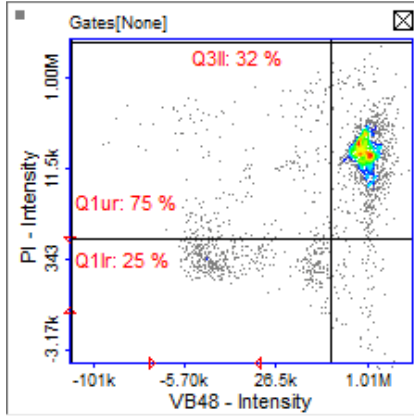


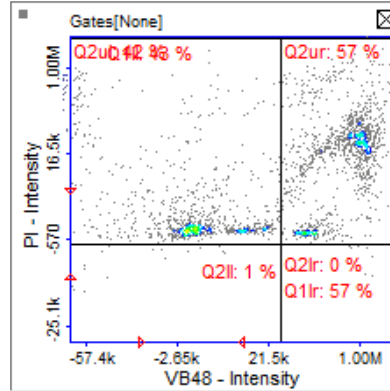
Figure 4.6 Combination of Inhibitors increases PC3 cell apoptosis. % Cell viability was lower in the presence of the inhibitors. % Cell viability was significantly lower in the presence of the inhibitors. Overall 5-FU alone reduced the cell viability by 38.55% ($p < 0.0001$). Pretreatment with Bisindolylmaleimide-I and Chloramidine together resulted in the maximum apoptosis throughout the study, 90.2% ($p < 0.0001$) on day 1 and 88.18% ($p < 0.0001$) on day 3 compared to 5-FU alone. The natural cell death occurred by day 3 which was reduced by 18% in the absence of drug and inhibitors. Chloramidine alone was more potent than Bisindolylmaleimide-I-pre-treatment by 81.9% ($p < 0.0001$) even on day 1 suggesting that Chloramidine is more potent as an inhibitor compared to Bisindolylmaleimide-I. Data presented are mean \pm SEM of three independent experiments performed in triplicate.

A: Bisin-I + 5-FU

24h post-treatment

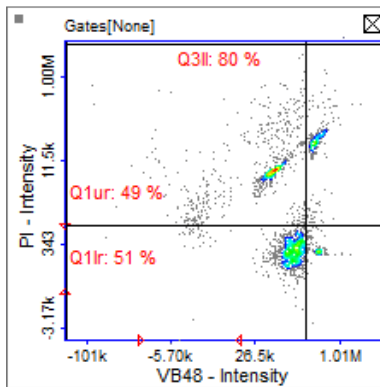


72h post-treatment

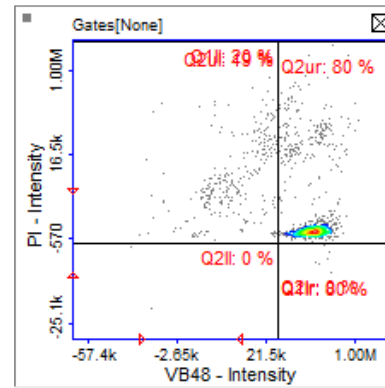


B: Chloramidine + 5-FU

24h post-treatment

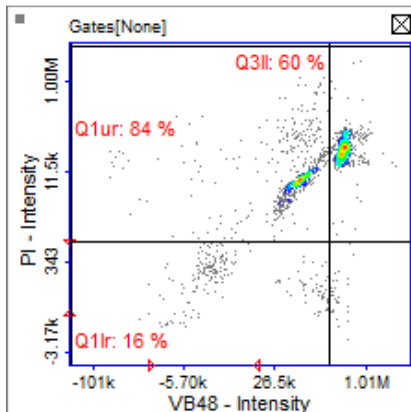


72h post-treatment

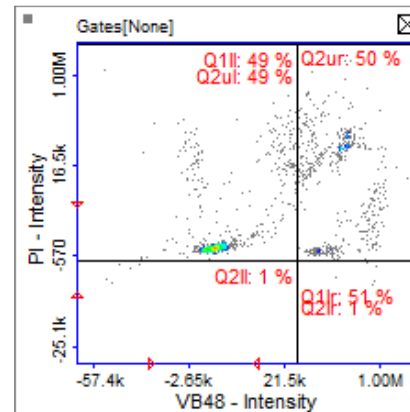


C: 5-FU + (Bis-I + Chlo)

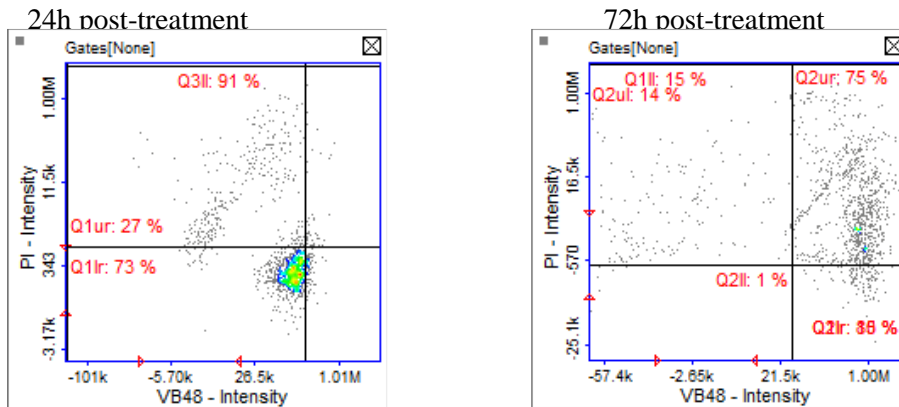
24h post-treatment



72h post-treatment



D: 5-FU



E: Control

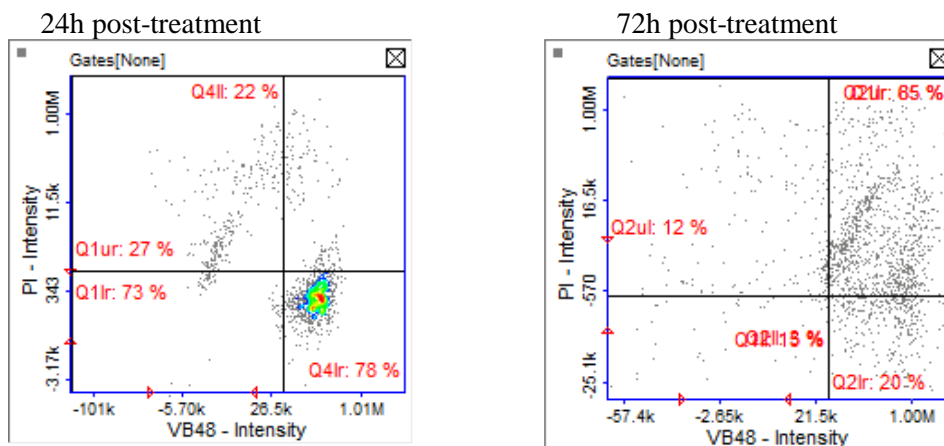


Figure 4.7 Multiplex assays demonstrating VitaBright-48™ staining following Cl-amidine-Bisindolylmaleimide-I pre-treatment/priming. PC3 cells were treated with 10 μ M Bisindolylmaleimide-I, 50 μ M chloramidine and 1 μ M 5-FU as shown in A-E. The cells were treated for 24h, 48h and 72h. Cells were stained with VB-48™, Acridine Orange (AO) and Propidium Iodide (PI) and analysed using the Vitality Assay and a NucleoCounter® NC-3000™. Scatter plots and histograms were obtained from the NucleoView™ NC-3000™ software. Polygons and markers in the displayed plots were used to separate the various cell populations. Plots show VitaBright-48™ intensity versus PI intensity. Nonviable cells were gated out based on propidium iodide uptake. Plots show VitaBright-48™ intensity versus PI intensity. Nonviable cells were gated out based on SYTOX green uptake. Chloramidine treatment was 52.40% ($p=0.0001$) more effective than Bisindolylmaleimide-I which was even increased in the presence of the combination by 70.32% ($p<0.0001$) resulting in less VB-48+ve, and more PI+ve cells even on day 3. However, Bisindolylmaleimide-I was strong in sensitising PC3 cells to 5-FU by at least 75% ($p<0.0001$) compared to 5-FU alone.

4.3.5 Pre-treatment with Bis-I abolish EV release Increasing the Cytotoxicity of Anti-cancer Drug-EVs

Bis-I is a strong EVinhibitor, so it became a prime candidate for examining the effect of EVinhibition on 5-FU activity. Addition of 5-FU EVs to the Bis-I pre-treated cells increased the apoptosis by 15.31% ($p=0.0011$) on day 1 which was lower but significant on day 3 by 10% ($p=0.0001$) compared to the direct treatment with 1 μM 5-FU-EVs (**Figure 4.9**). The apoptosis was lower when cells were washed after Bis-I pre-treatment by 13.69% ($p=0.0043$) even on day 3. The trend in the results was maintained throughout the 72 h period but the cell viability was significantly reduced by 19.19% ($p=0.0012$) even in the absence of inhibitor and chemotherapy suggesting that natural cell death occurs after a few days. Washing cells after pre-treatment with inhibitor resulted in the apoptotic cells which were 51% of Annexin- V (+ve) and 10% PI (+ve).(**Figure 4.10**). This was however less by 14.46% ($p= 0.0015$) compared to cells that were left unwashed after pre-treatment. This close synergy of inhibitor-drug interaction can elicit a favourable response facilitating effective chemotherapy as summarised in (**Figure 4.8**).

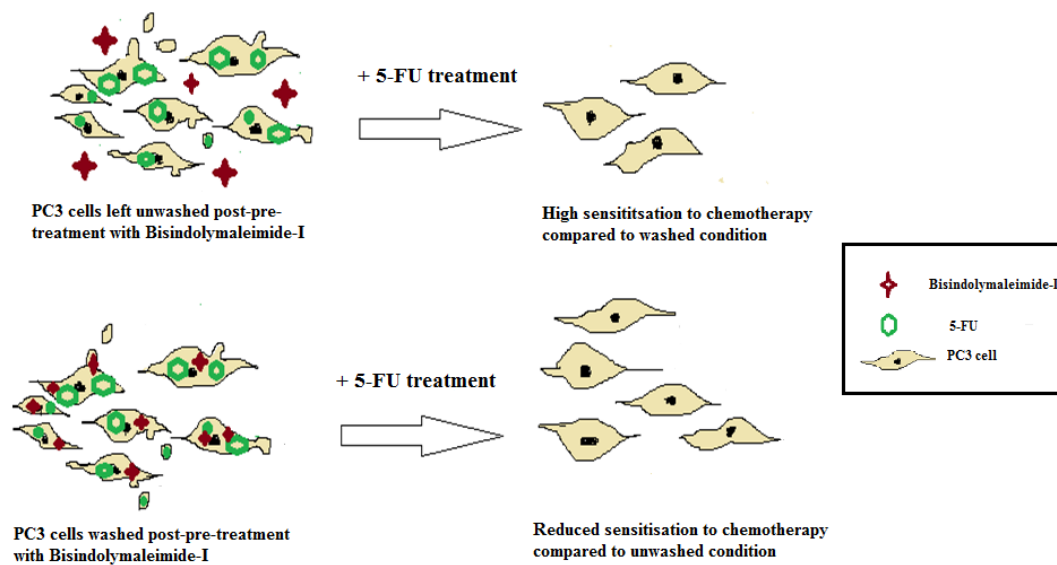


Figure 4.8 Schematic representation of the synergistic effect of EVinhibitor and chemotherapy. Bisindolymaleimide-I internalisation increased the sensitisation of PC3 cells to 5-FU therapy. However pre-treatment left ‘unwashed’ increases the sensitisation by at least by 15% compared to ‘washed’ condition. The natural synergy between EV inhibitor and chemotherapy is more successful in cancer cell sensitisation to effective chemotherapy.

Apoptosis of PC3 in the presence of Bis-I + 5-FU

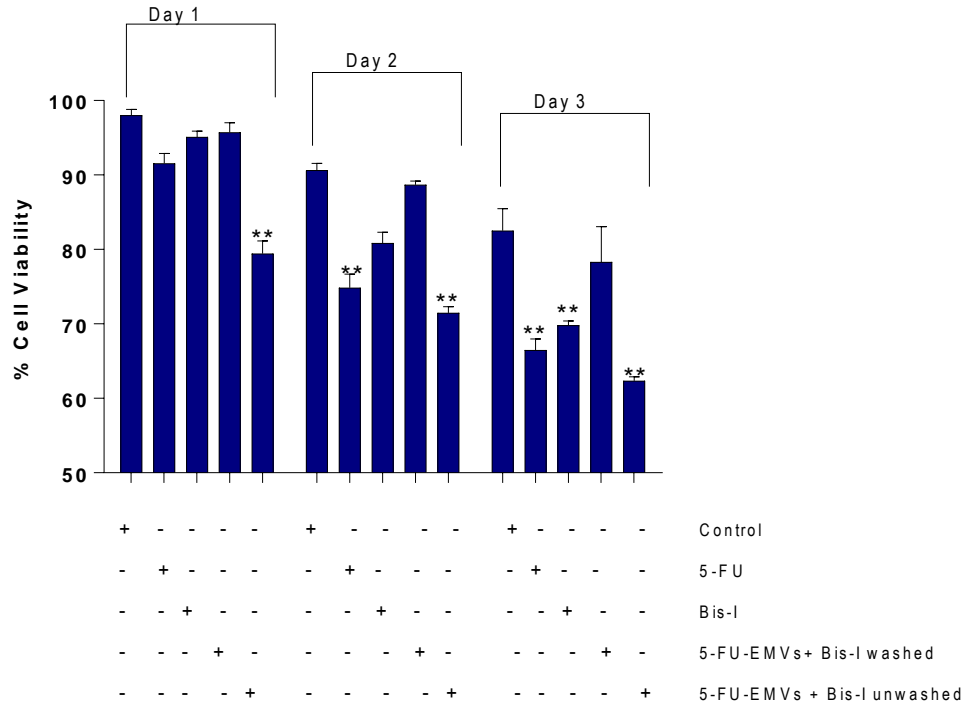
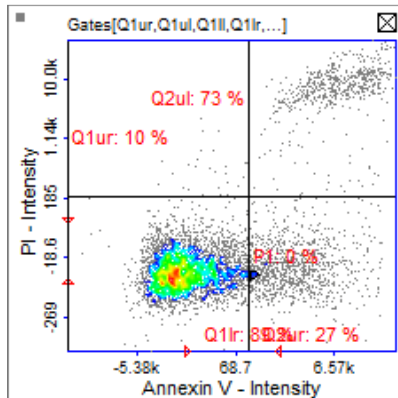
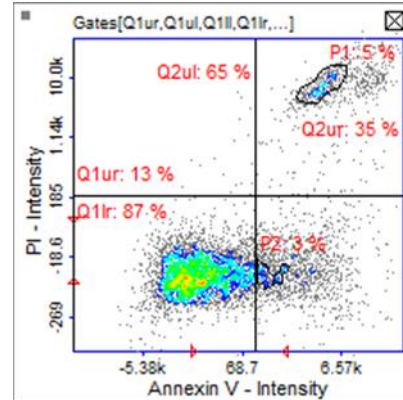


Figure 4.9 Presence of Bis-I abolishes EV release enhancing the Chemotherapeutic Cytotoxicity. Cells were treated with 1µM 5-FU-EVs following Bisin-I pre-treatment. Bisin-I pretreated cells were then either washed or unwashed before treating with 5-FU-EVs. % cell viability was significantly reduced by 10 % on day 1 which was increased to 15% by day 3 compared to respective untreated controls. However, pre-treatment of cells with Bisindolymaleimide-I had a significant effect on lowering total viable cells by less than 9% ($p=0.2649$) in washed condition by 21% ($p= 0.0003$) in unwashed condition compared to untreated control on day 3. Bisindolymaleimide-I pre-treatment even was more sensitising than direct 5-FU treatment of the cells. Increased sensitisation increased the apoptosis by 10% on day 1 ($p=0.0001$). This trend was however conserved throughout the study. Apoptosis was significantly affected in cells which were washed after Bisindolymaleimide-I pre-treatment. The % cell viability was higher than direct 5-FU treatment by 12.5% ($p= 0.0362$) on day 3. Data presented are mean \pm SEM of three independent experiments performed in triplicate. ** $p < 0.05$ was considered statistically significant compared to the untreated control.

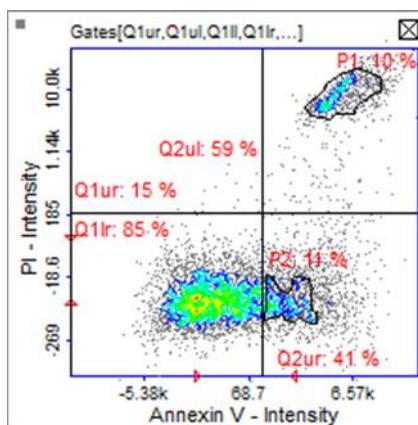
A. Control



B. 1 μ M 5-FU



C. 1 μ M 5-FU+Bisin-I (Unwashed)



D. 1 μ M 5-FU+ Bisin-I (Washed)

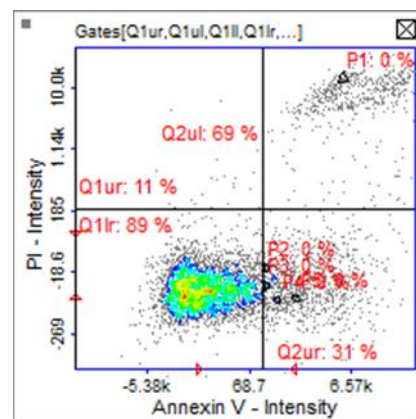


Figure 4.10 Multiplex assays demonstrating Annexin-V staining following Bisindolylmaleimide-I pre-treatment/priming. PC3 cells were treated with 10 μ M Bisindolylmaleimide-I, and 1 μ M 5-FU as shown in A-D. The cells were treated for 24h, 48h and 72h. Cells were stained with Hoechst-33342, Annexin V FITC conjugate and Propidium Iodide (PI) and analysed using the Annexin V Assay and a NucleoCounter[®] NC-3000[™]. Scatter plots and histograms were obtained from the NucleoView[™] NC-3000[™] software. Quadrants and markers in the displayed plots were used to demarcate the various cell populations. Bisindolylmaleimide-I treatment increased the sensitisation of PC3 cells to 5-FU-EVs by 15.31% ($p=0.0011$) compared to without Bisindolylmaleimide-I treatment. However, there is 10% more PI+ve cells in unwashed condition (Plot C) compared to washing after treatment with 5-FU-EVs. This suggests that there is at least a 10% increase in late apoptosis when more time is allowed to absorb 5-FU-EVs ($p=0.0001$).

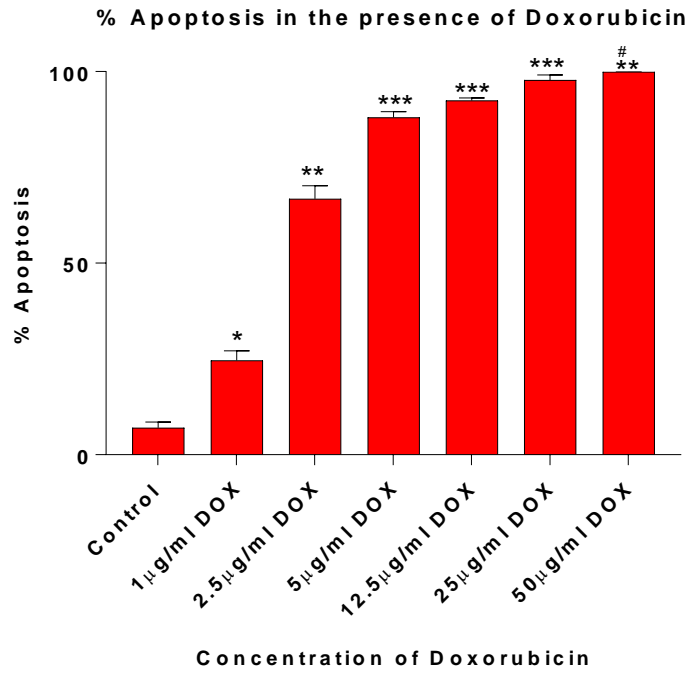
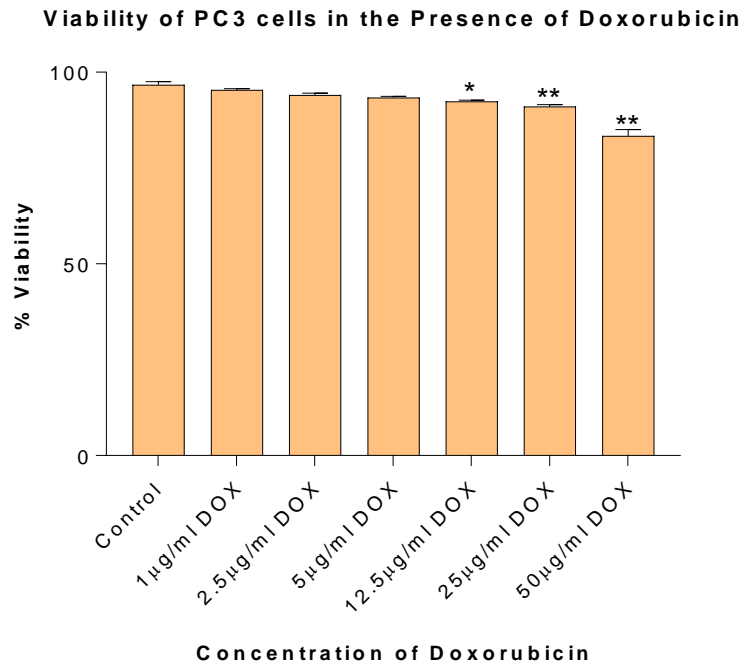
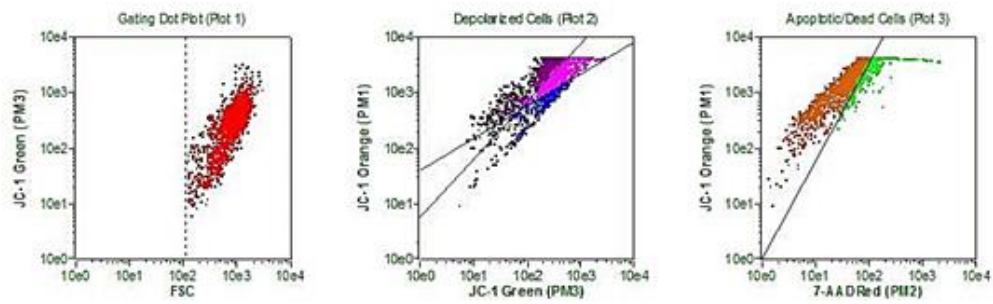
A**B**

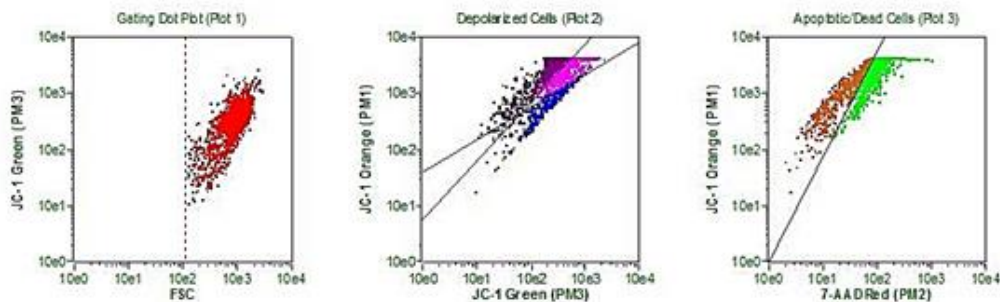
Figure 4.11 5µg/ml of DOX was the optimum concentration to treat PC3 cells. **A**, % apoptosis increased with increasing concentration of DOX. 59.7% increase in apoptosis was seen in the presence of just 1µg/ml which was increased by 28.65% to reach the maximum inhibition of 100% when treated with 5 µg/ml. **B**, there was no detrimental effect on cell viability on using 5µg/ml which only decreased by 5.1% compared to the untreated. * < 0.05 was considered statistically significant compared to the control, # <0.05 was considered statistically significant compared to 5µg/ml.



Analysis Results:

	Count	Cells /mL	% of Total	PM3 MFI	PM1 MFI	PM2 MFI
Polarized Cells (UL, Plot 2)	984	3.76e04	49.20%	267.27	2565.17	-
Depolarized Cells 1 (UR, Plot 2)	731	2.79e04	36.55%	477.94	2237.46	-
Depolarized Cells 2 (LR, Plot 2)	263	1.00e04	13.15%	226.34	567.92	-
Depolarized Cells 3 (LL, Plot 2)	22	8.40e02	1.10%	26.18	209.45	-
Apoptotic/Dead Cells (Right, Plot 3)	496	1.89e04	24.80%	-	2858.80	157.93
Gated Events	Total Count	% Inside Gate	FSC Mean			
-	2000	-	989.85			

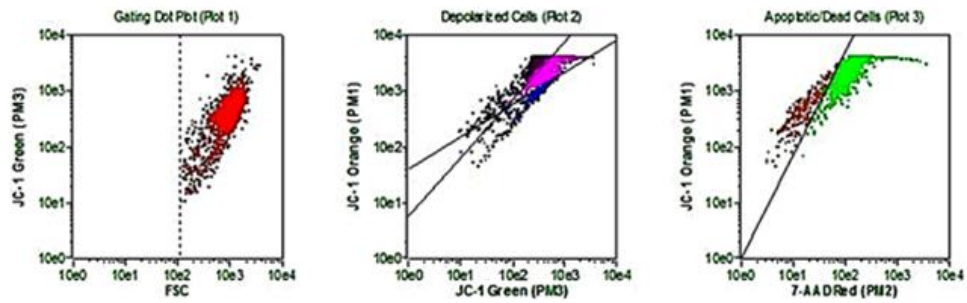
1µg/ml



Analysis Results:

	Count	Cells /mL	% of Total	PM3 MFI	PM1 MFI	PM2 MFI
Polarized Cells (UL, Plot 2)	1099	5.61e04	54.95%	284.34	2738.02	-
Depolarized Cells 1 (UR, Plot 2)	624	3.19e04	31.20%	486.33	2350.28	-
Depolarized Cells 2 (LR, Plot 2)	259	1.32e04	12.95%	250.79	641.56	-
Depolarized Cells 3 (LL, Plot 2)	18	9.19e02	0.90%	30.33	244.00	-
Apoptotic/Dead Cells (Right, Plot 3)	1427	7.29e04	71.35%	-	2640.91	105.54
Gated Events	Total Count	% Inside Gate	FSC Mean			
-	2000	-	1003.88			

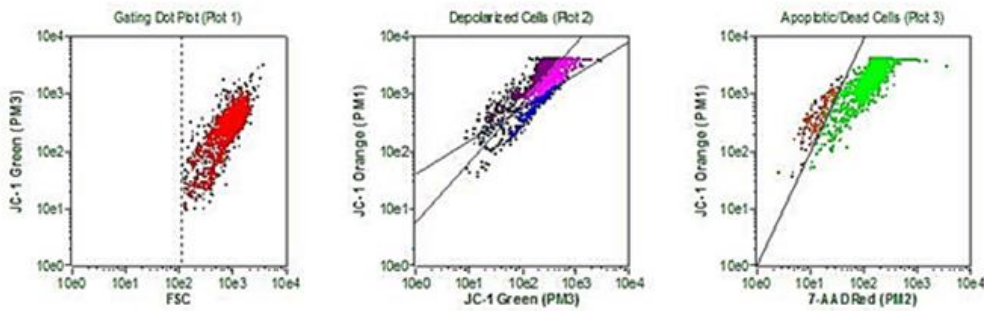
2µg/ml



Analysis Results:

	Count	Cells /mL	% of Total	PM3 MFI	PM1 MFI	PM2 MFI
Polarized Cells (UL, Plot 2)	824	4.75e04	41.20%	321.34	2852.54	-
Depolarized Cells 1 (UR, Plot 2)	928	5.35e04	46.40%	528.84	2501.26	-
Depolarized Cells 2 (LR, Plot 2)	236	1.36e04	11.80%	330.56	748.19	-
Depolarized Cells 3 (LL, Plot 2)	12	6.92e02	0.60%	21.83	205.58	-
Apoptotic/Dead Cells (Right, Plot 3)	1811	1.04e05	90.55%	-	2617.10	172.91
Gated Events	Total Count	% Inside Gate	FSC Mean			
-	2000	-	1093.93			

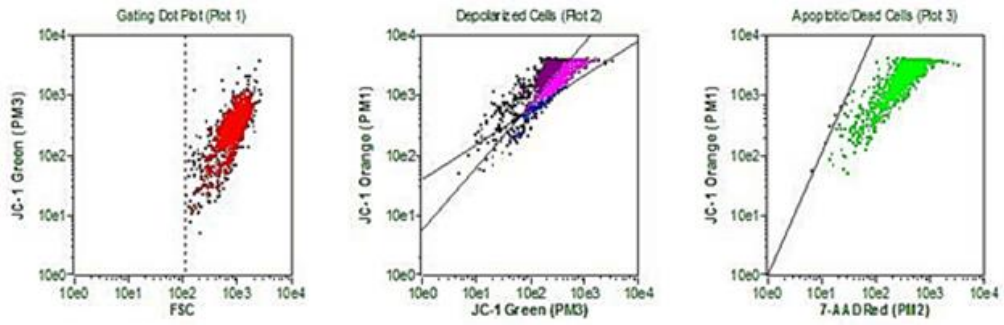
5µg/ml



Analysis Results:

	Count	Cells /mL	% of Total	PM3 MFI	PM1 MFI	PM2 MFI
Polarized Cells (UL, Plot 2)	892	4.61e04	44.60%	266.82	2459.00	-
Depolarized Cells 1 (UR, Plot 2)	833	4.30e04	41.65%	422.39	2122.65	-
Depolarized Cells 2 (LR, Plot 2)	251	1.30e04	12.55%	211.10	590.65	-
Depolarized Cells 3 (LL, Plot 2)	24	1.24e03	1.20%	24.67	210.67	-
Apoptotic/Dead Cells (Right, Plot 3)	1872	9.67e04	93.60%	-	2164.04	173.84
Gated Events	Total Count	% Inside Gate	FSC Mean			
-	2000	-	1043.90			

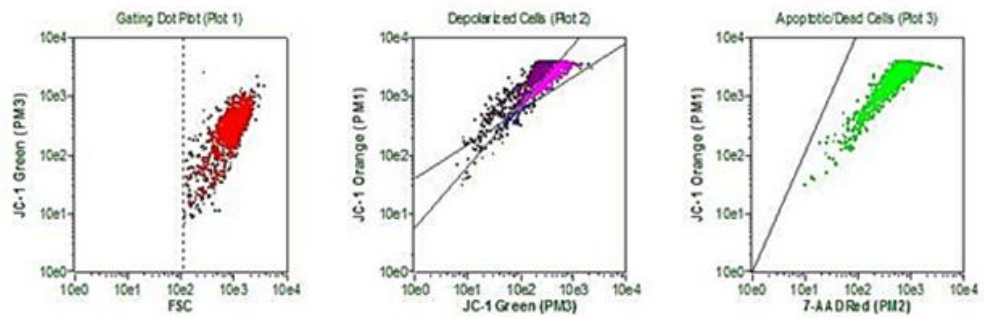
12.5µg/ml



Analysis Results:

	Count	Cells/mL	% of Total	PM3 MFI	PM1 MFI	PM2 MFI
Polarized Cells (UL, Plot 2)	1232	8.36e04	61.60%	270.81	2641.13	-
Depolarized Cells 1 (UR, Plot 2)	626	4.25e04	31.30%	461.09	2265.03	-
Depolarized Cells 2 (LR, Plot 2)	124	8.41e03	6.20%	196.33	545.10	-
Depolarized Cells 3 (LL, Plot 2)	18	1.22e03	0.90%	26.44	221.11	-
Apoptotic/Dead Cells (Right, Plot 3)	1996	1.35e05	99.80%	-	2375.74	467.58
Gated Events	Total Count	% Inside Gate	FSC Mean			
-	2000	-	974.34			

25µg/ml



Analysis Results:

	Count	Cells/mL	% of Total	PM3 MFI	PM1 MFI	PM2 MFI
Polarized Cells (UL, Plot 2)	1301	1.12e05	65.05%	268.42	2481.22	-
Depolarized Cells 1 (UR, Plot 2)	605	5.23e04	30.25%	466.89	2441.22	-
Depolarized Cells 2 (LR, Plot 2)	70	6.05e03	3.50%	120.14	417.24	-
Depolarized Cells 3 (LL, Plot 2)	24	2.07e03	1.20%	23.33	196.33	-
Apoptotic/Dead Cells (Right, Plot 3)	2000	1.73e05	100.00%	-	2369.46	752.19
Gated Events	Total Count	% Inside Gate	FSC Mean			
-	2000	-	1110.56			

50µg/ml

Figure 4.12 Apoptosis of PC3 cells after treating with different concentrations of DOX. PC3 cells were treated with 1-50 µg/ml of DOX and a mitochondrial membrane potential assay was performed using the Guava flow cytometer to determine levels of apoptosis. JC-1, a fluorescent cationic dye along with dead cell dye, 7-AAD, was used to determine the % polarization/depolarization. 90.55% of cells reached apoptosis when treated with 5 µg/ml which reached 99% in the presence of 25 µg/ml. However, there was a rapid increase in apoptosis when treated with 2 µg/ml which increased by 64.8% resulting in a 71% apoptosis.

4.3.6 Optimisation of DOX Concentration to be Used in Apoptosis Studies

A Mitochondrial membrane potential assay was used to determine the effective concentration of DOX in this series of experiments. The JC-1 green fluorescence increased steadily as the DOX concentration increased, clearly exhibiting increased percentage of depolarised cells at higher concentrations (**Figure 4.12**). 90.5% of the cells were affected only at 5 µg/ml of DOX with a 5.1% decrease in cell viability. This was only 10% less than the effect of 50 µg/ml but the cell viability in the presence of the highest concentration was reduced by nearly 10% ($p=0.0158$) (**Figure 4.11B**). This pointed to the use of 5 µg/ml DOX in future experiments.

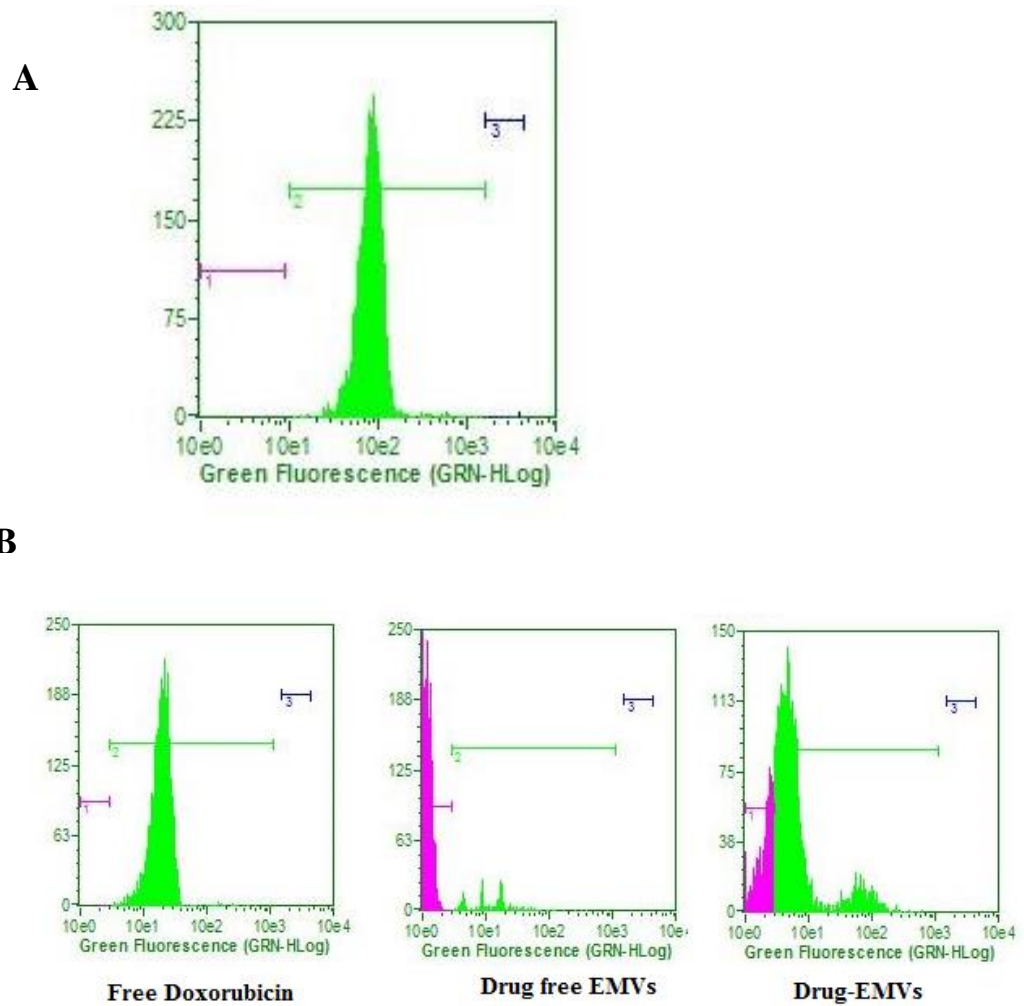


Figure 4.13 Flow cytometry confirmation of drugs encapsulated in EVs. **A**, Annexin V labelling revealed that 99.64% of the vesicles isolated were Annexin V positive which confirms that most are MVs. **B**, encapsulation of fluorescent labelled-DOX was carried out followed by a 4h incubation of EVs with drug at 37°C. Only 64.8% of the vesicles were labelled with the drug. A positive control of free-drug (99.04%) and a negative control of just EV-free RPMI were used to confirm the validity of the results. The experiment was repeated thrice, and the average was noted for final values.

4.3.7 PC3-cell derived, annexin-V positive EV Drug Encapsulation

EVs isolated from PC3 cells were 99.64% positive for Annexin V-FITC labelling (**Figure 4.13A**). The EVs were processed for DOX loading and analysed by flow cytometry. Less than 65% of the EVs were DOX positive which was a 40% decrease compared to the free-drug (**Figure 4.13B**). This was however distinguishable from the DOX-untreated, control EVs.

4.3.8 Cl-amidine significantly inhibits EV release in PC3 cells

EV release was significantly inhibited by Cl-amidine up to 99.6% ($p=0.0004$). In contrast, the anti-cancer drug DOX pronouncedly increased the EV release by 97.67% compared to the untreated control ($p<0.0001$). However, Cl-amidine pre-treatment managed to reduce the EV release up to 69.63% compared to the DOX only treated ($p<0.0001$). The outcome remarkably encourages the use of EV inhibition in order to increase the sensitisation of cancer cells to chemotherapy (**Figure 4.14**).

4.3.9 Fluorescence Microscopy analysis of Anti-cancer Drug transfer via EVs

Figure 4.15 summarises the effect of EV inhibition on the sensitisation to chemotherapeutic drug, DOX, delivered via EVs. 4h post-incubation only 5.76% of the Cl-amidine untreated cells were stained with DOX which still represented a 42.4% reduction compared to those that were stained following Cl-amidine pre-treatment. This was increased significantly after 24 h incubation. Less than 65% cells exhibited DOX in Cl-amidine pre-treated cells while only 30% of the cells were affected following co-incubation with DOX-EVs. This clearly depicts that Cl-amidine pre-treatment has increased the sensitisation of the PC3 cells to drug-EVs.

EMV release in PC3 cells

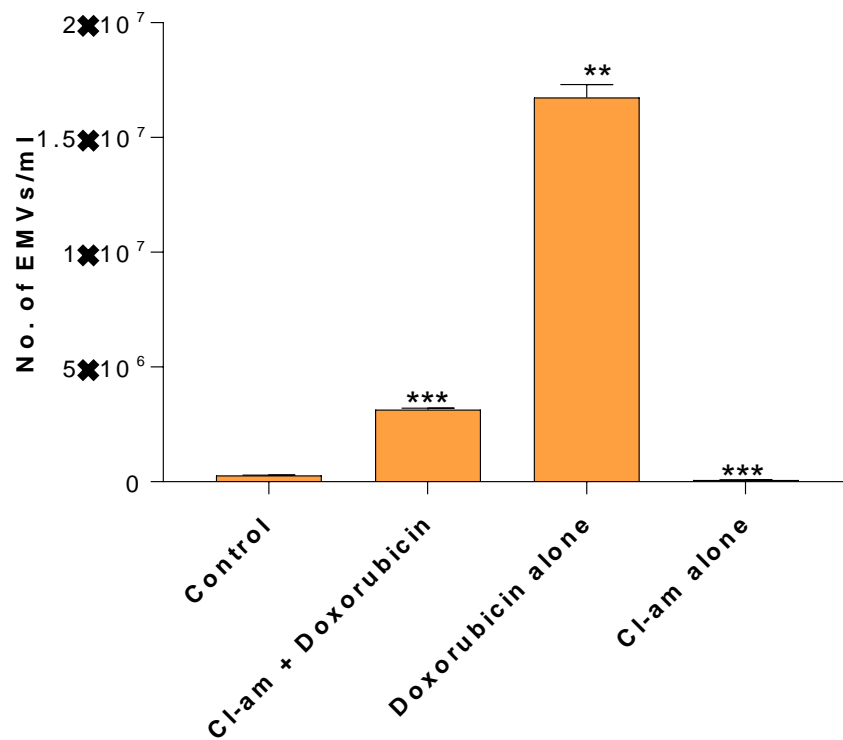


Figure 4.14 EV release in the presence of DOX and pan-PAD inhibitor, Cl-amidine. EV release was at its highest from PC3 cells when treated with DOX ($p < 0.0001$). In contrast where the cells were treated with Cl-amidine, this inhibited the EV shedding by 99.6% compared to DOX treatment which was also lower than the untreated control by 81.09% ($p = 0.0004$). However, Cl-amidine pre-treatment pronouncedly reduced the EV shedding by 69.63% ($p < 0.0001$) compared to Dox on its own. The average of three independent experiments was considered.

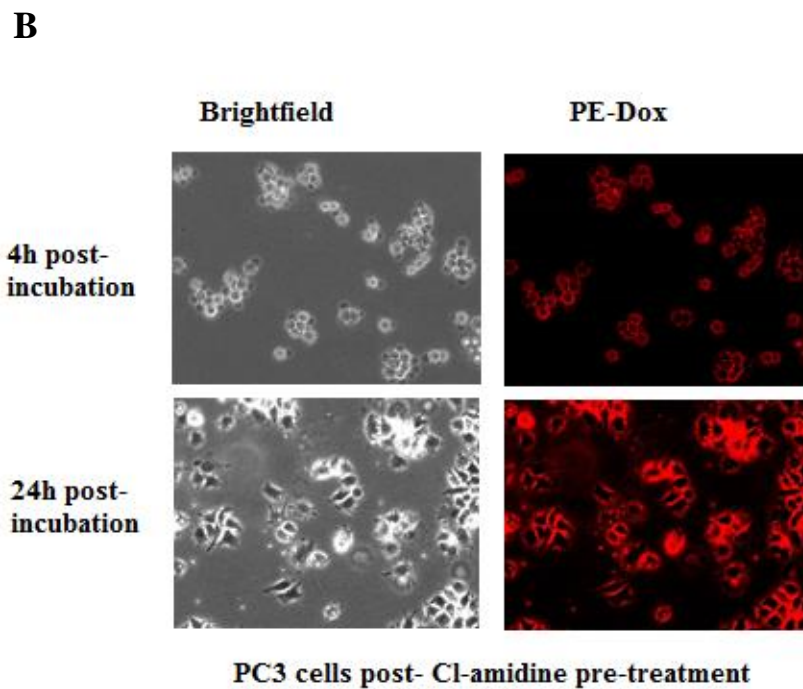
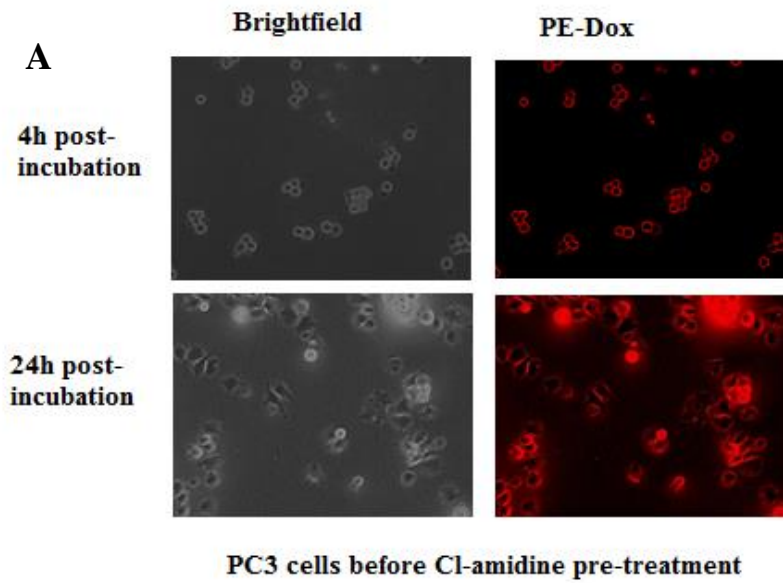
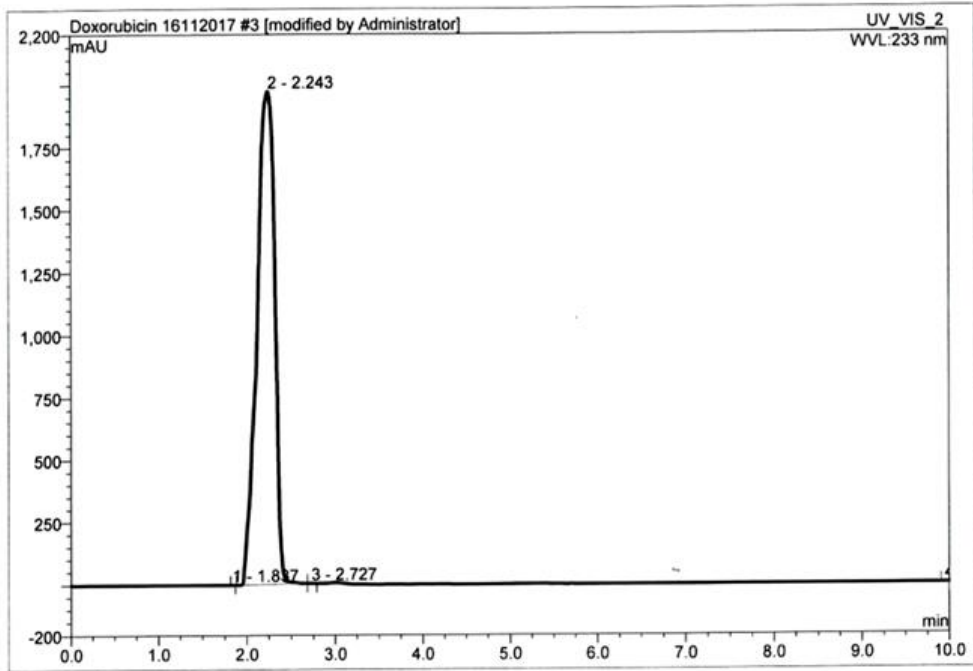
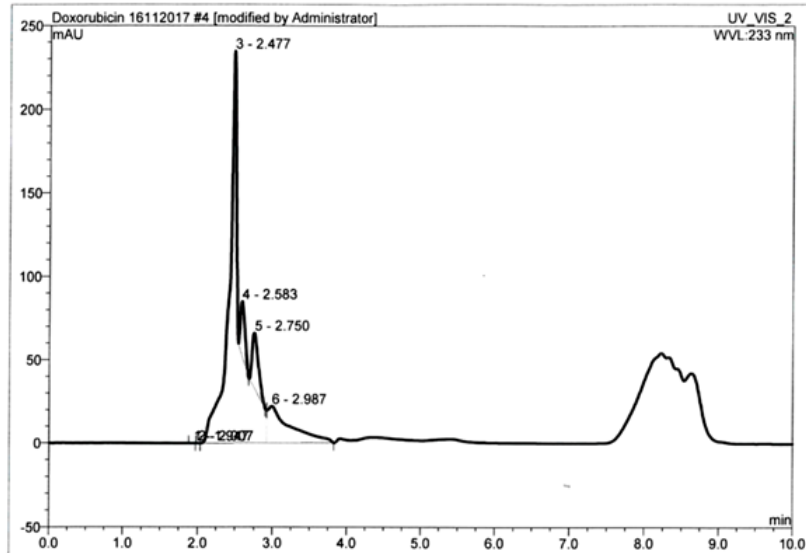


Figure 4.15 Fluorescent microscopy analysis of Cl-amidine pre-treatment sensitising PC3 cells to DOX-EVs. PC3 cells were incubated with DOX-EVs for 4h and 24h at 37 °C. **A**, only 30% of the PC3 cells without pre-treatment of Cl-amidine was labelled with DOX after 24h incubation. **B**, this was increased in Cl-amidine pre-treated cells where 64% of the total cell population showed the drug transfer via DOX-EVs. The experiment was repeated thrice, and representative images have been presented.



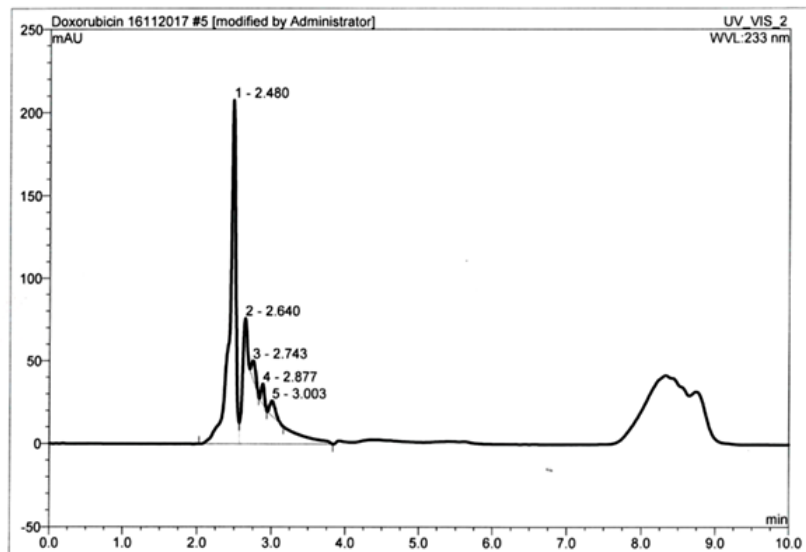
No.	Ret.Time min	Peak Name	Height mAU	Area mAU*min	Rel.Area %	Amount	Type
1	1.84	n.a.	0.007	0.000	0.00	n.a.	BMB
2	2.24	n.a.	1970.473	458.217	99.99	n.a.	BM *
3	2.73	n.a.	0.739	0.055	0.01	n.a.	MB*
4	9.95	n.a.	0.011	0.001	0.00	n.a.	BMB*
Total:			1971.230	458.273	100.00	0.000	

Dox-standard



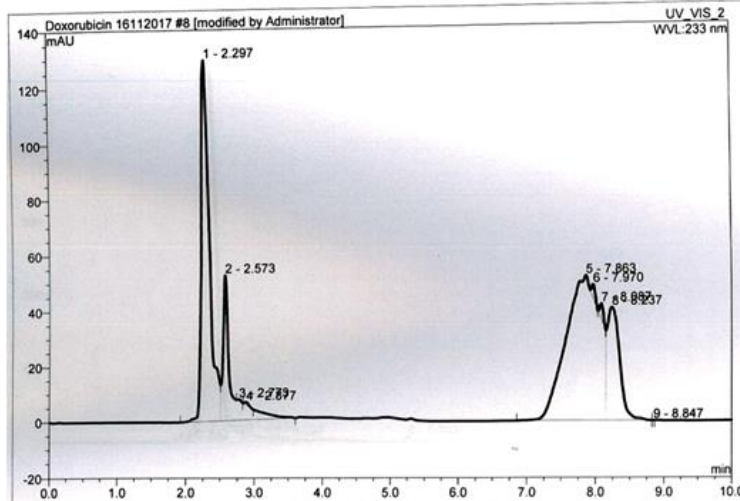
No.	Ret.Time min	Peak Name	Height mAU	Area mAU*min	Rel.Area %	Amount	Type
1	1.95	n.a.	0.028	0.001	0.00	n.a.	BMB
2	2.01	n.a.	0.010	0.000	0.00	n.a.	BMB
3	2.48	n.a.	234.875	41.675	75.64	n.a.	BM
4	2.58	n.a.	31.652	2.304	4.18	n.a.	Rd
5	2.75	n.a.	32.840	3.225	5.85	n.a.	Rd
6	2.99	n.a.	22.054	7.893	14.32	n.a.	MB
Total:			321.461	55.098	100.00	0.000	

Control cells



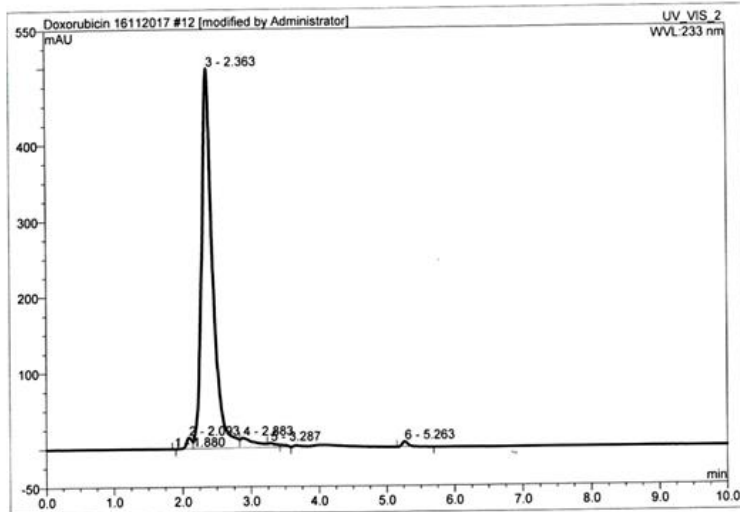
No.	Ret.Time min	Peak Name	Height mAU	Area mAU*min	Rel.Area %	Amount	Type
1	2.48	n.a.	207.640	19.389	46.14	n.a.	BM *
2	2.64	n.a.	75.991	20.442	48.65	n.a.	MB*
3	2.74	n.a.	10.648	0.794	1.89	n.a.	Rd
4	2.88	n.a.	11.962	0.608	1.45	n.a.	Rd
5	3.00	n.a.	9.038	0.788	1.88	n.a.	Rd
Total:			315.279	42.021	100.00	0.000	

Control EMVs



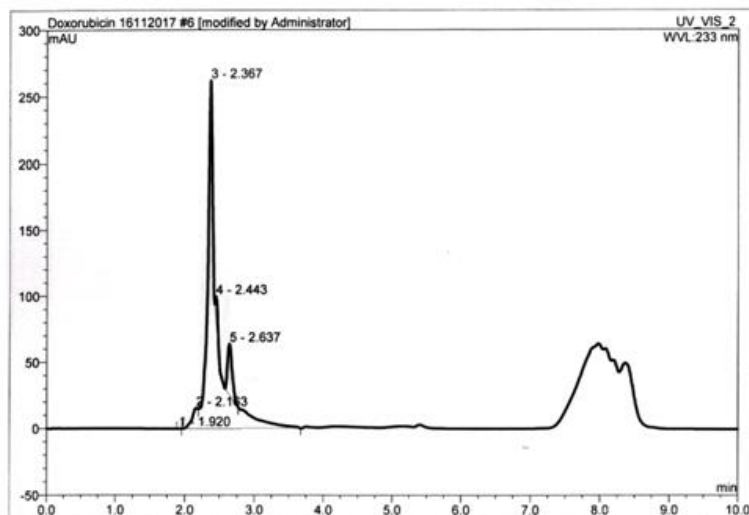
No.	Ret.Time min	Peak Name	Height mAU	Area mAU*min	Rel.Area %	Amount	Type
1	2.30	n.a.	129.292	17.862	28.15	n.a.	BM *
2	2.57	n.a.	52.394	7.131	11.24	n.a.	MB*
3	2.77	n.a.	0.602	0.029	0.05	n.a.	Rd
4	2.88	n.a.	0.920	0.064	0.10	n.a.	Rd
5	7.86	n.a.	51.620	29.348	46.24	n.a.	BM *
6	7.97	n.a.	4.834	0.285	0.45	n.a.	Rd
7	8.09	n.a.	5.469	0.316	0.50	n.a.	Rd
8	8.24	n.a.	40.277	8.429	13.28	n.a.	MB*
9	8.85	n.a.	0.004	0.000	0.00	n.a.	BMB
Total:			285.411	63.464	100.00	0.000	

Dox- treated cells



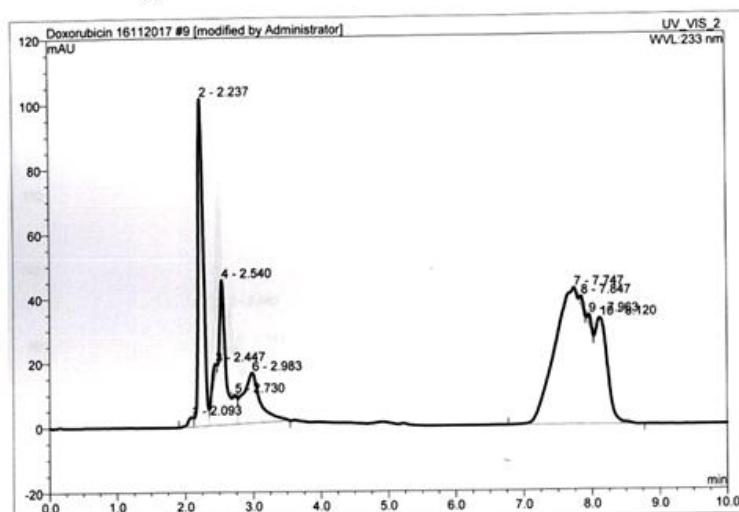
No.	Ret.Time min	Peak Name	Height mAU	Area mAU*min	Rel.Area %	Amount	Type
1	1.88	n.a.	0.006	0.000	0.00	n.a.	BMB
2	2.09	n.a.	14.458	1.391	1.41	n.a.	BM
3	2.36	n.a.	498.265	91.989	93.33	n.a.	M
4	2.88	n.a.	13.064	4.360	4.42	n.a.	MB
5	3.29	n.a.	1.037	0.072	0.07	n.a.	Rd
6	5.26	n.a.	7.201	0.749	0.76	n.a.	BMB
Total:			534.030	98.562	100.00	0.000	

Dox-treated EMVs



No.	Ret.Time min	Peak Name	Height mAU	Area mAU*min	Rel.Area %	Amount	Type
1	1.92	n.a.	0.006	0.000	0.00	n.a.	BMB
2	2.16	n.a.	15.327	1.555	3.40	n.a.	BM
3	2.37	n.a.	262.170	40.447	88.41	n.a.	MB
4	2.44	n.a.	18.119	0.854	1.87	n.a.	Rd
5	2.64	n.a.	38.117	2.891	6.32	n.a.	Rd
Total:			333.740	45.747	100.00	0.000	

Cl-amidine pre-treated cells



No.	Ret.Time min	Peak Name	Height mAU	Area mAU*min	Rel.Area %	Amount	Type
1	2.09	n.a.	2.880	0.275	0.53	n.a.	BM*
2	2.24	n.a.	101.230	9.026	17.38	n.a.	M*
3	2.45	n.a.	3.718	0.315	0.61	n.a.	Ru
4	2.54	n.a.	44.890	6.845	13.18	n.a.	M*
5	2.73	n.a.	1.053	0.046	0.09	n.a.	Rd
6	2.98	n.a.	15.509	4.522	8.71	n.a.	MB*
7	7.75	n.a.	42.111	23.728	45.69	n.a.	BM*
8	7.85	n.a.	2.670	0.168	0.32	n.a.	Rd
9	7.96	n.a.	3.027	0.175	0.34	n.a.	Rd
10	8.12	n.a.	32.749	6.836	13.16	n.a.	MB*
Total:			249.839	51.937	100.00	0.000	

Cl-amidine pre-treated EMVs

Figure 4.16 HPLC chromatograms of the effect of EV inhibition on DOX retention in PC3 cells. PC3 cells were treated with 50 µg/ml of Doxorubicin, with a retention time of 2.243 min. EVs were isolated following DOX treatment and analysed on HPLC. DOX-treated cells resulted in a 129.292 mAU (20.60% of the total) while EVs were of 498.265 mAU which comprised 79.39% of the total. In contrast, Cl-am pre-treatment resulted in higher retention of the drug within cells (72.14%) while only 27.86% was seen in EVs. Isolation was carried out at 233 nm.

Absorbance of Doxorubicin by PC3 cells and PC3-EMVs analysed by HPLC

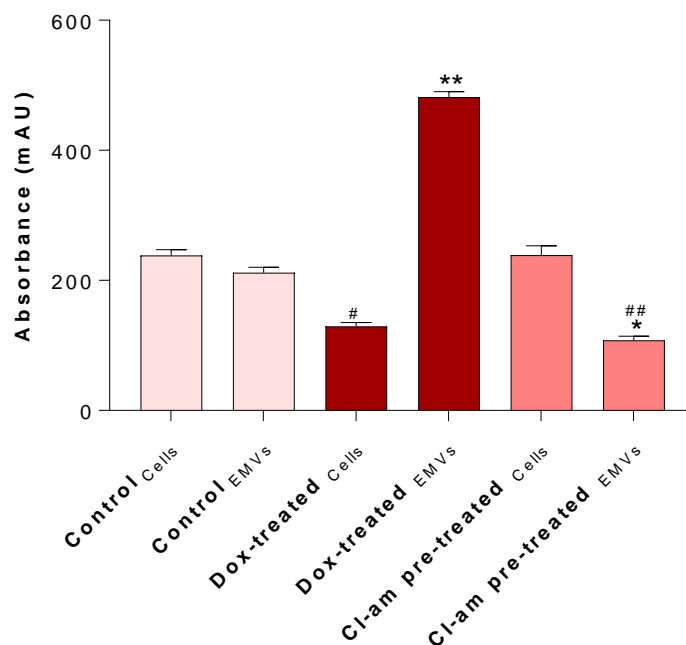


Figure 4.17 Cl-amidine pre-treatment increases sensitisation of PC3 cells to Doxorubicin. In the absence of Cl-amidine pre-treatment, 74% of the drug was absorbed by DOX-EVs ($p=0.0012$) as opposed to the cells. While the Cl-am pre-treatment increased the cellular uptake of the drug by 50.68% ($p=0.0118$). The experiment was repeated thrice, and the average considered. * = significance compared to its subset and # = significance compared to the control.

4.3.10 HPLC analysis confirms the importance of EV inhibition on the increased Effect of Anti-cancer Drug

A variety of chromatographic conditions and sample preparation methods were experimented upon before establishing the used method to achieve optimum conditions for reasonable peak separation of the analyte. **Figure 4.17** summarises the results that represent the chromatographs in **Figure 4.16**. It was quite apparent that the Cl-am pre-treatment decreased the drug expulsion by 61.39% ($p=0.0129$). There was 74% increase in DOX in EVs in the absence of the pre-treatment ($p=0.0012$). More than 78% of the drug was expelled within EVs in the absence of the Cl-am pre-treatment ($p=0.0015$). Interestingly EV inhibition increased the drug retainability by 50.68% in cells ($p=0.018$). Untreated cells and EVs were used as the negative control to validate the results.

4.3.11 Fluorescence Spectrometry Analysis further confirms that EV inhibition Increases the Effectiveness of Anti-tumour Therapy

The absorbance and fluorescence intensity in DOX-treated cells and EVs was analysed in the presence and absence of Cl-am pre-treatment. **Figure 4.18** undoubtedly shows that there was very much less DOX absorbance in cells that were not pre-treated with Cl-am which was reduced by 18.67% ($p=0.0060$) compared to that following pre-treatment. In contrast, absorbance in EVs under the same condition had a significant increase of 50.58% ($p=0.0022$) compared to that following pre-treatment. Similarly, apoptotic cells had a reduced absorbance, 35.33%, following Cl-am pre-treatment. Equally, it was very interesting to see that intensity results followed the same direction (**Figure 4.19**). Fluorescence intensity was higher in the presence of Cl-am pre-treatment by 53.16% ($p=0.0021$). A distinct reduction of 61.54% was seen in the supernatant of the pre-treated cells ($p=0.0257$). The outcome has further underlined the significance of EV inhibition on operative chemotherapy.

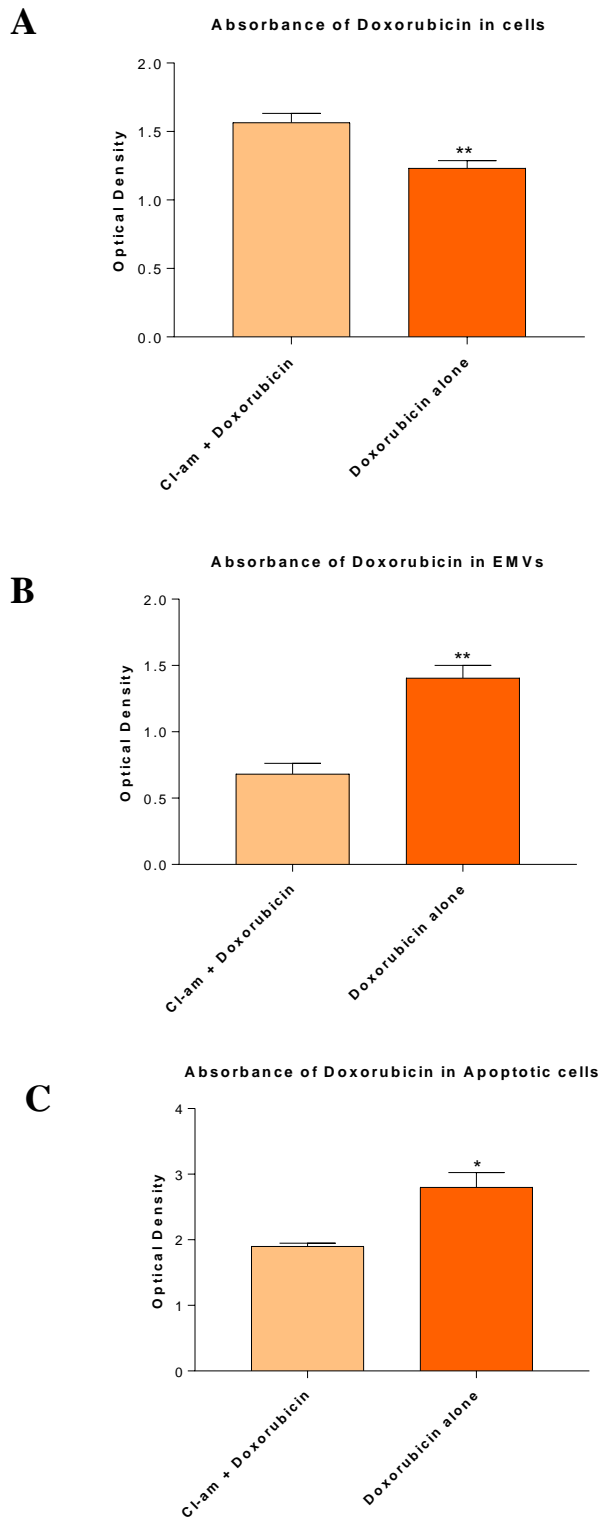


Figure 4.18 Absorbance of DOX by PC3 cells and PC3-EVs analysed by fluorescent spectroscopy. **A**, DOX absorption was higher in Cl-am pre-treated cells by 18.67% compared to no pre-treatment ($p=0.0060$). **B**, DOX absorbance was higher in EVs in the absence of Cl-am pre-treatment ($p=0.0022$). **C**, Apoptotic cells had a reduced absorbance post-pre-treatment with Cl-am by 35.33%. The experiment was repeated thrice and average \pm SEM presented.

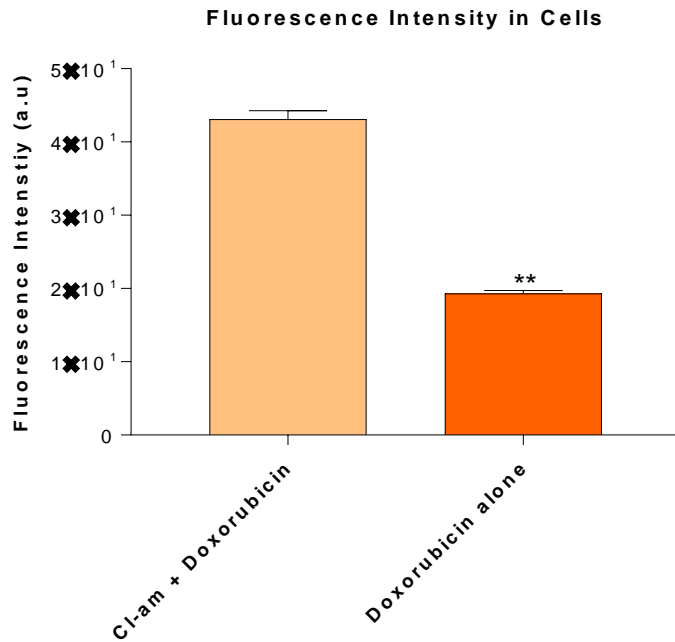
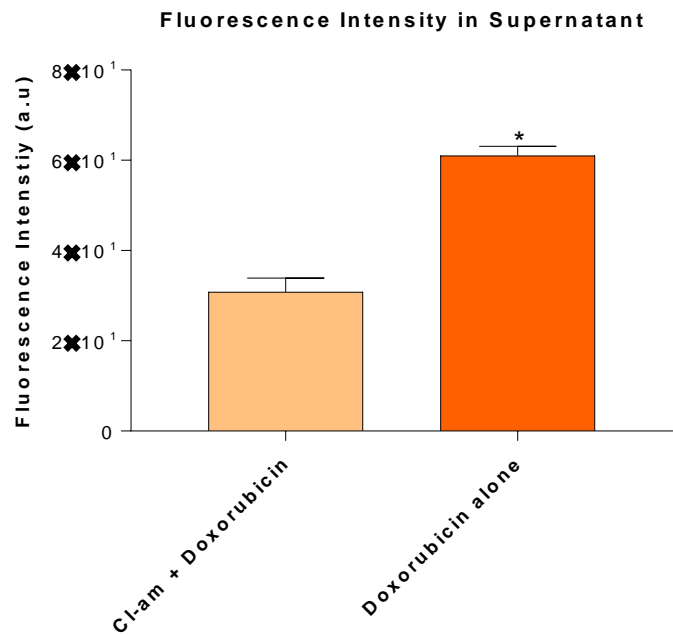
A**B**

Figure 4.19 Fluorescence intensity of PC3 cells and supernatant analysed by fluorescence spectroscopy. **A**, High fluorescence intensity was recorded in the Cl-am pre-treated cells compared to when it was absent ($p=0.0021$). In contrast, this was reduced in the supernatant by 41.45% ($p=0.0257$). **B**, Cells solely treated with DOX, however, had a 69.2% reduced fluorescence intensity compared to the supernatant ($p<0.0001$).

4.4 Discussion

Conducting apoptosis assays further justified the significance of using EV inhibitors in cancer therapy in order to minimise the expulsion of anti-cancer drug, therefore increasing its effectiveness. Pre-treatment with nicotine repressed the EV release thereby improving the drug effectiveness both with respect to PC3 (**Figure: 4.2.and 4.3**) and MCF7 cells (**Figure: 4.4. and 4.5**). Treatment with 25 μ M nicotine resulted in a relatively high percentage of propidium iodide stained (dead) cells compared with 50 μ M nicotine. However, there was substantial apoptosis in both PC3 and MCF7 in the presence of nicotine in contrast to the untreated controls. This further suggests that nicotine at smaller concentrations can be safely used to advance the therapeutic potential of anti-cancer drugs minimising chemoresistance.

It was important to determine the use of EVs as drug delivery vehicles. Therefore, EVs loaded directly with 5-FU were used to target the PC3 cells as shown in **Figures 4.1, 4.9 and 4.10**. Washing cells after pre-treatment with Bis-I resulted in low apoptosis compared to unwashed condition. This prolonged EV inhibition through Bis-I in the intercellular environment preventing the efflux of 5-FU-EVs from cells causing increased apoptosis. Furthermore, it was well established that the inhibition of EVs increases the drug efficacy compared to treatment solely with the anti-cancer drug. This phenomenon was further explained through apoptosis assays where it was found that the % of annexin-V positive cells increased throughout the 72 h period with a greater increase in the presence of Bis-I + 5-FU compared to the other subjects. There was a natural decline in viable cells by day 3 of the experiment suggesting natural cell death.

It was essential to test the hypothesis using a second anti-cancer drug with a different mode of action. Therefore, Doxorubicin was used in the subsequent array of experiments. Interestingly results further confirmed that inhibition of EVs is crucial to maintain a constant intracellular concentration of chemotherapeutic drug in order to elicit an effective response against the cancer cells. Cl-amidine oncemore was found to be an outstanding EV inhibitor that managed to remarkably reduce the EV biogenesis and release. HPLC, fluorescence microscopy and fluorescence spectrometry data strongly suggested that EV inhibition increased the susceptibility of the cancer cells to DOX. Though changes in drug concentration in cells were increased upon EV inhibition and drug was detected in released EVs, these changes were small as detected by HPLC and fluorescence microscopy (**Figures 4.15 and 4.17**) but significant enough to be noted. Furthermore, there was success in packaging the DOX into EVs compared to producing 5-FU-EVs previously. Enhanced susceptibility of PC3 cells to DOX was shown through a range of techniques to demonstrate the importance of EV inhibition in increasing anti-cancer drug effectiveness. These experiments are very promising, and this approach should be used to advance the development of future cancer drug therapy. Various studies have

concentrated on packaging vesicles and nanoparticles with therapeutic mRNA and various synthetic reagents to target cancer cells (Piktel et al., 2016). Nano-drug delivery can be active or passive. Passive drug delivery is based on the fact that tumor vasculature is characterized by discontinuous epithelium, impaired lymphatic drainage and reduced uptake of the interstitial fluid in contrast to normal blood vessels with firmly sealed endothelium. Subsequent accumulation of macromolecules provides the environment supporting the passive transport of nanotherapeutics to the target site (Bertrand et al., 2014) while active drug delivery involves the binding of ligands on the nanoparticles to surface receptors on target cancer cells (Byrne et al., 2008, Shah et al., 2013). Similar studies have shown that anti-cancer drugs such as Docetaxel (DTX) and Methotrexate (MTX) have been carried in EVs in these particular cases also being quantified through HPLC. The inhibition of the release of such drug-EVs was targeted in xenograft models of prostate cancer with the result of decreasing the rate of increase of the implanted tumour as well as increased apoptosis (Jorfi et al., 2015). Pascucci and co-workers have demonstrated that Mesenchymal stromal cells (MSCs) are able to package and deliver drug through their EVs. This was shown using a MSC murine cell line, SR4987. The release of paclitaxel (PTX) from SR4987 in the conditioned medium (CM) was checked by HPLC and the anti-tumor activity of both CM and EVs was tested on the human pancreatic cell line CFPAC-1 (Pascucci et al., 2014). A similar study on exosome mediated drug delivery has been reported where DOX was packaged into exosomes through electroporation and transferred to α v integrin-positive breast cancer cells *in vitro* as demonstrated by confocal imaging and flow cytometry. The study also showed that the intravenous application of drug-exosomes increased the specificity of the target therapy without overt toxicity (Tian et al., 2014).

HPLC data can be improved by using alternative methods. The mobile phase can be changed accordingly to obtain more clean peaks which can improve the quality of the results. Also, the cells can be treated with the inhibitor and the drug for an extended duration which will increase the drug retainability in the cells giving rise to distinguishable results. Using high-sensitivity HPLC detectors could improve the performance of peak detection and integration for small quantities of materials being analysed. Also using a column with a smaller diameter will enable the analysis of small quantities of the sample which will be an advantage in such studies. Locatelli and peers have suggested other improvements, specifically that ‘the most common choice for improving chromatographic performance is the use of columns packed with low-diameter particles to obtain efficiency improvement, optimal velocity, and mass transfer’ to prevent the pressure build up in the column (Locatelli et al., 2012).

In addition, relative intensities and absorption spectra are hampered by the sensitivity of the absorption and fluorescence properties of most chromophores to their microenvironment. Hence these give rise to environment-specific results (Resch-Genger et al., 2005) which can result in

inaccuracy. Therefore, it is important to standardise the methodology to improve the quality control of the procedure and increase the reliability of the results.

It must be noted that whilst using drug-EVs elicits an apoptotic response it is less compared to direct addition of the drug either in the presence or absence of the inhibitor/inhibitors. However, this can be overcome by using an EV inhibitor at the same time. This not only increases the susceptibility of the cancer cells to the drug but allows the use of very low concentrations of the drug to stimulate the same response in the cells. Of course, the additional benefit of encapsulating the drug within an EV is the protection afforded by an autologous vesicle. This phenomenon can be further tested using different anti-cancer drugs to increase the diversity and reproducibility of the results.

Chapter 5: Cannabidiol is a Novel Inhibitor of Extracellular Vesicle Biogenesis and Release in Cancer Cells

5.0 Cannabidiol (CBD) is a Novel Inhibitor of Extracellular Vesicle Biogenesis and Release in Cancer Cells

5.1 Introduction

CBD is generally safe at therapeutic doses, shows biphasic effects on the immune system, and has demonstrated anti-cancer activity *in vivo* (Massi et al., 2013, Velasco et al., 2016, Velasco et al., 2017). This study therefore aimed to investigate putative modulatory effects of CBD on EV release and to further establish whether CBD had combinatory effects with the recently described EV inhibitor Cl-amidine (Kosgodage et al., 2017, Kholia et al., 2015). For proof of principle three cancer cell lines, prostate cancer (PC3), hepatocellular carcinoma (HEPG2) and breast adenocarcinoma (MDA-MB-231) were used. The effects of CBD on EV release are discussed in this chapter. Our findings suggest a new link between the emerging understanding of anti-cancer effects of CBD and its modulatory effects on EV biogenesis in cancer cells which has been described for the first time by our team (Kosgodage et al., 2018).

Effect of CBD on two glioblastoma cell lines was also assessed. 5 μ M CBD was more effective in other cancer cell lines on EV release compared to 1 μ M, therefore 5 μ M of CBD was used in these tests. It was essential to see the combinatory effect of an EV inhibitor and chemotherapy. Temozolomide (TMZ) is an oral alkylating agent used to treat glioblastoma multiforme (GBM) and astrocytomas (Lee, 2016). It is an imidazotetrazine derivative of the alkylating agent dacarbazine and a prodrug of the anti-cancer drug Temodar. TMZ is known to induce cell cycle arrest at G2/M and to eventually lead to apoptosis and has been widely used in concomitantly with radiotherapy against melanomas as well (Zhang et al., 2012). However this therapy has not always been successful as some glioblastoma cell lines exhibit resistance to TMZ (Perazzoli et al., 2015). As a result it was an idea to investigate whether EVs play a role in driving the resistance mechanism and to whether EV inhibition can overcome this issue. As a consequence the latter part of this section has focussed on EV inhibition in two glioblastoma cell lines, LN229 (TMZ-sensitive) and LN18 (TMZ-resistant). CBD has been used as the EV inhibitor along with TMZ as the anti-cancer drug (Kosgodage et al., 2019).

5.2 Methods

5.2.1 Cell viability assays

EasyCyte 8HT flow cytometer and ViaCount assay were used to count and determine viability of cells before the start of every experiment and to assess cell viability after treatment with EV inhibitors, as previously described (**section 2.6.1**)

5.2.3 Effects on EV biogenesis using Cannabidiol (CBD) and Cl-amidine

For assessment of effects of CBD and Cl-amidine on EV generation, PC3, HEPG2 and MDA-MB-231 cells were seeded at a density of 3.8×10^5 cells/well, in triplicate, in 12-well microtitre plates, using pre-warmed serum- and EV-free RPMI 164. To ensure that the medium was EV free, it was centrifuged at $70,000g / 24$ h and filtered through a $0.22 \mu\text{m}$ pore size membrane before use. The cells were then incubated with CBD (1 or $5 \mu\text{M}$), Cl-amidine ($50 \mu\text{M}$) or with a combination of CBD ($5 \mu\text{M}$) and Cl-amidine ($50 \mu\text{M}$), for 60 min at $37^\circ\text{C} / 5\% \text{CO}_2$, while control cells were treated with either DMSO (0.001%) or serum free-RPMI for CBD and Cl-amidine respectively. The following concentrations of CBD were used: $1 \mu\text{M}$ or $5 \mu\text{M}$ in 0.001% DMSO, based on clinically relevant doses for CBD (Bergamaschi et al., 2011); while Cl-amidine was used at $50 \mu\text{M}$ concentration (in PBS) as previously determined as an optimal dose for maximum EV inhibition in several cancer cell lines (Kosgodage et al., 2017). For testing of a combinatory effect on EV release, CBD was applied at $5 \mu\text{M}$ together with Cl-amidine at $50 \mu\text{M}$ concentrations. After the 1h incubation period, the supernatants from each well were collected from the cell preparations, transferred to sterile 1.5 ml Eppendorf tubes (kept on ice) and centrifuged at $200g$ for 5 min at 4°C to remove the cell debris. The resulting supernatants were kept on ice and subsequently treated for isolation of EVs, as described in (**section 2.5.1**) to include both exosomes and MVs based on previously established protocols (Kosgodage et al., 2017, Kholia et al., 2015). Each experiment was repeated three times and performed in triplicate.

5.2.4 Effect of Temozolomide (TMZ) on Glioblastoma cell lines

A range of concentration of TMZ was tested on both LN18 and LN229 cells for 1h. EasyCyte 8HT flow cytometer and ViaCount assay were used to count and determine viability of cells after the treatment as described in (section 2.6.1).

5.2.5 Effect of CBD on TMZ treatment in LN18 and LN229 cells

LN18 and LN229 cells were seeded at a density of 3.8×10^5 cells/well, in triplicate, in 12-well microtitre plates, using pre-warmed serum- and EV-free RPMI 1640. One set of cells were incubated with CBD 5 μ M for 1h and then treated with TMZ 800 μ M for 1h. The next two sets of cells were either treated with CBD 5 μ M or TMZ 800 μ M alone for 1h. Control cells were treated with DMSO (0.001%). CBD 5 μ M in 0.001% DMSO was used based on clinically relevant doses for CBD (Bergamaschi et al., 2011) and previously established methods in the laboratory. The supernatants from each well were collected from the cell preparations, transferred to sterile 1.5 ml Eppendorf tubes (kept on ice) and centrifuged at 200g for 5 min at 4°C to remove the cell debris. The resulting supernatants were kept on ice and subsequently treated for isolation of EVs, as described in (section 2.5.1) to include both exosomes and MVs based on previously established protocols (Kosgodage et al., 2017). Each experiment was repeated three times and performed in triplicate.

5.3 Results

5.3.1 CBD inhibits EV release in PC3 cells

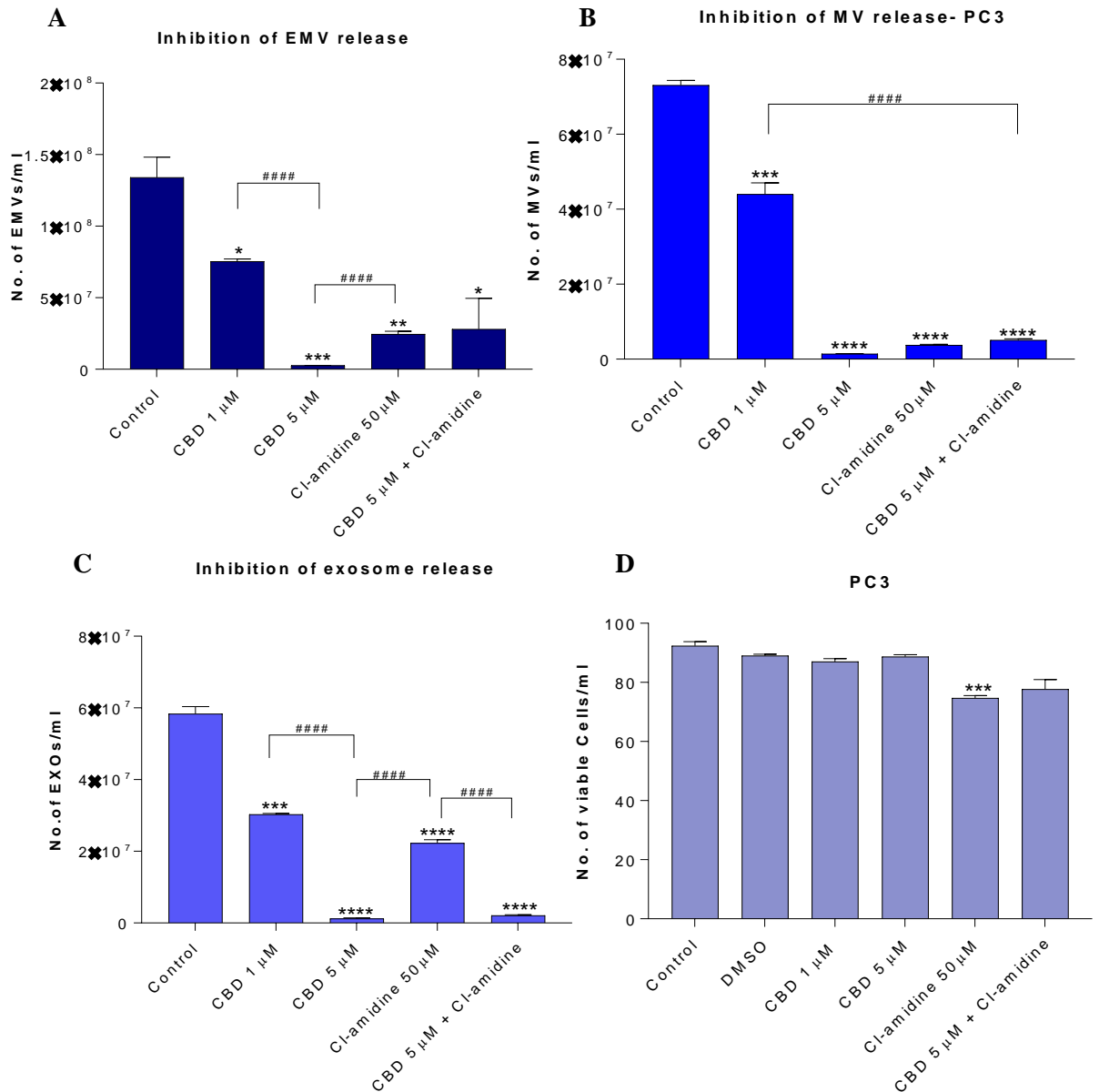


Figure 5.1 Effect of CBD on PC3-derived EV release. A-C, CBD significantly inhibits total EV, exosome and MV release from PC3 EVs represent all vesicles 0-900 nm (A); microvesicles (MV) are 100-900 nm (B) and exosomes are vesicles <100 nm (C); D, Cancer cell viability was not significantly affected by the levels of CBD used in these experiments after 1 h incubation 1 μM CBD resulted in a 5.6% decrease in cell viability ($p=0.1583$), and 5 μM CBD in a 2.2% decrease in cell viability ($p=0.7247$) compared to DMSO. However Cl-amidine resulted in a significant reduction ($p=0.0005$) compared to the treated control cells. The experiments were repeated three times and the data presented are mean \pm SEM of the results (* $p \leq 0.05$; ** $p \leq 0.01$; *** $p \leq 0.001$; **** $p \leq 0.0001$ vs Control; Differences between CBD and Cl-amidine treatment group is further indicated as # $p \leq 0.05$; ## $p \leq 0.01$; ### $p \leq 0.001$; #### $p \leq 0.0001$)

Pre-treatment of PC3 cells with both 1 μ M and 5 μ M CBD, for 1h before EV isolation, resulted in a significant reduction of total EV release compared to the DMSO treated control cells (44.5% and 49.1% reduction of EV release for 1 μ M ($p=0.0149$) and 5 μ M ($p=0.0008$) CBD respectively) (**Figure 5.1A**). The inhibitory effect by 5 μ M CBD on total EV release was greater than observed with Cl-amidine ($p=0.0001$), while Cl-amidine had a significantly stronger EV inhibitory effect than 1 μ M CBD ($p=0.0001$).

When using CBD (5 μ M) in combination with Cl-amidine no additional change in total EV inhibition was found compared to single inhibitors. Analysis of inhibitory effects on exosome, showed that both CBD and Cl-amidine significantly reduced the number of vesicles released compared to untreated PC3 cells (98.0% versus 66.1%; $p=0.0001$ and $p=0.0001$ respectively). A significantly stronger inhibitory effect was observed for 5 μ M CBD than with Cl-amidine ($p=0.0001$), while 1 μ M CBD was less effective, inhibiting exosome release by 51.3% compared to control ($p=0.0002$). Combinatory treatment with 5 μ M CBD and Cl-amidine gave similar results as single CBD (5 μ M) inhibitor treatment (96.6%; $p=0.0001$ compared to control) (**Figure 5.1C**). CBD mediated MV release was significant for both 1 μ M (38.5%; $p=0.0009$) and 5 μ M (98.1%; $p=0.0001$) compared to non-treated control cells, although 5 μ M CBD was significantly more effective than 1 μ M CBD ($p=0.0002$). The effect of 5 μ M CBD alone was similar in reducing MV release as seen for Cl-amidine compared to control cells (95.6%; $p=0.0001$) while combinatory treatment of CBD (5 μ M) and Cl-amidine did not exhibit a further additive effect on MV release (93.6%; $p=0.0001$ compared to control) (**Figure 5.1B**).

Cell viability was not significantly affected by the levels of CBD used after 1h incubation (**Figure 5.1 D**). 1 μ M CBD resulted in a 5.6% decrease in cell viability ($p=0.1583$), and 5 μ M CBD in a 2.2% decrease in cell viability ($p=0.7247$) compared to DMSO treated control cells. In comparison, cell viability was affected to some extent by Cl-amidine (20%; $p=0.0005$ compared to PBS treated control cells).

5.3.2 Effect of CBD on EV release in HEPG2 cells

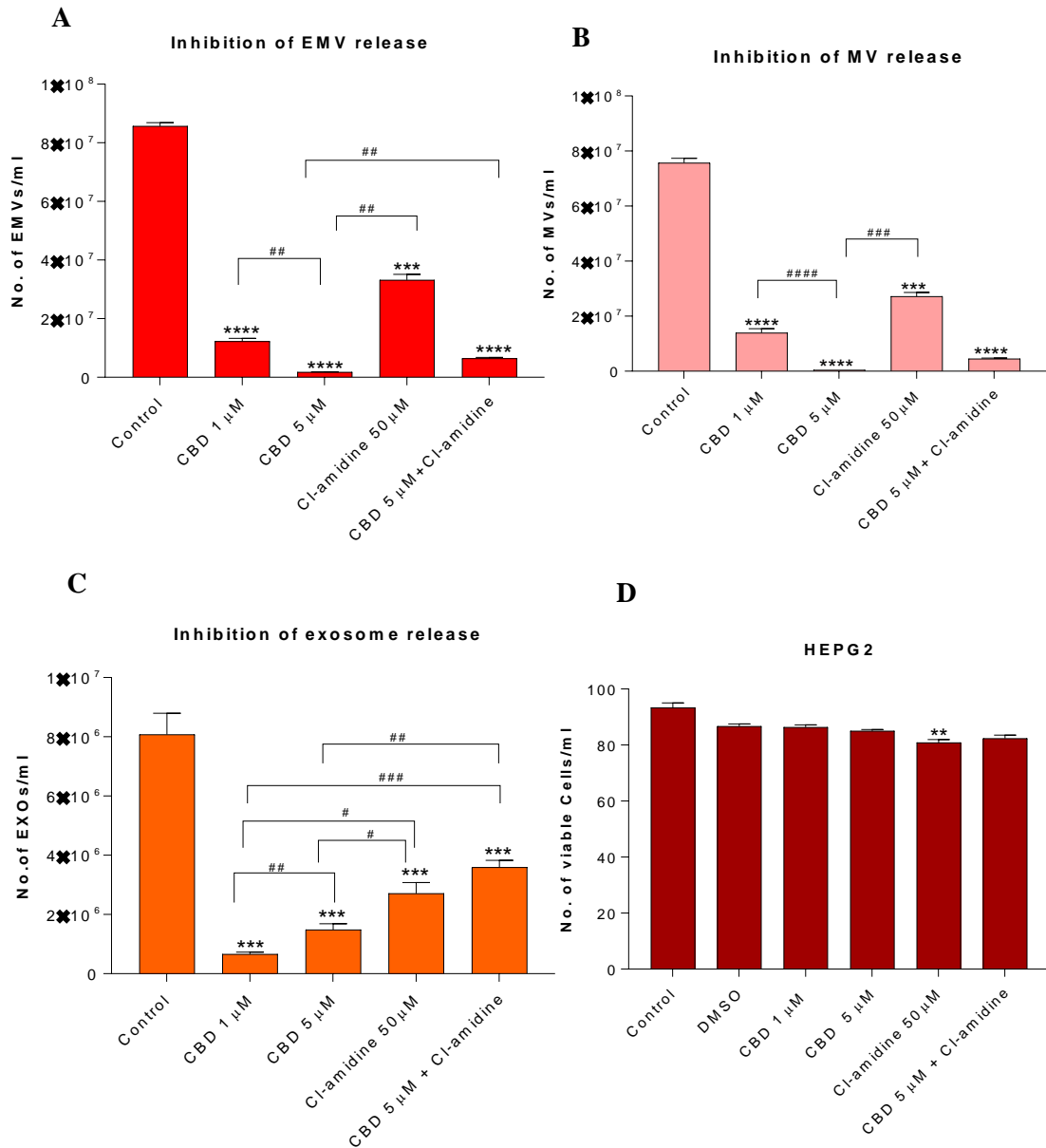


Figure 5.2 Effect of CBD on HEPG2-derived EV release. A-C, CBD significantly inhibits total EV, exosome and MV release from HEPG2 cells. EVs represent all vesicles 0-900 nm (A); microvesicles (MV) are 100-900 nm (B); exosomes are vesicles <100 nm (C). D, CBD does not affect cell viability of HEPG2 cells after 1h treatment. However, Cl-amidine significantly reduces the cell viability ($p=0.0033$). The experiments were repeated thrice and the data presented are mean \pm SEM of the results ($*p \leq 0.05$; $**p \leq 0.01$; $***p \leq 0.001$; $****p \leq 0.0001$ vs Control; Differences between CBD and Cl-amidine treatment group is further indicated as $\#p \leq 0.05$; $\##p \leq 0.01$; $\###p \leq 0.001$; $\####p \leq 0.0001$).

Pre-treatment of HEPG2 with both 1 μ M and 5 μ M CBD resulted in a significant reduction of total EV release compared to the DMSO treated control cells (86.7%; $p=0.0001$ and 97.9%; $p=0.0002$ respectively) and was more potent than for Cl-amidine (61.9%; $p=0.0002$) compared to control (**Figure 5.2A**). Combinatory treatment with 5 μ M CBD and Cl-amidine resulted in a significantly higher inhibition compared to Cl-amidine alone ($p=0.0058$). This was 91.9% ($p=0.0002$) compared to untreated control.

The inhibitory effect of CBD on MVs was significant in HEPG2 cells for both 1 μ M (86.1%; $p=0.0001$) and 5 μ M (99.6%; $p=0.0001$) concentrations of CBD compared to control cells, with 5 μ M CBD being significantly more effective ($p=0.0001$) (**Figure 5.2 B**). MV inhibitory effects of Cl-amidine in comparison were 61.1% compared to control ($p=0.0007$), while combinatory treatment of CBD (5 μ M) and Cl-amidine showed a similar effect on total EV release (96.2%; $p=0.0001$) as CBD alone.

Analysis of inhibitory effects on exosomes showed that both concentrations of CBD (1 μ M and 5 μ M) were more effective (91.6%; $p=0.0005$ and 84.0%; $p=0.0009$; respectively) than Cl-amidine (68.4%; $p=0.0026$). The lower dose of CBD (1 μ M) was the most potent inhibitor of exosome release in this cancer cell type. Combinatory treatment with 5 μ M CBD and Cl-amidine resulted in less exosome inhibition (57.9% compared to control; $p=0.0039$) than any of the single inhibitor treatments (**Figure 5.2C**).

Cell viability of HEPG2 cells was not apparent. Both 1 μ M and 5 μ M CBD caused 1.18% decreased cell viability ($p=0.1890$ and $p=0.2746$ respectively) compared to DMSO treated control cells. Cl-amidine reduced the cell viability by 11% ($p=0.0033$) compared to PBS treated control cells (**Figure 5.2D**).

5.3.3 Effect of CBD on EV release in MDAMB231 cells

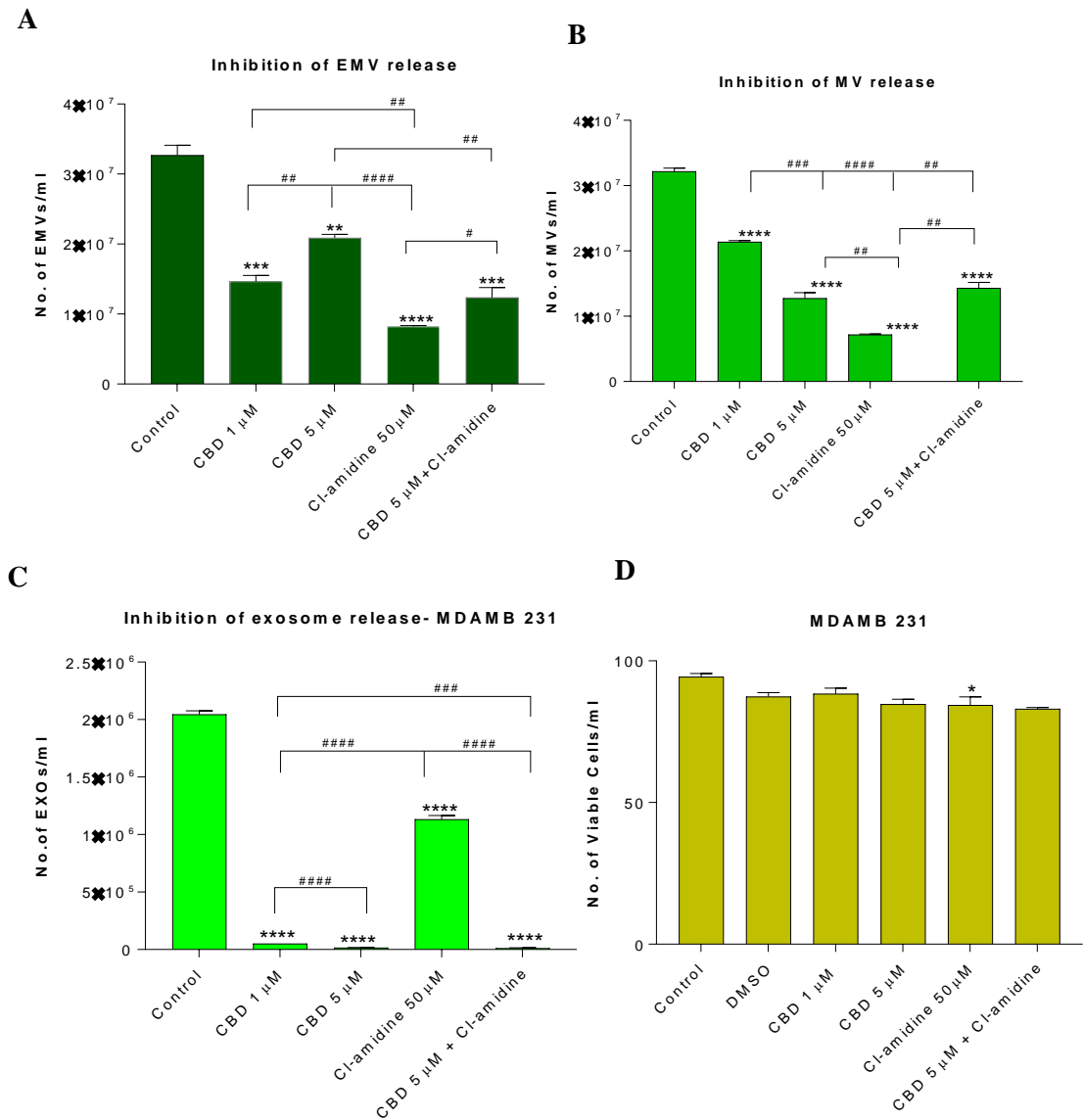


Figure 5.3 Effect of CBD on MDAMB231-derived EV release. A-C, EVs represent all vesicles 0-900 nm (A); MVs are 100-900 nm (B) and exosomes are vesicles <100 nm (C). D, CBD does not affect cell viability of cells after 1h treatment. However, Cl-amidine significantly reduces the cell viability ($p=0.0353$). The experiments were repeated three times and the data presented are mean \pm SEM of the results (* $p \leq 0.05$; ** $p \leq 0.01$; *** $p \leq 0.001$; **** $p \leq 0.0001$ vs Control; Differences between CBD and Cl-amidine treatment group is further indicated as # $p \leq 0.05$; ## $p \leq 0.01$; ### $p \leq 0.001$; #### $p \leq 0.0001$).

Pre-treatment of MDA-MB-231 with CBD resulted in a significant reduction of total EV release compared to the untreated control (53.4%; $p=0.0001$ and 42.9%; $p=0.0001$, respectively) but was a less potent total EV inhibitor than Cl-amidine (75.9%; $p=0.0001$ compared to control). When using CBD (5 μM) in combination with Cl-amidine, a significantly ($p=0.0052$) higher inhibition was observed compared to 5 μM CBD alone, while there was no significant difference compared to 1 μM CBD treatment ($p=0.2474$). Compared to control treated cells the combinatory treatment resulted in a 55.1% reduction of total EVs ($p=0.0006$) (**Figure 5.3A**).

The inhibitory effect of CBD on MVs was significant for both concentrations but seemed to be less effective than Cl-amidine. CBD showed 34.4% ($p=0.0001$) inhibition at 1 μM , and 56.5% ($p=0.0001$) inhibition at 5 μM , compared to control, with 5 μM CBD being a significantly more effective ($p=0.0007$) total MV inhibitor. In comparison, MV inhibitory effects of Cl-amidine were higher, at 77.8% compared to control ($p=0.0001$), while combinatory treatment of CBD (5 μM) and Cl-amidine showed a similar effect on total MV release (52.7%; $p=0.0001$) as 5 μM CBD alone (**Figure 5.3B**)

Analysis of inhibitory effects on exosomes showed that both concentrations of CBD (1 μM and 5 μM) were similarly potent. CBD 1 μM inhibited the EV release by 97.5% ($p=0.0001$) and CBD 5 μM by 99% ($p=0.0001$). This was stronger compared to Cl-amidine which only inhibited exosome release by 46.7% ($p=0.0001$) compared to control treated MDA-MB-231 cells. Combinatory treatment with 5 μM CBD and Cl-amidine resulted in similar effects on exosome inhibition as CBD alone (99.5%; $p=0.0001$) (**Figure 5.3C**). CBD did also not affect MDA-MB-231 cell viability significantly compared to DMSO treated control cells, with a 3.5% decrease observed in 1 μM CBD ($p=0.7090$) and 5.4% decrease in 5 μM CBD treated cells ($p=0.3081$) and by 5.3% for MDA-MB- 231 ($p=0.0353$) in the presence of 50 μM Cl-amidine compared to PBS treated control cells (**Figure 5.3D**).

5.3.4 Optimum concentration of TMZ to treat Glioblastoma cell lines

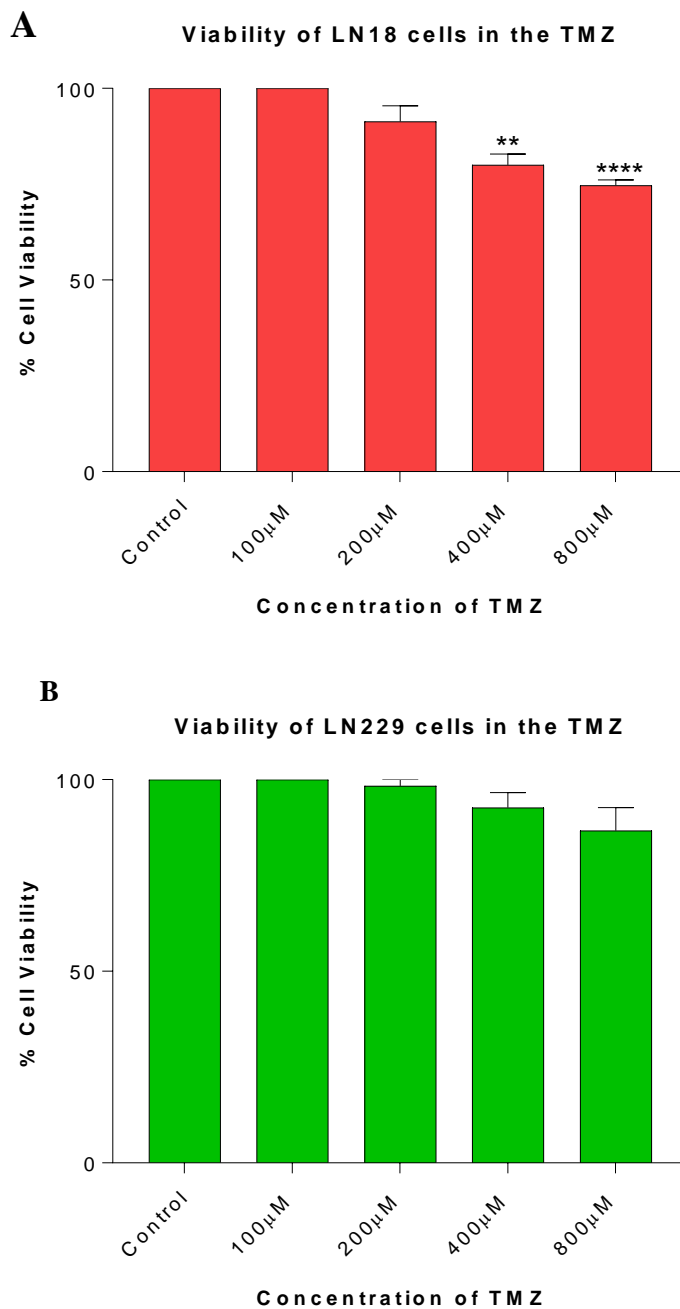
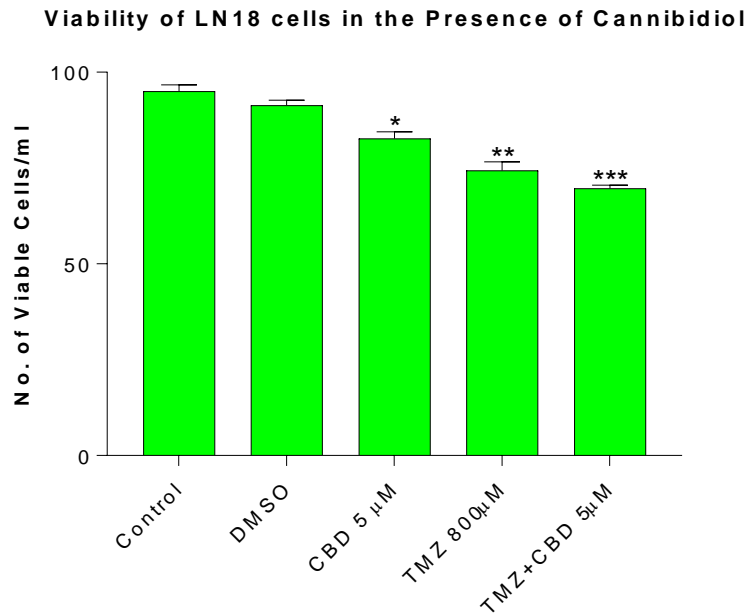


Figure 5.4 GBM cells LN18 and LN229 tolerate similar TMZ concentration. A range of concentrations of TMZ was tested against the GBM cell lines. **A**, LN18 was more sensitive to lower concentration of TMZ compared to LN229. There was a 15% reduction in cell viability in the presence of 400 µM ($p=0.0023$) while the maximum decrease was recorded in the presence of 800µM which was 23 % ($p<0.0001$). **B**, In contrast only 5% decrease was recorded with 800 µM in LN229 which was the maximum ($p=0.0907$). The experiments were repeated three times and the data presented are mean \pm SEM of the results. Therefore, 800µM TMZ was used in subsequent experiments.

5.3.5 Effect of CBD and TMZ treatment on the viability of GBM cells

A



B

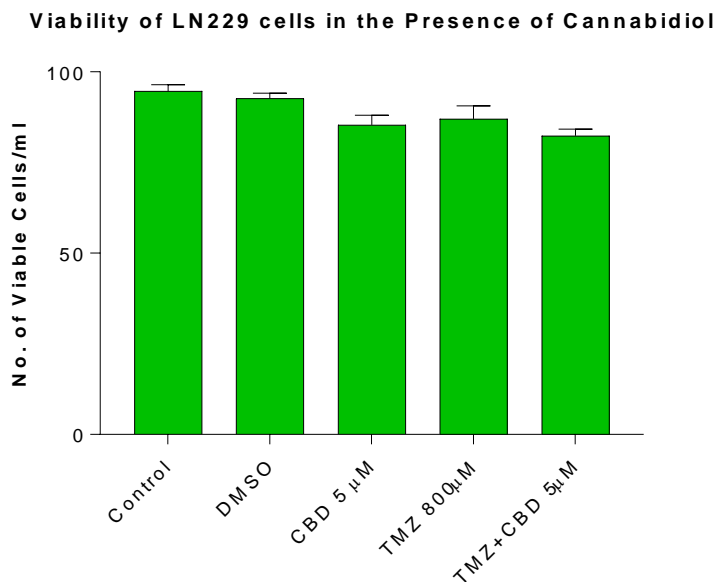


Figure 5.5 Glioblastoma cell viability is minimally affected following CBD and TMZ treatment. A, LN18 exhibited maximum decrease of 27.37% ($p=0.002$) in cell viability following combination therapy. **B,** There was no significant effect on cell viability. Similarly, combination therapy with CBD and TMZ resulted in the maximum reduction in viable cells, 12.77% ($p=0.0085$). The experiments were repeated three times and the data presented are mean \pm SEM of the results.

5.3.4 Optimum concentration of TMZ to treat Glioblastoma Multiforme (GBM) cell lines

In order to determine the optimal concentration, a range of concentrations of TMZ was tested on both LN229 and LN18 cells. LN18 exhibited minimal effect on cell viability in the presence of even the highest TMZ concentration, 800 μ M (23%; $p < 0.0001$). However, both 200 μ M and 400 μ M resulted in 10% and 15% reduction in cell viability respectively ($p = 0.1018$; 0.0023). There was no effect on cell viability in the presence of 100 μ M (**Figure 5.4A**).

In contrast the effect of TMZ on LN229 was low. 800 μ M of TMZ only resulted in a 5% reduction in cell viability ($p = 0.0907$) compared to the untreated control. This was also evident in other concentrations used in the experiment. 200-400 μ M only resulted in 2% and 5% decrease respectively ($p = 0.3739$; 0.1355). Similar to LN18, cell viability was not affected in the presence of 100 μ M (**Figure 5.4B**).

EV inhibition was modulated via CBD while TMZ was used as the anti-cancer drug. CBD had the least effect on cell viability which only reduced by 9.47% ($p = 0.0173$) compared to the DMSO treated control in LN18. However, cell viability was not negatively affected when this effect was compared with that of TMZ (9.76%; $p = 0.0464$) and combinatory therapy (15.85%; $p = 0.0027$). TMZ significantly reduced the cell viability (18.68%; $p = 0.0032$) and a further reduction by 24.18% was seen in the presence of combinatory therapy ($p = 0.0002$).

LN229 cells were less affected by CBD treatment, the cell viability being reduced by 7.61% ($p = 0.0732$). This was however reduced compared to that with TMZ (2.29%; $p = 0.7290$) and combination treatment (3.53%; $p = 0.4081$) while TMZ treatment resulted in a less negative effect on cell viability which was 5.43% ($p = 0.2187$) (**Figure 5.5B**). Combinatory therapy only reduced the cell viability by 10.87% ($p = 0.0118$). These changes were not significant compared to the effect seen on LN18 (**Figure 5.5A**).

5.3.6 Effect of EV inhibition on TMZ-treated LN229 GBM cells

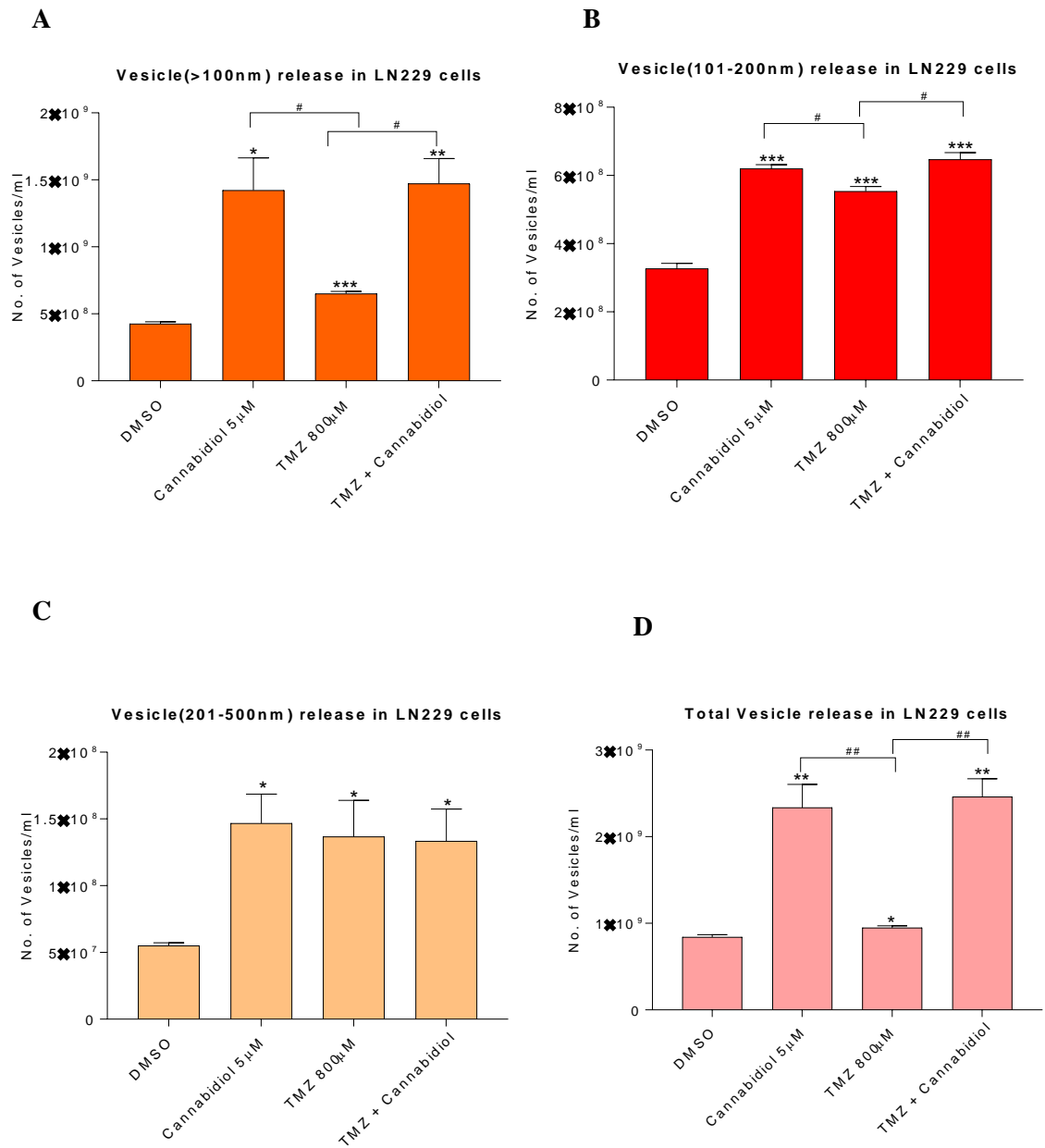


Figure 5.6 CBD modulated vesicle release is increased compared to TMZ treatment in LN229. A-D, suggest that EV inhibition does not affect TMZ in combinatory treatment. However, TMZ alone increases the release of 101-500 nm sized vesicles by 50 % ($p=0.0008$) compared to the control. However sole TMZ treatment reduced <100nm-sized vesicles as well as the total EVs by at least 45% ($p=0.0006$). The combinatory effect of both treatments increased EVs in all subpopulations by at least 49% ($p=0.0316$). EV subpopulations were determined via size-exclusion nanosight analysis (>100nm-exosomes; 101-200 nm and 201-500 nm- MVs). The experiments were repeated three times and the data presented are mean \pm SEM of the results.

Pre-treatment with CBD increased >100nm-sized vesicles compared to the untreated control by 64.88% ($p=0.0144$). It also increased the effect by 15.5% compared to cells treated with TMZ alone and combinatory therapy by 22.48% ($p=0.0326$ and $p=0.8772$). Treatment with TMZ alone did increase the exosome release by 58.44% compared to the control ($p=0.006$) but was less compared to that of CBD and combination (8.26%; $p=0.0115$). Combination therapy stimulated the exosome release by 54.7% ($p=0.0049$) (**Figure 5.6A**).

TMZ stimulated vesicle release the least in all subpopulations compared to the proposed EV inhibitor, CBD. This was also apparent in 101-200nm-sized vesicles which was increased by 40.19% ($p=0.0008$) but was lower than CBD by 17.19% ($p=0.0653$) and combination therapy by 22.06% ($p=0.046$) (**Figure 5.6B**). CBD stimulated the vesicle release by 50.47% ($p=0.0001$) which was higher than the combination therapy by 5.88% although not significant ($p=0.3169$). The stimulation of vesicles in the presence of both CBD+ TMZ was lower compared to exosomes but was increased by 53.38% compared to the untreated control ($p=0.0002$)

Figure 5.6C resulted in the highest stimulation of vesicles by sole TMZ treatment which was by 49% ($p=0.0406$) but was low compared to CBD (16.67%; $p=0.7891$) but had no difference compared to the combination therapy. CBD was again the highest in stimulating vesicle release. It stimulated a 57.5% increase compared to the control and 16.67% compared to the combined treatment ($p=0.0140$ and $p=0.7025$ respectively). Combination therapy increased the vesicle release by 49% which was similar to TMZ alone ($p=0.0316$).

Total EVs were further increased by CBD by 60.38% ($p=0.0051$) compared to the control which was higher than TMZ (40.95%; $p=0.006$). Combination therapy stimulated the total EVs by 62.18% ($p=0.0015$). Although not significant, this was higher than CBD by 4.55% ($p=0.7339$). This was however lower than sole TMZ treatment by 43.64% ($p=0.0020$). TMZ inhibited the stimulated EV release by 32.9% ($p=0.0392$) compared to the control. Total EVs were stimulated in the presence of all treatments (**Figure 5.6D**).

5.3.7 Effect of EV inhibition on TMZ-treated LN18 GBM cells

Pre-treatment with CBD decreased >100nm-sized vesicles significantly compared to the untreated control by 28.95% ($p=0.0066$). It also reduced the effect by 19.8% compared to cells treated with TMZ alone and combinatory therapy by 19% ($p=0.0255$ and $p=0.0376$). Treatment with TMZ alone did increase the exosome release by 11.4% compared to the control ($p=0.4978$) but was less compared to that of combined treatment (17.69%; $p=0.2471$). Combination therapy stimulated the exosome release by 12.28% ($p=0.3827$) (**Figure 5.7A**).

CBD was a pan-inhibitor of LN18-derived vesicles. This was also apparent in 101-200nm-sized vesicles which was reduced by 23.96% ($p<0.0001$). The inhibition achieved was also lower than sole TMZ treatment by 2.26% ($p=0.2378$) and combination therapy by 19.35% ($p<0.0001$) (**Figure 5.7B**). TMZ also inhibited the vesicle release by 20.21% ($p=0.0003$) which was higher than CBD (2.26%; $p=0.2378$) but lower than the combination therapy by 44.58% which stimulated the vesicle release ($p=0.0002$). The stimulation of vesicles in the presence of both CBD+ TMZ was 4.17% compared to the untreated control ($p=0.4818$)

Both CBD and combinatory treatment significantly inhibited the vesicle release. TMZ was the only vesicle stimulator. Vesicle release was increased by 1.1% ($p=0.7160$) but was significantly higher compared to CBD (55%; $p=0.0010$) and by 59.44% ($p=0.0010$) compared to the combination therapy. CBD stimulated the vesicle release by 55.56% ($p=<0.0001$). However, it was lower than the inhibitory effect in the presence of both CBD and TMZ treatment by 12.5% ($p=0.0363$) which was 61.11% compared to the DMSO control ($p=<0.0001$) (**Figure 5.7.C**).

Total EVs were further reduced by TMZ treatment alone by 56.17% ($p=0.0001$) compared to the control. This inhibitory effect was however significantly higher than that exerted by CBD (24.64%; $p=0.0012$) and exhibited opposing effects to combination therapy which increased the total EVs by 60% compared to sole TMZ ($p=<0.0001$) and by 10.26% ($p=0.0724$) compared to the untreated control. This was higher than CBD by 46.15% ($p<0.0001$). CBD also inhibited total EVs by 40% ($p=0.0002$) compared to the control. Total EVs were inhibited in the presence of CBD and TMZ on its own but was stimulated in the presence of the reagents in synergy (**Figure 5.7D**).

5.3.8 Size exclusion analysis of vesicle release in GBM cell lines

The results suggest that overall vesicle release is significantly higher in TMZ-sensitive LN229 cells compared to the TMZ-resistant LN18 cells (**Figure 5.8**). This is apparent in all subpopulations. Total EV release was decreased by 11.97% ($p= 0.0385$). Although not significant, the lowest reduction was seen with the MV population in the 101-200 nm range which was just 11.03% ($p=0.4103$). <100nm-sized vesicle release in LN18 was reduced by 17.38% compared to that released by LN229 ($p=0.0005$). LN229 had a significant increase in 201-500nm-sized MV release by 57.59% compared to LN18 ($p=0.0006$).

5.3.7 Effect of EV inhibition on TMZ-treated LN18 GBM cells

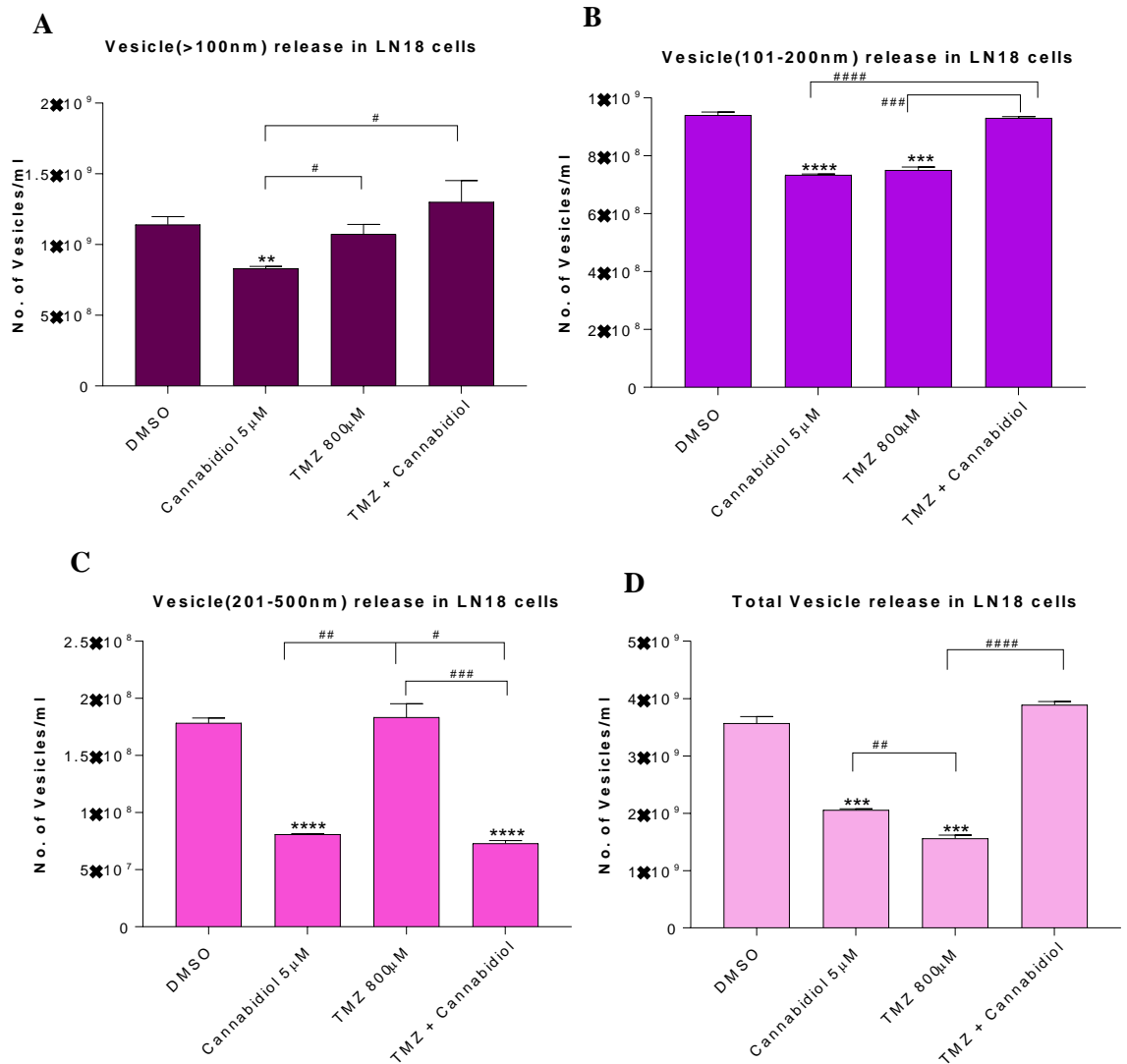


Figure 5.7 CBD modulated vesicle release is decreased compared to the TMZ treatment in LN18. A-D, CBD significantly inhibited the vesicle release in all subpopulations by 25% with the highest recorded in 201-500nm vesicles which was 55.56% ($p < 0.0001$). Total EVs were reduced by 56.17% ($p = 0.0001$) following TMZ treatment. Nevertheless, combined effect of CBD and TMZ increased the overall EV release by at least 10% with the exception of the 201-500 nm subpopulation which resulted in a significant reduction of 61.11% compared to the control ($p < 0.0001$). EV subpopulations were determined via size-exclusion nanosight analysis (>100nm-exosomes; 101-200nm and 201-500nm- MVs). The experiments were repeated three times and the data presented are mean \pm SEM of the results.

5.3.8 Comparison of Size Exclusion Vesicle release in GBM cell lines

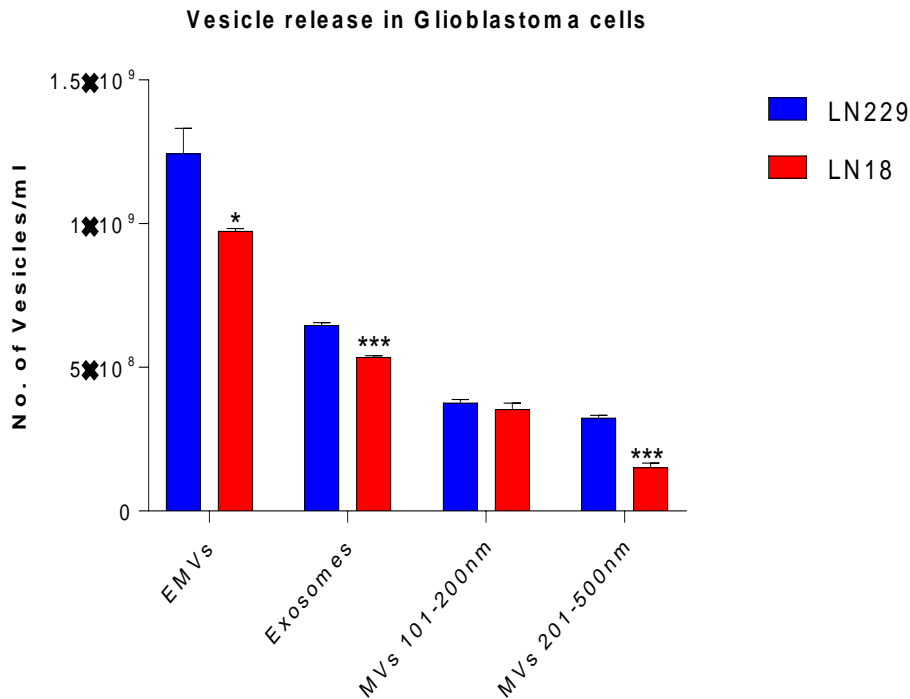


Figure 5.8 LN18-derived EV release is significantly lower than TMZ-sensitive LN229. There is an overall reduction in the release of all vesicle subpopulations in LN18 compared to LN229. However, 201-500 nm-sized vesicle release is lowest, at 57.59%, compared to the rest of the groups ($p=0.0006$). There was only 11.03% reduction in 101-200nm-sized vesicle release which was not statistically significant. Total EVs were only affected by 11.97% ($p=0.0385$). EV subpopulations were determined via size-exclusion nanosight analysis (>100nm-exosomes; 101-200 nm and 201-500 nm- MVs). The experiments were repeated three times and the data presented are mean \pm SEM of the results.

5.4 Discussion

This chapter discusses a novel and potential inhibitor of EV release in cancer cell lines which is also a novel finding for functions of CBD. The different cancer cell lines tested here (prostate cancer PC3, hepatocellular carcinoma HEPG2, breast adenocarcinoma MDA-MB-231, GBM cell lines, LN18 and LN229) showed that CBD consistently inhibited exosome release and also had significant, although more variable, modulating effects on MV release. This study was the base for the recently published research findings (Kosgodage et al., 2018, Kosgodage et al., 2019) that highlights this novel function of CBD on EV release for the first time. This is of high relevance for optimised therapeutic application in various EV-mediated pathologies.

There has been a significant interest in EV inhibition during the past few years as it plays a considerable role in metastasis and other EV-associated disease statuses. This has been reported throughout this work by comparing the efficacy of different pharmacological agents in inhibiting EV biogenesis and release. Published research findings from the previous chapters of this study as well as previous work carried out in the same laboratory have outlined the importance in using EV inhibition as a novel therapeutic strategy (Kholia et al., 2015, Kosgodage et al., 2017). Here, the impact of PAD inhibition on prostate cancer was highlighted using Cl-amidine and 5-FU as well as MTX as anti-cancer drugs. Furthermore, novel EV inhibition pathways were introduced to the field which have shown success compared to that were previously experimented. Many researches have been conducted to increase sensitisation of cancer cells to chemotherapy. Consequently, the presented study on CBD was an interesting approach to develop a novel EV inhibition pathway.

As shown in the results, CBD has consistently affected the EV profiles of different cancer cells tested. However its effect was significant in exosome inhibition while MV subpopulations varied. This EV modulation was in some instances more potent than Cl-amidine. It was also interesting to observe different effects on different EV subpopulations that differed between the cancers. In PC3 cells, 5 μ M of CBD was more effective than 1 μ M CBD in inhibiting total EVs, exosomes and MV subpopulations. In the HEPG2 hepatocellular carcinoma cells 5 μ M CBD had the main impact on total EV and MV release, while 1 μ M CBD most significantly affected exosome release. Overall, the potency of CBD to inhibit all subsets of EVs tested here was most marked in the HEPG2 cells. In MDA-MB-231 cells the inhibitory effect of CBD was particularly marked for exosome release, while total MV release was less inhibited by CBD compared to Cl-amidine (Kosgodage et al., 2019).

Recent studies in this invasive breast cancer cell line have suggested an active role of exosomes in increased cell movement and metastasis (Harris et al., 2015). The increase in MVs released in response to CBD treatment was specific for the MDA-MB-231 cells. This may indicate a higher

sensitivity of this particular cancer cell line to CBD and may also be a sign of pseudoapoptotic responses, where increased membrane permeability and leakage of reactive oxygen species (ROS) and other apoptotic factors is still low enough for the cell to turn the apoptosome into MVs for export of hazardous agents via pseudoapoptosis (Kosgodage et al., 2018, Inal et al., 2012). Using a combination therapy of CBD and Cl-amidine resulted in different effects on the various EV subsets and varied between the three cancer cell lines. In general, Cl-amidine did not have additive effects on the inhibitory effect of EV release compared to CBD alone, while the combinatory treatment was more effective on some subsets than Cl-amidine alone, as was observed on exosome release in PC3 cells and on MV release in HEPG2 cells. Similarly, combinatory treatment did not show more effect than CBD or Cl-amidine alone on exosome release from HEPG2 cells.

Interestingly, in MDA-MB-231 cells, Cl-amidine counteracted the increased CBD-mediated release observed for the total EVs when used in combination, bringing the amount of vesicles release below the level of sole CBD treatment. Overall the results presented here suggest that the two EV inhibitors act on different pathways involved in MV and exosome release. While previously, Cl-amidine has been shown to act on MV biogenesis via increased cytoskeletal actin deimination and nuclear PAD translocation, indicative of changes in histone deimination (Kholia et al., 2015), CBD may act in part through modulation of mitochondrial metabolism as described earlier (Kosgodage et al. 2018).

The application of CBD in EV inhibition was further tested using GBM cell lines, LN18 and LN229. Previously, CBD has been shown to enhance effects of TMZ (Torres et al., 2011). In this study we also have used TMZ in conjunction with CBD to study the effect of CBD-mediated EV inhibition on the GBM treatment. Previously conducted research confirmed that the anti-cancer drug itself stimulated the EV release in the presence of DOX and 5-FU (Lange et al., 2017b, Aubertin et al., 2016). However, an opposing effect was visualised in TMZ-sensitive LN229 cells where EV release was inhibited following TMZ treatment alone. This was true in all subsets of EVs. CBD did not act as an inhibitor in this cell line which promoted hyper-vesiculation in the presence of combined treatment with CBD and TMZ. In contrast, TMZ stimulated the EV release in all EV subpopulations (exosomes and MVs) but the TMZ-resistant cell line, LN18, exhibited the previously demonstrated phenomenon, TMZ stimulating EV release in exosomes and MV subpopulations. This also portrayed significant EV inhibition in the presence of CBD compared to the control treatment. Nevertheless, only the large MV subset (201-500nm) revealed a significant decrease in EVs in the presence of combined therapy which may indicate pseudoapoptotic responses. In addition, both cell lines varied in the proportional amounts of total EVs, MVs and exosomes released under standard conditions (**Figure 5.8**). LN229 resulted in a significant release of vesicles in all subpopulations compared

to LN18. Further work on miRNA profiling and other cargo profiling of these vesicle subtypes will have to be carried out to confirm whether LN229 vesicles contain for example protective miRNAs which would further support the observations made so far (Kosgodage et al., 2018b, Kosgodage et al., 2019).

However, from the results observed, the TMZ-resistant LN18 responded to CBD treatment favourably. This suggests that CBD-EV inhibition can certainly overcome the TMZ resistance in this cell line and encourages further testing to investigate both *in vitro* and *in vivo*.

The expanded repertoire of EV inhibiting agents, including CBD along with its sensitising effects on cancer cells to cisplatin-mediated apoptosis (Kosgodage et al. 2018), indicates a therapeutic potential for sensitisation of cancer cells to chemotherapy, as has been demonstrated for other promising EV inhibitors (Vader et al., 2014, Nishida-Aoki et al., 2017, Kholia et al., 2015, Kosgodage et al., 2017). Importantly, such EV-modulating agents could be used to circumvent the use of high doses of chemotherapeutic drug minimising its side effects but enhancing effective inhibition of tumour growth *in vivo*. The results in this chapter have shown the ability of CBD to inhibit EV release. However further work will have to be carried out to fully understand its beneficial EV-mediated effects in cancer therapy.

Chapter 6: Isolation of Bacterial Outer Membrane Vesicles (OMVs)

6.0 Isolation of Bacterial Outer Membrane Vesicles

6.1 Introduction

The research focus on bacterial outer membrane vesicles (OMVs) has grown rapidly in the recent years. Using nanovesicles as drug delivery vehicles has fascinated researchers in the EV field. Therefore using OMVs in targeted therapy and in drug delivery has encouraged the development of such new therapies. Wang and colleagues have demonstrated its use in vaccine development (Wang et al., 2018) while Gujrati and co-workers have demonstrated the importance of its use in drug delivery against cancer cells. Bioengineered bacterial OMVs of a mutant strain of *E.coli* with low immunogenicity were used to kill cancer cells (Gujrati et al., 2014) in a cell-specific manner by delivering small interfering RNA (siRNA) targeting kinesin spindle protein (KSP). These vesicles were engineered to generate OMVs displaying a human epidermal growth factor receptor 2 (HER2)-specific affibody in the membrane as a targeting ligand (Gujrati et al., 2014). The advantages of using OMVs in therapy have been highlighted in a recent study by Bitto and Kaparakis-Liaskos (Bitto and Kaparakis-Liaskos, 2017). 'Natural immunogenicity and self-adjuvanting capability' (Bitto and Kaparakis-Liaskos, 2017), controls cell and antibody-mediated immune responses. These, together with its cost-effectiveness to produce, temperature-stability, and safety when used in humans make them more potent to be used as vaccines.

OMVs have been widely used as neoadjuvants. The recent rise in the incidence of whooping cough has resulted in the use of *Bordetella pertussis*-OMV vaccines compared to the current approved whole cell *B. pertussis* vaccine which showed a rise in humoral response in mice (Raeven et al., 2016, Gaillard et al., 2014). Similarly, increasing antibiotic resistance in cases of *Staphylococcal* infections has encouraged *S. aureus* vaccine studies. It also reported that vaccination of mice with *S. aureus* OMV resulted in much stronger cell-mediated and humoral responses (Choi et al., 2015). The inclusion of a lipid functional group attached to the target protein that drives membrane tethering or fusion of the target protein directly to a transmembrane OM protein has been described as the mechanisms for anchoring desired pharmacological reagents (Alves et al., 2016b).

PAD catalyses the citrullination of arginine residues and has been found in *Porphyromonas gingivalis* (*P.gingivalis*), a Gram-negative bacterium that causes chronic periodontitis (Gully et al., 2014a, Maresz et al., 2013). The association of PADs in *P.gingivalis* has opened new avenues for research by linking different disease statuses such as oral cavity disease to rheumatoid arthritis. However no significant data is available to confirm the presence of PAD in the *E.coli* genome, also a Gram-negative bacterial species, although arginine deiminase has

been identified. The deiminating activity of arginine deiminase of *E.coli* has though not been shown until in this thesis. Association of PAD inhibitors of EV release and thus potential effects on arginine deiminase in OMV release, led to the current study to evaluate an effect of PAD inhibition on OMV release in *E.coli*.

Previous research findings demonstrate the effect of EV inhibition on enhanced cancer therapy successfully. This together with rapid advancements in the therapeutic use of OMVs has encouraged the direction in this chapter to apply OMV inhibition to develop their therapeutic potential by minimising multi-drug resistance associated with such treatment. This will also increase the sensitisation of the cells to OMV-mediated drug delivery and adjuvant therapy which will be an innovative approach for the establishment of an OMV-targeted treatment. This section of the study has utilised *E.coli* and *S.aureus* to isolate OMVs and identify their characteristics. The latter part of the chapter has focussed on pharmacological OMV inhibition in both Gram-positive and Gram-negative bacteria with the idea to exploit this in successful improvement of antibiotic and phage therapy.

6.2 Materials & Methods

6.2.1 Maintenance of *E.coli* cultures

E.coli cultures were maintained by plating on Müeller-Hinton agar plates and sub culturing was performed each week. *S. aureus* were maintained in nutrient agar plates and subculturing was performed each week.

6.2.2 Preparation of Outer Membrane Vesicles (OMVs)

Two different methods were used as suggested in the literature to prepare *E.coli*- OMVs. However subsequent experiments utilised ultracentrifugation method. *S.aureus*- OMVs were prepared using ultracentrifugation method in experiments.

6.2.2.1 Centrifugation Method

Bacteria were allowed to grow for 24h at 37°C and 5% CO₂ and OMV isolation was carried out. OMVs were isolated from the supernatant of the bacterial culture medium which was initially centrifuged once at 400 g for 10 min to remove the cells. The resultant supernatant was then centrifuged again at 4000g this time for 1h at 4°C to remove cell debris. The resultant supernatant was centrifuged at 25,000g for 1h at 4°C. The isolated OMV pellet was resuspended in ultracentrifuged and sterile filtered (0.22µm) DPBS and centrifuged again at 25,000g for 1h at 4°C to remove proteins such as albumin possibly bound to the OMV membrane surface. The OMV pellet was resuspended in sterile filtered (0.22µm) PBS and the isolated OMVs then used immediately or stored at -80°C for future experiments. For OMV associated experiments the

bacterial growth medium and DPBS was used after ultracentrifugation at 75,000 g for 24h to obtain a medium minimally contaminated with vesicles.

6.2.2.2 Ultrafiltration Method

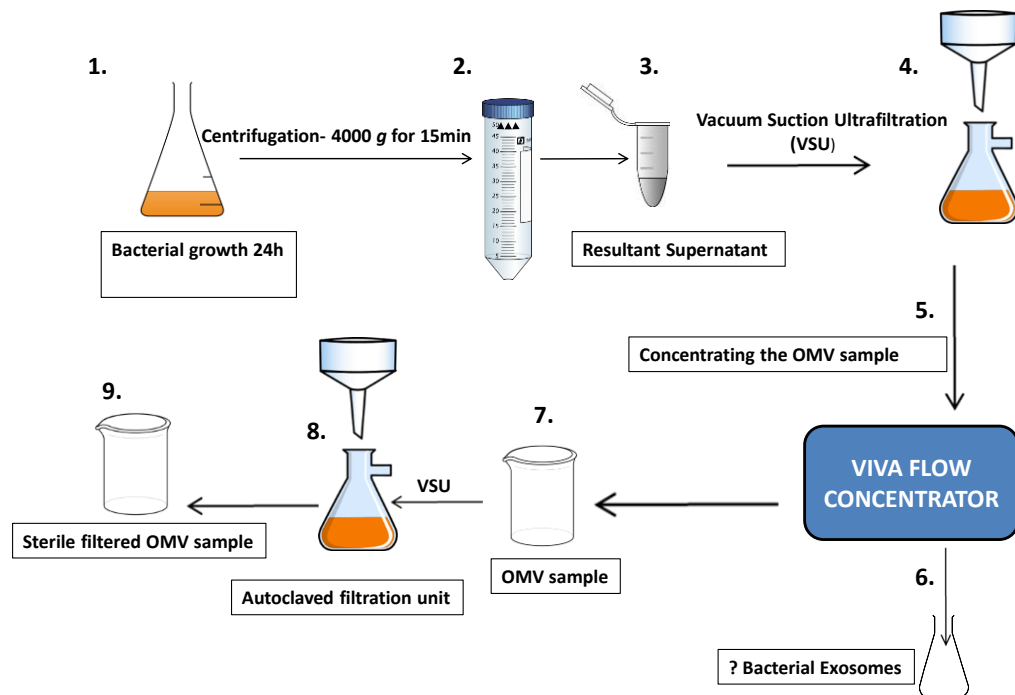


Figure 6.1 Ultrafiltration method of OMV isolation. The diagram shows the steps of OMV isolation through ultrafiltration. The product of step 6 was assumed to be exosome-like vesicles which were quantified as shown in (Figure 6.2.1) and (Figure 6.2.2). Between step 8 and 9, the filtration unit was autoclaved to ensure a sterile filtrate of OMVs was obtained.

Bacterial samples were allowed to grow for 24 h and then centrifuged at (4000 g for 15 min) to remove intact bacteria. The resultant supernatant was subject to vacuum suction filtration using a vacuum pump method. Concentration of the culture filtrate was performed through pumping the filtrate through a viva flow concentrator to ensure the OMV sample was concentrated sufficiently and to allow accurate quantification. The filtrate was assumed to contain bacterial exosomes and was sterile filtered using a 0.22µm sterile filter. The remaining supernatant was subject to a subsequent vacuum suction filtration this time using the autoclaved unit to ensure a sterile OMV sample was obtained. Both samples were quantified using the nanosight LM10.

6.2.3 Immunoprecipitation (IP)

To determine the proteins that had been citrullinated by the PAD enzymes when stimulated for microvesiculation, cell lysates from *E.coli* and *E.coli*-derived OMVs were immunoprecipitated

(Catch and Release v2.0 IP kit, Millipore) with the pan-citrulline F95, PAD2, PAD3 and PAD4 antibodies.

6.2.3.1 Materials and Reagents

- 1x Wash buffer - Diluted from 10X catch release buffer (provided in kit)
- Spin columns
- Capture tubes
- 1.5 ml microcentrifuge tubes (Eppendorf)
- Antibody affinity ligand - provided in the kit
- F95, PAD2, PAD3 and PAD4 antibodies
- Denaturing elution buffer with β -Mercaptoethanol (5% v/v) added immediately before use.
- Milli-Q water – For dilution of throughout, wash and elution buffers

6.2.3.2 IP Protocol

Spin columns, capture tubes and 1.5 ml microcentrifuge tubes to be used were labelled. Caps and snap-off plugs located at the bottom of the spin columns were removed and stored for later use. Individual spin columns were then inserted into individual capture tubes and centrifuged at 2000 g for 30 s to remove the resin slurry buffer. The columns were then washed twice with 405 μ l of 1x wash buffer (provided in kit) at 2,000 g for 30 s. The snap-off plugs removed earlier were then plugged back into the spin columns.

As per the manufacturer's directions a volume of combined reagents had to be determined to add to the spin columns as follows: 528 μ g of *E.coli* cell lysate and 54.45g of OMV lysate, 5 μ l of F95, PAD2, PAD3 and PAD4 antibodies, affinity ligand (10 μ l - fixed volume) and 1x wash buffer (the volume of which was adjusted to 500 μ l final volume). After determining the volumes required for each of the reagents mentioned above, they were added in the respective spin columns in the following order: 1x wash buffer, cell lysate, primary antibodies, and antibody capture affinity ligands. The spin columns were then capped and incubated at 4°C on a rotator overnight.

Post incubation, the spin columns were inserted in capture tubes with the snap-off plugs removed and centrifuged at 2,000 g for 30s. The flow-through was transferred to 1.5 ml microcentrifuge tubes and stored at -20°C for later analysis. The columns were then washed

three times with 400 µl of 1x wash buffer spinning at 2,000 g for 30s. Each of the washes were collected in one tube and stored at -20°C for later analysis if required.

The columns were then placed in fresh capture tubes and the protein eluted by adding 250 µl of 1x denaturing elution buffer containing 5% β-Mercaptoethanol and centrifuging at 2,000 g for 30 s. For maximum recovery of the protein a successive elution step was carried out with 4x denaturing buffer instead. The eluate was then stored at -20°C for Western blot analysis.

E. coli and *E. coli*-OMVs were washed three times with cold PBS at 400 g for 5 min and lysed with B-PER buffer (as per **section 2.2.6**). 528 µg of *E. coli* cell lysate and 54.45g of OMV lysate were then immunoprecipitated with antibodies and eluate analysed for deiminated proteins by immunoblotting.

6.2.4 Western blot analysis of citrullinated/deiminated proteins from *E. coli* and *E. coli*-derived OMVs

In order to compare protein profiles of citrullinated proteins between *E. coli* and *E. coli*-OMVs, cell and vesicle lysates were subjected to Western blot analysis. Briefly, 50 µg of cell lysates were separated by SDS-PAGE using 4–20% Mini-Protean TGX protein gels (BioRad, U.K) and transferred to a nitrocellulose membrane as per (**section 2.9.1-2.9.4**). Western blotting using PAD2, PAD3, PAD4, as well as the monoclonal F95 mouse IgM antibody, that was raised against a deca-citrullinated peptide and specifically detects protein citrulline (Nicholas and Whitaker, 2002), for the detection of putative deiminated/citrullinated sites in *E. coli* and *E. coli*-OMVs. Approximately 5 µg of protein was loaded per lane, even loading being assessed using Ponceau S staining (Sigma, U.K.); membranes were thereafter blocked in 5% bovine serum albumin (BSA) in Tris buffered saline with 0.01% Tween20 (TBS-T) for 1 h, followed by incubation at 4 °C overnight with the primary antibodies (F95 [1:2000], PAD2[1:1000], PAD3[1:1000], PAD4 [1:1000] (BioRad, U.K). Membranes were then washed three times in TBS-T, incubated at room temperature for 1 h with HRP-conjugated secondary antibodies (anti-mouse IgM –F95 and anti-rabbit IgM-PAD4 1:4000 (BioRad, U.K.), followed by six washes in TBS-T before visualisation with ECL (Amersham, U.K.). Membranes were imaged using the UVP transilluminator (UVP BioDoc-IT™ System, U.K.).

6.2.5 Mass Spectrometry analysis of citrullinated/deiminated proteins from *E. coli* and *E. coli*-derived OMVs

In order to identify proteins that were citrullinated during OMV release, 54.45 µg of *E. coli* cell lysate and OMV lysate were immunoprecipitated with F95 and PAD4 antibody and eluted with 250 µl of non-denaturing buffer four times successively for maximum recovery of protein. The eluate was then subjected to mass spectrometry analysis as per (**section 2.10.7**).

6.2.6 Effect of pharmacological EV Inhibitors on *E. coli*-OMV Release

E. coli was cultivated using EV-free Mueller-Hinton broth for 24h. The cells were washed at 4,000g for 10min and seeded in triplicate in micro centrifuge tubes. EGTA (1.5mM), Bisindolylmaleimide-I (10 μ M), Imipramine (25 μ M), Y27632(1 μ M) and D-pantethine(1mM) were added in triplicate and incubated for 1h at 37°C in 5% CO₂. OMV isolation was carried out according as described earlier(**section 5.2.1.1**).The experiment was repeated thrice and the OMVs were quantified using NTA analysis (Nanosight LM10).

6.2.7 Effect of pharmacological PAD inhibitors on *E. coli*-OMV Release

E. coli cultures were prepared as mentioned before(**section 6.2.2**). PAD2 inhibitor AMF30a (5 μ M), PAD4 inhibitor, GSK199 (10 μ M) and pan PAD inhibitor, Cl-am(50 μ M) were added in triplicate and incubated for 1h at 37°C in 5% CO₂. OMV isolation was carried out according to **section 6.2.2.1**.The experiment was repeated thrice and the OMVs were quantified using NTA analysis (Nanosight LM10).

6.2.8 Effect of pharmacological EV and PAD inhibitors on *S. aureus*- OMV Release

S. aureus cultures were prepared as mentioned above(**section 6.2.2**). Both pharmacological EV and PAD inhibitors were added in triplicate and incubated for 1h at 37°C in 5% CO₂. OMV isolation was carried out according to **section 6.2.2.1**.The experiment was repeated thrice and the OMVs were quantified using NTA analysis (Nanosight LM10).

6.3 Results

6.3.1 Isolation of Bacterial OMVs

Ultrafiltration and ultracentrifugation have widely been used in OMV isolation. The data presented both in (**Figure 6.2.1**) and (**Figure 6.2.2**) suggests that ultrafiltration is efficient in the isolation of differently sized particles. However, using the centrifugation method has appreciated the abundance of both exosome-like vesicles (OEXos) and OMVs in samples. Nevertheless, ultrafiltration has resulted in a higher yield of vesicles compared to centrifugation. The experiments described henceforth have utilised the centrifugation method as it was important to see the effect on vesicles as a general population.

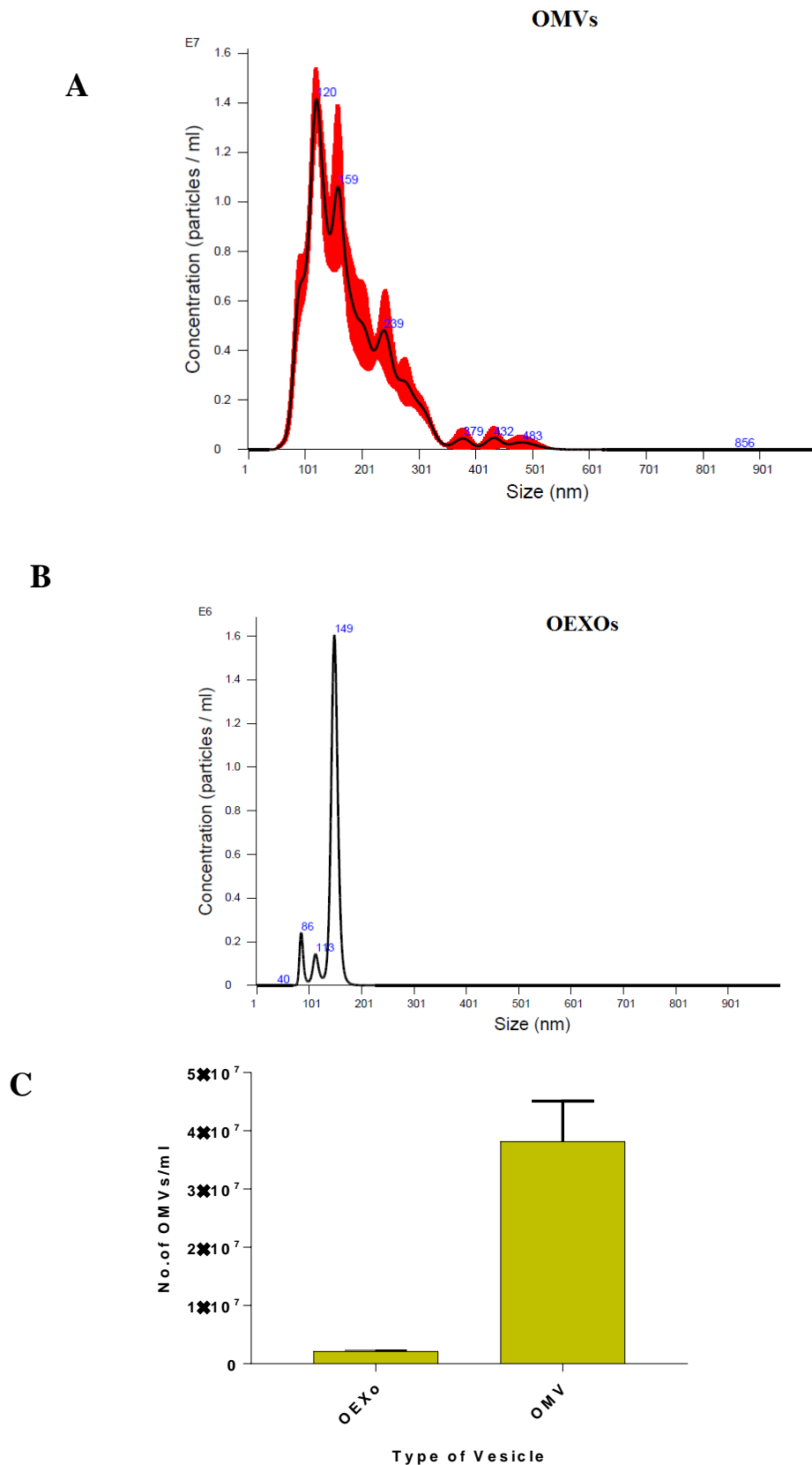
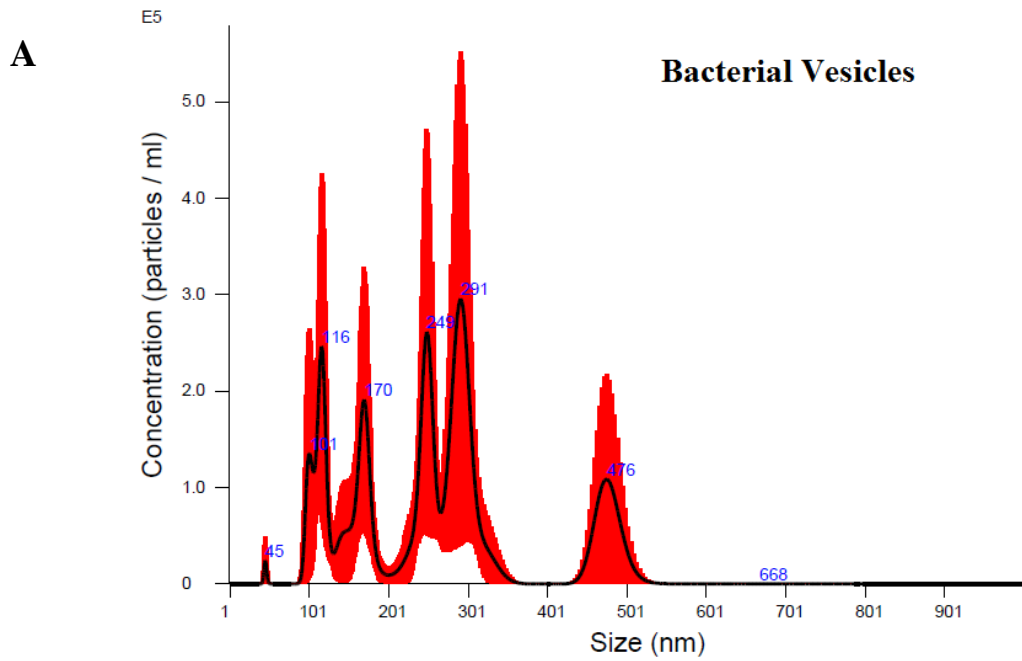


Figure 6.2.1 Size distribution of vesicles using ultrafiltration. A, OMV vesicles are larger than the **B**, OEXo vesicles which suggest that adopting the ultrafiltration method as described in Fig 5.1 clearly distinguishes between the two types, exosomes and microvesicles. **C**, demonstrates that the yield of OMVs are higher than OEXo by atleast 85% ($p < 0.001$). The experiment was repeated three times and the data presented are mean \pm SEM of the results.



B Isolation of Outer membrane vesicles via ultracentrifugation

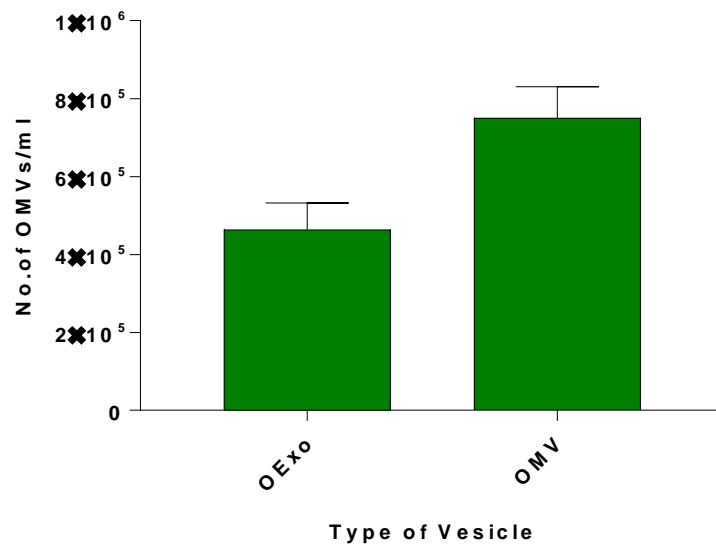


Figure 6.2.2: Size distribution of vesicles using centrifugation. A, Both OMV and OExo are visible on this plot. B, still suggests that the yield of OMV is still higher at least by 30% ($p=0.018$) compared to OExo. Experiment was repeated twice and the data presented are mean \pm SEM of the results.

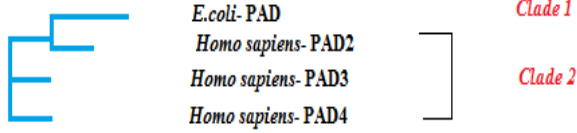
6.3.2 Phylogenetic reconstruction of *E.coli*-PAD sequences

Two well supported clades were formed within the Neighbour-joining phylogeny (**Fig. 6.3**), which suggests that *E. coli* PAD is closely associated with human PAD2 but that it carries similarities to PAD3 and PAD4. This is supported by the multiple sequence alignment which was generated through clustal omega (Sievers and Higgins, 2018), a method of progressive alignment construction. PAD *E. coli* has 220 amino acids (aa) while PAD2, 3 and 4 have 665, 663, 664 aa respectively. There are many positions that have a single, fully conserved residue in all 3 proteins while some conservation of similarity between *E. coli*, PAD2 and PAD3 is visible that scores > 0.5 in the Gonner PAM matrix. Very few weakly similar properties are detected between the two species. This clearly demonstrates that *E. coli* PAD and human PAD are evolutionary related.

6.3.3 Detection of PAD enzymes and citrullinated/deiminated proteins in *E. coli* via Western blot Analysis

E. coli and *E. coli*-OMV samples were analysed by Western blotting for total deiminated proteins (F95), deiminated PAD2, PAD3 and PAD4. Bands in the size range of 100, 75, 37–50 and 20 kDa were revealed for total deiminated proteins (F95) in both *E. coli* and OMVs. The presences of PADs were verified by detection of an expected band at 75/76 kDa which was stronger in PAD4 but faint in PAD3 and PAD2 (**Figure 6.4**). These results correlated with those observed in OMVs suggesting that the deiminated proteins, as detected by F95 positive proteins, have been transferred to the OMVs from *E. coli*.

A



B

<i>E.coli</i> -	-----mmgkiitva-----	9
PAD2	dvdadrdgvve--knpkkaswtwgpegggailvncdretpwlpkedcrdekvykedl	178
PAD3	dcdlncegr--qdrnfvdkrqvwgpgsyggillvncdrddpscdvqndcdqhvhlqdl	177
PAD4	caditrtgkvkptravkdqrtwtwgpcgggailvncdrdnlessamceddevldsedl	177
	* *: *	
<i>E.coli</i> -	-----	9
PAD2	kdmsqmilrtkqpdrlpagyeivlyismsdsdkvgfyvenpff-gqryihilgrrklyh	237
PAD3	edmsvmvlrtqgpaalfddhklvllhtssydakraqvfhicgpedvceayrhvlgqdkv-s	236
PAD4	qdmslmtlstktpkdfnhtlvtlhvarsemdkvrvfqatrgkl-sskcsvvlgpkwps	236
<i>E.coli</i> -	-----ghkkg-----	14
PAD2	vvkytggsaellffveglcfpdegfsglvsihvsllleymaqdipltpiftdtvifriapw	297
PAD3	yevprlhgdeerffveglsfpdagftglisfhvtllddsnedfsaspiftdtvvfrvapw	296
PAD4	ylmvpggkhnmdfyvealafpdtdfpglitltislldtsnllepeavvfqdsvvfrvapw	296
	.. *	
<i>E.coli</i> -	i-----gkstvlcslcvvirkgktacfletdsq-gs	45
PAD2	imtpnilppvsvfvccmkdnylflkevknlvektncelkvcfqylnrgdrwiqdeiefgy	357
PAD3	imtpstlpplevyvrnrntcfvdavaelarkagcklticpqaenrndrwiqdemelgy	356
PAD4	imtpntqppqevyacsifenedflksvttlamkakcklticpeenmddqwmqdemeigy	356
	* .. *. * : * . : : : *	
<i>E.coli</i> -	ik-----dfieerktnarlseipyfecytdipamvqklaarfdyfvdtpgmkspafvk	99
PAD2	ieaphkgfpvvlvsprdgnlkdfpvke-----llgpdfgyvtrepl-fesvtsld	406
PAD3	vqaphktlpvfvdsprngelqdfpykr-----ilgpdfgyvtrepr-drsvsgld	405
PAD4	iqaphktlpvfvdsprnrglkefpikr-----vmgpdfgyvttrgpq-tggisgld	405
	: : . : : * : : * . : . * . * . : : .	
<i>E.coli</i> -	alscadilftfvepgsgieintlgrlvfdiktaqagvnpmskawivlnkcstnpsdseas	159
PAD2	sfgnlevsppvtvng---ktyplgriligss-fplsggrrmtk--vvr-----dflkaq	454
PAD3	sfgnlevsppvvang---keyplgriliggn-lpgssgrrvtq--vvr-----dflhaq	453
PAD4	sfgnlevsppvtvrg---keyplgrilfgdscypsndsrqmhq--alq-----dflsaq	454
	: : . : . * : * : : : . . . : . : . *	
<i>E.coli</i> -	elrkqlnddpdlvpvrqriymrtah-----kkayncmgmvhey	198

PAD2	qvqapvelysdwlvtvghvdefmsfvpiipgtkkflllmastsacyklfreakqkdghgeaim	514
PAD3	kvqppvelfdwlvavghvdeflsvfpapdgkgfrmlaspgacfkfgekqkcgghgrall	513
PAD4	qvqapvklysdwlvsvghvdeflsvfpapdrkgfrlllasprscyklfgeqqneghgeall	514
	::: :: *** * : :: . :: : * *	
E.coli-	ddkrgnk-----argevellketdii-----	220
PAD2	fkglggms-skritinkilsneslvqenlyfqrcldwrdilkkelglteqdiidlpalf	573
PAD3	fqqvvddeqvktisinqvlsnkdlinynkfvqscidwnrevlkrrelglaecdiidipqlf	573
PAD4	fegikkkkqg---kiknilsnkltrehnsfvercidwnrellkrelglaesdiidipqlf	571
	. : * * * * *	
E.coli-	-----	220
PAD2	kmdedhraraffpnmvnmivldkdlgipkpfqgqveeccclemhvrglleplglectfid	633
PAD3	kte-rkkataffpdlvnmvlvlgkhlqipkpfqpiingcccleekvrslleplglhctfid	632
PAD4	klkefskaeaffpnmvnmvlvlgkhlqipkpfqpvgrccleekvcslleplglqctfin	631
E.coli-	-----	220
PAD2	disayhkflgevhcgtnvrrkpfkwhmvp	665
PAD3	dftpyhmlhgevhcgtnvcrkpfkwhmvp	664
PAD4	dfftyhirhgevhcgtnvrrkpfkwhmvp	663

Figure 6.3 Neighbour joining tree and Multiple Sequence Alignment (MAP) showing phylogenetic clustering of *E.coli*- PAD. The evolutionary analysis was inferred using the Neighbour-Joining method under the conditions of the Poisson distance correction model in MEGA6. Bootstrap values > 50 based on 1,000 replicates are shown as nodal support. Where Clade 1, contains *E. coli* sequence and Clade 2 contains human PAD2, PAD3 and PAD4 sequences. **B**, MAP indicates the evolutionary relationship between the two species; (*) indicates positions which have a single, fully conserved residue;(:) indicates conservation between groups of strongly similar properties - scoring > 0.5 in the Gonnet PAM 250 matrix;(.) indicates conservation between groups of weakly similar properties - scoring =< 0.5 in the Gonnet PAM 250 matrix.

6.3.3 Detection of PAD enzymes and citrullinated/deiminated proteins in *E.coli* and observation of transfer in *E.coli*-OMVs

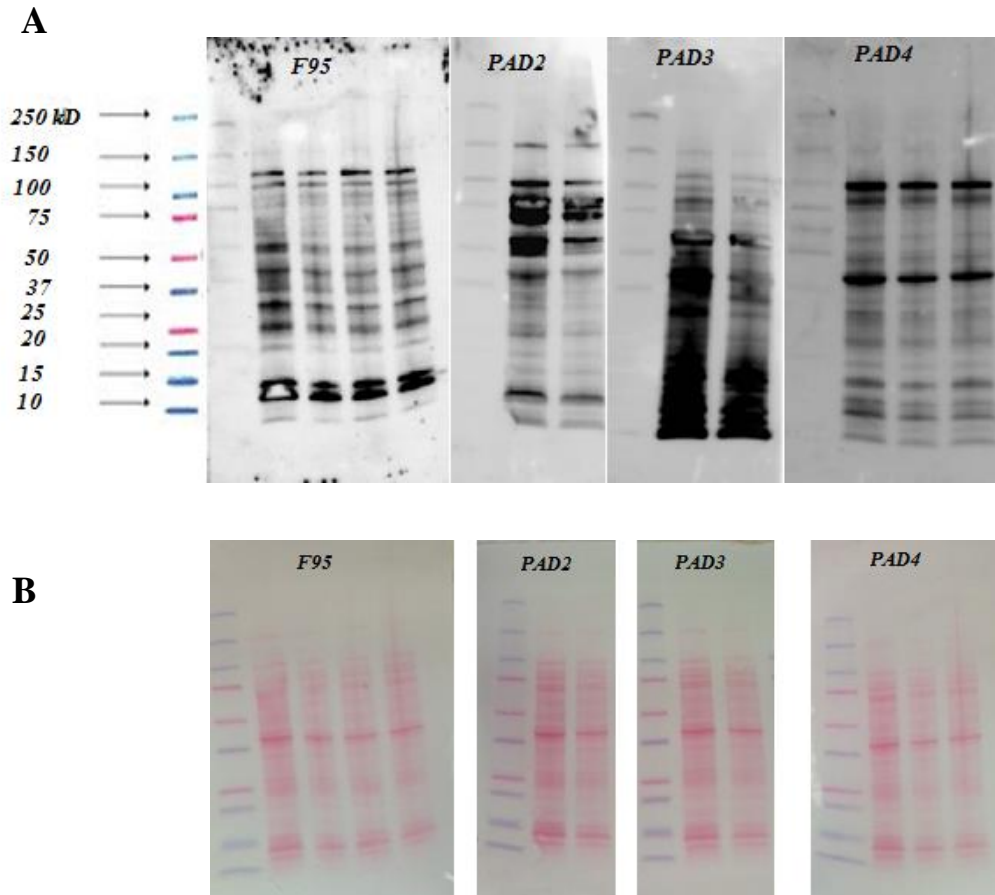


Figure 6.4 Western blotting of deiminated proteins in *E.coli* and OMVs. **A**, *E. coli* and *E. coli*-OMVs were analysed for total deiminated proteins (F95), PAD2, PAD3 and PAD4. Bands in the size range of 37-50 and 75-76 and 20 kDa were revealed for pan-deimination antibody (F95). PAD was detected as an expected band of 75-76 kDa with PAD4 being very prominent. PAD2 and PAD3 were less expressed. **B**, Ponceau S staining (PoncS) is shown to confirm that even loading was carried out. Lane 1 contains Precision Plus Protein Standard (161-0376, BioRad, U.K.), F95, lanes 2-3 contain two *E. coli* samples, lanes 4-5 contains 2 OMV samples; PAD2 and PAD3, lane 2 contains *E. coli* sample and lane 3 contains OMV sample; PAD4, lanes 2-3 contains *E. coli* sample while lane 4 contains the OMV sample.

6.3.4 Immunoprecipitation and Protein Identification

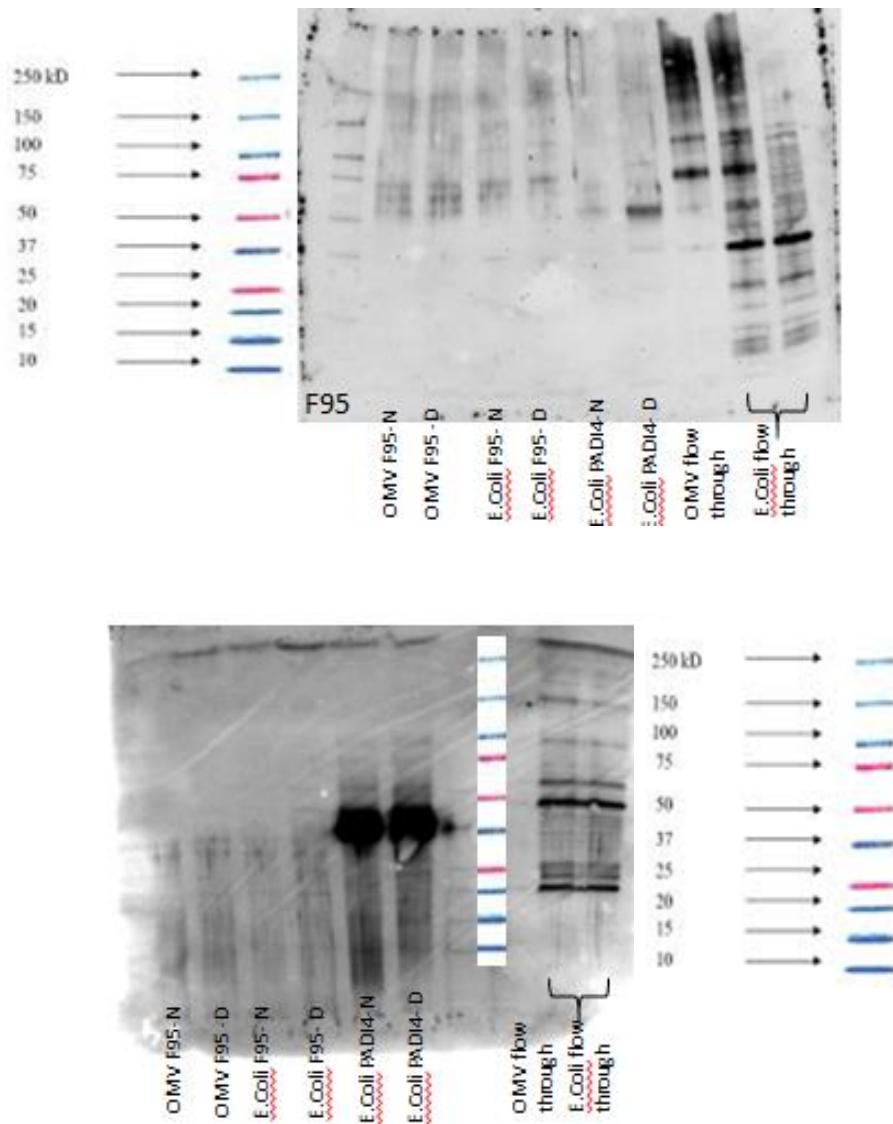


Figure 6.5 Immunoprecipitated deiminated proteins (F95) and PAD4 from *E.coli* and OMVs. IP was performed on *E. coli*-F95 and OMV-F95 as well as *E. coli*-PAD4. F95 blot, Lanes 8-10 has a band at 37kDa corresponding to F95. However, the band in lane 8 is faint compared to lanes 9-10. *E. coli* PAD4 blot has a significant band at 49kDa which corresponds to *E. coli*-PAD. Bands are detected in the size range of 100, 75, 37–50 and 20 kDa and were identified by proteomic analysis. Lane 1 contains Precision Plus Protein Standard (161–0376, BioRad, U.K.)

6.3.5 LC-MS/MS analysis of citrullinated proteins in *E.coli* and *E.coli*-OMVs

6.3.5.1 Common deiminated proteins identified in *E.coli*-F95, *E.coli*-PAD4 and OMVs-F95

UniProt ID	Protein name	MS2 intensities			Score (p<0.05)
		E.coli F95	E.coli PAD4	OMV F95	
Q1R6H3	30S ribosomal protein S15	128707	61762	67181	585.62
P04949	Flagellin	704599	1E+06	9488.7	653.24
P0A906	Outer membrane lipoprotein SlyB	289574	555800	10565	632.79
Q1R636	30S ribosomal protein S4	22719	44378	3554.4	289.35

Table 2: Deiminated proteins identified in *E.coli* and *E.coli*-OMVs. Deiminated proteins were isolated by immunoprecipitation using the pan-deimination F95 and PAD4 antibodies, analysed by LC-MS/MS. Ions score is $-10 \cdot \log(P)$, where p is the probability that the observed match is a random event. Individual ions scores > 16 indicated identity or extensive homology (p< 0.05). Protein scores were derived from ions scores as a non-probabilistic basis for ranking protein hits. Cut-off was set at Ions score 20. Values with 2 or more peptides per protein and a score of >50 were considered.

6.3.5.2 Unique deiminated proteins identified in *E.coli* -F95

UniProt ID	Protein name	MS2 Intensity	
		<i>E.coli</i> -F95	Score (p<0.05)
B7MQF2	Trigger factor	81193	192.72
B7NKH1	UPF0227 protein YcfP	11941	166.86
B7MSJ0	RNA-binding protein Hfq	256917	132.47
Q1R638	50S ribosomal protein L17	126430	128.85
Q1R602	50S ribosomal protein L3	69461	254.77
Q1R619	50S ribosomal protein L24	6484.4	75.48
B7N255	Protein-export protein SecB	136512	77.044
P14407	Fumarate hydratase class I, anaerobic	15233	78.27
P0A9S6	Glycerol dehydrogenase	220449	441.19
P69799	PTS system mannose-specific EIIAB component	94232	56.71
B7MRV6	Serine--tRNA ligase	16845	55.11

Table 3: Deiminated proteins identified in *E.coli*-F95 sample. Deiminated proteins were isolated by immunoprecipitation using the pan-deimination F95 antibody, analysed by LC-MS/MS. Ions score is $-10 \cdot \log(P)$, where p is the probability that the observed match is a random event. Individual ions scores > 16 indicated identity or extensive homology (p< 0.05). Protein scores were derived from ions scores as a non-probabilistic basis for ranking protein hits. Cut-off was set at Ions score 20. Values with 2 or more peptides per protein and a score of >50 were considered.

6.3.5.3 Unique deiminated proteins identified in *E.coli* –PAD4

UniProt ID	Protein name	MS2 Intensity	
		<i>E. coli</i> PAD4	Score (p<0.05)
P0A8N5	Lysine--tRNA ligase, heat inducible	321997	300.12
Q8X9L0	ATP-dependent zinc metalloprotease FtsH	1E+06	151.09
B7MRC1	Regulator of sigma D	23402	247.53
P0ABC5	Modulator of FtsH protease HflC	66850	189.23
Q1R5V0	50S ribosomal protein L10	478659	218.99
Q8X4S5	Arabinose 5-phosphate isomerase GutQ	486219	120.37
Q1R6A9	50S ribosomal protein L13	99365	135.62
P0AA45	Ribosomal small subunit pseudouridine synthase A	50727	162.27
A7ZML6	Succinylornithine transaminase	232079	73.58
B7MPT2	Curved DNA binding protein	6123.2	90.68
P69911	Glutamate decarboxylase beta	387378	72.46
A7ZY39	Cyclic pyranopterin monophosphate synthase accessory protein	17232	67.03
Q1R613	50S ribosomal protein L16	475140	95.53
Q1R358	30S ribosomal protein S18	312269	103.87
P07014	Succinate dehydrogenase iron-sulfur subunit	48651	157.85
P42632	PFL-like enzyme TdcE	29499	66.01
P0AGL3	Putative reactive intermediate deaminase TdcF	161746	80.57
Q8X7I0	UPF0339 protein YegP	6121.7	87.63
Q0TFD0	Acetyl-coenzyme A carboxylase carboxyl transferase subunit beta	156916	99.12
P0A6A5	Acetate kinase	79146	70.42
P0A9Q3	Aerobic respiration control protein ArcA	19035	60.23
A8A0U0	Succinylornithine transaminase	28022	73.51
P0A9H4	Inducible lysine decarboxylase	716567	78.26
Q8FJM0	DNA protection during starvation protein	51562	65.43
B7N1L1	Glycine--tRNA ligase beta subunit	23006	87.76

B7N2S2	ATP-dependent protease ATPase subunit HslU	398703	52.01
B7N2Q7	ATP-dependent 6-phosphofructokinase isozyme 1	57552	62.75
B7UJ59	Polyribonucleotide nucleotidyltransferase	5914.7	70.94
B7MZ76	CTP synthase	17163	59.39
B6I184	50S ribosomal protein L25	56618	57.85
Q0TA78	DNA-directed RNA polymerase subunit beta	102175	72.91
B6HZE3	30S ribosomal protein S2	226035	68.17
B7NGD4	30S ribosomal protein S6	151007	61.19
C4ZUJ7	30S ribosomal protein S12	396281	110.55
Q8XBT3	Universal stress protein G	36115	159.67
P0AF94	2-iminobutanoate/2-iminopropanoate deaminase	22468	105.18

Table 4: Deiminated proteins identified in *E.coli*-PAD4 sample. Deiminated proteins were isolated by immunoprecipitation using the PAD4 antibody, analysed by LC-MS/MS. Ions score is $-10 \cdot \log(P)$, where p is the probability that the observed match is a random event. Individual ions scores > 16 indicated identity or extensive homology ($p < 0.05$). Protein scores were derived from ions scores as a non-probabilistic basis for ranking protein hits. Cut-off was set at Ions score 20. Values with 2 or more peptides per protein and a score of > 50 were considered.

6.3.5.4 Deiminated proteins identified in OMV-F95

A

UniProt ID	Protein name (short)	Gene name	MS2 Intensity	
			OMV F95	Score (p<0.05)
Q1R6H3	30S ribosomal protein S15	rpsO	67181.14	585.62
P04949	Flagellin	fliC	9488.724	653.24
P0A906	Outer membrane lipoprotein SlyB	slyB	10565.21	632.79
Q1R636	30S ribosomal protein S4	rpsD	3554.363	289.35
B7L6J2	Threonine--tRNA ligase	thrS	8718.552	371.78
P21513	Ribonuclease E	rne	8574.855	369.58
P02925	D-ribose-binding periplasmic protein	rbsB	6973.666	270.86
P63285	Chaperone protein ClpB	clpB	30537.26	227.63
B5YWX8	50S ribosomal protein L25	rplY	4326.5	51.12

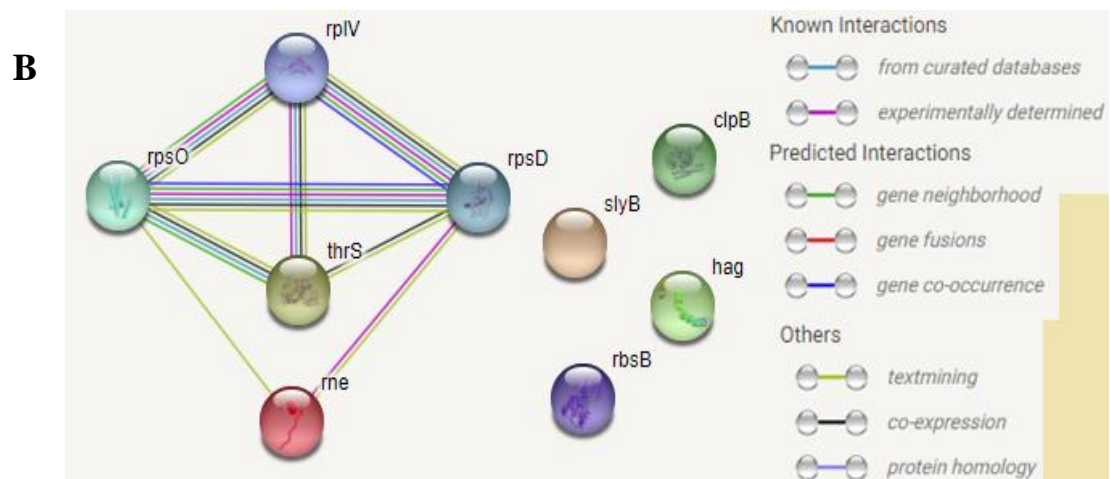


Figure 6.6 Deiminated proteins identified in *E.coli*-OMV-F95 sample. Deiminated proteins were isolated by immunoprecipitation using the F95 antibody, analysed by LC-MS/MS. **A**, all deiminated proteins identified in OMV sample. These contain all proteins which had a score of >50. **B**, String analysis of OMV-F95 proteins revealed nine proteins. Only 5 out of 9 proteins were associated with each other at least through text mining. Ions score is $-10 \cdot \log(P)$, where p is the probability that the observed match is a random event. Individual ions scores > 16 indicated identity or extensive homology ($p < 0.05$). Protein scores were derived from ions scores as a non-probabilistic basis for ranking protein hits. Cut-off was set at Ions score 20. Values with 2 or more peptides per protein and a score of >50 were considered for **A**.

6.3.5. Identification of deiminated proteins from *E. coli* and *E. coli*-OMVs by Immunoprecipitation

Proteins from *E. coli* and OMVs were immunoprecipitated using the pan-deimination F95 antibody (both *E. coli* and OMVs) and PAD4 antibody (*E. coli* only) (**Figure 6.5**). Bands were significant at 37, 75 and 100kDa in *E. coli* samples that corresponds to F95. Similar bands were observed with respect to the OMV sample with the exception of the 37kDa band being very weak. Although the PAD4 corresponds to a band at 70-75kDa (Magnadottir et al., 2018), there are occasions that it has reacted with lower bands as well. This confirms our findings which had a very strong band at around 50kDa that corresponds to PAD4 but non-specific bands were also present at low molecular weights and may also represent proteins binding to *E. coli* PAD. The OMV sample did not react to the PAD antibody which suggests that the bands seen in *E. coli* samples correlate to the PAD immunoprecipitation.

6.3.6 Mass spectrophotometry analysis of immune-precipitated proteins from *E. coli* and *E. coli*-OMVs

Immunoprecipitated proteins from *E. coli* and OMV samples were analysed by LC-MS/MS. Deiminated protein candidates included immunogenic, cytoskeletal, nuclear and metabolic proteins, and are listed in **Tables 2-4** and **figure 6.6**. **Table 1**, summarise the common proteins in all samples that had 2 or more peptides and a protein score of >50. There were more proteins identified in *E. coli* samples that were unique to both F95 (**Table 3**) and PAD4 (**Table 4**). Nine proteins were identified from the *E. coli* OMV protein sample (**Figure 5.3.6 A**) after citrullinated protein enrichment using an F95 antibody immunoprecipitation method. Only 30s ribosomal protein S15 was unique to OMVs (**Figure 5.3.6 C**). Threonine—tRNA ligase (thrS), has not yet been reported in *E. coli* OMVs. However, peptides are only present in the *E. coli* F95 and *E. coli* PAD4 samples. There is however the potential that this maybe a novel identification in OMVs and that it is thus connected with the other proteins identified in the OMV fraction.

STRING analysis was carried out to assess if Threonine—tRNA ligase is interconnected with the other proteins in the OMV associated proteins (**Figure 6.6 B**). This shows that 5 of the 9 proteins are associated with each other at least through text mining. The novel *E. coli* OMV protein Threonine—tRNA ligase is co-expressed with 30s ribosomal protein S15 (rpsO), 30s ribosomal protein S4 (rpsD) and 50S ribosomal protein L22 (rplV) as well as being experimentally determined to interact with rplV.

6.3.7 Effect of EV inhibitors on OMV Inhibition

To observe effect of EV inhibitors on OMV release was encouraging (**Figure 6.7**). This represents the effect of the inhibitors previously used for EV experiments in human cancer cells. It is evident that these inhibitors have a significant effect also on OMV release which suggests that they can be used further in investigations similar to apoptosis experiments as described in previous sections. Imipramine is the most potent OMV inhibitor, but all reagents have shown marked reduction in OMVs. Imipramine resulted in the strongest inhibition of 72.38% ($p < 0.0001$) with a reduction of only 4.12% in cell viability. This was higher than EGTA (1.04%) which least affected the cells with only an inhibition of 21.56% ($p = 0.0048$). Bis-I was the second strongest inhibitor, 67.95% ($p < 0.0001$) which only reduced the cell viability by 6.25%. Both pantethine and Y27632 resulted in less than 50% inhibition, 21.09% ($p = 0.0027$) and 43.03% ($p = 0.0004$) respectively with greater effect on cell viability with pantethine reducing it by 25% and Y27632 by 12.5%.

6.3.8 Effect of PAD inhibitors on OMV Biogenesis and Release

Figure 6.8 represents the effect of the PAD inhibitors on OMV release. Only Cl-amidine had previously been used in EV experiments in human cancer cells. GSK199, a PAD4 inhibitor, is more potent with 66.36% inhibition ($p = 0.0001$) but all reagents showed a noticeable reduction in OMVs. However, GSK199 had the highest effect on viability with a 23.86% reduction. BBCl-am, is the second best inhibitor with 53.79% inhibition ($p < 0.0001$) and a reduction of 19.32% of viable cells. Cl-amidine resulted in a 42.42% inhibition ($p = 0.0001$) with 18.18% decrease in cell viability while AMF30a, a PAD2 inhibitor, only resulted in 28.18% ($p = 0.0116$) with a 14.73% viability. Cl-amidine has been widely used as a pan-PAD inhibitor so it was interesting to appreciate the effectiveness compared to other specific inhibitors. BBCl-am reduced the number of OMVs by 19.7% ($p = 0.0014$) and GSK199 by 41.58% ($p = 0.0024$). Interestingly AMF30a stimulated OMVs compared to Cl-amidine by 19.8% ($p = 0.0742$).

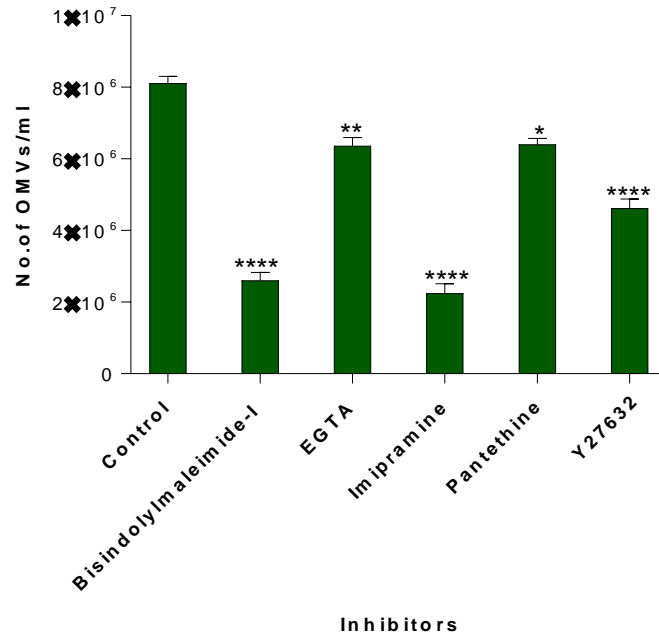
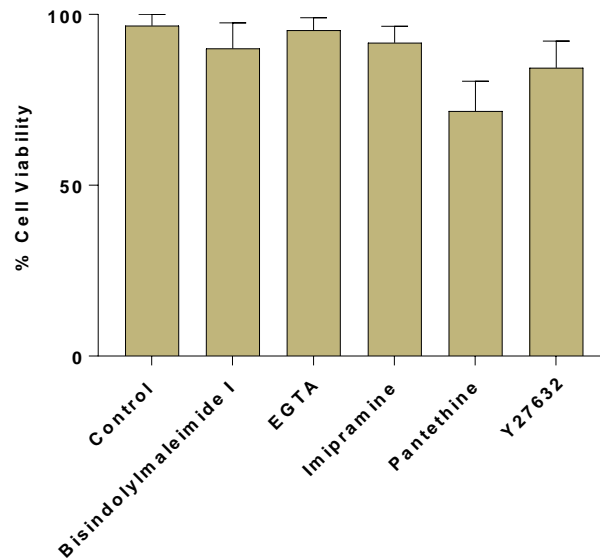
A**Inhibition of OMV production in *E. coli*****B****Bacterial Growth in the Presence of OMV inhibitors**

Figure 6.7 Effect of inhibitors on OMV inhibition. A, All reagents used in the experiment have shown clear inhibition. However, Imipramine and Bisindolylmaleimide-I were more potent inhibitors of OMV release by 73.4% and 63.19% respectively ($p < 0.0001$). However, Imipramine-mediated inhibition was more significant to Bisindolylmaleimide-I by 27.5% ($p = 0.3630$). Y27632 resulted in a 38.45% inhibition which was better compared to the latter. EGTA and Pantethine reduced the OMVs by 14.97% ($p = 0.0048$, $p = 0.0027$). B, except for pantethine (35.5% viability), there is no detrimental effect on healthy cells which suggests that using these reagents in future experiments is advisable. The experiment was repeated twice and the data presented are mean \pm SEM of the results.

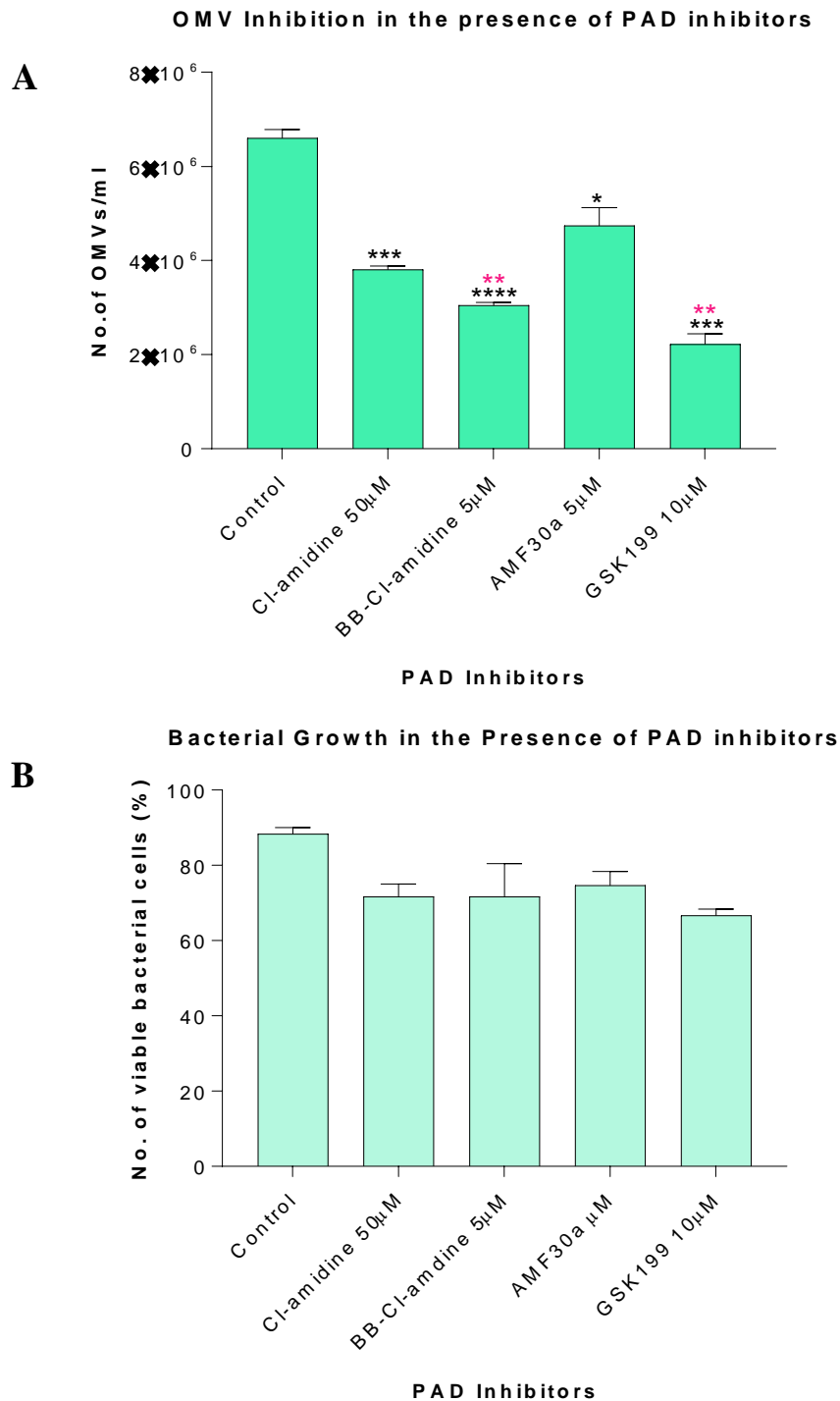


Figure 6.8 Effect of PAD inhibitors on OMV biogenesis and release in *E. coli*. **A**, All reagents used in the experiment have shown clear inhibition. However, GSK199 and BB-Cl-amidine inhibit OMV release significantly by 59.07% and 51.23% respectively ($p < 0.0001$). Pan PAD inhibitor, Cl-amidine affected the inhibition less compared to BB-Cl-amidine by 20% ($p = 0.0014$) and GSK199 by 42% ($p = 0.0024$). However, it was more potent than PAD2 inhibitor, AMF30a by 19.19% ($p = 0.0742$). * = significance compared to the control; ** = significance compared to Cl-amidine. **B**, There is no detrimental effect on healthy cells which suggests that using these reagents in future experiments is advisable. The experiment was repeated three times and the data presented are mean \pm SEM of the results.

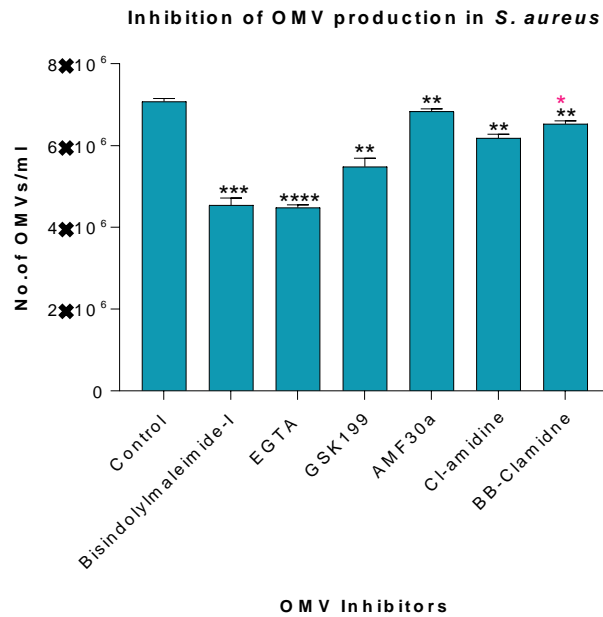
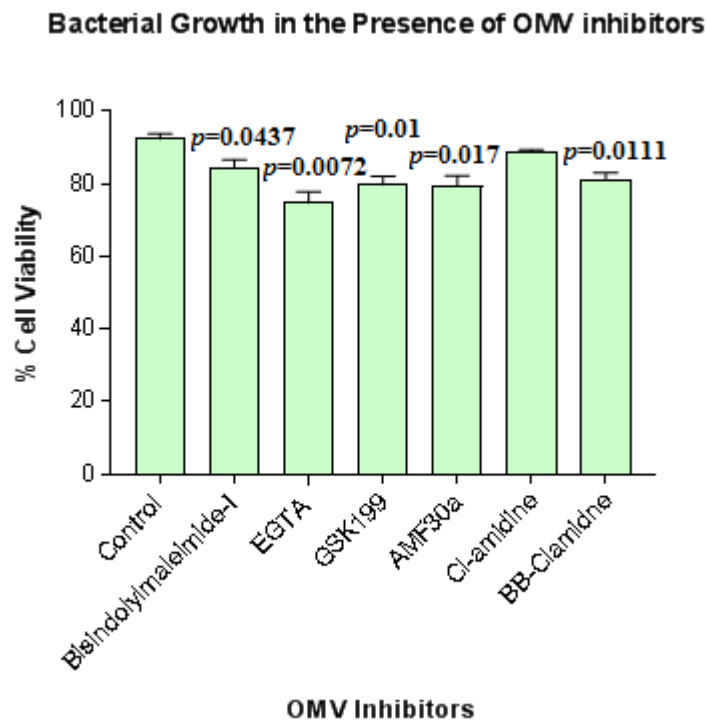
A**B**

Figure 6.9 Effect of inhibitors on *S.aureus* OMV biogenesis and release. A, All reagents used in the experiment except for AMF30a and BB-Clamidne have shown clear inhibition. However, EGTA (36.63%) and Bisindolylmaleimide-I (35.79%) inhibits OMV release significantly (* $p=0.0002$ and $p<0.0001$ respectively). BB-Clamidne has a significant effect compared to Cl-amidine (* $p=0.0412$). B, There is no detrimental effect on healthy cells with only EGTA resulting in 18.48% reduction in cell viability which suggests that using these reagents in future experiments is advisable. The experiment was repeated three times and the data presented are mean \pm SEM of the results.

6.3.9 Effect of inhibitors on *S. aureus*-OMV Biogenesis and Release

A selected range of OMV inhibitors was used to examine the effect as shown in **(Figure 6.9)**. Both Bisin-I and EGTA showed significant inhibition with Bisin-I having less effect on cell viability, 8.69% compared to EGTA which was 18.48%. PAD inhibitors were less effective but still had significant effects ($p < 0.0001$) compared the control treatment. GSK199 resulted in the highest inhibition of 22.49% ($p = 0.0018$) PAD2 inhibitor showed only 3.39 % ($p = 0.0606$) and BB-Clamidine ($p = 0.0061$) being only 7.64% OMV inhibition and were thus significantly lower in their capacity for OMV inhibition compared to that in *E. coli*. However, Cl-amidine resulted in a 12.5% inhibition with the lowest effect on cell viability, 3.26% which was 5.36% more effective compared to its modified reagent, BB-Clamidine ($p = 0.0412$). Overall the OMV inhibition was less than 40% in the presence of inhibitors which suggests that they are less effective in Gram-positive species compared to that of Gram-negative.

6.4 Discussion

Vesicles released from *E. coli* were isolated utilising both ultrafiltration and ultracentrifugation. Ultrafiltration resulted in a pure population of both OMVs and OExos. However, ultracentrifugation was chosen as the preferred method in order to examine the effect on vesicles as a general population as the yield was higher in both OExo and OMVs which has been considered collectively in future experiments. Other researchers have taken similar approaches during OMV preparation in Gram-negative bacteria (Klimentova and Stulik, 2015, McCaig et al., 2013) which suggests that there are different methods to ensure a pure isolate is obtained. The OMVs were quantified using ananosight LM10 which has also recently been used by other researchers (Roier et al., 2016a). Other detection methods include flow cytometry (Wieser et al., 2014) and direct labelling of OMVs with lyophilic dyes such as PKH(O'Donoghue and Krachler, 2016).

OMVs have been reported in different contexts by many researchers to fall in the size range of 10-300nm (Huang et al., 2016, Kulkarni et al., 2015). However, in the main the literature cites the OMVs to be 20-250nm in size. Our Nanosight Tracking Analysis (NTA) plots in **Figures 6.3.1 and 6.3.2** suggest that OMVs can be larger in size. Nevertheless, work carried out in this study has considered vesicles in the 20-250nm range as OMVs to enable standardisation.

PAD has been reported as a protein that is solely expressed in *P. gingivalis* (Bielecka et al., 2014, Mangat et al., 2010), and the citrullinome of *gingivalis* has been published (Stobernack et al., 2016) while arginine deiminases have been reported in various bacteria, but hitherto not with deiminating activity. Our findings in this chapter firmly corroborate the presence of citrullinated proteins in *E. coli* through immunoprecipitation and Mass spectrometry analysis. Though PAD association with *P. gingivalis* has been looked at previously, our study was the first to investigate the possibility of PAD-like activity in *E. coli* species. Western blot analysis gave rise to strong bands in the presence of F95 (a pan-deimination antibody detecting deiminated proteins, Nicholas and Whitaker, 2002) and also detected a PAD-like protein as assessed by cross-reactivity with PAD-antibodies. Identification of PAD-positive bands with low molecular weight correlates with previous research carried out on *P. gingivalis* with band sizes ranging

between 43 to 49 kDa (Bielecka et al., 2014, Gabarrini et al., 2015). However, evolutionary relationship analysis by the means of the phylogenetic tree and the multiple sequence alignment strongly suggested that *E. coli* PAD is closely connected to human PAD2 (**Figure 6.3**). Nevertheless, PAD in *P. gingivalis*, also a Gram-negative bacterium is believed to be evolutionarily unrelated to mammalian PAD despite the fact that both catalyze the same chemical reaction (Rodriguez et al., 2009). *E. coli* PAD has shown to be evolutionarily connected with human PAD2 (**Figure 6.3 A**) (Magnadóttir et al., 2018). However, inhibition assays clearly demonstrated that PAD4 inhibitor, GSK199 has been effective in both Gram-positive and Gram-negative bacteria compared to PAD2 inhibitor, AMF30a. **Figure 6.8 and 6.9** which prompted the investigation to its presence primarily in *E. coli*. It may nevertheless also be possible that the confirmation of the *E. coli* PAD may be more similar to the human PAD4, although the sequence is more PAD2 related, and thus the PAD4 specific GSK199 inhibitor may be more effective than the other PAD-inhibitors. This will require further investigation. Immunoprecipitation results suggest that *E. coli* deiminated proteins as seen in the F95 immunoprecipitation data. Interestingly, total deiminated proteins were captured by anti-F95 in both *E. coli* and OMV samples and although fewer deiminated proteins were identified in the OMVs, it still confirms that lateral transfer of deiminated proteins occurs via OMVs. OMV-mediated genetic predisposition has been confirmed in other studies. Bielecka and colleagues observed a total citrullination of C5a post-treatment with *P. gingivalis*-OMVs as opposed to *in vitro* treatment of C5a with PAD. This vastly contributes to immune evasion decreasing the chemotactic ability of neutrophils (Bielecka et al., 2014). Identification of threonine-tRNA ligase for the first time in OMVs was particularly interesting. Presence of only a single peptide is concerning but interaction with other proteins is shown by string analysis (**Figure 6.6 B**). Threonine-tRNA ligase also known as threonine-tRNA synthetase is a 642 aa long protein present in *E. coli* belonging to the family of aminoacyl-tRNA synthetases. This is present in all IP samples. They link amino acids to their cognate transfer RNAs (tRNA) in aminoacylation reactions that establish the connection between a specific amino acid and a nucleotide triplet anticodon embedded in the tRNA (Schimmel, 2008). Its involvement in RNA splicing and transcriptional and translational regulation might play an important role in protein deimination.

30S ribosomal protein is one of the primary rRNA binding proteins that bind directly to 16S rRNA where it helps nucleate assembly of the platform of the 30S subunit by binding and bridging several RNA helices of the 16S rRNA (Gao et al., 2003). 30S ribosomal protein S4 (rpsD) and S15 (rpsO) were present in all deiminated samples including the OMVs. This has been previously reported as a substrate of PAD4 mediated citrullination in HEK 293T (Guo et al., 2011). This confirms its presence in both F95 and PAD4 *E. coli* IP samples. All commonly

expressed proteins including chaperone protein, ribonuclease, outer membrane lipoprotein, 50S ribosomal protein L22 and flagellin are believed to be either substrates or products of protein deimination (Claushuis et al., 2018). **Figure 5.3.7** depicts the clear inhibition of OMV release in the presence of previously used EV inhibitors. Imipramine was the most potent (72.38% reduction) in inhibiting OMV release compared to other reagents. The least effective was pantethine (21.09%) which also resulted in a 25% reduction in cell viability compared to the untreated control. Overall all reagents used in this study have demonstrated OMV inhibition in *E. coli* which suggests they can be used in antibiotic sensitivity assays and phage-mediated cytotoxicity in subsequent experiments. Also **Figure 6.8** clearly demonstrates that inhibition of vesicle release via PAD inhibition is successful. PAD4 inhibitor, GSK199 was significantly effective compared to other reagents used. Although the extent of inhibition was less than with other OMV inhibitors as shown in (**Figure 6.7**), PAD reagents can still be used in future experiments for bacterial OMV inhibition with minimal effect on cell viability. Neutrophil extracellular trap (NET) formation is a well known mechanism of the immune system for bacterial killing. It has been found that PAD4-mediated chromatin decondensation is essential to form NETs and is a main player in histone-mediated bacterial killing (Bicker and Thompson, 2013). PAD4 association with NETosis therefore increases innate immunity. Here, PAD-inhibition in *E. coli* showed a different anti-bacterial mechanism by inhibiting OMV release from the bacteria, which may further sensitize them to killing and also prevent them from carrying out immune evasive strategies, including via the release of OMVs. Many studies on OMVs have been based on Gram-negative bacterial species (Bonnington and Kuehn, 2014, Roier et al., 2016b, Perez-Cruz et al., 2013). OMV release in *S. aureus* has been previously shown by different groups in the field (Olsen and Amano, 2015, Gurung et al., 2011). Interestingly our study has demonstrated that inhibition of biogenesis and release of OMVs is seen in Gram-positive bacterial species as well. Nonetheless the OMV inhibition in the presence of the same inhibitors was seen to be lower compared to *E. coli*. However, Bisin-I and EGTA were more potent than PAD inhibitors (**Figure 6.9**).

My results suggest that EV inhibitors used previously on eukaryotic cells (Kosgodage et al., 2017) are successful inhibitors of OMV release from bacteria, which prompts further investigation. The increased hydrophobicity of the reagents (**Table 1**) is an attribute likely to lead to increased cell penetration, which is visible in the results. Both EGTA and Bisin-I are less hydrophobic compared to the PAD inhibitors which are more successful in OMV inhibition in both Gram-positive and Gram-negative bacteria. Nevertheless, this type of study has not previously been conducted on bacterial OMVs, according to the literature, which makes it more interesting to express the results and steer its use in combatting antibiotic resistance and

possibly increasing the bacterial cell's susceptibility to bacteriophage therapy as highlighted in **Figure 6.10**.

Both CBD and nicotine have shown to effectively inhibit EV release in previous chapters. CBD is also well known to possess anti-bacterial properties (Appendino *et.al.* 2008, Hernández-Cervantes *et.al.* 2017). Previous research has looked into the anti-bacterial effect of nicotine. According to a study by Pavia and colleagues this revealed that nicotine is effective against both Gram-positive and Gram-negative bacteria and fungal pathogens (Pavia *et.al.* 2000). Later in the field, a group lead by Zaidi also clearly portrayed the anti-bacterial effect of nicotine against both groups of bacteria, *E.coli* and *P. aeruginosa* being Gram-negative and *S. faecalis* being the only Gram-positive bacterial species that were used in the study. It had no effect on *S. aureus* (Zaidi *et.al.* 2012). However, no studies have been performed in relation to their capacity in OMV inhibition. Therefore, it will be very interesting to investigate the potency of CBD and Nicotine in OMV inhibition in the future.

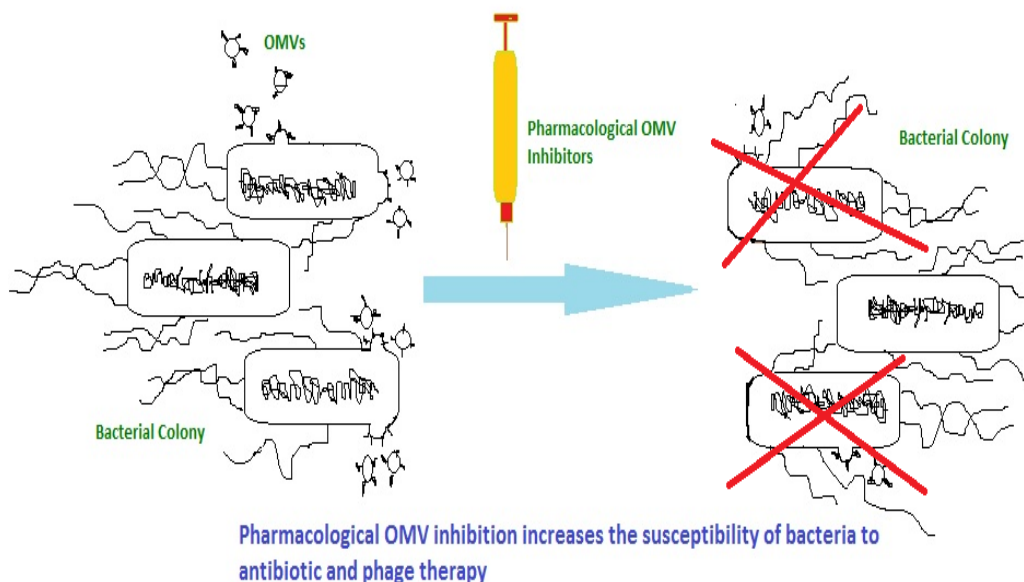


Figure 6.10 Formulaic representation of the effect OMV inhibition could have on antibiotic and phage therapy. Synthesis of OMVs from bacterial cells mimics the attack by hosts' innate and adaptive immune system increasing its virulence in disease. Therefore, OMV inhibition increases the susceptibility of bacterial cells to anti-bacterial therapy.

Better OMV isolation techniques such as optiprep and a combination of density gradient centrifugation and ultrafiltration needs to be used to purify the vesicles and improve the quality of results as suggested by experts in the field (Rompikuntal et al., 2015, Elluri et al., 2014, Alves et al., 2016b). Also it is crucial that the size range of OMVs to be standardised in the field to enable accurate quantification of vesicles that significantly affect the development of accurate detection methods and therapeutic strategies. Better OMV isolation techniques such as optiprep and a combination of density gradient centrifugation and ultrafiltration needs to be used to purify the vesicles and improve the quality of results as recently suggested (Rompikuntal et al., 2015, Elluri et al., 2014, Alves et al., 2016b).

It will certainly be interesting to conduct IP and Western blotting on *S. aureus* samples to identify deiminated proteins which can directly correlate with inhibition of OMV release data obtained in this study.

Chapter 7: Effect of Inhibiting OMV release on Antibiotic Activity and Phage Therapy

7.0 Effect of Inhibiting OMV Release on Antibiotic Activity and Phage Therapy

7.1 Introduction

This chapter investigates the potential of using OMV inhibitors to enhance antibiotic activity against *E. coli* and follows on from the previous work that I conducted (Chapter 6) and that other colleagues conducted in CMIRC (Kholia et al., 2015, Jorfi et al., 2015) investigating the effect of inhibiting the release of vesicles from cancer cells to enhance, by sensitizing cells, their response to chemotherapeutic treatment. The same reagents used in the previous chapter will be followed to determine their effect on the antibiotic activity via the disc diffusion method and Minimum Inhibitory Concentration (MIC) followed by Minimum Bactericidal Concentration (MBC). A range of antibiotics was used to determine the effect of these OMV inhibitors and the MIC experiment was performed using just Colistin. The Disc Diffusion method uses antibiotic-impregnated discs to determine the antibiotic sensitivity of bacteria. MIC is a measure of the concentration of the antibiotic needed to eliminate the visible bacterial growth. MBC is the minimum concentration of antibiotic needed to kill the bacteria.

7.1.1 Colistin

Colistin (Polymyxin E) is a non-ribosomal peptide with a molecular weight of approximately 1200Da, (**Figure 7.1**), and is synthesized by *Paenibacillus polymyxa*, a Gram-positive bacterium. This antibiotic is seen as the ‘antibiotic of the 21st century’ (Yu et al., 2017). It acts on the lipoglycans and endotoxins of the Gram-negative bacterial cell membrane. Colistin also known as polymyxin E, belongs to the group of Polymyxinantibiotics that was first isolated in Japan and used to treat Gram- negative bacterial infections (Livermore et al., 2011). These together with Polymyxin B are the only Polymyxins used clinically.

Its mechanism of action is widely described by microbiologists, and essentially it is a bactericidal drug that directly binds to lipopolysaccharides(LPS) and phospholipids in the outer cell membrane of Gram-negative bacteria and competitively displaces divalent cations from the phosphate groups of lipids(Falagas et al., 2005). This disruption to the cell membrane integrity causes leakage of intracellular contents leading to bacterial death.

It is also known to bind and neutralise LPS and avert pathophysiological effects of endotoxin in the circulation (Yahav et al., 2012, Falagas et al., 2005).MIC values for Colistin ranged between 2-16µg/ml in the literature (Moskowitz et al., 2010, Rojas et al., 2017). Therefore, the current study extended this range from 0.015µg/ml to 64µg/ml.

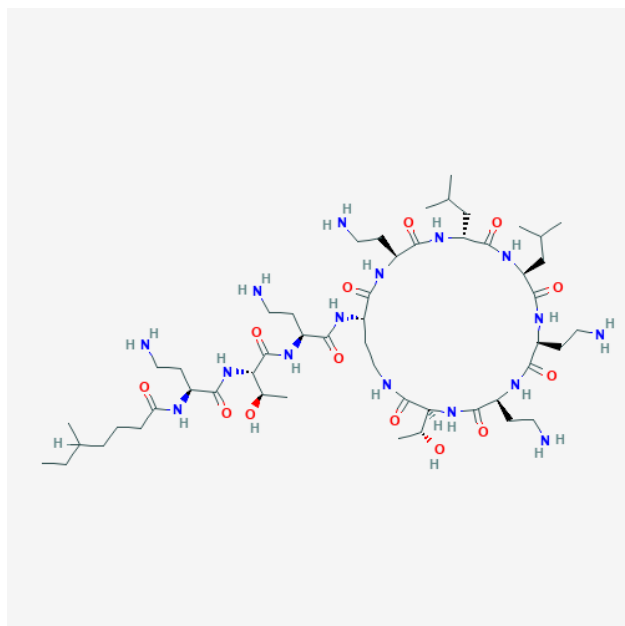


Figure 7.1. The molecular structure of Colistin. Colistin is a combination of the cyclic polypeptides colistin A and B with a molecular weight of 1155.455g/mol .

7.1.2 Vancomycin

Vancomycin is effective against Gram-positive bacterial species including *Staphylococcus*, *Streptococcus* and *Listeria*. It is recommended to be administered intravenously and is prescribed for serious skin, blood-borne and joint infections and meningitis caused by methicillin-resistant *S. aureus* (MRSA). It is a unique glycopeptide that is structurally unrelated to any other antibiotic (Ng et al., 2014). There is sufficient evidence that vancomycin alters the permeability of the cell membrane and selectively inhibits ribonucleic acid synthesis. Induction of bacterial L-phase variants from susceptible organisms with vancomycin is extremely difficult, and such variants are unstable. Stable L-phase variants induced by other agents are susceptible to vancomycin (Watanakunakorn, 1984). Abundant usage of vancomycin in studies (Goldstein et al., 2018) related to *Staphylococcus spp.* was the main reason to use it in the current study against *S.aureus*. The majority of MIC values for vancomycin have been recorded in the range of 1.5-2µg/ml (Maclayton et al., 2006, Kshetry et al., 2016) but there are some studies where a MIC value of 8µg/ml and higher have been reported (Jiang et al., 2017, Lepe et al., 2014). Therefore, a MIC confirmation test starting from a concentration of 8µg/ml was carried out and the MIC was considered accordingly.

7.1.3 OMV inhibition and Phage Therapy

My earlier description of pharmacological inhibition of OMV release as a means of enhancing antibiotic therapy, also has a potential to promote the effectivity of bacteriophage (phage) therapy, where phage are used to lyse bacteria (Inal, J. *AITE* 2004) especially if OMV play a

role as a decoy to phage infection. Lambda phage was the virus chosen against *E.coli*. The Pan-PAD inhibitor, Cl-amidinewas to be used as described in the previous chapter. In this study, the effect of OMVs and the inhibitor have been analysed in terms of phage titre (plaque forming units) and the results illustrate the effect.

7.1.4 Phage Therapy

Phage therapy describes the therapeutic use of viruses that have a lytic life cycle after infecting their host bacteria. This has been widely used to treat pathogenic bacterial infections(Sulakvelidze et al., 2001). It is important that the specific phage is used that targets the particular bacteria. The specificity of this treatment is likely to be much narrower than available antibiotic therapies. The limited host range is an advantage as phage therapy is thus lessadverse to side-effects and off-target effects, compared to the use of antibiotics which can destroy the normal gut flora resulting in adverse side-effects. Phage resistance is also possible just as with antibiotic resistance but the rate of appearance is lower and it is comparatively much easier to develop new phage strains than developing a novel antibiotic. As bacteria evolve resistance, the relevant phages naturally evolve alongside(Lin et al., 2017). When ‘superbugs’ (resistant bacteria) appear, the super phage already attacks it. The phage will have to be isolated from the same environment.

Phages are ideal for localised use as they penetrate deeper as long as the infection is present unlike antibiotics which are surface treatments. Also phage stop reproducing once the targeting host has been destroyed(Abedon et al., 2011). Therefore, it has no detrimental effect on the surrounding healthy tissue. Furthermore, phages do not build up secondary resistance as seen with antibiotics. Phage therapy should be improved as a solution to multi-drug resistance.

7.1.5 Lambda Phage

Lambda phage (λ) is an enterobacteriaceae infecting virus which was discovered by Esther Lederberg in 1949 (Rajagopala et al., 2011). It consists of an Icosahedral head, measuring around 50-60 nm in diameter, containing double-stranded linear DNA as its genetic material. Its flexible tail is 150nm long and may contain tail fibres. Its genome is dsDNA of 48.5KB(Casjens and Hendrix, 2015). λ is a temperate phage which has two possible life cycles after infecting its *E. coli* host, both a lytic and lysogenic one(Clokie et al., 2011). A typical lytic cycle involves the multiplication and release of phage progeny into the extracellular space. To maintain this ‘lysogenic’ state λ has evolved an elaborate pathway of site-specific recombination that inserts the viral chromosome into the chromosome of the host, using specific sites on the phage (attP) and bacterial (attB) chromosomes(Clokie et al., 2011).

7.2 Methods

7.2.1 Disc Diffusion Method

Discs impregnated with Colistin, Rifampicin, Erythromycin, Kanamycin and Vancomycin were used in this study. Agar plates were prepared as described previously (**section 2.11.1**). Solutions of inhibiting reagents of appropriate concentrations (EGTA, 1.5mM; Bisindolylmaleimide-I, 10 μ M; Imipramine, 25 μ M; Y27632, 1 μ M; D-pantethine, 1mM) were prepared and sterile paper discs were soaked in each reagent. An inhibitor disc was placed in the middle while an antibiotic disc was placed equi-distant to the inhibitor disc. These results were then graphically represented as in **Section 7.3.1**.

7.2.2 Effect of OMV inhibitors on MIC of Colistin

An *E. coli* suspension was prepared by inoculating a few colonies from an *E. coli* plate and mixing well with sterile distilled water. This was incubated overnight at 37°C. Müller Hinton Broth was prepared as stated earlier (**section 2.9.2**) on the day of the experiment. This experiment used 64 μ g/ml as the starting concentration. 100 μ l of Colistin was added to the first triplicate and mixed well. This then followed using the doubling dilution method whereby 100 μ l from each triplicate was transferred to the next set of triplicates until the concentration reached 0.015 μ g/ml. A triplicate of control with no antibiotic added was also prepared. 20 μ l of the bacterial suspension was added to each well and mixed thoroughly (the total well volume being 220 μ l). The remaining sets of wells of the plate followed the same pattern but had the inhibiting reagents (**Figure 7.2**). This was then incubated overnight at 37°C. The transparent wells were recorded for MIC values. The MIC values of antibiotic treated control wells were then compared to the wells treated with both inhibiting reagent and antibiotic.

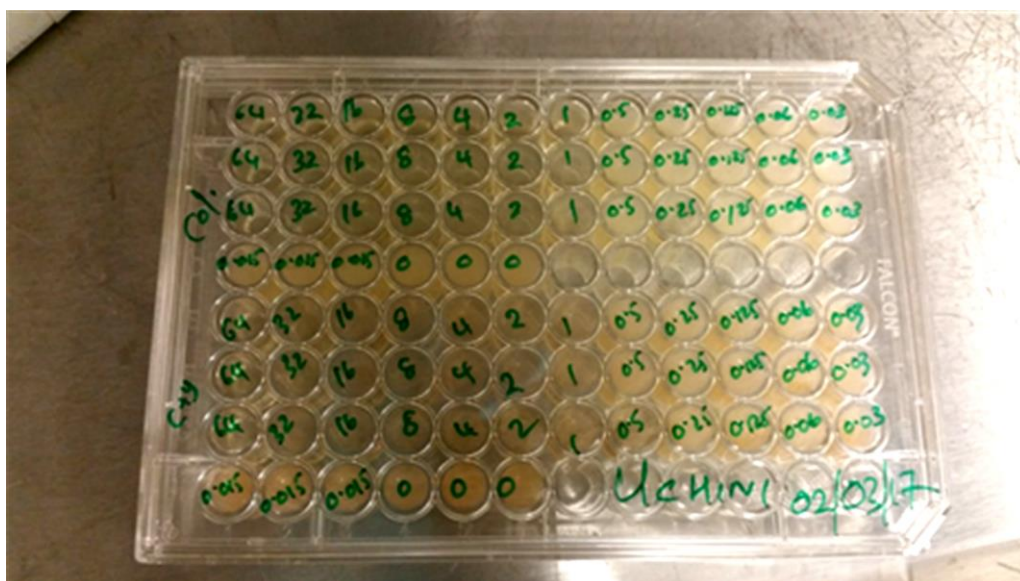


Figure 7.2: MIC of Colistin. The 96-well microtitre well plates were arranged as shown with appropriate volumes of the antibiotic, inhibiting reagents and the bacterial suspension as described. Upon incubation, the wells were compared to the untreated control and transparent wells were considered for MIC values.

7.2.3 Isolation and Propagation of Lambda Phage

The phage kit, 200201/ Gigapack III Gold Packaging Extract, 4 Rxn from Agilent technologies was used as the source of lambda phage and *E. coli* VCS257. The isolation was carried out adhering to the manufacturer's guidelines. Phage propagation was initiated by adding 5ml of SM buffer to the highly confluent phage plate as shown in **Figure 7.8**. It was left on the shaker for 2h at room temperature after which the SM buffer was pipetted off and spun at maximum speed (25,000g for 10min). The supernatant was either immediately used or stored at 4°C for future experiments.

7.2.4 Effect of phage concentration on OMV Release

The isolated phage was used to prepare serial dilutions in SM buffer to examine the effect on OMV production. An overnight culture of *E. coli* grown in LB broth to an OD of 0.5 was used in all experiments. 10µl of phage from each dilution was mixed with 200µl of *E. coli* suspension and incubated at 37°C for 1h. The OMV isolation was carried out as described in **section 5.2.1.1**. Phage concentration was calculated and expressed in Plaque Forming Units per ml (PFU/ml).

7.2.4.1 Effect of incubation time on OMV Release

The isolated phage was used to prepare serial dilutions in SM buffer to examine the effect on OMV production. An overnight culture of *E.coli* grown in LB broth to an OD of 0.5 was used in all experiments. 10µl of phage from each dilution was mixed with 200µl of *E. coli* suspension and incubated at 37°C for different durations (0, 5, 10, 15 and 20min). The OMV isolation and quantification were carried out as described previously (**section 6.2.1**). Phage concentration was calculated and expressed in Plaque Forming Units per ml (PFU/ml).

7.2.4.2 Effect of PAD inhibition on OMV Release

Chloramidine (Cl-amidine), a pharmacological inhibitor of PAD enzyme has been shown to affect EV synthesis and release (**Fig 3.7**). Its presence in *E. coli* (**Section 6.3.4**) was confirmed by immunoprecipitation and Western blotting. Therefore, it was interesting to examine its effect on OMV synthesis. An overnight culture of *E.coli* grown in LB broth was used in the experiment. The cells were washed at 4,000 g for 10min and seeded in triplicate in micro-centrifuge tubes. 50µM of Cl-am was added separately into each tube and incubated for 24h at 37°C in 5% CO₂. OMV isolation was carried out according to **section 6.2.1**. The experiment was repeated thrice and the OMV count was determined using NTA analysis (Nanosight NS500).

7.2.4.3 PAD Inhibition Enhances Phage Concentration

The aim here was to determine the effect of pharmacological OMV inhibition on phage propagation. An overnight culture of *E. coli* grown in LB broth up to an OD of 0.5 was used. 200µl of *E. coli* was incubated with 50µM of Cl-amidine for 60min which was then incubated with 10µl of 10⁻⁴ phage for 20min. 5ml of Top Agar was added to the mixture and poured on pre-warmed bottom agar plates. The plates were incubated overnight at 37°C in 5% CO₂. The experiment was carried out in triplicate. Phage concentration was calculated and expressed in Plaque Forming Units per ml (PFU/ml).

7.2.5 Effect of addition of OMVs on Phage Therapy

With a view to identifying whether adding OMVs affects the phage concentration, the following experimental set-up was prepared: different concentrations of isolated OMVs were added to 10µl of 10⁻⁴ lambda phage and incubated for 60min at 37°C. Then 200µl of an overnight culture of *E. coli* was added to the phage-OMV mixture and further incubated for 20min at 37°C. 5ml of Top Agar was added to the mixture and poured on pre-warmed bottom agar plates. The plates were incubated overnight at 37°C in 5% CO₂. The experiment was carried out in triplicate. Phage concentration was calculated and expressed in Plaque Forming Units per ml (PFU/ml).

7.2.6 Transmission Electron Microscopy imaging of Lambda phage and phage-OMV Interaction

10^{-3} of phage stock was used for TEM imaging of phage. $1.7\mu\text{l}$ of a 10^{-3} dilution of phage stock (of titre 5.8×10^8 PFU/ml) was mixed with $3.6\mu\text{l}$ of a 10^{-1} dilution of OMV stock (1.4×10^8 OMVs/ml) and incubated for 30min at 37°C in 5% CO_2 . TEM was carried out as described previously (section 2.12).

7.3 Results

7.3.1 OMV inhibitors enhance the effect of antibiotic activity against *E.coli*

The investigation into finding an effective inhibitor of OMV release from bacteria was important to examine their possible role in enhancing antibiotic activity. Initial data as presented in **Figure 7.3** clearly shows the effect of OMV inhibitors on antibiotic activity. Rifampicin has shown to be the most responsive to inhibitors compared to other antibiotics. However, of the OMV inhibitors, GSK199 was effective against erythromycin, increasing its effectivity, measured as a percentage increase in the measured zone of inhibition on the lawn of *E. coli* by 88.9 % ($p=0.0025$); rifampicin by 56.72% ($p=0.0561$) and colistin by 14.62% ($p=0.2495$). Bisin-I was active against rifampicin and kanamycin increasing their effectivity by 42.62% and 17.9% respectively ($p=0.0263$ and $p=0.0122$). PAD inhibition was superficially effective against all antibiotics used in the study. BB-Cl-amidine was the most potent PAD inhibitor which was mostly effective together with rifampicin. It increased the zone of inhibition by 106.45% ($p=0.0025$). Nonetheless, Cl-amidine was also effective across the study and was most effective in combination with erythromycin (35.6%, $p=0.0572$). Also, Bis-I and EGTA had quite similar effects with rifampicin with an overall increase of zone of inhibition by at least 40% with Bis-I ($p=0.0263$) and with EGTA being 100% ($p=0.0005$). EGTA increased the effectiveness of erythromycin by 50% ($p=0.0093$). The zone of inhibition as a result of Kanamycin activity was increased with bisin-I by 16.96% ($p=0.0595$), with Cl-amidine by 38.76% ($p=0.0390$) and with BB-Cl-amidine by 65.62% ($p=0.0186$). Vancomycin had no activity against *E. coli* suggesting that it is only effective against Gram-positive bacterial species. Zhou and colleagues have clearly stated that *E. coli* is resistant to vancomycin as it cannot significantly penetrate outer membrane. However, the synergy between different antibiotics was used to monitor the improved effectiveness. The results indicated that the effect was insignificant on growth inhibition or cell killing (Zhou et al., 2015) which supports our thesis findings.

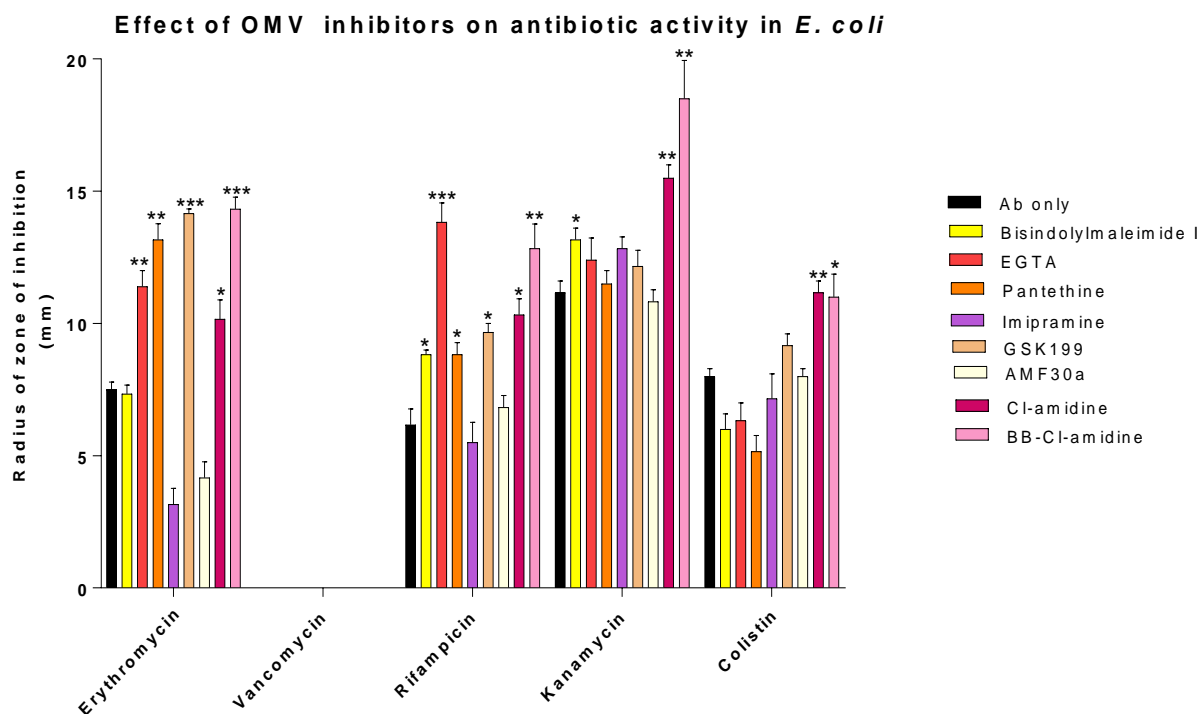


Figure 7.3. Using OMV inhibitors increase the antibiotic activity against *E. coli*. All antibiotics (Abs) except for vancomycin were shown to have significant increases in their zones of Inhibition. EGTA was effective against Erythromycin and Rifampicin increasing the measured zones as a measure of activity by 50% ($p=0.0093$) and 100% ($p=0.0005$) respectively. GSK199, Cl-amidine and BB-Cl-amidine were all effective against all antibiotics tested. BB-Cl-amidine resulted in the highest inhibition of all. It increased the zones of inhibition by 37.5% ($p=0.0351$) for colistin, erythromycin by 90% ($p=0.0006$), rifampicin by 106.45% ($p=0.0025$) and kanamycin by 65.18% ($p=0.0186$). However, the PAD2 inhibitor, AMF30a exerted an antagonist effect opposed to other PAD inhibitors with respect to all antibiotics except Rifampicin. Although not significant, the zone of inhibition was increased by 13.33% ($p=0.0572$). Bisindolylmaleimide-I was effective against rifampicin and kanamycin increasing their activity by at least 44.3% ($p=0.0263$) and 16.96% ($p=0.0595$) respectively. Pantethine increased the zone of inhibition by 75.47% ($p=0.0034$) with respect to erythromycin and by 43.11% in combination with rifampicin ($p=0.0153$). Kanamycin was the least affected antibiotic in the presence of OMV inhibitors. Cl-amidine was 38.76% ($p=0.0390$) effective and BB-Cl-amidine was 65.62% ($p=0.0186$) effective against Kanamycin. Vancomycin was not effective against Gram-negative bacterial colonies as it did not result in a zone of inhibition even in the presence of any of the used antibiotics alone. Importantly, there were no zones of inhibition seen in the plates which were only treated with the inhibitor discs which clearly shows that there is no sole effect exerted by the inhibitors on bacterial growth. The experiment was carried out two times and the data presented are mean \pm SEM of the results.

7.3.2 Effect of OMV Inhibitors on MIC value of Colistin against *E. coli*

The MIC value of Colistin against Gram-negative bacteria has been inconsistently reported in the literature so it was essential to investigate this further. The data presented in **Figure 7.4** reveals the effect of OMV inhibitors on the MIC of Colistin. It was interesting to see that all reagents used managed to decrease the MIC value of Colistin by more than 50%. BB-Cl-amidine and Cl-amidine resulted in the lowest MIC values producing an 88% reduction in MIC ($p=0.0001$ and $p=0.0002$ respectively) while GSK199 lowered the MIC by 76% ($p=0.0004$). Though the MIC of Colistin in the presence of EGTA was higher compared to the others, this still resulted in a 52% reduction compared to the untreated control ($p=0.0183$).

7.3.3 OMV inhibitors enhances the effect of antibiotic activity against *S. aureus*

OMV inhibitors had a significant effect on Vancomycin with Cl-amidine being more potent with 42.67% increase in antibiotic effectivity ($p=0.0354$) (**Figure 7.5**). EGTA, GSK199 and Bisin-I increased the zone of inhibition by atleast 16% ($p=0.0022$). However, Kanamycin and colistin had the highest effect imposed by OMV inhibitors. EGTA was effective against kanamycin which increased the zone of inhibition by 12.24% ($p=0.0351$) and Colistin by 10.96% ($p=0.0296$). However, EGTA did affect rifampicin as Bisin-I, which increased the effectiveness by 8.47% ($p=0.1448$). Bisin-I was also active against kanamycin increasing antibiotic effectivity by 19.42% ($p=0.0166$) and colistin by 19.35% ($p=0.0351$). GSK199 was also active against rifampicin, increasing the zone of inhibition by 10.06% ($p=0.0202$). BB-Cl-amidine was also effective against erythromycin and kanamycin which managed to increase the zone of inhibition by 18.22% ($p=0.0234$) and 28.98% ($p=0.0101$) respectively. Cl-amidine was also active against rifampicin which increased the zone of inhibition by 6.43% ($p=0.0239$), kanamycin by 20.81% ($p=0.0055$) and colistin by 21.53% ($p=0.0444$). Overall a significant effect of PAD inhibition was noted in antibiotic activity against *S. aureus*.

Minimum Inhibitory Concentration(MIC) of *E. coli* in the presence of Colistin and OMV Inhibitors

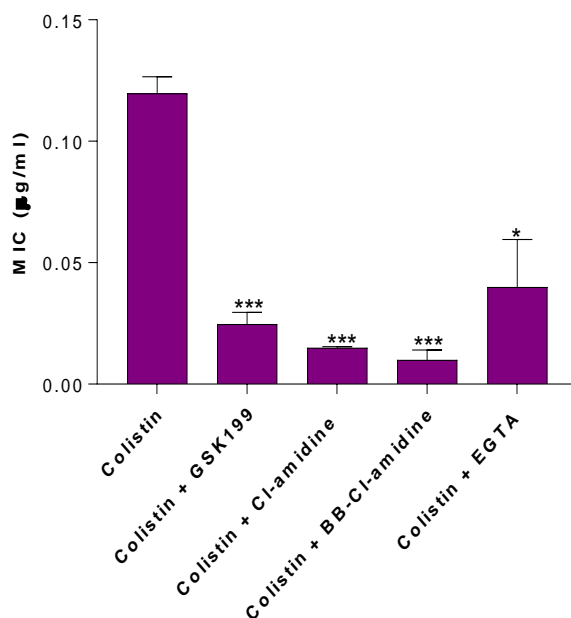


Figure7.4 OMV inhibitors reduce the MIC value of Colistin. All OMV inhibitors managed to lower the MIC value of Colistin by 50%. However, BB-Cl-amidine was the most potent which reduced the MIC by 91.59% ($p=0.0002$). Cl-amidine decreased MIC by 87.39% being the second most potent inhibitor against colistin. However, both GSK199 and EGTA were effective by 74.79% ($p=0.0004$) and 66.3% ($p=0.0183$) respectively in lowering MIC. Although not significant, EGTA was 75% less effective than BB-Cl-amidine in reducing MIC ($p=0.2065$). GSK199 was less potent compared to BB-Cl-amidine by 25% ($p=0.4879$). Nevertheless there was no effect on MIC with Colistin in the presence of only the inhibitors which clearly shows that there is no sole effect exerted by the inhibitors on bacterial growth. The experiment was repeated three times and the data presented are mean \pm SEM of the results.

Effect of OMV inhibitors on antibiotic activity in *S. aureus*

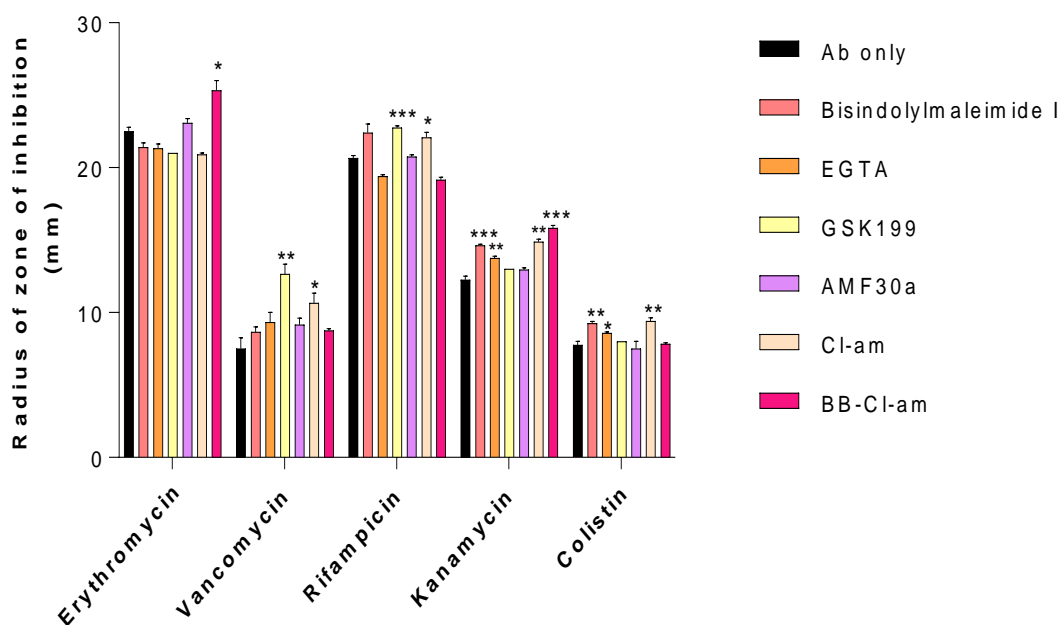


Figure 7.5 Using OMV inhibitors increase the antibiotic activity against *S.aureus*. OMV inhibitors were active against all antibiotics used. However, Vancomycin, Rifampicin, Kanamycin and Colistin were shown to produce a significant increase in their zones of Inhibition. Vancomycin was affected by Bisindolylmaleimide-I which increased its zone of inhibition by 16% ($p=0.1181$). GSK199 and Cl-amidine were more potent against vancomycin which increased its effectiveness by at least 40% ($p=0.0250$ and $p=0.1562$). Cl-amidine was also effective against Rifampicin, Kanamycin and Colistin which also increased the zone of inhibition by 6.43% ($p=0.1077$), 20.81% ($p=0.0055$) and 21.53% ($p=0.0444$) respectively. GSK199 was also active against Rifampicin which increased the zone of inhibition by 10.06% ($p=0.0202$). BB-Cl-amidine was shown to increase the zone of inhibition by 18.22% ($p=0.0234$) against Erythromycin and by 28.98% ($p=0.0101$) against Kanamycin. EGTA and Bisindolylmaleimide-I were also potent against all antibiotics with Erythromycin being the exception. The PAD inhibitors were more effective in conjunction with antibacterial therapy against Gram positive bacterial species. There were no zones of inhibition seen in the plates which were only treated with the inhibitor discs which clearly shows that there is no sole effect exerted by the inhibitors on bacterial growth. The experiment was carried out three times and the data presented are mean \pm SEM of the results.

MIC of *S.aureus* in the presence of Vancomycin and OMV Inhibitors

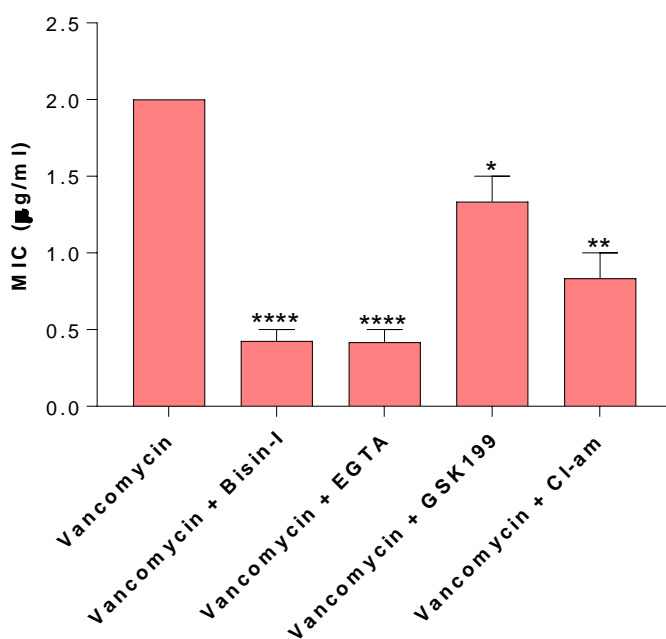


Figure 7.6 OMV inhibitors reduce the MIC value of Vancomycin. All OMV inhibitors managed to lower the MIC value of Vancomycin by at least 50%. However, Bisindolylmaleimide-I (Bisin-I) and EGTA were the most effective reducing the MIC of vancomycin by 75% ($p=0.0004$ and $p=0.0001$ respectively). GSK199 was the least effective in combination with vancomycin which only resulted in a 25% decrease in MIC ($p=0.0161$). GSK199 was less effective compared to the most effective inhibitors by 80% ($p=0.0079$). Cl-amidine increased the effectiveness of vancomycin by at least 62.5% ($p=0.0022$). This was lower than that of the most potent inhibitors by 75% ($p=0.0158$). It was however more effective than GSK199 by 37% ($p=0.0550$). Nevertheless, there was no effect on MIC of Collistin in the presence of only the inhibitors which clearly shows that there is no sole effect exerted by the inhibitors on bacterial growth. The experiment was repeated three times and the data presented are mean \pm SEM of the results.

7.3.4 Effect of OMV Inhibitors on MIC value of Vancomycin against *S. aureus*

The MIC value of Vancomycin against *S. aureus* was inconsistently noted in the literature so it was essential to investigate this further. **Figure 7.6** reveals the effect of OMV inhibitors on the MIC of Vancomycin. The reagents that were more effective in **Figure 7.5** were used in this experiment. It was interesting to see that all reagents used managed to decrease the MIC value by at least 25%. Bisin-I and EGTA resulted in the lowest MIC value of 0.5µg/ml producing a 75% reduction ($p<0.0001$). PAD inhibitors together managed to reduce the MIC by 37.5% with Cl-amidine being more effective resulting in a 50% reduction ($p=0.0022$) while GSK199 only lowered MIC by 25% ($p=0.0161$). The results suggest that these inhibitors can be used in future experiments.

7.3.5 Propagation of Lambda phage

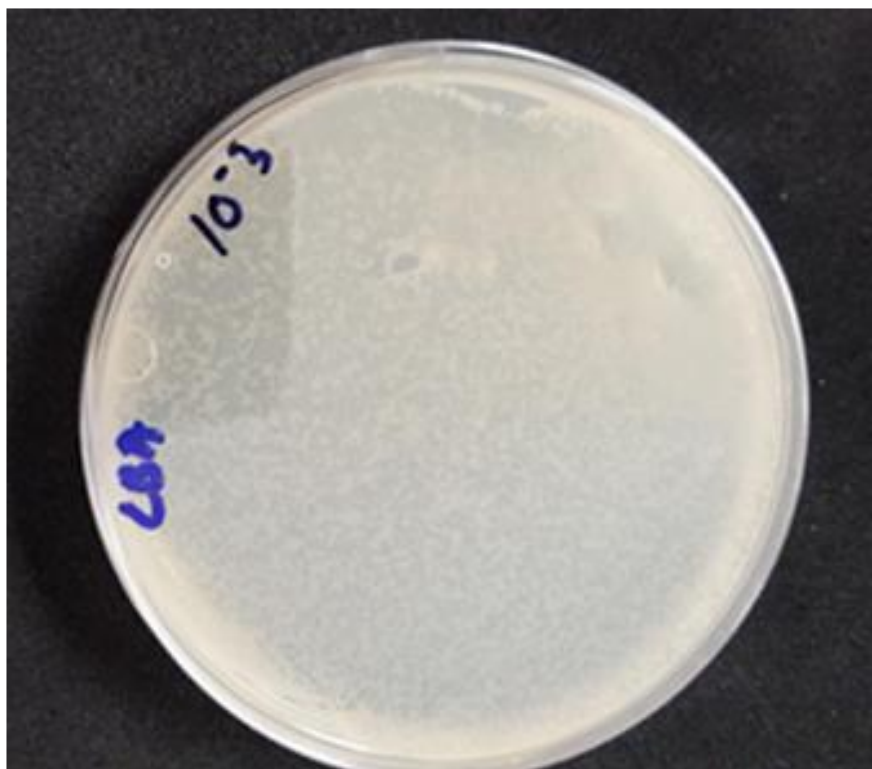


Figure 7.7 Lambda phage propagated at 10^{-3} concentration. This plate was used in phage propagation.

7.3.6 Effect of phage concentration on OMV Release

It was very interesting to observe the effect of phage itself on the release of OMVs from its targeted cell, *E. coli*. It is very well established that the presence of a high concentration of phage promotes OMV release which in turn can have a decoy effect on phage activity (Shabbir et al., 2016, Reyes-Robles et al., 2018b, Kulkarni et al., 2015, Seed, 2015, Tabib-Salazar et al., 2018, Górski et al., 2017). This is another type of defence mechanism adopted by bacteria in order to combat phage attack which may result in the building up of resistance towards phage therapy. The results obtained emphasise the importance in using low phage concentrations to actively sensitise the bacterial cells to phage therapy. Multiplicity of Infection (MOI) effectively indicates the concentration of infectious agents (phage in this case) that attack each bacterial cell during an infection. As the MOI decreases so does the OMV release As shown in **Figure 7.8A** and **Figure 7.8B** the lowest phage titre of 4.4×10^4 reduced the OMV count by 73.15% ($p=0.0002$) compared to the highest OMV concentration recorded in the study in the presence of a phage titre of 9.4×10^8 . Compared to using the highest phage titre, a titre of 5×10^5 reduced the OMV concentration by 69% ($p=<0.0001$). There was a 54.23% decrease in OMV release when the MOI was decreased from 6.27 to 0.05 ($p=0.0055$). The overall effect of decreased MOI from 6.27 to its lowest of 0.0004 reduced the OMV count by 73.15%. Therefore a 10^{-4} phage dilution (5.8×10^8 PFU/ml) was used as the standard in all experiments.

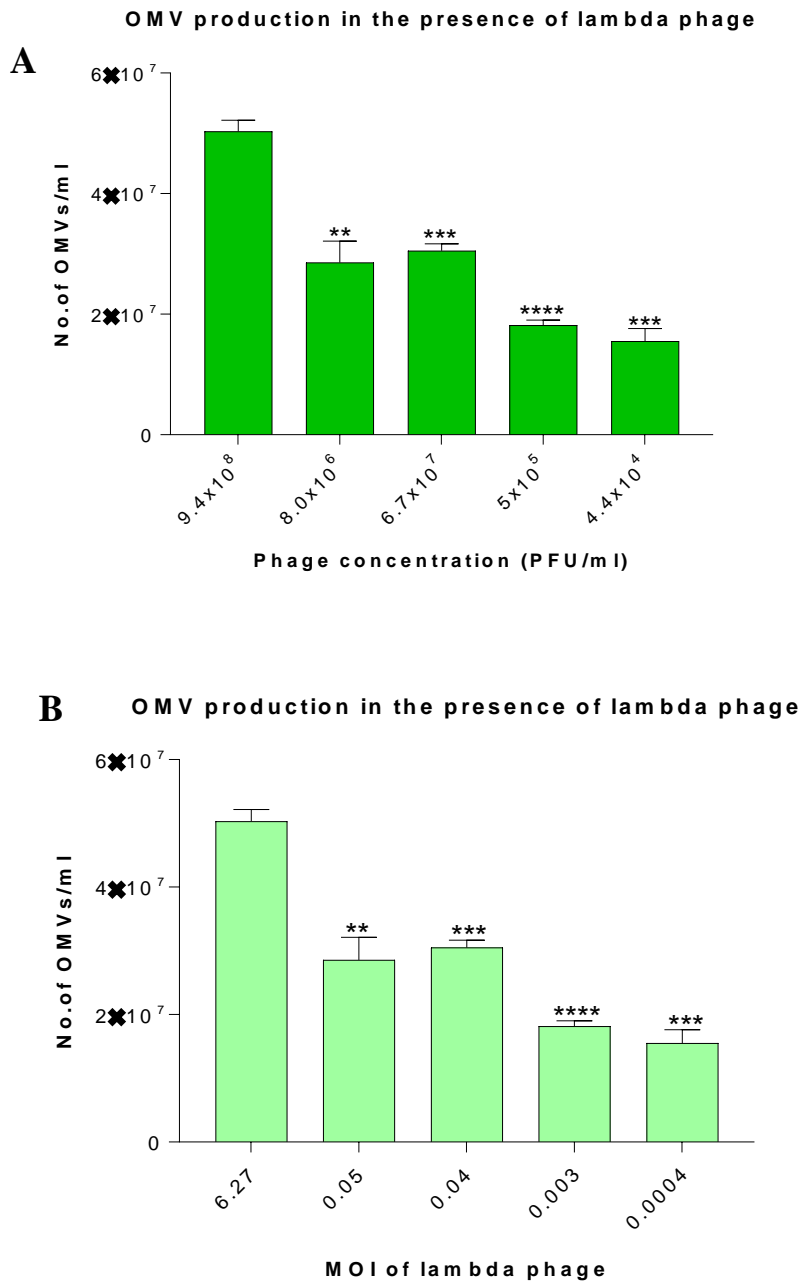


Figure 7.8 Effect of phage concentration on OMV release. **A**, Phage concentration has a significant effect on OMV release. As the phage concentration decreased so did the number of OMVs released. The OMV concentration was the lowest at the phage titre of 4.4×10^4 PFU/ml. This was a reduction of 73.14% ($p=0.0002$) compared to the highest OMV concentration recorded in the study in the presence of a phage titre of 9.4×10^8 PFU/ml. The second lowest phage titre, 5×10^5 PFU/ml reduced the OMV concentration by 69% ($p<0.0001$) compared to the highest phage titre. This was however 25.25% higher than the lowest OMV concentration ($p=0.3107$). **B**, At a MOI of 0.0004 the lowest OMV concentration released from bacteria was detected, which was a drastic reduction of 73% ($p=0.0002$) compared to the highest MOI of 6.27. As the MOI of phage reduced so did the OMV concentration, showing a dose response of phage on OMV release. An MOI of 0.05 MOI reduced the OMV concentration by 54.25% ($p=0.0055$). However an MOI of 0.04 was shown to stimulate OMV release by 24% ($p=0.6301$). The MOI should be considered when investigating novel aspects of phage therapy. The experiment was repeated three times and the data presented are mean \pm SEM of the results.

7.3.7 Effect of phage-OMV incubation time on the release of OMVs

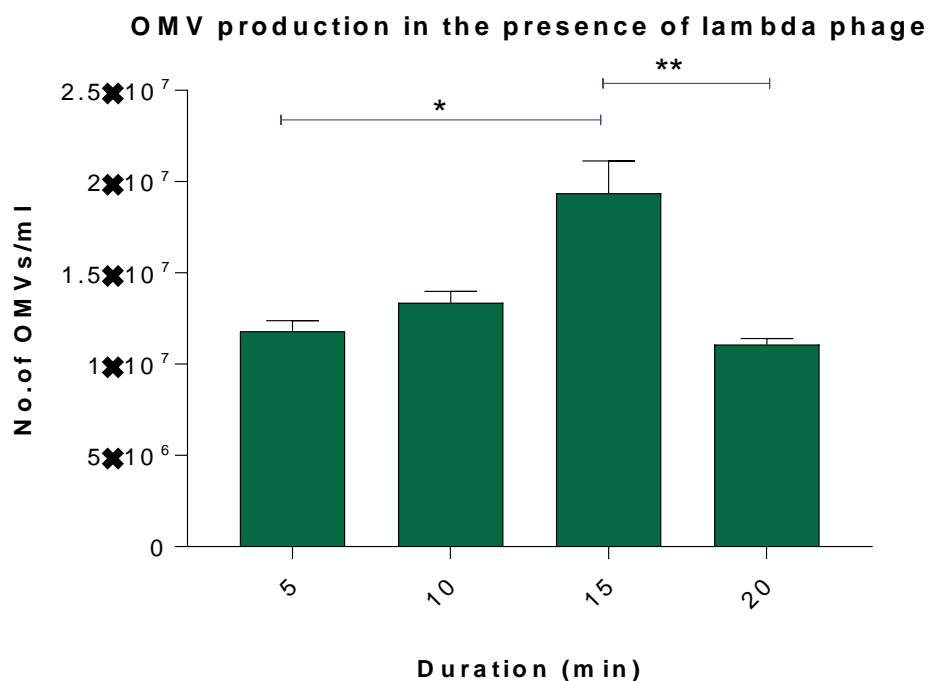


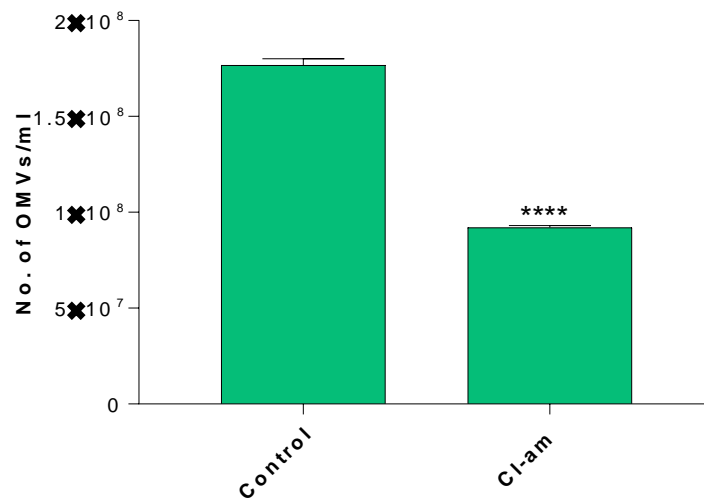
Figure 7.9 Effect of Incubation time on OMV release. The graph symbolises the significance of incubation time of phage and bacteria on OMV release. The concentration of OMVs increased steadily for 15min which was followed by a rapid decline. OMV concentration increased by 11.7 % in the first 5 min ($p=0.1365$) which was further increased by 36.12% ($p=0.0327$). This was however rapidly decreased by 49.8% after 15min ($p=0.0099$) which was only 10.93% compared to the starting OMV concentration at 5min ($p=0.3331$). The overall OMV reduction was calculated to be 43.6% ($p=0.0073$). The experiment was repeated three times and the data presented are mean \pm SEM of the results.

There was a significant increase in OMV production ($p=0.0073$) within the first 15min of incubation by 11.72% (10 min) and 36.12% (15 min). However, there was a significant decrease in OMV release for incubation periods beyond that (20 min; $p=0.0099$). The concentration of OMVs released at 20 min was even lower than the starting concentration of OMVs by 6.27 % ($p=0.3331$). However previous experiments carried out in the field suggest that 15min incubation is optimal for *E. coli*-phage initial interaction.

7.3.8 Pharmacological inhibition of PAD significantly improves therapeutic usage (in phage therapy) of Lambda Phage

PAD catalysed citrullinated proteins are known to be present in *E. coli* (sections 6.3.4 and 6.3.5). **Figure 7.10A** illustrates the effect of pharmacological inhibition of PAD via Cl-amidine as significantly reducing the number of OMVs released compared to untreated control by 48.06% after 1h incubation ($p<0.0001$). Moreover, the data presented in **Figure 6.9B** clearly shows that the presence of OMVs obstructs the (receptor-mediated) binding of phage to *E. coli* as the titre of free phage then able to infect *E. coli* in the subsequent plaque assay is dose-dependently diminished with increasing OMV concentration. Although it was not significant, addition of 10 OMVs reduced the phage activity (measured as the phage titre) by 13.3 % ($p=0.1987$). In contrast, phage activity reduced by 97.92% after the addition of 10^3 OMVs. This significant reduction ($p=<0.0001$) was however restored by 99.01% ($p=<0.0001$) when the OMV synthesis and release was inhibited. Pharmacological inhibition of PAD by Cl-am has increased phage particles that are available to potentially cause bacterial lysis by 45.45% compared to Cl-am untreated *E. coli* and phage control ($p=0.0052$) and by 52.73% compared to addition of 10-fold OMVs ($p=0.0002$). Thus OMV inhibition would be expected to reduce the capacity of bacteria to use OMVs as decoys for infection with phage. Negative controls of samples without phage (just *E. coli* and OMVs) were used in the experiment to confirm that the plaques were only visible in the presence of phage and not as a result of the interaction of *E. coli* with introduced OMVs.

A Inhibition of *E.coli*-derived Outer Membrane Vesicles



B Plaque Assay of *E.coli* + Lambda Phage

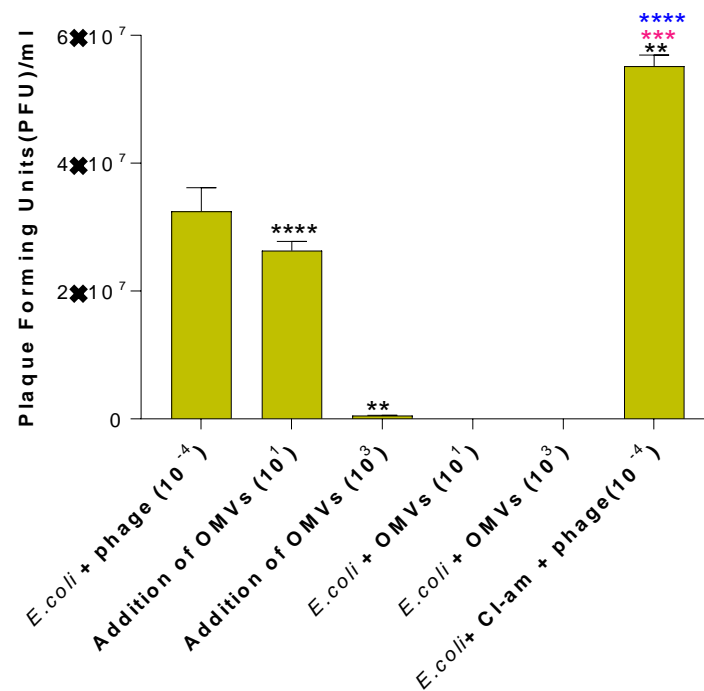


Figure 7.10 Effect of PAD inhibition on OMV release and its impact on Phage activity. Addition of OMVs significantly reduced the PFU in the samples ($p=0.0010$ in the presence of 10^3 OMVs). OMV ‘absorption’ of phage was intimated by the significant increase in phage titre (PFU/ml) in Cl-amidine-treated sample ($p=0.0052$). This was significantly higher by 42.85% ($p<0.0001$) compared to addition of 10^1 OMVs and 99% compared to the addition of 10^3 OMVs ($p<0.0001$). Additions of OMVs to *E.coli* samples were taken as negative control to confirm that changes were only observed in the presence of lambda phage. (*= significance compared to the control; **= significance addition of 10^3 OMVs compared to the Cl-am treated; ***=significance addition of 10^1 OMVs compared to the Cl-am treated. The experiment was repeated three times and the data presented are mean \pm SEM of the results.

7.3.9 Electron Microscopy Imaging confirms the likelihood of a phage-OMV Interaction during Bacterial Infections

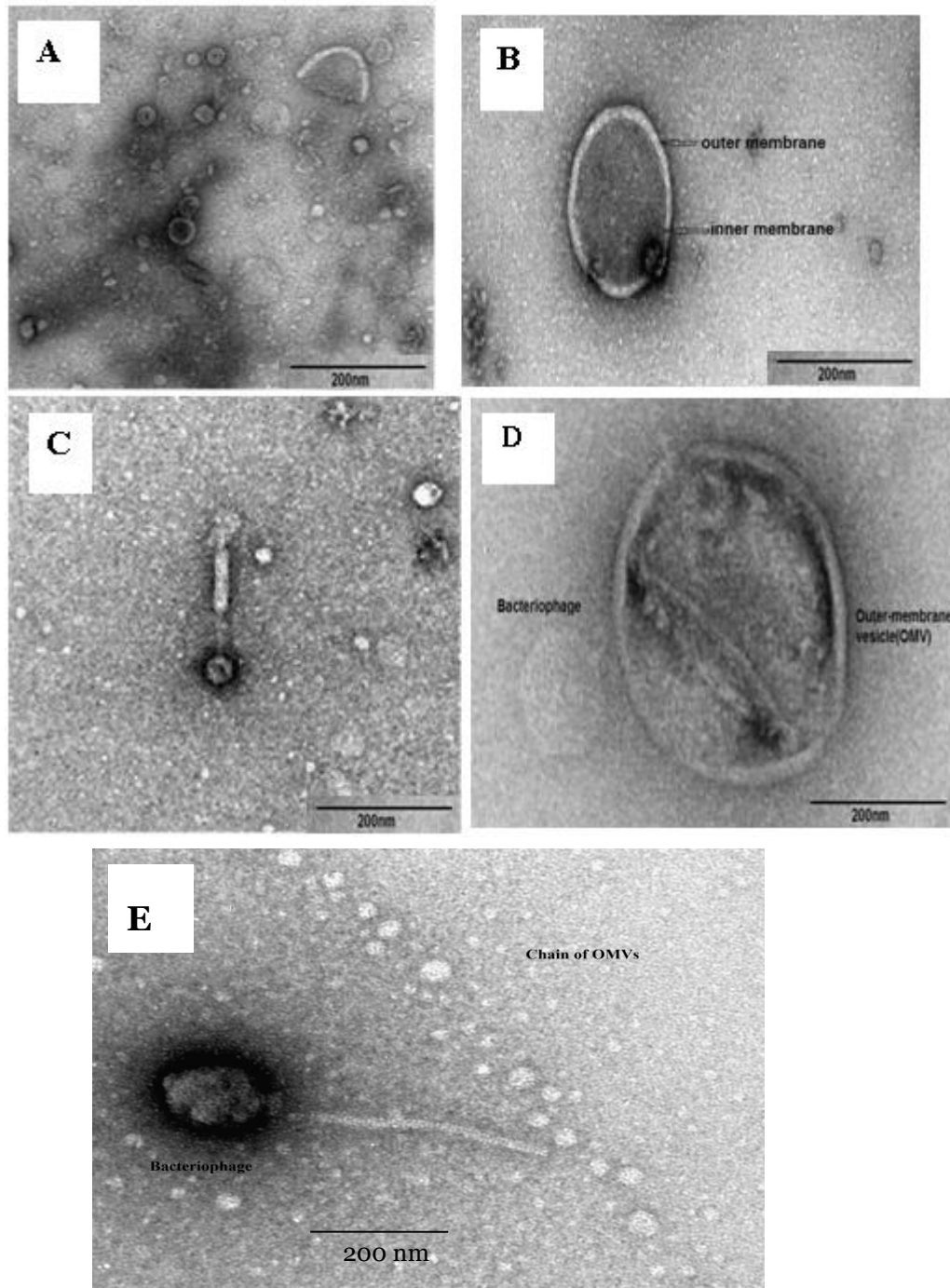


Figure 7.11 Negative stain TEM micrographs of OMVs after incubation with lambda phage. 10^{-3} dilution of phage stock of titre 5.8×10^8 PFU/ml) was mixed with 10^{-1} dilution of OMV stock (1.4×10^8 OMVs/ml) and incubated for 30min at 37°C in 5% CO_2 . The particles were stained with 1% (w/v) uranyl acetate following incubation. **A**, poydispersed population of OMVs were observed. **B**, an enlarged image of membrane bound *E. coli*-OMV. **C**, lambda phage with icosahedral head, sheath, tail and fibres. **D**, a clear image of OMV-phage interaction. **E**, phage attachment to a chain of OMVs.

Transmission electron microscopy was used to confirm OMV isolation by morphology and average size estimations. It was also used to visualize any lambda phage-OMV complexes. **Figure 7.11A** and **Figure 7.11B** show OMVs isolated from *E. coli*. The sample was clearly poly-dispersed with the majority of vesicles ranging in size from 20- 50nm while some were 100-207nm in diameter. **Figure 7.11C** is a micrograph of lambda-phage with an icosahedral-shaped head measuring approximately ranging in size from 27nm to 36.7nm in width, showing the contractile sheath (tail) ranging in length from 101nm to 260nm and the tail fibres ranging in length from 200-315nm. Many complexes between lambda and OMVs were visualised as in **Figure 7.11D** and **Figure 7.11E**. It was particularly interesting to identify the formation of chains of OMVs in complex samples (phage and OMVs) which were totally absent from samples of where only OMVs were present.

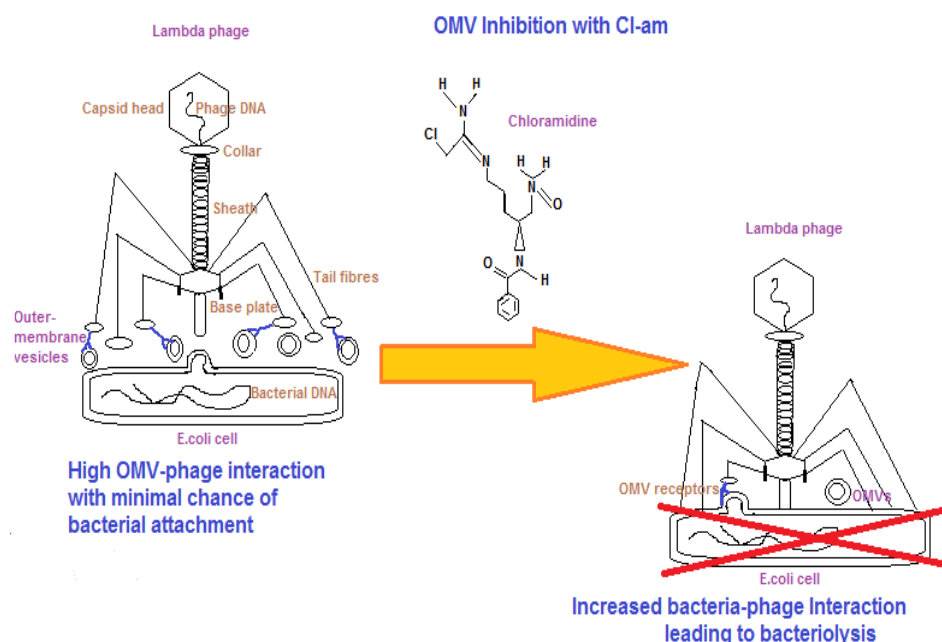


Figure 7.12 Schematic representation of the effect Cl-am- mediated OMV inhibition on phage therapy. Synthesis of OMVs from *E.coli* cells promotes vesicle-receptor mediated interaction with phage particles arresting the bacterial-phage interaction. Pre-treatment of *E.coli* cells with Cl-am hinders OMV release. This promotes the phage-bacterial interaction leading to phage-mediated bacteriolysis.

7.4 Discussion

This section has elucidated the importance of OMV inhibition on enhanced susceptibility of both Gram-positive and Gram-negative bacterial species to antibiotic therapy. Upon OMV inhibition, *E. coli* was more sensitive to erythromycin, rifampicin, colistin and kanamycin. There was no vancomycin activity on *E. coli* which confirms its limited effectiveness on Gram-positive species. Colistin had a significant effect in this study (**Figure 7.1**) clearly demonstrating that colistin activity is enhanced in the presence of certain inhibitors. This is further illustrated in **Figure 7.4** where the inhibiting reagents have significantly decreased the MIC value of colistin which suggests that lower concentrations of the antibiotic can be used to treat infections with minimal damage to healthy cells.

It has been shown that the presence of calcium decreases the effect of colistin mediated damage in *Paenibacillus polymyxa* which suggests that Ca^{2+} modulates a protective barrier against colistin (Wang et al., 2017). EGTA is a calcium chelator which can mop up the excess calcium present in the intercellular environment which acts synergistically with colistin to elicit a bactericidal effect. This together with its role in OMV inhibition enhances the antibiotic activity. Polymyxin B is a PKC inhibitor (Robinet et al., 2005).

Although there is no evidence of Polymyxin E (colistin) being involved in PKC inhibition, the presence of PKC inhibitor, Bisin-I, is shown to cease OMV secretion. This might thereby decrease drug expulsion and increase bioavailability of colistin. Also, Vincent and colleagues have demonstrated that *E. coli* cells contain both a protein-tyrosine kinase and a phosphotyrosine-protein phosphatase (Whitmore and Lamont, 2012). So Bisin-I might be acting on these pathways and stop phosphorylation which is another mechanism by which *E. coli* undergoes apoptosis. Similarly, Imipramine, an inhibitor of A-SMase (Kosgodage et al., 2017) is directly involved in OMV inhibition as described in **section 3.4**. Therefore imipramine is likely to improve the bacterial cell's ability to retain the antibiotic within the bacterial cells augmenting its activity.

Pharmacological inhibition of OMV release has not been communicated previously. However many groups have discussed the use of OMVs as drug delivery vehicles (Jain and Pillai, 2017, Gujrati et al., 2014, Wang et al., 2018, Gerritzen et al., 2017, Jan, 2017a, Ellis and Kuehn, 2010). The exact mechanism for packaging proteins and other reagents in OMVs has not been fully understood but Alves and colleagues have successfully managed to insert an enzyme, phosphotriesterase (PTE) in OMVs which enables its activity to be maintained when subjected to elevated temperatures, iterative freeze-thaw cycles and lyophilisation. This was designed by creating a synthetic linkage between PTE and a highly expressed transmembrane porin protein (OmpA) known to be abundant in OMVs (Alves et al., 2016a). The same group has shown that

bacterial OMVs can be used as nano-bioreactors in cancer therapy. A mutant *E. coli* strain that exhibits reduced endotoxicity toward human cells was engineered to generate OMVs displaying a human epidermal growth factor receptor 2 (HER2)-specific affibody in the membrane as a targeting ligand. Systemic injection of siRNA-packaged OMVs caused targeted gene silencing and induced highly significant tumour growth regression in an animal breast cancer model (Alves et al., 2016a). The effect of PAD inhibition on bacterial species has been discussed previously only on oral bacteria (Mangat et al., 2010). This has been only in the context of its correlation to rheumatoid arthritis (Montgomery et al., 2016) whereas there has been no reporting on PAD-related OMV inhibition in bacterial species let alone in *E.coli* or *S.aureus*. The work presented herein has clearly shown that PAD-mediated OMV inhibition has a significant effect on antibiotic activity, reducing MIC values specifically on colistin and vancomycin. Interestingly, this effect was reduced in *S. aureus* which suggests that there might be different mechanisms of OMV biogenesis and release involved. Additional experiments using different OMV inhibitors will be useful. However the PAD-mediated OMV inhibition remarkably increased in *S. aureus* which suggests that Gram-positive species might be more sensitive to PAD enzyme. Looking forward, this needs to be examined in a range of Gram-positive and Gram-negative species in order to reach a definite conclusion.

This study has shown that using OMV inhibitors strongly improves antibiotic activity. One might speculate that this could be due to minimising drug expulsion by bacterial cells and so increasing their capacity to retain antibiotic; this in turn allows a more effective bactericidal activity. Consequently this plays an important role in minimising antibiotic resistance as minimal doses of the antibiotic can be administered that can still provoke a bactericidal effect. Further work is needed to fully establish this phenomenon.

Bacteriophage-OMV interaction has been widely expressed (Klimentova and Stulik, 2015, Shabbir et al., 2016, Manning and Kuehn, 2011, Jan, 2017b, Simmons et al., 2018) which in view of the capacity described in this thesis to modulate OMV release, made it a particularly interesting topic to further investigate. Identification of novel OMV inhibitors and their influence on improved antibacterial therapy set the background for the research undertaken in this chapter. It was also of interest to investigate the effect of phage itself on OMV synthesis and release. **Figure 7.8** clearly demonstrated that the lower phage concentration resulted in a low level OMV release and **Figure 7.9** depicted that a shorter incubation time increases the OMV concentration. These findings confirmed the optimal conditions recommended according to the literature. A 10^8 to 10^{10} PFU/ml concentration of phage stock was used in the experiments

with an initial *E.coli*- phage interaction interaction time of 15min before plating up. This was then followed by 24h incubation at 37°C. However, countable phage particles were observed when the stock was diluted down to 10^{-5} to 10^{-7} (Bonilla et al., 2016, Wang et al., 2006). Therefore, as the MOI decreases so does the OMV concentration. These findings are consistent with the research work on T4 and *E.coli* by Manning and co-workers (Manning and Kuehn, 2011).

OMVs released by bacteria elicit a subtle defensive effect that has been a challenge to develop successful therapy. Our previous research findings in the thesis evaluated the importance of OMV inhibition on improved antibiotic therapy *in vitro*. It has also been shown that the presence of OMVs decreases the virulence of phage allowing the bacterial cells to be resistant to such therapy leading to the possible therapeutic use of phage against bacterial infection. *E. coli* uses this defence mechanism to maximise the binding of phage particles to OMVs instead of the bacterial cells to maximise the survival in such conditions as shown in **Figure 7.10** Addition of OMVs from 10-fold to 1000-fold reduced the MOI from 0.1 to 0.0001 significantly reduced which increased the chance of phage binding to OMVs by 85%. This in turn reduced the phage infection in bacterial cells drastically. Further calculations revealed that approximately 24 phage particles are mopped up by each OMV particle which decreases its infectivity. This phenomenon has also been demonstrated in other bacterial species in the presence of various bacteriophages including T7 and T4(Reyes-Robles et al., 2018b, Tzipilevich et al., 2017, Shabbir et al., 2016). Having seen the detrimental effect caused by OMVs and previous findings of OMV inhibition improving the antibiotic therapy *in vitro*, I was encouraged to investigate whether OMV inhibition similarly could stimulate the phage activity. The Pan-PAD inhibitor, Cl-amidine was used for OMV inhibition. The clear demonstration of the presence of PAD enzyme and citrullinated (deiminated) proteins in *E.coli* in previous chapters lead to the use of Cl-amidine in this section. As discussed previously, there was a significant improvement in phage infection in the presence of Cl-amidine. It considerably reduced the number of OMVs available to bind to phage particles consequently increasing the chance and the rate of phage binding to *E.coli*. This strongly suggest that OMV inhibition is the key to drive the maximum infection potential of lambda phage leading to successful phage therapy. These findings were confirmed via electron microscopy as shown in **Figure 7.11**. This was able to demonstrate the binding of lambda phage to OMVs which further confirmed our conclusion. TEM further signified the abundance of OMVs in the smaller size range of 20-50nm. In addition to the phage attachment to isolated OMVs, the TEM images in the study also revealed bacteriophage binding to multiple chains of OMVs as shown in (**Figure 7.11 E**). Similar chains of bacterial vesicles have been seen in *Myxococcus xanthus* TEM images as reported by a US research group (Berleman et al., 2016). Furthermore, Bohuszewicz and colleagues has also reported the

presence of similar structures in *Shewanella oneidensis* MR-1. These ‘nanowires’ were seen in atomic force microscopy images produced during the study (Bohuszewicz et al., 2016). *S. oneidensis* is a gram-negative, anaerobic species that is notable for metal iron reduction. Pirbadian and colleagues very interestingly has reported the presence of these chains of vesicles *in vivo* concluding that they offer an ‘extracellular electron transport pathway’ (Pirbadian et al., 2014) linking the respiratory system of the microorganism to the external. Therefore, it can be concluded that these outer membrane protrusions closely associated with OMVs are functional energy distributors. **Figure 7.12** is a schematic representation of how further research can aid in advancing OMV-mediated phage therapy.

Furthermore previous research has highlighted that Arginine deiminase (ADI) present in certain bacterial species including the oral cavity microorganism, *Porphyromonas gingivalis* (*P. gingivalis*) inhibits the microorganism’s capacity for surface attachment (Cugini et al., 2013). This prompts the question whether inhibition of the enzyme would facilitate the binding of phage to *E. coli* in addition to mopping up the OMVs. Furthermore, a study reported that in *P. gingivalis*, PAD-mediated citrullination of a critical C-terminal arginine of the anaphylatoxin C5a disabled the protein function that resulted in reduced chemotaxis of neutrophils and diminished calcium signalling in the pro-monocytic cell line U937 transfected with the C5a receptor (C5aR) (Bielecka et al., 2014). This phenomenon can be applied to *E. coli* as well in that PAD inhibition through Cl-amidine modulates different pathways to elicit a favourable response for phage attachment resulting in bacterial killing.

Overall, the results presented in this chapter have presented the significance of OMV inhibition on effective antibiotic and phage therapy (**Figure 7.12**). This original research reveals for the first time the potential of pharmacological inhibition of OMV release on enhanced antibiotic sensitivity and effective phage therapy. Nevertheless, with further improvement this will be a valuable innovation against antibiotic resistance and enriched phage therapy. As a consequence, this phenomenon can be used to improve novel drug intervention and prognosis in bacterial infections.

Chapter 8: Discussion

8.0 Discussion

Over the past decade there has been a rapid interest in the association of extracellular vesicles (also known as EVs in the study) in various disease statuses. Scientists from different fields in biomedicine have been able to apply knowledge of the EV field in terms of EVs' capacity for intercellular communication to explain the nature of disease biogenesis and progression. As a result, since the foundation of the International Society for Extracellular Vesicles (ISEV) (Araldi et al., 2012) there has been an immense drive, with several papers dedicated throughout the literature and in the *Journal of Extracellular Vesicles* to standardizing the isolation and characterization of EVs. This urgent need has enabled EV researchers to develop sophisticated isolation and quantitation techniques that have improved the outcome of such studies (Thèry et al., 2018)

Previous research has highlighted the role of EVs modulating intercellular communication which has been shown to be key to the progression of several diseases, including infectious disease, autoimmune disease, cancer and neurodegenerative disease (Rodrigues et al., 2018, Turpin et al., 2016, Candelario and Steindler, 2014). Other diseases such as cardiovascular disease and diabetes have also attracted the attention of practitioners to the EV field (van Niel et al., 2018). The great interest in EV-mediated intercellular communication has been due to the cargo that EVs are able to deliver. This includes various species of RNA such as miRNA, lncRNA as well as proteins and lipids that EVs are able to deliver to recipient cells. Therefore, '...the 'language' of EVs is by its nature combinatorial, multifaceted, and contextually complex' (Maas et al., 2017).

Through this interest in EVs in mediating and exacerbating disease and our increased understanding of their means of communicating such macromolecules to recipient cells EV researchers have naturally taken an interest in further applications of EV biology. This has taken the path of either modulating their production to for example ameliorate disease progression or of capitalizing on their lipid bilayer, vesicular nature with a lumen that may carry therapeutics, whether drugs or siRNA and the capacity to specifically engineer targeting moieties into their surface to develop their use as drug delivery vehicles. EV-based targeted therapy has thus had a significant impact on clinically led investigations. (van der Meel et al., 2014, Kim and Kim, 2017, Armstrong and Stevens, 2018) and the prospect of EV modulation (removal of EVs from the system) has also showed recent promise (Karasu et al., 2018, Guo et al., 2018). Either way EV-led research has significantly contributed to the development of novel therapeutic interventions.

A large focus of the work presented in this thesis has focussed on pharmacological elimination of EVs and the impact of so doing on reducing disease progression and improving prognosis

following successful treatment. Different cancer models have been used in this investigation along with different anti-cancer drugs to show the significance of EV inhibition. The study looked at the effect of a range of pharmacological agents which according to the signaling pathways they were known to inhibit could be potential EV inhibitors. Some were used previously in research but this has been the only study so far to have collectively presented the effect of these novel EV inhibitors in reducing EV biogenesis and pronouncedly sensitising the cancer cells to lower dosages of chemotherapeutic agents that have fallen out of favour because of too many adverse side-effects at the high concentrations that are needed to be effective or other chemotherapies where it is anyway desirable to reduce dosages while maintaining effectivity. In an extension to this theme, the work presented in this thesis has then applied this knowledge into identifying any possibilities of inhibition of OMV (Outer Membrane Vesicle) biogenesis in both Gram-positive and Gram-negative bacterial species. Somewhat surprisingly, this approach has proved successful, revealing a conserved mechanism of EV and OMV release, and as a consequence the capacity to modulate OMV biogenesis has been further applied to stimulating antibiotic sensitivity and phage-mediated bacterial clearance. Some of the successful discoveries throughout this research have been made available to the scientific community (Kosgodage et al., 2017, Kosgodage et al., 2018a, Kosgodage et al., 2018b, Kosgodage et al., 2019).

8.1 Identification of novel EV inhibitors and their effect on EV Biogenesis and Release

The study was initiated by looking at a range of reagents in their capacity to inhibited EV release in prostate cancer cells, PC3. Some of these pharmacological agents have been described in the literature previously. However, there have been only a handful of studies in connection with EVs. A detailed investigation of the literature combined with preliminary empirical data derived in this thesis brought about a range of agents that were tested along with appropriate initial concentrations to be used. Also it was essential to carry out a pathway analysis of EV biogenesis and release to examine the role of each reagent used on overall EV inhibition. Both flow cytometry and nanoparticle tracking analysis was used to quantify the EVs which facilitated determining the effectiveness of each pharmacological reagent as a potential EV inhibitor.

It was interesting to identify the most pathways which were most effective at inhibiting EV release because as the next stage of the study, pharmacological agents were then used in apoptosis studies, to see if they could promote chemotherapeutic-mediated cytotoxicity. Two pathways were considered initially, PKC-mediated signaling and the dimerization of pantothenic acid linked by disulphide cystamine which blocks PS externalization (a crucial event during EV release). Both pathways were therefore targeted by their respective inhibitors,

Bisindolylmaleimide-I (Bisin-I) and D-pantethine and both were shown to indeed inhibit EV biogenesis.

Similarly, the effect of protein citrullination (also termed deimination) has been widely studied both by our group and many researchers. It is associated with many disease models including rheumatoid arthritis (RA), cardiovascular disease, alzheimer's and cancer (Fert-Bober et al., 2015, Lange et al., 2017b, Wong and Wagner, 2018, Mohanan et al., 2012). The enzyme mediating this post-translational modification is peptidyl arginine deiminase or PAD (Lange et al., 2017a). The formation of the Neutrophil Extracellular Trap (NET) generally is part of the host defence mechanism (Kruger et al., 2015). However, NETosis together with PAD4 activity which produces citrullinated neoantigens that promote autoimmune diseases such as RA could cause injurious effect (Franck et al., 2018, Kenny et al., 2017). For this reason there has been a strong drive to inhibit PAD to thereby eliminate such adverse effects. Our group has previously tested Cl-amidine, a pan-PAD inhibitor in association with EVs (Kholia et al., 2015). This further encouraged its use in the present study. Cl-amidine-mediated PAD inhibition was strongly involved in EV inhibition (**Figures 3.7, 3.8, and 3.9**). This suggests that PADs play a crucial role in EV biogenesis and release.

It should be noted that pharmacological inhibition of other proposed pathways of EV biogenesis and release were also likely to be affected to some extent although not pronounced. D-pantethine did affect the cell viability significantly which strongly suggested ruled it out in potential clinical use (**Figure 3.7A**). It was interesting to note the inhibitory effect of nicotine on EV release. A previous study also looked into the level of plasma microvesicles (MVs) in smokers and non-smokers and the effect of nicotine on MV release was also monitored (Grant et al., 2011). Whilst it was found that smokers (albeit this aspect of the study being restricted to a very small sample size) had reduced plasma MV levels compared to non-smokers, and that nicotine inhibited MV release from the promonocytic cell line, THP-1, more recent studies show that cigarette smoke extract stimulates exosome release in Airway Epithelial Cells (ACE) (Benedikter et al., 2017). This study however did not use nicotine but cigarette smoke extract which is a complex mixture of chemicals, and looked at exosome release alone. A similar study was carried out to determine the effect of tobacco smoke extract (TSE) on vesiculation in human macrophages derived from THP-1 cells. Macrophages are a key participant in extracellular matrix damage. The study concluded that exposure to TSE induced the release of proteolytically active microvesicles from THP-1-macrophages (Li et al., 2013). The positive previously obtained effects observed for nicotine on EV inhibition encouraged its testing in apoptosis studies along with Bisin-I and Cl-amidine (**Figure 3.10B and Figure 3.10C**). Nicotine may possess different properties in different cell types so it will be interesting to

examine the effect of pure nicotine used in this study on alveolar epithelial cells (AEC) to clarify any inconsistency found in the current results.

8.2 Combinatory effect of Protein Kinase C and PAD inhibition together with Nicotine treatment augments the effectiveness of Chemotherapy

Multi-drug resistance either intrinsic or acquired has been increasingly problematic in recent years (Salgia and Kulkarni, 2018, Housman et al., 2014, Baguley, 2010, Mansoori et al., 2017). Despite extensive research efforts in recent years, multi-drug resistance remains a major problem. The use of nanotechnology has fortunately given promise (Liu et al., 2016, Conde et al., 2013, Qi et al., 2017). This result of this research has prolonged the duration of drug-cell interaction and prevented the physiological damage during drug delivery to the target organ. However rapid genomic reshuffling in terms of mutations in cancer cells (and microorganisms) has meant that multiple strains of a disease have evolved. Various resistance mechanisms adopted have not only led to host defence mechanisms being weak, but progressive build-up of drug resistance has limited the success of targeted therapy (Moiseenko et al., 2017, Shah et al., 2016, Friedman, 2016).

The next section of the study focussed on an alternative to using nanotechnology to minimise if not overcome the magnitude of drug-resistance in anti-cancer therapy. Many researchers have used different methods to increase sensitivity of cancer cells to treatment and EV inhibition-mediated sensitisation has been effective as was previously reported by the Inal lab (Jorfi et al., 2015, Kholia et al., 2015) with respect to prostate cancer (PCa). This study aimed at using novel inhibitors both individually and in combination to increase drug sensitivity. This approach was tried in both PC3 cells (a PCa cell line) and MCF7 cells (a breast cancer cell line) *in vitro*. Nicotine and Cl-amidine was tested individually and in combination together with 5-FU in both PC3 and MCF7 cells. Apoptosis was drastically affected in the presence of inhibitors, more so than 5-FU alone. This suggested that EV inhibition had favourably sensitised the cancer cells to chemotherapy. This was further examined in the presence of Cl-amidine coupled with Bisin-I in PC3 cells. The outcome was similar to that observed previously. Essentially, Cl-amidine and Bisin-I-mediated EV inhibition was pronouncedly higher than the inhibition mediated by individual reagents on their own and significantly higher than 5-FU alone (**Figures 4.2 to 4.8**). Both Annexin V and VB-48 cell vitality assays showed increased cancer cell apoptosis in the presence of 5-FU and EV inhibitors. This further signifies the importance of EV inhibition in cell sensitisation to anti-cancer treatment.

Addition of EVs carrying 5-FU to Bisin-I pre-treated cells (**Figures 4.8 and 4.9**) increased the % apoptosis considerably compared to that observed in the absence of pre-treatment. This further justified the importance of EV inhibition in effective therapy. However the apoptosis that

resulted from direct treatment with 5-FU was higher compared to that obtained from the addition of drug-loaded EVs.

This strategy of limiting EV release during chemotherapy was then repeated with a second anti-tumour drug, doxorubicin (DOX). Fluorescence microscopy, spectrophotometry and HPLC were used to observe the effect of pretreating cancer cells with Cl-amidine for the capacity to sensitize cancer cells to chemotherapy. Collectively the results supported the hypothesis that EV inhibition increases anti-cancer drug effectiveness. Interestingly, nanosight analysis revealed that DOX alone increased the EV release markedly. This has been proven in the literature which is another valid reason to pharmacologically inhibit EV release in order for increased drug retention and effectiveness (Chulpanova et al., 2018, Sun et al., 2018, Sadovska et al., 2015). However on the same note, Cl-amidine pronouncedly inhibited EV release which once more confirmed previous findings.

With a view to using EVs as drug delivery vehicles PC3 EVs were incubated with DOX for 4 and 24h to generate DOX-EVs (that is EVs encapsulating DOX). PC3 cells were treated with these DOX-EVs 65% of which were shown to be DOX-positive (**Fig. 4.13**). This was confirmed by fluorescent microscopy (**Fig. 4.15**). Cl-amidine pre-treatment facilitated the retention of DOX delivered by DOX-EVs (drug-EVs) in PC3 cells. By fluorescence microscopy increased DOX fluorescence was also observed after Cl-amidine inhibition of EV release suggesting increased retention of drug in the PC3 cells. This further confirmed the importance of EV inhibition on drug efficacy. This was then supported by HPLC data (**Figure 4.16**). An increase of 51% drug internalisation was noticed following Cl-amidine pre-treatment compared to its absence (**Figure 4.17**). Fluorescent spectroscopy data also supported this observation. DOX intensity and absorption was increased in Cl-amidine pre-treated cells compared to the absence of pre-treatment (**Figures 4.18 and 4.19**) further highlighting the significance of EV inhibition on minimising drug expulsion.

The experimental data to this point emphasised the importance of EV inhibition on increasing drug efficacy. Release of EVs from tumour cells minimises the period of drug retention and reduces the concentration of drug in the cells thereby reducing the ability of the drug to induce apoptosis. This has thus encouraged the use of increased dosages of anti-cancer treatment which has deleteriously affected the patient prognosis. Pharmacological EV inhibition not only increases the drug retention capacity but also encourages the use of minimum dose of drug which can increase the level of tolerance of chemotherapy in patients. Not many studies have concentrated on this but successful research has been undertaken that supports the current findings (Ivanov, 2014, Kosgodage et al., 2017, Datta et al., 2018). The research findings by Datta and co-workers., looked into inhibitors of exosome biogenesis and release in PC3 cells

through immunoblot analysis of protein markers of the endosomal sorting complex required for transport (ESCRT)-dependent and ESCRT-independent pathways(Datta et al., 2018). Koch and colleagues have also established that chemical depletion of ATP-transporter A3 (ABCA3) inhibited the release of exosomes. Therefore, pre-treatment of B cell lymphoma cells with ABCA3 inhibitor, Indomethacine augmented the retention of both doxorubicin and pixantrone increasing its cytostatic efficacy (Koch et al., 2016)

8.3 CBD-mediated EV inhibition: A novel implication of its Activity

Cannabidiol(CBD) is a naturally occurring cannabinoid constituent of cannabis(Atakan, 2012). The prescription drug of cannabidiol, Epidiolex is known to prevent the breakdown of a chemical in the brain reducing psychotic symptoms (Devinsky et al., 2014, Maroon and Bost, 2018, Zuardi et al., 2012, Iffland and Grotenhermen, 2017). It is therefore effective against anxiety, bipolar disorder, seizures, multiple sclerosis, Parkinson's disease, and schizophrenia (McGuire et al., 2018, Stampanoni Bassi et al., 2017, Tambaro and Bortolato, 2012). This study further elaborates its potential use as an EV inhibitor for the first time. CBD activity was been tested in multiple cancer cell lines including, PC3, MDA-MB-231, HEPG2, LN18 and LN229 in which CBD has consistently affected the EV profiles differently but had a significant effect on exosome release across all cell lines. This effect was also more apparent than Cl-amidine treatment in some instances.

Using a combination therapy of CBD and Cl-amidine resulted in different effects on the various EV subsets and varied between the three cancer cell lines. Combinatory treatment was more effective on some subsets than Cl-amidine alone, as was observed on exosome release in PC3 cells and on MV release in HEPG2 cells. Interestingly, in MDA-MB-231 cells, Cl-amidine counteracted the increased CBD-mediated release observed for the total EVs when used in combination. Previously, Cl-amidine has been shown to act on MV biogenesis via increased cytoskeletal actin deimination and nuclear PAD translocation, indicative for changes in histone deimination (Lange, 2016, Dreyton et al., 2014, Witalison et al., 2015, Kholia et al., 2015). A recent study proposed that CBD may act in part through modulation of mitochondrial metabolism as described (Kosgodage et al., 2018a)

Previously, CBD has been shown to enhance effects of TMZ (Torres et al., 2011). In this study we also have used TMZ in conjunction with CBD to study the effect of CBD-mediated EV inhibition on glioma treatment. CBD treatment did not express any favourable activity on glioma cell line, LN29. TMZ, anti-glioma therapy itself inhibited EV release whereas CBD resulted in hyper-vesiculation. In contrast, LN18 (the TMZ-resistant cell line) (Würstle et al., 2017)exhibited opposing activity in the presence of both TMZ and CBD. Nonetheless, both cell lines varied in the proportional amounts of total EVs, exosomes and MVs, released under

standard conditions (**Figure 7.8**). LN229 resulted in a significant release of vesicles in all subpopulations compared to LN18.

Further work on miRNA profiling of these vesicle subtypes will have to be carried out to ensure whether LN229 vesicles contain protective miRNAs which would then support the observations made so far. The results presented in this section achieved the aim of enhancing anti-cancer therapy and minimising drug resistance. TMZ-resistant LN18 responded to CBD treatment favourably which means its resistance was overcome. The effects of CBD on EVs, described here, may explain some of the beneficial effects that have been observed for GBM in response to CBD treatment in combination with TMZ (Ivanov, 2014).

As with previously suggested EV inhibitors, CBD has enhanced the effectivity of chemotherapy in cell cultures, which could lead to treatment using lower doses of chemotherapeutic drugs, thus minimising side-effects and result in equally effective inhibition of tumour growth *in vivo*.

8.4 OMV isolation and the identification of PAD- mediated citrullination/deimination in *E. coli*

The technology for isolation of OMVs and that is used to characterize them has slightly lagged behind that used on EVs from eukaryotic cells (Dauros Singorenko et al., 2017). Initially two techniques of OMV isolation were adopted in this study; ultracentrifugation was by far the preferred method as it met the requirements of high yield and rapid isolation which was applied throughout the chapters (**Figures 5.3.1 and 5.3.2**).

In the next part of the project PAD-mediated citrullination in *E. coli* was investigated. In bacteria, PAD has been reported as a protein that is exclusively expressed in *P. gingivalis* (Scher and Abramson, 2013, Gabarrini et al., 2015, Gully et al., 2014b). The findings presented in this section firmly substantiated the presence of citrullinated proteins in *E. coli* through immunoprecipitation and Mass spectrometry analysis. Though PAD association with *P. gingivalis* has been looked at previously (Jenning et al., 2017, Xibille-Friedmann et al., 2014), my study was the first to investigate the presence of PAD in *E. coli*.

The phylogenetic relationship between *E. coli* PAD and *Homo sapiens* (*H. sapiens*) was first identified in this study which revealed that *E. coli* PAD is closely associated with *H. sapiens* PAD2. This was further confirmed by MAP analysis (**Figure 5.3.3**). Citrullinated proteins resulted from PAD2, PAD3, PAD4 and F95 mediated catalysis were identified in *E. coli* and *E. coli*-OMV isolates. Western blotting resulted in bands in the size range of 37-50 and 75-76 and 20 kDa for pan-deimination antibody (F95). PAD was detected at an expected band of 37-50 kDa

with PAD4 being very prominent. PAD2 and PAD3 were less expressed. Identification of citrullinated proteins in OMV isolates confirmed lateral transfer of proteins in vesicles. This vesicle-mediated horizontal gene transfer (Fulsundar et al., 2014a, Biller et al., 2014, Hasegawa et al., 2015) was noticed in previous research that has increased the chance of bacterial survival. The outcome of IP further confirmed the findings. *E. coli* PAD proteins are predicted to have a size of 49 kDa which was noticed in the blot following IP. This establishes the prominent separation and detection of *E. coli* PAD-mediated protein citrullination.

Mass spectrometry following IP further revealed the unique citrullinated proteins identified in the samples. This identified Threonine-tRNA ligase for the first time in OMVs. String analysis shows interactive partners (**Figure 5.3.6 B**). 30S ribosomal protein S4 (rpsD) and S15 (rpsO) were present in all deiminated samples including those obtained from OMVs. This has been previously reported as a substrate of PAD4-mediated citrullination in HEK 293T (Guo et al., 2011). This confirms its presence in both F95 and PAD4 *E. coli* IP samples. All commonly expressed proteins including chaperone protein, ribonuclease, outer membrane lipoprotein, 50S ribosomal protein L22 and flagellin are believed to be either substrates or products of protein deimination (Magnadóttir et al., 2018).

OMV inhibition assays were performed on both Gram-positive and Gram-negative bacteria. Interestingly, PAD4 inhibitor, GSK199 was an effective PAD inhibitor (**Figure 5.3.8 and 5.3.9**). The presence of a prominent band corresponding to anti-PAD4 activity strongly confirmed the effectiveness of GSK199 in OMV inhibition, as this seems thus to be related to a PAD4-like activity. Interestingly, total deiminated proteins were captured by anti-F95 in both *E. coli* and OMV samples.

The strongest OMV inhibition in *E. coli* was in the presence of Imipramine whereas EGTA was the weakest. Nevertheless all other inhibitors influenced OMV inhibition differently. In contrast to the reagent activity seen in Gram-negative bacterial-OMVs, inhibition in Gram-positive bacterial was enhanced by EGTA. Both Bisin-I and EGTA showed significant inhibition.

PAD inhibitors were more effective in inhibiting *E. coli*-OMVs production than *S. aureus*-OMVs, GSK199 being the most potent inhibitor, but all PAD inhibitors showed a strong capacity to reduce OMV biogenesis. However this was not true with Gram positive-OMVs, the PAD-mediated OMV release not being affected by PAD-inhibitors. Overall the inhibition of OMV release was below 40% in the presence of pan-PAD inhibitors, suggesting that they are less effective in Gram-positive species than Gram-negative.

There has been no similar previous research undertaken on this subject. Therefore this study of OMV inhibition in both Gram-positive and Gram-negative species is the first to combine OMV modulation with improvement of antibiotic sensitivity and phage therapy, and identifying a novel PAD-specific pathway of OMV release.

8.5 OMV inhibition enhances Gram-positive and Gram-negative bacterial Antibiotic Sensitivity and increases Susceptibility to Bacteriophage Therapy

Upon OMV inhibition, *E.coli* was more sensitive to erythromycin, rifampicin and colistin but did not show any effect in the presence of kanamycin. There was no vancomycin activity on *E.coli* which confirmed its limited effectiveness on Gram-positive species. Susceptibility to colistin was significantly affected by OMV inhibition (**Figure 6.2**). This encouraged the use of lower concentrations of the antibiotic to treat infections with minimal damage to healthy host cells. There was however a distinct difference between the species.

This work has clearly shown that PAD-mediated OMV inhibition has a significant effect on antibiotic activity resulting in reduced MIC values specifically when using colistin on *E.coli* and vancomycin on *S.aureus*. Interestingly, this effect was reduced in *S.aureus* suggesting that there might be different mechanisms of OMV biogenesis and release involved. This however is in line with previous results obtained on PAD-mediated OMV inhibition. PAD inhibitors were more potent in inhibiting OMV release by *E. coli* compared to *S. aureus*. A maximum inhibition of 60% was recorded in the presence of GSK199 in *E. coli* which was far less in *S. aureus* being only 22.49%. Similarly Cl-amidine exerted a 30% maximum inhibition on *E.coli* OMVs but was only 12.5% in *S. aureus*. The least effect was in the presence of AMF30a, PAD2 inhibitor. Only 3.39% inhibition was observed in *S. aureus*. This was at least 20% less compared to the effect on *E. coli* OMVs. BB-Cl-amidine was 51.23% effective in *E. coli* but only decreased the OMV release in *S. aureus* by 7.64%. These results strongly indicate that PAD effect is minimal in *S. aureus* compared to *E. coli*.

As discussed previously, where inhibition of EV release enhanced anti-cancer drug sensitivity, the results presented in this thesis have similarly shown an enhanced antibiotic activity. Much of the evidence surrounding the work to increase drug sensitivity by inhibiting EV release in cancer cells pointed to the inhibition resulting in retention of drug within cells. The hypothesis that a similar mechanism may operate in prokaryotes with regard inhibition of OMV release and possible antibiotic retention (resulting in reduced levels of antibiotic being equally effective); however, will need more empirical data to be able to make a judgement.

Bacteriophage-OMV interaction has been widely described in the field (Kharina et al., 2015, Reyes-Robles et al., 2018a, Klimentová and Stulík, 2015). These researchers have quite

logically expressed the OMV interaction with bacteria as a potential barrier to phage infection and therefore an impediment to effective phage therapy. Just as for anti-cancer drugs stimulating EV release, data presented here shows phage itself to stimulate OMV release (**Figure 7.3**). This work showed that the lower phage concentrations resulted in a low OMV release and that shorter incubation time resulted in increasing levels of OMV release (**Figure 7.4**). It has previously been shown that OMVs decrease the virulence of phage allowing the bacterial cells to be resistant to such therapy (Tzipilevich et al., 2017, Ellis and Kuehn, 2010, Schwechheimer and Kuehn, 2015, Klimentova and Stulik, 2015)

My data presented also showed that increased addition of (externally isolated) OMVs to *E. coli* reduced the phage infection significantly. These findings are consistent with the research work on T4 and *E. coli* (Manning and Kuehn, 2011). Manning and colleagues have also looked at the effect of OMVs on T4 virulence. The remaining irreversible phage concentration was determined following chloroform pre-treatment. The results suggested that inactivation of T4 phage occurred very quickly following addition of OMVs. 80% reduction of free phage was observed within 5min of co-incubation with OMVs which also can be used to support our findings of shorter incubation time resulting in increased levels of OMVs. It further confirmed that phage-OMV binding is not only instant but also irreversible (Manning and Kuehn, 2011). Further research has shown OMVs comprise a natural defence mechanism used by bacteria to prevent phage attack (Manning and Kuehn, 2011, Kuehn and Kesty, 2005, Altindis et al., 2014, Schwechheimer and Kuehn, 2013, Kharina et al., 2015). Much of the research of this thesis has tried to dissect EV and OMV biogenesis and through this to find pharmacological inhibitors of EV and OMV release in eukaryotic and prokaryotic cell respectively. This ability to modulate OMV release was then used uniquely in the data presented in this thesis to use an approach to modulate OMV release with a view to removing the protection they afford bacteria from infection with phage and therefore to enhance the efficacy of phage therapy. To begin with the pan-PAD inhibitor, Cl-amidine was used for OMV inhibition. This resulted in a significant improvement in phage infection in the presence of Cl-amidine. A significant reduction of OMVs released and therefore present in the immediate environment of the bacteria suggested that there was a significantly decreased chance of OMVs successfully acting as decoys to infection and a greater chance for phage tail fibers to adhere to bacterial receptors resulting in infection and then lysis. This strongly suggests that OMV inhibition is the key to drive the maximum infection potential of lambda phage leading to successful phage therapy. These findings were further reinforced by electron microscopy as shown in (**Figure 7.7**) which shows the binding of lambda phage to OMVs.

Previous research showed Arginine deiminase(ADI) inhibiting the surface attachment in *P.gingivalis* (Cugini et al., 2013). This prompts the question as to whether inhibition of the

enzyme could facilitate the binding of phage to the *E.coli* bacterium in addition to stopping OMV release. Intriguingly the finding by Cugini et al that PAD inhibition in bacteria prevented attachment may be due to OMVs themselves facilitating the attachment process. Thus inhibiting OMV release would result in decreased attachment to host. This would be akin to the finding from the groups of Inal and Ramirez who showed attachment of *Giardia intestinalis* to intestinal epithelial cells (Evans-Osses et al., 2017) and more appropriately results using different bacteria showing OMVs to be involved in attachment to host cells (MacDonald and Kuehn, 2012).

The hypothesis still remains unconfirmed but this thesis has begun to collate data supporting the role of OMV modulation and the associated improvements in antibiotic therapy and possibly phage therapy. Therefore it will be interesting to see whether similar improvements of activity as a result of OMV inhibition are seen in other bacteria-bacteriophage complexes to improve the therapeutic use of Cl-amidine. OMV inhibition using other suggested novel inhibitors in the study will be important also to further confirm the existing data.

As part of further studies it would be useful to visualise the phage-OMV interaction by means of fluorescent microscopy using membrane staining. Using a PAD gene knock-out model of *E. coli* would also make a useful control to confirm the effect of Cl-amidine. Looking further ahead it would also be interesting to test the OMV inhibition in a murine model of *E. coli* infection in order to show its applicability *in vivo* in terms of improving both antibiotic and phage therapies. It would also be important to visualise phage attachment in Gram-positive bacteria once more by electron microscopy. Overall these strategies will open new avenues to improve current antibacterial therapy and minimise therapeutic resistance.

8.6 Summary and Concluding Remarks

Extracellular vesicles (EVs) are important mediators of intercellular communication. They have been widely accepted as playing a key role in disease progression and used in many therapeutic strategies. This thesis has focused on a small aspect of the importance of these key players in developing novel therapies primarily in cancer. This has been achieved successfully *in vitro* using a variety of cancer cell-lines, numerous potential EV inhibitors and a range of different anti-cancer drugs as evidenced by the increased sensitisation of cells to therapy and interestingly an alternative to minimise multi-drug resistance.

An unexplained role of Cannabidiol is revealed for the first time in this study. Its use as a potential EV inhibitor was clearly established through utilisation of multiple cancer cell lines. It was fascinating to report the diverse function of CBD on EVs released in different cancers. This has not only made the reader aware of a novel role of CBD but has encouraged other researchers

to test its potency in anti-cancer effectivity. Interestingly CBD had a pronounced effect on the TMZ-resistant, LN18 cells encouraging its use to overcome drug resistance.

The final focus was bacterial outer membrane vesicles (OMVs). Their isolation, characterisation and quantification are well detailed in the study. The thesis, for the first time has demonstrated OMV inhibition with respect to both Gram-positive (*S.aureus*) and Gram-negative bacteria (*E.coli*) using various reagents. It has also highlighted the presence of PAD in *E.coli* for the first time through detecting the presence of citrullinated proteins via immunoprecipitation, Western blotting and mass spectrometry analysis. The investigator has also presented the different modes of OMV inhibition by using a range of reagents. The reader is then able to appreciate the implication of OMV inhibition in increasing antibiotic sensitivity and bacteriophage therapy for the first time. This observation has been confirmed using a range of antibiotics and lambda phage. Electron microscopy imaging has added value to depict the significance of OMV inhibition on enhanced phage therapy.

The findings of the study have clearly shown selective pharmacological inhibition with respect to EVs and OMVs (**Figure 7.13**). However most of the reagents used have been effective in inhibiting both type of vesicles. There is a higher lipid composition in Gram-negative cell membrane compared to Gram-positive cell membranes, meaning that lipid soluble reagents more easily penetrate *E.coli* compared to *S.aureus*. This phenomenon also can be applied to the greater effect of inhibitors on EVs and Gram-negative OMVs compared to that of Gram-positive. Some inhibitors were only tested against EVs. CBD and nicotine possess antibacterial properties as outlined previously. However, there is no research undertaken in relation to its application in OMVs. Therefore, it will be interesting to test this hypothesis. Previous research has revealed the use of the second pan-PAD inhibitor BB-C1-amidine (Jang et al., 2017), PAD2 specific inhibitor AMF30a (Muth et al., 2017) and PAD4 specific inhibitor GSK199 (Slade et al., 2015). Therefore, in this study these inhibitors were used against bacterial OMVs.

It was also interesting to observe the effect of inhibitors on different types of vesicle. PAD inhibition was more potent in EV inhibition as C1-amidine was more effective against PC3-cell derived EVs and as shown earlier in the study in MCF-7 cell derived EVs (**Table 5**). Non-PAD inhibition was more successful in Gram-positive OMV inhibition compared to Gram-negative, EGTA was more potent in Gram-positive but was significantly less in Gram-negative OMV inhibition. However, Bisin-I did not elicit a major opposing response in release of MVs from Gram-positive or Gram-negative bacteria. Furthermore, PAD4 inhibitor, GSK199 was more effective against both bacterial OMVs compared to PAD2-mediated inhibition via AMF30a. Hydrophobicity of the reagents as described in **Table 1** could have played a significant role in cell penetration hence the differential effect on EV and OMV release. A recent review has

demonstrated the presence of different types of vesicles released from both Gram-negative and Gram-positive bacteria. (Toyofuku et al., 2019). The composition of cell membrane plays a major role in vesiculation. Presence of a thickened peptidoglycan cell wall in Gram-positive restricts the penetration of most of the drugs into the cells which suggests the need of an alternative receptor-mediated transport system (Liu et al., 2018). However, the high lipid content of the Gram-negative cell membrane with a thin layer of peptidoglycan increases membrane fluidity thus facilitating OMV release (Roier et al., 2016). It also makes it easier for the lipid soluble drugs to penetrate the bacterial cell easily to elicit a favourable response which is also apparent from our results.

The majority of the inhibitors were investigated against PC3 cells. A diverse group of cancer cells were used in the CBD study which made it a successful comparative study. This finding should now be used with regards to the effect of different inhibitors of EV release from cancer cells.

Gram-negative OMV inhibition	Gram-positive OMV inhibition	EV inhibition
EGTA	Bisin-I	Cl-amidine
Bisin-I	GSK199	Pantethine
GSK199	BB-Cl-amidine	EGTA
Cl-amidine	Cl-amidine	Bisin-I
BB-Cl-amidine	AMF30a	Imipramine
AMF30a	EGTA	Y27632

Table 5. Comparative analysis of the effect of different inhibitors on EV and OMV release. PAD inhibition was more potent in EV inhibition compared to OMV inhibition. However, PAD-specific inhibition was noted in OMVs with PAD4-mediated OMV inhibition being successful. Non-PAD inhibition was effective against Gram-positive OMV inhibition and EV inhibition compared to Gram-negative OMV inhibition.

Inhibitors on release of EVs and OMVs

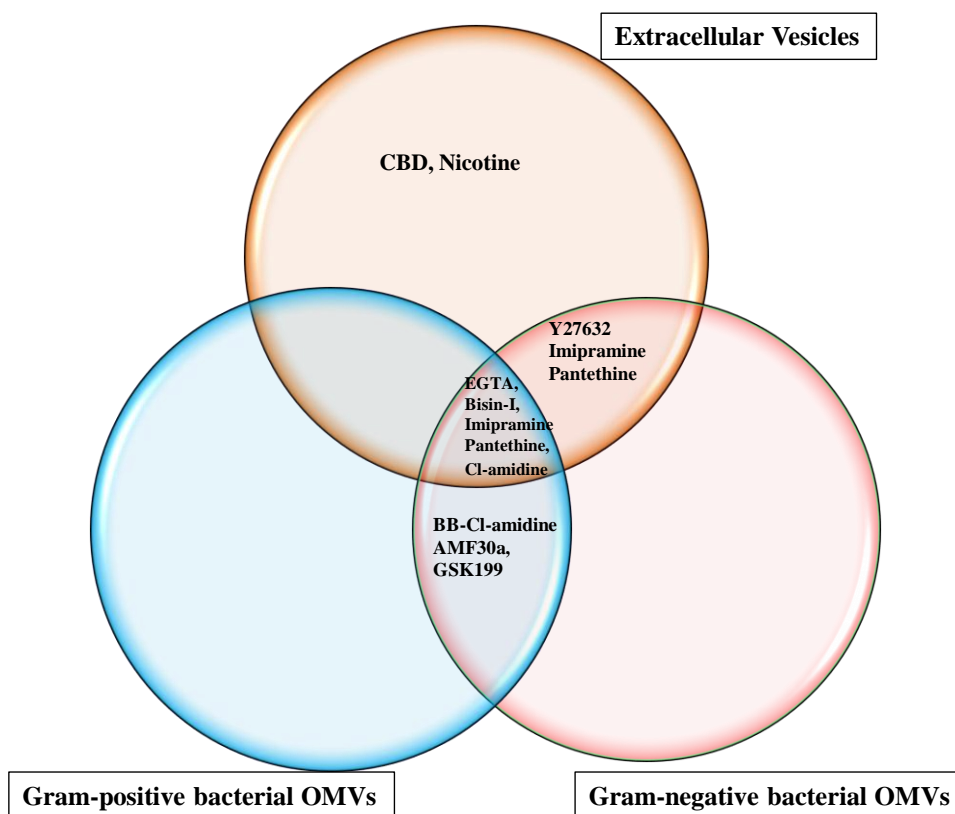


Figure 7.13. Identification of common inhibitors of EVs and OMVs. Venn diagram illustrates that most of the potential inhibitors used in the study were capable of inhibiting all type of vesicles. PAD inhibitors, BB-Cl-amidine, GSK199 and AMF30a were only tested in bacteria. However, Y27632, Imipramine and Pantethine were only potent against EVs and Gram-negative bacteria. This may be due to the low lipid content of the Gram- positive cell membrane which then need a different transporter system for cell penetration. Furthermore, CBD and nicotine were only tested against EVs.

This thesis therefore presents a collection of potential novel therapeutic strategies developed through both EV inhibition in carcinogenesis and Outer Membrane Vesicle inhibition in bacterial infections.

9.0 Appendix

9.1 Complete Proteomic Analysis of *E.coli* and *E.coli*-derived OMVs

UniProt ID	Protein name (short)	Gene name	number of unique peptides			MS2 intensities			best_ protein score	sum score	samples
			Sample 1	Sample 2	Sample 3	Sample 1	Sample 2	Sample 3			
			<i>E.coli</i> F95	<i>E.coli</i> PA D4	OMV F95	<i>E.coli</i> F95	<i>E.coli</i> PA D4	OMV F95			
Q8X9B6	Biotin carboxylase	accC	1				8219.04		49.8	49.8	1
P0A9Q6	Acetyl-coenzyme A carboxylase carboxyl transferase subunit beta	accD	3	3		10170.15	21748.649		130.77	224.59	2
Q0TFD0	Acetyl-coenzyme A carboxylase carboxyl transferase subunit beta	accD		2			156916.305		99.12	99.12	1
P0A9G7	Isocitrate lyase	aceA	2	1		207418.3	302355.52		88.61	126.09	2
P0AFG8	Pyruvate dehydrogenase E1 component	aceE	8	9		144390.2	211469.821		323.68	608.51	2
P06959	Dihydropyridyl lysine-residue acetyltransferase component of pyruvate dehydrogenase complex	aceF	8	6		583182.8	1471690.61		285.02	547.58	2
P0A6A5	Acetate kinase	ackA		2			79145.638		70.42	70.42	1
P36683	Aconitate hydratase B	acnB	1	1		47979.66	60431.904		207.76	340.93	2
B7MTM4	Acyl carrier protein	acpP	1			54078.05			23.71	23.71	1
P0AE07	Multidrug efflux pump subunit AcrA	acrA		1			115575.999		45.61	45.61	1
P31224	Multidrug efflux pump subunit AcrB	acrB	1	1		91864.08	27081.852		69.46	94.22	2
P2418	Multidrug	acrE	1			58880.44			35.04	35.04	1

0	export protein AcrE							4	
Q8X5 T5	Acetyl- coenzyme A synthetase	acs	1		56659.86		36.17	36.1 7	1
P0A9 Q8	Aldehyde- alcohol dehydrogenase	adhE		1	16626.90 4		542.93	542. 93	1
P0AE 10	Alkyl hydroperoxide reductase subunit C	ahpC	1	4	64627.09 4	570140.1 4	158.76	314. 22	2
Q8X3 W8	Alanine-- tRNA ligase	alaS	1	3	12755.68	14569.64 1	79.57	119. 11	2
P0080 5	L- asparaginase 2	ansB	1	1	15888.17	28337.13	38.03	71.0 3	2
P0A9 Q3	Aerobic respiration control protein ArcA	arcA		2		19035.19	60.23	60.2 3	1
B7MR 48	Acetylmornithine deacetylase	argE		1		107868.8 1	45.19	45.1 9	1
Q8X5 W4	Phospho-2- dehydro-3- deoxyheptona te aldolase, Trp-sensitive	aroH	1		4800.6		25.69	25.6 9	1
Q8XD S0	Aspartate ammonia- lyase	aspA	9	3	41866.05	22582.04 3	392.45 36715	476. 7536 7	2
P0050 9	Aspartate aminotransferase	aspC		1		40123.23 5	36.89	36.8 9	1
B7L6 M2	Succinylornithine transaminase	astC	16	10	217900.4	366167.8 65	475.7	838. 54	2
B7US C9	Succinylornithine transaminase	astC	13	9	290787.6	167965.7 04	345.62	603. 61	2
B7M VM7	Succinylornithine transaminase	astC	12	8	753161.3	1573119. 98	368.09	676. 8	2
A7ZM L6	Succinylornithine transaminase	astC		3		232079.3 16	73.58	73.5 8	1
A8A0 U0	Succinylornithine transaminase	astC		2		28021.86 9	73.51	73.5 1	1
Q8X5 98	Succinylornithine transaminase	astC	1	1	2839.005	16188.23 2	363.03	656. 42	2
B7N2 H3	ATP synthase subunit alpha	atpA	7	5	17275.58	25477.84 4	278.97	428. 67	2

B7N2 H0	ATP synthase epsilon chain	atpC		1			50390.40 3	40.92	40.9 2	1
A8A6 J5	ATP synthase subunit beta	atpD	3	8		242535.7	1784489. 81	242.64	303. 31	2
B7N2 H1	ATP synthase subunit beta	atpD	4	5		393488.4	1393864. 1	266.67	441. 04	2
B7N2 H2	ATP synthase gamma chain	atpG	1	1		25752.43	52398.21 6	40.52	73.4 2	2
P0A9 H4	Inducible lysine decarboxylas e	cadA		2			716567.2 5	78.26	78.2 6	1
P7663 2	CRISPR system Cascade subunit CASB	casB	1			48439.74		37.18	37.1 8	1
B7MP T2	Curved DNA binding protein	cbpA		3			6123.157 6	90.68	90.6 8	1
P0AB M9	Cytochrome c-type biogenesis protein CcmH	ccmH	1	2		5425.614	6263.335	41.12	72.1 9	2
P0A9 66	Chemotaxis protein CheW	cheW		1			6079.74	40.65	40.6 5	1
P6328 5	Chaperone protein ClpB	clpB	1	1	1	5169079	5833442. 7	227.63	430. 06	3
P0AC K0	cAMP- activated global transcriptiona l regulator CRP	crp	4	9		93378.67	298240.1 94	479.3	689. 38	2
P6978 4	Glucose- specific phosphotransf erase enzyme IIA component	crp	3	4		242379.4	408741.3 9	157.56	296. 21	2
P0A9 Y8	Cold shock- like protein CspC	cspC		1			14612.86 4	25.76	25.7 6	1
P0AB J2	Cytochrome bo(3) ubiquinol oxidase subunit 2	cyoA	1			33604.2		43.07	43.0 7	1
B7N1 F1	Siroheme synthase	cysG		1			231691.8 45	20.21	20.2 1	1
P0AE B4	D-alanyl-D- alanine carboxypepti dase DacA	dacA	11	12		1993153	3989363. 58	565.99	1057 .64	2
B7M NN7	4-hydroxy- tetrahydrodipi	dapB	2	2		88421.6	472167.7 8	88.45	123. 88	2

	colinate reductase									
Q8X8 Y7	2,3,4,5-tetrahydropyridine-2,6-dicarboxylate N-succinyltransferase	dapD	1	1	44638.34	435885.28	29.79	50.88	2	
P0AE E0	DNA-cytosine methyltransferase	dcm	1		3012.168		25.22	25.22	1	
P0AB N7	Anaerobic C4-dicarboxylate transporter DcuA	dcuA	1	1	14725.33	37571.091	94.06	157.92	2	
B7MT C9	Phosphopentomutase	deoB	2		4098.075		40.28	40.28	1	
P0AB S3	RNA polymerase-binding transcription factor DksA	dksA		1		8272.797	22.76	22.76	1	
B7M NM2	Chaperone protein DnaJ	dnaJ	1	1	5226.309	40686.87	43.92	75.73	2	
P0A6 Z0	Chaperone protein DnaK	dnaK	1	1	204589.7	98262.38	386.58	718.01	2	
P0AE G0	Dipeptide transport system permease protein DppB	dppB		1		7462.026	21.12	21.12	1	
B7M QR6	DNA protection during starvation protein	dps	1	5	49293.94	397406.814	179.03	324.33	2	
Q8FJ M0	DNA protection during starvation protein	dps		2		51561.816	65.43	65.43	1	
B7MZ 75	Enolase	eno	1	1	73150.26	113597.72	358.57	709.67367	2	
P0A9 W4	Energy-dependent translational throttle protein EttA	ettA	1	1	61002.77	67219.11	47.22	77.92	2	
P0A9 54	3-oxoacyl-[acyl-carrier-protein] synthase 1	fabB	1		7902.669		47.06	47.06	1	
P0AE K2	3-oxoacyl-[acyl-carrier-protein] reductase FabG	fabG		1		4225.648	56.61	56.61	1	

P0AE K5	Enoyl-[acyl- carrier- protein] reductase [NADH] FabI	fabI	1	2		4621.212	64691.11 5	96.9	154. 53	2	
P0AB 72	Fructose- bisphosphate aldolase class 2	fbaA	1	5		2382.267	17559.62 7	165.26 12477	187. 7712 5	2	
P5959 0	Chaperone protein FimC	fimC	1			42662.38		31.55	31.5 5	1	
P0A9 L3	FKBP-type 22 kDa peptidyl- prolyl cis- trans isomerase	fkIB	1	1		26969.75	59181.50 7	28.96	52.2 7	2	
P0494 9	Flagellin	fliC	10	14	2	704598.6	1146224. 24	^{9488.7} 24	653.24	1305	3
Q1R9 R9	GTP cyclohydrolas e 1	folE	3	2		589202.6	741671.7 4	123.62	236. 04	2	
P0036 3	Fumarate reductase flavoprotein subunit	frdA	1	1		3390.246	4483.52	57.26	99.8 9	2	
B7MP 32	Ribosomal recycling factor	frf		1			2181.198	36.06	36.0 6	1	
Q8X9 L0	ATP- dependent zinc metalloprotea se FtsH	ftsH		6			1159639. 11	151.09	151. 09	1	
P0A9 A8	Cell division protein FtsZ	ftsZ	1	1		16559.87	16662.99 9	68.18	89.3 8	2	
Q8X4 P8	Fumarate hydratase class I, aerobic	fumA	3	4		407340.7	604730.9 73	114.04	216. 36	2	
P1440 7	Fumarate hydratase class I, anaerobic	fumB	2			15232.67		78.27	78.2 7	1	
P0A9 B1	Ferric uptake regulation protein	fur	22	19		1534314	1421004. 09	732.46 36715	1459 .517 3	2	
B7N0 X6	Elongation factor G	fusA	7	9		483355.8	1142360. 97	356.45	637. 69	2	
B7ND U8	Elongation factor G	fusA	1			57190.14		316.36 36715	316. 3636 7	1	
P2552 6	Succinate- semialdehyde dehydrogenas e [NADP(+)] GabD	gabD		1			136760.4 23	32.28	32.2 8	1	

P58228	Glutamate decarboxylase alpha	gadA	8	8	57333	94579.335	312.35	577.22	2
P69911	Glutamate decarboxylase beta	gadB		3		387378.17	72.46	72.46	1
Q8FHG5	Glutamate decarboxylase beta	gadB		1		23077.826	72.69	72.69	1
P0A9B3	Glyceraldehyde-3-phosphate dehydrogenase	gapA	11	10	566896.6	570950.754	448.05	766.15	2
P0A9B6	Putative glyceraldehyde-3-phosphate dehydrogenase C	gapC		1		17560.102	35.4	35.4	1
P0A9S6	Glycerol dehydrogenase	gldA	2		220449.1		441.19	441.19	1
B7N176	Glycogen synthase	glgA	7	9	102277.9	262501.719	355.81	706.33	2
Q1R5J7	Glycogen synthase	glgA	6	6	518282.8	978486.705	292.77	577.97	2
Q8XEG2	Glutamine--fructose-6-phosphate aminotransferase [isomerizing]	glmS	1	4	40677.99	187964.543	536.14	1035.05	2
A7ZPK7	Glutamate--tRNA ligase	gltX		1		7927.44	33.96	33.96	1
B7MY10	Serine hydroxymethyltransferase	glyA	5	4	28752.94	35118.91	199.0136715	329.11734	2
B7N1L1	Glycine--tRNA ligase beta subunit	glyS		2		23005.6158	87.76	87.76	1
Q8XD88	Guanylate kinase	gmk	1		30770.63		21.72	21.72	1
B7MPN9	2,3-bisphosphoglycerate-dependent phosphoglycerate mutase	gpmA	1		43889.44		23.86	23.86	1
B7MYL2	Autonomous glycyl radical cofactor	grcA	3	4	327409.2	1445352.32	234.73	383.83	2
B7MIR4	Autonomous glycyl radical cofactor	grcA	3	4	224635.4	1189183.3	188.81	290.95	2
Q0T9P8	60 kDa chaperonin	groL	9	9	33034.06	61275.832	477.38	831.31	2

A1AJ 51	60 kDa chaperonin 1	groL1	15	12	317080.7	180363.6 75	504.5	883. 25	2
Q19N J4	60 kDa chaperonin 2	groL2	6	7	703376.3	1227065. 95	256.99	503. 59	2
Q1R3 B7	10 kDa chaperonin	groS	4	2	46761.72	60904.69 8	131.21 36715	212. 6436 7	2
B7M YA6	Protein GrpE	grpE		1		5408.954	51.76	51.7 6	1
P0AC 59	Glutaredoxin- 2	grxB	2	2	253146.2	637131.5 6	89.14	151. 4	2
P0AD G8	Inosine-5'- monophospha te dehydrogenas e	guaB		1		5275.682	27.22	27.2 2	1
Q8X4 S5	Arabinose 5- phosphate isomerase GutQ	gutQ		4		486219.4 05	120.37	120. 37	1
P0AE T3	Acid stress chaperone HdeB	hdeB		1		25340.94	94.64	94.6 4	1
P3213 1	Oxygen- independent coproporphyr inogen III oxidase	hemN		1		244051.1 79	28.32	28.3 2	1
P0AC B9	Protein HemY	hemY	3	3	45377.47	215596.8 08	155.4	241. 68	2
P0AB C5	Modulator of FtsH protease HflC	hflC		5		66849.55 8	189.23	189. 23	1
P0AB C8	Protein HflK	hflK	5	8	550602.2	1654879. 03	420.85	598. 43	2
B7MS J0	RNA-binding protein Hfq	hfq	4		256916.9		132.47	132. 47	1
P0AC E8	HIT-like protein HinT	hinT	5	4	48687.09	47522.30 1	231.05	376. 53	2
B7N1 S3	ADP-L- glycero-D- manno- heptose-6- epimerase	hldD	1	1	5405.202	3741.466	40.58	70.5 8	2
P0AC G0	DNA-binding protein H-NS	hns	3	4	40401.71	50673.61 2	129.48	240. 95	2
P0895 7	Type I restriction enzyme EcoKI M protein	hsdM		1		61548.18	29.4	29.4	1
B7N2 S2	ATP- dependent protease ATPase subunit HslU	hslU		2		398702.7 26	52.01	52.0 1	1

P0A6 Z5	Chaperone protein HtpG	htpG	2	3	4380.75	17582.38 9	160.1	209. 12	2
P0AC F2	DNA-binding protein HU- alpha	hupA	2	4	18452.03	96330.11 97	174.13	238. 87	2
P0AC F6	DNA-binding protein HU- beta	hupB		1		38401.36	33.07	33.0 7	1
P0AA N4	Hydrogenase isoenzymes nickel incorporation protein HypB	hypB	1		4406.638		50.65	50.6 5	1
B7MZ 27	D- phenylhydant oinase	hyuA		1		8175.753 6	31.92	31.9 2	1
P0A9 W7	Acid stress protein IbaG	ibaG	3	2	16776.79	35776.44 5	79.18	132. 6	2
B7N1 Z1	Small heat shock protein IbpA	ibpA	2	2	9821.772	9303.624	95.58	180. 83	2
B7N2 D2	Small heat shock protein IbpB	ibpB	3	1	66906.29	123676.5 93	125.75	204. 2	2
P0820 0	Isocitrate dehydrogenas e [NADP]	icd	6	1	601762.5	44659.42	188.54	360. 72	2
B7M NN1	Isoleucine-- tRNA ligase	ileS		1		2933.824	40.26	40.2 6	1
Q1R6 H0	Translation initiation factor IF-2	infB	1	1	9979.556	10560.88 4	51.63	82.9 7	2
A7ZU G1	Catalase- peroxidase	katG		1		39981.33 7	23.71	23.7 1	1
P0AB 78	2-amino-3- ketobutyrate coenzyme A ligase	kbl	1	1	4434.879	18208.60 8	43.85	73.4 1	2
P2186 5	Sensor protein KdpD	kdpD		1		2085.633	23.1	23.1	1
B7MT Z9	2-dehydro-3- deoxyphosph ooc-tonate aldolase	kdsA		1		75229	48.97	48.9 7	1
B7M NQ3	Glutathione- regulated potassium- efflux system ancillary protein KefF	kefF	1	1	17840.59	19691.29	27.65	52.4 5	2
P0A9 P2	Dihydrolipoyl dehydrogenas e	lpdA	7	6	98884.65	119226.6 62	335.04	575. 84	2
P0AB 39	Penicillin- binding protein	lpoB	1		7220.348		31.18	31.1 8	1

	activator									
	LpoB									
P69778	Major outer membrane lipoprotein	lpp	6	3	90253.11	163080.87	149.27	296.16	2	
P0ACJ2	Leucine-responsive regulatory protein	lrp	1	2	4064.236	6108.7366	49.11	74.9	2	
B7MYZ0	S-ribosylhomocysteine lyase	luxS	4	6	306210.9	1515951.92	189.99	276.87	2	
B7LEA1	S-ribosylhomocysteine lyase	luxS	1	2	5577.112	11211.972	64.82	104.2	2	
E0IWI3	Diaminopimelate decarboxylase	lysA	1		4361.5		23.39	23.39	1	
P0A8N3	Lysine--tRNA ligase	lysS		1		13274.055	46.3	46.3	1	
P0A8N5	Lysine--tRNA ligase, heat inducible	lysU		7		321997.371	300.12	300.12367	1	
P76558	NADP-dependent malic enzyme	maeB		1		2393.8921	26.6	26.6	1	
P69799	PTS system mannose-specific EIIAB component	manX	2		94232.46		56.71	56.71	1	
P69807	Mannose permease IID component	manZ		1		10940.919	20.23	20.23	1	
B6I1V4	Malate dehydrogenase	mdh	4	4	832640.7	1788561.48	218.67	418.82	2	
Q0TCN0	Malate dehydrogenase	mdh	4	2	91096.26	32903.832	218.38	268.83	2	
P37353	2-succinylbenzoate--CoA ligase	menE	1		9193.93		21.81	21.81	1	
P77781	1,4-dihydroxy-2-naphthoyl-CoA hydrolase	menI	1		2642.538		76.78	76.78	1	
P0ABB9	Magnesium -transporting ATPase, P-type 1	mgtA		1		3954.304	22.84	22.84	1	
P0AEZ5	Septum site-determining protein MinD	minD		1		27457.737	21.78	21.78	1	

P63388	Probable phospholipid import ATP-binding protein MlaF	mIaF	1		4800.6		25.69	25.69	1
P54746	Mannosylglycerate hydrolase	mngB		1		14874.105	20.93	20.93	1
B7MQN7	Cyclic pyranopterin monophosphate synthase accessory protein	moaC	6	6	740836.5	1327054.6	199.75	375.05	2
A7ZY39	Cyclic pyranopterin monophosphate synthase accessory protein	moaC		3		17231.85	67.03	67.03	1
P32125	Molybdopterin-guanine dinucleotide biosynthesis adapter protein	mobB	2	1	11182.77	4190.38	83.18	111.7	2
P00393	NADH dehydrogenase	ndh		1		4306.996	84.07	84.07	1
B7MYF2	Nucleoside diphosphate kinase	ndk	2	3	97655.26	149204.5	56.35	102.73	2
P0A764	Nucleoside diphosphate kinase	ndk	2	1	11030.94	12477.588	50.72	98.39	2
B7NR9	Nickel-responsive regulator	nikR	1	1	20081.3	64273.8	111.15	184.42	2
B7UL33	Nickel-responsive regulator	nikR	1		64264.6		20.94	20.94	1
B7MXG5	NADH-quinone oxidoreductase subunit C/D	nuoC		1		2487.342	28.53	28.53	1
P0AFD2	NADH-quinone oxidoreductase subunit E	nuoE	2	2	17505.05	53040.801	101.62	151.15	2
P31979	NADH-quinone oxidoreductase subunit F	nuoF	1		4427.308		22.73	22.73	1
Q8XCX2	NADH-quinone oxidoreductase subunit G	nuoG	5	4	29390.6	39332.474	121.38	234.64	2
P0AF F8	Transcription termination/a	nusA		1		10447.7727	41.89	41.89	1

	ntermination protein NusA									
B7M QD1	N utilization substance protein B homolog	nusB		1		4264.065		40.42	40.4 2	1
P0A9 11	Outer membrane protein A	ompA	26	28		376301.4	639014.0 18	1045.1	1989 .78	2
P0AA 18	Transcription al regulatory protein OmpR	ompR	1	1		12755.68	4925.856	39.54	68.0 6	2
P0C0 L2	Peroxioredoxin OsmC	osmC	1	4		33791.23	721805.4 86	124.32	151. 09	2
P0AD B2	Osmotically- inducible lipoprotein E	osmE	1	1		4085.12	6470.59	35.25	56.3 8	2
P0AF H9	Osmotically- inducible protein Y	osmY	3	3		152214.8	403707.3 6	92.33	181. 49	2
P1531 9	Chaperone protein PapD	papD	1			1638.998		21.41	21.4 1	1
B7N2 Q7	ATP- dependent 6- phosphofru ctokinase isozyme 1	pfkA		2			57552.04	62.75	62.7 5	1
P0699 9	ATP- dependent 6- phosphofru ctokinase isozyme 2	pfkB	1			9622.43		51.16	51.1 6	1
P0937 3	Formate acetyltransfer ase 1	pflB	15	9		297271.4	444181.2 42	441.75	768. 88	2
A8A4 66	Phosphoglyce rate kinase	pgk	2	4		177327.3	1082788. 4	168.13	251. 23	2
Q8XD 03	Phosphoglyce rate kinase	pgk	1	1		52794.29	58935.94	217.31	399. 66	2
B7UJ 59	Polyribonucle otide nucleotidyltra nsferase	pnp		2			5914.682	70.94	70.9 4	1
B7N0 U9	Polyribonucle otide nucleotidyltra nsferase	pnp	1	1		10006.96	14293.99 5	53.96	84.0 4	2
P0700 1	NAD(P) transhydroge nase subunit alpha	pntA	1	1		59337.06	149039.4 2	50.79	89.6 8	2
P2353 8	Phosphoenolp yruvate synthase	ppsA	2	4		79410.2	414087.3 87	187.44	254. 12	2
P0A7 19	Ribose- phosphate	prs	1	1		106292.1	118090.9 98	189.19	329. 79	2

	pyrophosphokinase									
P0A9 M8	Phosphate acetyltransferase	pta	10	5		722931.5	1153871.86	310.28 36715	478. 90734	2
P0AA 06	Phosphocarrier protein HPr	ptsH	2	3		271328	997502.415	114.33	193. 82	2
P0883 9	Phosphoenolpyruvate-protein phosphotransferase	ptsI	2	2		40895.88	139961.489	72.25	125. 33	2
B7MS J5	Adenylosuccinate synthetase	purA	2	2		23459.6	47643.372	120.77	169. 5	2
B1LN C6	Phosphoribosylaminoimidazole-succinocarboxamide synthase	purC		2			129627.771	44.28	44.2 8	1
P3705 1	Formyltetrahydrofolate deformylase	purU	5	9		35994.79	84004.292	333.37	490. 54	2
P0A4 40	Formyltetrahydrofolate deformylase	purU	2	1		423342.5	120189.2	357.91	687. 55	2
P0954 6	Bifunctional protein PutA	putA	1			5358.864		36.88	36.8 8	1
P2159 9	Pyruvate kinase II	pykA	4	8		13954.18	39846.8954	310.88	477. 44	2
P0AD 61	Pyruvate kinase I	pykF	1	3		30297.19	188820.279	144.84	176. 54	2
B7MZ 76	CTP synthase	pyrG		2			17162.516	59.39	59.3 9	1
P0AA 55	Protein QmcA	qmcA	1	1		5092.593	9497.072	55.01	89.9 9	2
P0AD 51	Ribosome-associated inhibitor A	raiA		1			158439.936	51.87	51.8 7	1
B7N0 J8	RNase adapter protein RapZ	rapZ	2	3		4366.437	12991.356	98.58	130. 87	2
P0292 5	D-ribose-binding periplasmic protein	rbsB	5	4	1	48977.3	178441.592	270.86	529. 27	3
P6941 2	Outer membrane lipoprotein RcsF	rscF		1			18626.172	50.583 6715	50.5 83671	1
B7M YJ9	Protein RecA	recA		1			1959.172	31.75	31.7 5	1
B7MR 01	ATP-dependent	rhlB		2			27936.015	39.3	39.3	1

		RNA helicase RhlB								
P25888	ATP-dependent RNA helicase RhlE	rhlE	1			2791.438		22.3	22.3	1
P0AG32	Transcription termination factor Rho	rho		1		6039.511		70.05	70.05	1
B7N0J6	3,4-dihydroxy-2-butanone 4-phosphate synthase	ribB	2	3		14414.36	31662.651	96.48	160.97	2
P25539	Riboflavin biosynthesis protein RibD	ribD		1		75194.039		52.6	52.6	1
B7MQD0	6,7-dimethyl-8-ribityllumazine synthase	ribH		2		101818.68		44.91	44.91	1
P36999	23S rRNA (guanine(745)-N(1))-methyltransferase	rlmA		1		47156.005		30.57	30.57	1
P21513	Ribonuclease E	rne	11	7	1	2351234	578948.991	^{8574.8} ₅₅ 369.58	688.48	3
Q1R5U9	50S ribosomal protein L1	rpIA	2	5		58648.11	929533.73	207.32	260.82	2
Q1R607	50S ribosomal protein L2	rpIB	6	6		4875830	3958421.57	294.04	526.89	2
Q1R602	50S ribosomal protein L3	rpIC	3			69461.01		254.77	254.77	1
Q1R604	50S ribosomal protein L4	rpID	1	3		23396.57	78412.143	128.55	179.68	2
Q1R620	50S ribosomal protein L5	rpIE	1	1		30716.26	270075.519	120.7	179.8	2
Q1R624	50S ribosomal protein L6	rpIF	3	1		62367.3	23478.829	386.53	698.42	2
Q1R357	50S ribosomal protein L9	rpII	7	7		22189.18	41732.75	264.24	502.53	2
Q1R5V0	50S ribosomal protein L10	rpIJ		5		478658.586		218.99	218.99	1
Q1R5U7	50S ribosomal protein L11	rpIK	1	2		14745.52	46332.552	109.61	180.71	2
Q1R5V1	50S ribosomal	rpIL	2	4		107919.6	458967.553	152.57	249.89	2

	protein										
	L7/L12										
Q1R6 A9	50S ribosomal protein L13	rplM		4		99364.50 58		135.62	135. 62	1	
Q1R6 17	50S ribosomal protein L14	rplN	2	6	208567.2	1085357. 31		214.15	285. 09	2	
Q1R6 30	50S ribosomal protein L15	rplO	1	1	212270	268996.1 64		218.58	360. 08	2	
P0241 3	50S ribosomal protein L15	rplO	1	1	43104.39	27467.12 92		204.44	364. 3	2	
Q1R6 13	50S ribosomal protein L16	rplP		3		475139.7 2		95.53	95.5 3	1	
Q1R6 38	50S ribosomal protein L17	rplQ	4		126430.3			128.85	128. 85	1	
Q1R6 26	50S ribosomal protein L18	rplR		1		6570.726		36.49	36.4 9	1	
Q1R8 B9	50S ribosomal protein L19	rplS	1	2	5878.179	21250.93 8		93.26	150. 51	2	
Q1RB 79	50S ribosomal protein L20	rplT	4	1	214207.4	318728.6 55		107.93	158. 75	2	
Q1R6 F0	50S ribosomal protein L21	rplU	2	3	9478.912	36519.67 8		115.09	164. 92	2	
Q1R6 10	50s ribosomal protein L22	rplV	1	1	1	204453.3	137499.1 89	^{4362.4} ₆₅	36.38	92.9 9	3
Q1R6 19	50S ribosomal protein L24	rplX	3		6484.408			75.48	75.4 8	1	
B5Y WX8	50S ribosomal protein L25	rplY	1	2	14513.39	330060.1 42		51.12	74.6 3	2	
B6I18 4	50S ribosomal protein L25	rplY		2		56617.96 2		57.85	57.8 5	1	
B1LK T4	50S ribosomal protein L25	rplY		1		16522.59 6		35.9	35.9	1	
Q1R4 V5	50S ribosomal protein L28	rpmB		1		35076.15		46.58	46.5 8	1	
Q1R6 29	50S ribosomal protein L30	rpmD	1		12062.56			35.02	35.0 2	1	
P0C20 3	50S ribosomal protein L31	rpmE	1		143944.3			59.18	59.1 8	1	

Q1R6 32	50S ribosomal protein L36 I	rpmJ1	1	2		10101.77	31294.47 8	75.35	122. 43	2
P0A7 Z6	DNA- directed RNA polymerase subunit alpha	rpoA	4	5		19232.49	37768.53 5	162.06	294. 31	2
B7MR B3	DNA- directed RNA polymerase subunit beta	rpoB	4	5		35417.39	125498.5 29	301.95	478. 14	2
Q0TA 78	DNA- directed RNA polymerase subunit beta	rpoB		2			102175.2 02	72.91	72.9 1	1
P0A8 T8	DNA- directed RNA polymerase subunit beta'	rpoC	9	7		1629679	1231105. 03	420.05 36715	764. 3836 7	2
P0057 9	RNA polymerase sigma factor RpoD	rpoD		1			10242.74 3	29.54	29.5 4	1
P0AG 67	30S ribosomal protein S1	rpsA	5	8		42099.26	168448.6 71	218.14	340. 19	2
Q1RG 21	30S ribosomal protein S2	rpsB	4	4		69125.29	573877.0 41	140.09	238. 28	2
B6HZ E3	30S ribosomal protein S2	rpsB		2			226034.9 49	68.17	68.1 7	1
Q1R6 12	30S ribosomal protein S3	rpsC	1	5		87762.57	1603406. 07	241.14	313. 52	2
Q1R6 36	30S ribosomal protein S4	rpsD	6	6	2	22718.9	44378.06 8	289.35	633. 87	3
Q1R6 27	30S ribosomal protein S5	rpsE	1	2		72767.1	245384.2 4	258.8	420. 06	2
B7NG D4	30S ribosomal protein S6	rpsF		2			151007.3 88	61.19	61.1 9	1
Q1R3 60	30S ribosomal protein S6	rpsF	1	1		185516.8	139620.3 27	63.22	115. 45	2
Q1R5 U2	30S ribosomal protein S7	rpsG	1	1		1411.526	3590.718	54.67	86.2 1	2
Q1R6 B0	30S ribosomal protein S9	rpsI	3	3		265882.3	591593.9 8	111.82	198. 68	2
Q1R6 01	30S ribosomal protein S10	rpsJ	6	7		312588	465910.7 58	272.01	515. 7	2

Q1R6 35	30s ribosomal protein S11	rpsK	5	2		210614.4	26547.39 6	154.58	259. 4	2	
Q1R5 U1	30S ribosomal protein S12	rpsL	3	3		98482.35	286514.0 72	145.38	258. 77	2	
C4ZU J7	30S ribosomal protein S12	rpsL		2			396280.7 2	110.55	110. 55	1	
Q1R6 33	30S ribosomal protein S13	rpsM	6	6		435893.5	578486.8 8	273.87	506. 3	2	
B5YS 55	30S ribosomal protein S15	rpsO	2	4		5450.814	34470.26 9	193.1	249. 31	2	
Q1R6 H3	30S ribosomal protein S15	rpsO	1	1	3	128707.1	61762.03 5	67181. 14	585.62	1235 .71	3
Q1R6 16	30s ribosomal protein S17	rpsQ		1			153927.8 37	26.14	26.1 4	1	
Q1R3 58	30S ribosomal protein S18	rpsR		3			312269.4 2	103.87	103. 87	1	
Q1RG H9	30S ribosomal protein S20	rpsT		1			1914.052	33.08	33.0 8	1	
B7MR 18	Regulator of ribonuclease activity A	rraA		1			2528.569	30.34	30.3 4	1	
B7MR C1	Regulator of sigma D	rsd		6			23401.74 9	247.53	247. 53	1	
P0AA 45	Ribosomal small subunit pseudouridine synthase A	rsuA		4			50727.44 4	162.27	162. 27	1	
P0AC 43	Succinate dehydrogenas e flavoprotein subunit	sdhA	21	19		663065.2	851727.6 16	922.35	1772 .5	2	
P0701 4	Succinate dehydrogenas e iron-sulfur subunit	sdhB		3			48650.99 2	157.85	157. 85	1	
B7N2 55	Protein- export protein SecB	secB	3			136512.2		77.043 6715	77.0 4367 1	1	
P0AG 91	Protein translocase subunit SecD	secD	1	1		5589.2	9121.068	37.34	69.9 8	2	
B7M QL5	tRNA 2- selenouridine synthase	selU	1			62528.36		25.69	25.6 9	1	
B7MR V6	Serine--tRNA ligase	serS	2			16844.89		55.11	55.1 1	1	
P0AE U9	Chaperone protein Skp	skp	1	1		57159.63	73421.10 3	45.52	86.0 5	2	

P3719 4	Outer membrane protein slp	slp	2	2		248008.1	308136.7 47	104.47	171. 6	2
P0A9 06	Outer membrane lipoprotein SlyB	slyB	11	15	2	289573.7	555800.0 37	^{10565.} ₂₁ 632.79	1231. .97	3
P0A9 L1	FKBP-type peptidyl- prolyl cis- trans isomerase SlyD	slyD	15	12		1605919	1829200. 46	706.17	1285. .23	2
B7M YQ8	SsrA-binding protein	smpB		1		68079.71 1		46.1	46.1	1
P0A9 52	Spermidine N(1)- acetyltransfer ase	speG		1		5172.028		27.37	27.3 7	1
P0AG E2	Single- stranded DNA-binding protein	ssb	3	1		192743.9	22773.38 7	97.95	118. 6	2
P0AF G3	2- oxoglutarate dehydrogenas e E1 component	sucA	9	8		78159.13	287168.1 84	474.24 36715	863. 5173 4	2
P0AF G6	Dihydrolipoyl lysine-residue succinyltransf erase component of 2- oxoglutarate dehydrogenas e complex	sucB	5	2		62720.66	36309.38 5	314.43	512. 98	2
B7M5 P1	Succinyl- CoA ligase [ADP- forming] subunit beta	sucC	6	5		70603.15	55332.06 06	177.37	340. 56	2
P0A8 38	Succinyl- CoA ligase [ADP- forming] subunit beta	sucC	8	3		423587.9	282917.6 49	220.89	338. 86	2
P0AG F1	Succinyl- CoA ligase [ADP- forming] subunit alpha	sucD	5	6		238748.5	463724.7 66	245.74	380. 9	2
P0A8 69	Transaldolase A	talA	1	2		42937.29	189704.0 88	33.12	57.5 5	2
P0A8 71	Transaldolase B	talB	1	3		55140.49	154683.5 79	94.81	125. 1	2
P0701 8	Methyl- accepting chemotaxis protein IV	tap		1		6429.138		32.23	32.2 3	1

P0701 7	Methyl- accepting chemotaxis protein II	tar	5	4		323323.2	698197.9 2	181.69	343. 65	2
P0AG F8	L-threonine dehydratase catabolic TdcB	tdcB		1			5570.586	27.34	27.3 4	1
P4263 2	PFL-like enzyme TdcE	tdcE		3			29499.43 4	66.01	66.0 1	1
P0AG L3	Putative reactive intermediate deaminase TdcF	tdcF		3			161745.9	80.57	80.5 7	1
B7N1 S0	L-threonine 3- dehydrogenas e	tdh		1			2487.342	40.47	40.4 7	1
B7M VJ7	Threonine-- tRNA ligase	thrS	12	10		257338.9	406729.2 42	441.53	739. 29	2
B7L6J 2	Threonine-- tRNA ligase	thrS	9	6	1	2097880	886276.7 22	^{8718.5} 52 371.78	776. 46	3
B7M QF2	Trigger factor	tig	5			81192.55		192.72	192. 72	1
B7N2 12	Tryptophanas e	tnaA	3	3		18024.02	68734.85 2	151.78	260. 69	2
P0AD I2	Transposon Tn3 resolvase	tnpR		1			120169.9 8	34.19	34.1 9	1
B7MP N1	Protein TolB	tolB		1			66870.90 69	39.78	39.7 8	1
P0A8 60	Triosephosph ate isomerase	tpiA		1			6734.41	81.48	81.4 8	1
P0A8 64	Thiol peroxidase	tpx		1			10666.86 6	40.75	40.7 5	1
P0A8I 6	tRNA (guanine- N(7)-) methyltransfe rase	trmB	1	1		114660.7	72873.14	75.86	101. 53	2
B7MP 30	Elongation factor Ts	tsf	4	1		319680.8	127523.2 35	112.82	148. 22	2
P0294 2	Methyl- accepting chemotaxis protein I	tsr	2	1		194745.1	56974.30 2	55.32	87.9 6	2
A7ZU J2	Elongation factor Tu 2	tuf2	1	1		424640.6	130264.3 35	476.59 36715	865. 9136 7	2
P0A6 N3	Elongation factor Tu	tufA	2	2		177541.5	176742.5 2	791.64	1446 .99	2
Q8XB J4	Oxidoreducta se UcpA	ucpA	2	2		85930.05	1001172. 69	51.74	87.8 5	2
P1275	Uridine	udp	1	3		29970.24	253864.4	96.26	147.	2

8	phosphorylase				01			93	
B7M YC5	Uracil phosphoribosyltransferase	upp	1	1	2043.835	3884.974	32.64	59.43	2
P0A4 P7	Universal stress protein F	uspF		1		20765.022	29.85	29.85	1
P3790 3	Universal stress protein F	uspF	1		1600.2		49.11	49.11	1
Q8XB T3	Universal stress protein G	uspG		2		36115.02	159.67	159.67	1
P0AD Z9	UPF0092 membrane protein YajC	yajC		1		50079.042	125.06	125.06	1
P0AF P6	GTP cyclohydrolase 1 type 2 homolog	ybgI	10	9	787612.7	826435.953	325.46	647.30367	2
P7581 8	Uncharacterized lipoprotein YbjP	ybjP		1		27057.319	42.47	42.47	1
B7M QX0	UPF0145 protein YbjQ	ybjQ	2	2	115091.8	326669.679	89.79	158.16	2
P0AB 16	Uncharacterized protein YccJ	yccJ		1		29737.46	38.15	38.15	1
B7MT N8	UPF0227 protein YcfP	ycfP	7	6	58229.52	76340.895	205.6	393.28	2
B7NK H1	UPF0227 protein YcfP	ycfP	5		11941.04		166.86	166.86	1
P3180 8	Uncharacterized oxidoreductase YciK	yciK	1	1	10328.12	9005.072	36.52	58.36	2
P7610 0	Uncharacterized acetyltransferase YdcK	YdcK	1		1356.867		23.21	23.21	1
P6446 5	Putative selenoprotein YdfZ	ydfZ	1		32119.58		32.34	32.34	1
P6717 6	Probable transcriptional regulatory protein YebC	yebC		1		3822.203	40.72	40.72	1
Q8X7 I0	UPF0339 protein YegP	yegP		3		6121.679	87.63	87.63	1
P0AD 34	UPF0381 protein YfcZ	yfcZ	2	2	97730.7	442109.535	96.17	148.97	2
P0AD E7	Uncharacterized protein YgaU	ygaU	1		6774.944		68.03	68.03	1

P65809	Uncharacterized protein YgeY	ygeY	3	1	173427	124008.885	87.29	114.69	2
Q8XD75	Uncharacterized protein YgfK	ygfK	1	2	37926.08	190107.22	213.72	286.6	2
P0ADT7	Putative acid-amine ligase YgiC	ygiC		1		5411.331	22.39	22.39	1
P0ADU3	Probable quinol monooxygenase YgiN	ygiN	2	3	152988	480285.351	105.23	139.93	2
P0ADW5	Putative cytochrome d ubiquinol oxidase subunit 3	yhcB	2	3	33406.26	99323.44	156.48	255.76	2
P28638	DNA adenine methyltransferase YhdJ	yhdJ		1		64097.775	28.02	28.02	1
P68207	UPF0337 protein YjbJ	yjbJ		1		62127.08	41.28	41.28	1
P0AF94	2-iminobutanolate/2-iminopropanoate deaminase	yjgF		2		22467.876	105.18	105.18	1
P39342	Uncharacterized protein YjgR	yjgR	1		1600.2		25.69	25.69	1
P64583	Uncharacterized protein YqjD	yqjD	4	5	279435.2	306374.886	122.44	221.75	2
P64588	Transcriptional regulator YqiI	yqiI	3	5	6270881	7515577.86	183.32	318.68	2
P64598	Uncharacterized protein YraP	yraP		1		13732.641	24.47	24.47	1
P0A9W9	Protein YrdA	yrdA		1		77292.988	53.34	53.34	1
Q8XB4	NAD(P)H dehydrogenase (quinone)	Z1423/ Z1504	2	1	6858.729	2050.472	59.56	105.18	2
B7N2R9	Cell division protein ZapB	zapB	1		55250.33		39.4	39.4	1
P0AAB0	Zinc resistance-associated protein	zraP	2	5	3052.526	36955.681	167.33	199.78	2

Table 4: Total proteomics data of *E. coli* and *E. coli*-derived OMVs. Sample 1, *E. coli*-F95; sample 2, *E. coli*-PAD4; sample 3, *E. coli*-OMV

9.1.2 Complete proteomic Analysis of unique *E.coli*-OMV proteins

UniProt ID	Protein name (short)	Gene name	number of unique peptides			MS2 intensities			Bestprotein score	Sum score	s a m p l e
			<i>E.coli</i> F95	<i>E.coli</i> PAD4	OMV F95	<i>E.coli</i> F95	<i>E.coli</i> PAD4	OMV F95			
Q1R6H3	30S ribosomal protein S15	rpsO	1	1	3	128707	61762.035	67181.1	585.62	1235.71	3
P04949	Flagellin	fliC	10	14	2	704599	1146224.2	9488.72	653.24	1305	3
P0A906	Outer membrane lipoprotein SlyB	slyB	11	15	2	289574	555800.04	10565.2	632.79	1231.97	3
Q1R636	30S ribosomal protein S4	rpsD	6	6	2	22718.9	44378.068	3554.36	289.35	633.87	3
B7L6J2	Threonine--tRNA ligase	thrS	9	6	1	2097880	886276.72	8718.55	371.78	776.46	3
P21513	Ribonuclease E	rne	11	7	1	2351234	578948.99	8574.86	369.58	688.48	3
P02925	D-ribose-binding periplasmic protein	rbsB	5	4	1	48977.3	178441.59	6973.67	270.86	529.27	3
P63285	Chaperone protein ClpB	clpB	1	1	1	5169079	5833442.7	30537.3	227.63	430.06	3
Q1R610	50S ribosomal proten L22	rplV	1	1	1	204453	137499.19	4362.47	36.38	92.99	3

Table 6: Total proteomics data of proteins isolated from *E.coli* and *E.coli* -derived OMVs. Sample 1, *E.coli*-F95; sample 2, *E.coli*-PAD4; sample 3, *E.coli*-OMV

9.2 Materials

9.2.1 Reagents & Solutions

Annexin V- apoptosis kit	Thermofisher
BCA protein assay kit	Thermofisher
Bisindolymaleimide I	Sigma-Aldrich
BSA (Bovine serumalbumin)	Sigma-Aldrich
BzATP	Sigma-Aldrich
Calpeptin	Sigma-Aldrich
Canabidiol	G W Pharma
Catch and Release v2.0 IP kit	Millipore
Chloramidine	A gift from Prof. Thompson
Cytochalacin D	Sigma-Aldrich
Colistin	Sigma-Aldrich
DAPI Vecta Shield mounting medium	Sigma-Aldrich
Doxorubicin	Sigma- Aldrich
DMSO	Fisher Scientific
D-pantethine	Sigma-Aldrich
DPBS	Sigma-Aldrich
EGTA	Sigma-Aldrich
Erythromycin	Sigma-Aldrich
5-Fluorouracil	Sigma-Aldrich
Guava ViaCount reagent	Guava Technologies,UK
HALT Protease Cocktail	Sigma-Aldrich
HEPES	Sigma-Aldrich
Imipramine	Sigma-Aldrich
Kanamycin	Sigma-Aldrich
Laemmli sample buffer	BioRad
Müller Hinton Agar	Sigma-Aldrich
Müller HintonBroth	Sigma-Aldrich
Nicotine	The Alchemists Cupboard

Paraformaldehyde	Sigma-Aldrich
Penicillin / Streptomycin	Sigma-Aldrich
Pkh26 cell labelling kit	Sigma-Aldrich
Propidium iodide	Sigma-Aldrich
Protein molecular weight marker	BioRad
Rifampicin	Sigma-Aldrich
RPMI	Sigma-Aldrich
Running buffer	BioRad
RIPA buffer	Sigma-Aldrich
SDS (Sodium dodecyl sulphate)	Sigma-Aldrich
TEMED	Sigma-Aldrich
TGX- ready gels	BioRad
Transfer Buffer	BioRad
Tris base	Sigma-Aldrich
Triton X-100 Trypsin/EDTA solution	Sigma-Aldrich
Trypsin/EDTA solution	Sigma-Aldrich
Tween 20	Sigma-Aldrich
Y27632	Sigma-Aldrich

9.2.2 Equipment

Beckman L8-70M Ultracentrifuge	Beckman
Cell culture flasks (75 cm ² , 25cm ²)	Fisher Scientific
Centrifuge 5804 R	Eppendorf
Centrifuge 5810 R	Eppendorf
ECL system	Amersham, UK
Eppendorf tubes (1.5ml)	Fisher Scientific
Fluorescence microscope (1X81)	Olympus Corporation, Germany
FLUOstar Omega plate reader	BMG Labtech, UK
Guava EasyCyte flow cytometer	Guava Technologies UK
Incubator Heraeus CO ₂ -Auto-Zero	Thermo Electron Corporation
NanoSightLM10	School of Pharmacy, UCL
NanoSight NS500	St. George's University
NucleoCounter® NC-3000™	Chemometec
Microcentrifuge 5417R	Eppendorf
Microplate (12-well)	Fisher Scientific
Microplate (24-well)	Fisher Scientific
Microplate (96-well)	Fisher Scientific
Nikon Inverted Microscope, TS100	Nikon Eclipse, Japan
Semi-dry transfer system	BioRad
Suction filtration apparatus	Kind provided
UVP Chemiluminescence	UVP BioDoc-IT™ System, U.K
Viva flow	Kindly provided (Dr. P. Matewele)

9.2.3 Antibodies

Anti-Annexin V	ImmunoTools
Anti-PAD2, Anti-PAD3, Anti-PAD4	BioRad
Mouse anti-IgG FITC	ImmunoTools
CD9-FITC, CD29-FITC, CD71-FITC, CD58-FITC	ImmunoTools
F95	BioRad

9.3 Experimental Solutions

9.3.1 Mammalian cell freeze medium

90% cell growth medium

10% DMSO

9.3.2 RIPA Lysis Buffer pH 7.4

1ml RIPA buffer

1:100 HALT protease inhibitor

9.4.1 Sample Buffer (10x)

2x laemmli sample buffer

5% beta mercaptoethanol

9.4.2 Running Buffer

30.0 g Tris base

144.0 g glycine

10.0 g of SDS

1000 ml of H₂O.-pH- 8.3 dilute to 1X before using

9.4.3 TBS buffer (10x)

To prepare 1000ml:

60.6 g Tris

87.6 g NaCl

1M HCl

Deionized water

9.4.4 Blocking buffer

5% BSA

TBS-T (1x TBS-T with 0.01% tween 20)

9.4.5 Transfer Buffer (10X)

15.2 g Tris (free base)

72.1 g Glycine

5.0 g SDS

Ultra pure water to 500 ml

9.4.6 Transfer Buffer (1X)

50 ml 10X Transfer Buffer

100 ml Methanol

350 ml Distilled water (Make fresh for each use)

10.0 References

- ABEDON, S. T., KUHL, S. J., BLASDEL, B. G. & KUTTER, E. M. 2011. Phage treatment of human infections. *Bacteriophage*, 1, 66-85.
- ACEVEDO, R., FERNANDEZ, S., ZAYAS, C., ACOSTA, A., SARMIENTO, M. E., FERRO, V. A., ROSENQVIST, E., CAMPA, C., CARDOSO, D., GARCIA, L. & PEREZ, J. L. 2014. Bacterial outer membrane vesicles and vaccine applications. *Front Immunol*, 5, 121.
- AKERS, J. C., RAMAKRISHNAN, V., NOLAN, J. P., DUGGAN, E., FU, C.-C., HOCHBERG, F. H., CHEN, C. C. & CARTER, B. S. 2016. Comparative Analysis of Technologies for Quantifying Extracellular Vesicles (EVs) in Clinical Cerebrospinal Fluids (CSF). *PLOS ONE*, 11, e0149866.
- ALFAROUK, K. O., STOCK, C.-M., TAYLOR, S., WALSH, M., MUDDATHIR, A. K., VERDUZCO, D., BASHIR, A. H. H., MOHAMMED, O. Y., ELHASSAN, G. O., HARGUINDEY, S., RESHKIN, S. J., IBRAHIM, M. E. & RAUCH, C. 2015. Resistance to cancer chemotherapy: failure in drug response from ADME to P-gp. *Cancer Cell International*, 15, 71.
- ALTEVOGT, P., BRETZ, N. P., RIDINGER, J., UTIKAL, J. & UMANSKY, V. 2014. Novel insights into exosome-induced, tumor-associated inflammation and immunomodulation. *Semin Cancer Biol*, 28, 51-7.
- ALTINDIS, E., FU, Y. & MEKALANOS, J. J. 2014. Proteomic analysis of *Vibrio cholerae* outer membrane vesicles. *Proc Natl Acad Sci U S A*, 111, E1548-56.

ALVES, N. J., TURNER, K. B., MEDINTZ, I. L. & WALPER, S. A. 2016a. Protecting enzymatic function through directed packaging into bacterial outer membrane vesicles. *Scientific Reports*, 6, 24866.

ALVES, N. J., TURNER, K. B. & WALPER, S. A. 2016b. Directed Protein Packaging within Outer Membrane Vesicles from Escherichia coli: Design, Production and Purification. *J Vis Exp*.

ANAGNOSTOU, V. K., LOWERY, F. J., ZOLOTA, V., TZELEPI, V., GOPINATH, A., LICEAGA, C., PANAGOPOULOS, N., FRANGIA, K., TANOUE, L., BOFFA, D., GETTINGER, S., DETTERBECK, F., HOMER, R. J., DOUGENIS, D., RIMM, D. L. & SYRIGOS, K. N. 2010. High expression of BCL-2 predicts favorable outcome in non-small cell lung cancer patients with non squamous histology. *BMC Cancer*, 10, 186.

ANDRE, F., CHAPUT, N., SCHARTZ, N. E., FLAMENT, C., AUBERT, N., BERNARD, J., LEMONNIER, F., RAPOSO, G., ESCUDIER, B., HSU, D. H., TURSZ, T., AMIGORENA, S., ANGEVIN, E. & ZITVOGEL, L. 2004. Exosomes as potent cell-free peptide-based vaccine. I. Dendritic cell-derived exosomes transfer functional MHC class I/peptide complexes to dendritic cells. *J Immunol*, 172, 2126-36.

ANDREOLA, G., RIVOLTINI, L., CASTELLI, C., HUBER, V., PEREGO, P., DEHO, P., SQUARCINA, P., ACCORNERO, P., LOZUPONE, F., LUGINI, L., STRINGARO, A., MOLINARI, A., ARANCIA, G., GENTILE, M., PARMIANI, G. & FAIS, S. 2002. Induction of lymphocyte apoptosis by tumor cell secretion of FasL-bearing microvesicles. *J Exp Med*, 195, 1303-16.

ANTEBI, Y. E., NANDAGOPAL, N. & ELOWITZ, M. B. 2017. An operational view of intercellular signaling pathways. *Current Opinion in Systems Biology*, 1, 16-24.

- ANTWI-BAFFOUR, S., ADJEI, J., ARYEH, C., KYEREMEH, R., KYEI, F. & SEIDU, M. A. 2015. Understanding the biosynthesis of platelets-derived extracellular vesicles. *Immunity, Inflammation and Disease*, 3, 133-140.
- APPENDINO, G., GIBBONS, S., GIANA, A., PAGANI, A., GRASSI, G., STAVRI, M., SMITH, E. & RAHMAN, M. 2008. Antibacterial Cannabinoids from *Cannabis sativa*: A Structure–Activity Study. *Journal of Natural Products* 71 (8), 1427-1430 DOI: 10.1021/np8002673
- ARALDI, E., KRAMER-ALBERS, E. M., HOEN, E. N., PEINADO, H., PSONKAANTONCZYK, K. M., RAO, P., VAN NIEL, G., YANEZ-MO, M. & NAZARENKO, I. 2012. International Society for Extracellular Vesicles: first annual meeting, April 17-21, 2012: ISEV2012. *J Extracell Vesicles*, 1, 19995.
- ARMSTRONG, J. P. K., HOLME, M. N. & STEVENS, M. M. 2017. Re-Engineering Extracellular Vesicles as Smart Nanoscale Therapeutics. *ACS nano*, 11, 69-83.
- ARMSTRONG, J. P. K. & STEVENS, M. M. 2018. Strategic design of extracellular vesicle drug delivery systems. *Advanced Drug Delivery Reviews*, 130, 12-16.
- ATAKAN, Z. 2012. Cannabis, a complex plant: different compounds and different effects on individuals. *Therapeutic Advances in Psychopharmacology*, 2, 241-254.
- AUBERTIN, K., SILVA, A. K. A., LUCIANI, N., ESPINOSA, A., DJEMAT, A., CHARUE, D., GALLET, F., BLANC-BRUDE, O. & WILHELM, C. 2016. Massive release of extracellular vesicles from cancer cells after photodynamic treatment or chemotherapy. *Scientific Reports*, 6, 35376.
- AUGER, I., MARTIN, M., BALANDRAUD, N. & ROUDIER, J. 2010. Rheumatoid arthritis specific autoantibodies to peptidyl arginine deiminase type 4 inhibit citrullination of fibrinogen. *Arthritis Rheum*, 62, 126-31.
- AYERS, L., NIEUWLAND, R., KOHLER, M., KRAENKEL, N., FERRY, B. & LEESON, P. 2015. Dynamic microvesicle release and clearance within the cardiovascular system: triggers and mechanisms. *Clin Sci (Lond)*, 129, 915-31.

BACHUR, N. R. 2002. Anthracyclines. In: BERTINO, J. R. (ed.) *Encyclopedia of Cancer (Second Edition)*. New York: Academic Press.

BADRNYA, S., BAUMGARTNER, R. & ASSINGER, A. 2014. Smoking alters circulating plasma microvesicle pattern and microRNA signatures. *Thromb Haemost*, 112, 128-136.

BAGULEY, B. C. 2010. Multiple drug resistance mechanisms in cancer. *Mol Biotechnol*, 46, 308-16.

BALAJ, L., LESSARD, R., DAI, L., CHO, Y.-J., POMEROY, S. L., BREAKFIELD, X. O. & SKOG, J. 2011. Tumour microvesicles contain retrotransposon elements and amplified oncogene sequences. *Nature communications*, 2, 180-180.

BARDAL, S. K., WAECHTER, J. E. & MARTIN, D. S. 2011. Chapter 20 - Neoplasia. In: BARDAL, S. K., WAECHTER, J. E. & MARTIN, D. S. (eds.) *Applied Pharmacology*. Philadelphia: Content Repository Only!

BARKALINA, N., JONES, C., WOOD, M. J. A. & COWARD, K. 2015. Extracellular vesicle mediated delivery of molecular compounds into gametes and embryos: learning from nature. *Human Reproduction Update*, 21, 627-639.

BARROS, F. M., CARNEIRO, F., MACHADO, J. C. & MELO, S. A. 2018. Exosomes and Immune Response in Cancer: Friends or Foes? *Front Immunol*, 9, 730.

BASU, P. S., MAJHI, R., GHOSAL, S. & BATASYAL, S. K. 2011. Peptidyl-arginine deiminase: an additional marker of rheumatoid arthritis. *Clin Lab*, 57, 1021-5.

BEER, K. B. & WEHMAN, A. M. 2017. Mechanisms and functions of extracellular vesicle release *in vivo*—What we can learn from flies and worms. *Cell Adhesion & Migration*, 11, 135-150.

BELLO-MORALES, R., PRAENA, B., DE LA NUEZ, C., REJAS, M. T., GUERRA, M., GALAN-GANGA, M., IZQUIERDO, M., CALVO, V., KRUMMENACHER, C. & LOPEZ GUERRERO, J. A. 2018. Role of Microvesicles in the Spread of Herpes Simplex Virus 1 in Oligodendrocytic Cells. *J Virol*, 92.

BENEDIKTER, B. J., VOLGERS, C., VAN EIJCK, P. H., WOUTERS, E. F. M., SAVELKOUL, P. H. M., REYNAERT, N. L., HAENEN, G., ROHDE, G. G. U., WESELER, A. R. & STASSEN, F. R. M. 2017. Cigarette smoke extract induced exosome release is mediated by depletion of exofacial thiols and can be inhibited by thiol-antioxidants. *Free Radic Biol Med*, 108, 334-344.

BERGAMASCHI, M. M., QUEIROZ, R. H., ZUARDI, A. W. & CRIPPA, J. A. 2011. Safety and side effects of cannabidiol, a Cannabis sativa constituent. *Curr Drug Saf*, 6, 237-49.

BERLEMAN, J. E., ZEMLA, M., REMIS, J. P., LIU, H., DAVIS, A. E., WORTH, A. N., WEST, Z., ZHANG, A., PARK, H., BOSNEAGA, E., VAN LEER, B., TSAI, W., ZUSMAN, D. R. & AUER, M. 2016. Exopolysaccharide microchannels direct bacterial motility and organize multicellular behavior. *The Isme Journal*, 10, 2620.

BERTRAND, N., WU, J., XU, X., KAMALY, N. & FAROKHZAD, O. C. 2014. Cancer nanotechnology: The impact of passive and active targeting in the era of modern cancer biology. *Advanced Drug Delivery Reviews*, 66, 2-25.

BHATTACHARYYA, A., CHATTOPADHYAY, R., MITRA, S. & CROWE, S. E. 2014. Oxidative Stress: An Essential Factor in the Pathogenesis of Gastrointestinal Mucosal Diseases. *Physiological Reviews*, 94, 329-354.

BIANCO, F., PERROTTA, C., NOVELLINO, L., FRANCOLINI, M., RIGANTI, L., MENNA,

E., SAGLIETTI, L., SCHUCHMAN, E. H., FURLAN, R., CLEMENTI, E., MATTEOLI, M. & VERDERIO, C. 2009. Acid sphingomyelinase activity triggers microparticle release from glial cells. *Embo j*, 28, 1043-54.

BICKER, K. L. & THOMPSON, P. R. 2013. The protein arginine deiminases: Structure, function, inhibition, and disease. *Biopolymers*, 99, 155-63.

BIELECKA, E., SCAVENIUS, C., KANTYKA, T., JUSKO, M., MIZGALSKA, D., SZMIGIELSKI, B., POTEMPA, B., ENGHILD, J. J., PROSSNITZ, E. R., BLOM, A. M. & POTEMPA, J. 2014. Peptidyl arginine deiminase from *Porphyromonas gingivalis* abolishes anaphylatoxin C5a activity. *J Biol Chem*, 289, 32481-7.

BILLER, S. J., SCHUBOTZ, F., ROGGENSACK, S. E., THOMPSON, A. W., SUMMONS, R. E. & CHISHOLM, S. W. 2014. Bacterial Vesicles in Marine Ecosystems. *Science*, 343, 183-186.

BINICI, J., HARTMANN, J., HERRMANN, J., SCHREIBER, C., BEYER, S., GULER, G., VOGEL, V., TUMULKA, F., ABELE, R., MANTELE, W. & KOCH, J. 2013. A soluble fragment of the tumor antigen BCL2-associated athanogene 6 (BAG-6) is essential and sufficient for inhibition of NKp30 receptor-dependent cytotoxicity of natural killer cells. *J Biol Chem*, 288, 34295-303.

BIRGE, R. B., BOELTZ, S., KUMAR, S., CARLSON, J., WANDERLEY, J., CALIANESE, D., BARCINSKI, M., BREKKEN, R. A., HUANG, X., HUTCHINS, J. T., FREIMARK, B., EMPIG, C., MERCER, J., SCHROIT, A. J., SCHETT, G. & HERRMANN, M. 2016. Phosphatidylserine is a global immunosuppressive signal in efferocytosis, infectious disease, and cancer. *Cell Death And Differentiation*, 23, 962.

BITTO, N. J. & KAPARAKIS-LIASKOS, M. 2017. The Therapeutic Benefit of Bacterial

Membrane Vesicles. *Int J Mol Sci*, 18.

BLANC, E., GOLDSCHNEIDER, D., FERRANDIS, E., BARROIS, M., LE ROUX, G., LEONCE, S., DOUC-RASY, S., BENARD, J. & RAGUENEZ, G. 2003. MYCN enhances Pgp/MDR1 gene expression in the human metastatic neuroblastoma IGR-N-91 model. *Am J Pathol*, 163, 321-31.

BLESSING, E. M., STEENKAMP, M. M., MANZANARES, J. & MARMAR, C. R. 2015. Cannabidiol as a Potential Treatment for Anxiety Disorders. *Neurotherapeutics*, 12, 825-36.

BOHUSZEWICZ, O., LIU, J. & LOW, H. H. 2016. Membrane remodelling in bacteria. *J Struct Biol*, 196, 3-14.

BOKHARI, M., CARNACHAN, R. J., CAMERON, N. R. & PRZYBORSKI, S. A. 2007. Culture of HepG2 liver cells on three dimensional polystyrene scaffolds enhances cell structure and function during toxicological challenge. *Journal of Anatomy*, 211, 567-576.

BONILLA, N., ROJAS, M. I., NETTO FLORES CRUZ, G., HUNG, S. H., ROHWER, F. & BARR, J. J. 2016. Phage on tap-a quick and efficient protocol for the preparation of bacteriophage laboratory stocks. *PeerJ*, 4, e2261.

BONNINGTON, K. E. & KUEHN, M. J. 2014. Protein selection and export via outer membrane vesicles. *Biochimica et Biophysica Acta (BBA) - Molecular Cell Research*, 1843, 1612-1619.

BRACHOVA, P., THIEL, K. W. & LESLIE, K. K. 2013. The Consequence of Oncomorphic TP53 Mutations in Ovarian Cancer. *International Journal of Molecular Sciences*, 14, 19257-19275.

BREEN, L., HEENAN, M., AMBERGER-MURPHY, V. & CLYNES, M. 2007. Investigation of the role of p53 in chemotherapy resistance of lung cancer cell lines. *Anticancer Res*, 27, 1361-4.

BROWN, L., WOLF, J. M., PRADOS-ROSALES, R. & CASADEVALL, A. 2015. Through the wall: extracellular vesicles in Gram-positive bacteria, mycobacteria and fungi. *Nat Rev Microbiol*, 13, 620-30.

BROWMAN, K.E., and FOX, G.B. 2007. Attention Deficit Hyperactivity Disorder, Editor(s): John B. Taylor, David J. Trigg, Comprehensive Medicinal Chemistry II, Elsevier, Pages 117-138,

BRUNETTI, D., DUSI, S., GIORDANO, C., LAMPERTI, C., MORBIN, M., FUGNANESI, V., MARCHET, S., FAGIOLARI, G., SIBON, O., MOGGIO, M., D'AMATI, G., TIRANTI, V. 2013. Pantethine treatment is effective in recovering the disease phenotype induced by ketogenic diet in a pantothenate kinase-associated neurodegeneration mouse model. *Brain : a journal of neurology*, 137(Pt 1), 57-68.

BYRNE, J. D., BETANCOURT, T. & BRANNON-PEPPAS, L. 2008. Active targeting schemes for nanoparticle systems in cancer therapeutics. *Advanced Drug Delivery Reviews*, 60, 1615-1626.

CANDELARIO, K. M. & STEINDLER, D. A. 2014. The role of extracellular vesicles in the progression of neurodegenerative disease and cancer. *Trends Mol Med*, 20, 368-74.

CARPINTERO-FERNÁNDEZ, P., FAFIÁN-LABORA, J. & O'LOGHLEN, A. 2017. Technical Advances to Study Extracellular Vesicles. *Frontiers in Molecular Biosciences*, 4, 79.

CASADO, P., RODRIGUEZ-PRADOS, J. C., COSULICH, S. C., GUICHARD, S.,

VANHAESEBROECK, B., JOEL, S. & CUTILLAS, P. R. 2013. Kinase-substrate enrichment analysis provides insights into the heterogeneity of signaling pathway activation in leukemia cells. *Sci Signal*, 6, rs6.

CASJENS, S. R. & HENDRIX, R. W. 2015. Bacteriophage lambda: early pioneer and still relevant. *Virology*, 0, 310-330.

CEDERVALL, J., DRAGOMIR, A., SAUPE, F., ZHANG, Y., ÄRNLÖV, J., LARSSON, E., DIMBERG, A., LARSSON, A. & OLSSON, A.-K. 2017. Pharmacological targeting of peptidylarginine deiminase 4 prevents cancer-associated kidney injury in mice. *OncImmunology*, 6, e1320009.

CHATTOPADHYAY, E. & ROY, B. 2017. Altered Mitochondrial Signalling and Metabolism in Cancer. *Frontiers in Oncology*, 7, 43.

CHAVEZ, K. J., GARIMELLA, S. V. & LIPKOWITZ, S. 2010. Triple Negative Breast Cancer Cell Lines: One Tool in the Search for Better Treatment of Triple Negative Breast Cancer. *Breast disease*, 32, 35-48.

CHIURCHIÙ, V., VAN DER STELT, M., CENTONZE, D. & MACCARRONE, M. 2018. The endocannabinoid system and its therapeutic exploitation in multiple sclerosis: Clues for other neuroinflammatory diseases. *Progress in Neurobiology*, 160, 82-100.

CHOI, S. J., KIM, M.-H., JEON, J., KIM, O. Y., CHOI, Y., SEO, J., HONG, S.-W., LEE, W. H., JEON, S. G., GHO, Y. S., JEE, Y.-K. & KIM, Y.-K. 2015. Active Immunization with Extracellular Vesicles Derived from *Staphylococcus aureus* Effectively Protects against Staphylococcal Lung Infections, Mainly via Th1 Cell-Mediated Immunity. *PLOS ONE*, 10, e0136021.

CHULPANOVA, D. S., KITAEVA, K. V., JAMES, V., RIZVANOV, A. A. & SOLOVYEVA, V. V. 2018. Therapeutic Prospects of Extracellular Vesicles in Cancer Treatment. *Frontiers in Immunology*, 9, 1534.

Chen, C., Lee, S., Yu, H., Huang, F., Chang, Y. 2015. Effects of nicotine on cell growth, migration, and production of inflammatory cytokines and reactive oxygen species by cementoblasts, *Journal of Dental Sciences*, 10(2), Pages 154-160,

CIOCCA, D. R. & CALDERWOOD, S. K. 2005. Heat shock proteins in cancer: diagnostic, prognostic, predictive, and treatment implications. *Cell Stress & Chaperones*, 10, 86-103.

CIREGIA, F., URBANI, A. & PALMISANO, G. 2017. Extracellular Vesicles in Brain Tumors and Neurodegenerative Diseases. *Frontiers in Molecular Neuroscience*, 10, 276.

CLAUSHUIS, T. A. M., VAN DER DONK, L. E. H., LUITSE, A. L., VAN VEEN, H. A., VAN DER WEL, N. N., VAN VUGHT, L. A., ROELOFS, J. J. T. H., DE BOER, O. J., LANKELMA, J. M., BOON, L., DE VOS, A. F., VAN 'T VEER, C. & VAN DER POLL, T. 2018. Role of Peptidylarginine Deiminase 4 in Neutrophil Extracellular Trap Formation and Host Defense during *Klebsiella pneumoniae*-Induced Pneumonia-Derived Sepsis. *The Journal of Immunology*.

CLOKIE, M. R. J., MILLARD, A. D., LETAROV, A. V. & HEAPHY, S. 2011. Phages in nature. *Bacteriophage*, 1, 31-45.

CONDE, J., DE LA FUENTE, J. & BAPTISTA, P. 2013. Nanomaterials for reversion of multidrug resistance in cancer: a new hope for an old idea? *Frontiers in Pharmacology*, 4.

CROESE, T. & FURLAN, R. 2018. Extracellular vesicles in neurodegenerative diseases. *Mol Aspects Med*, 60, 52-61.

CROWN, J., O'LEARY, M. & OOI, W. S. 2004. Docetaxel and paclitaxel in the treatment of breast cancer: a review of clinical experience. *Oncologist*, 9 Suppl 2, 24-32.

CUGINI, C., STEPHENS, D. N., NGUYEN, D., KANTARCI, A. & DAVEY, M. E. 2013. Arginine deiminase inhibits Porphyromonas gingivalis surface attachment. *Microbiology*, 159, 275-285.

CUNNINGHAM, D. & YOU, Z. 2015. In vitro and *in vivo* model systems used in prostate cancer research. 2015.

DAI, X., CHENG, H., BAI, Z. & LI, J. 2017. Breast Cancer Cell Line Classification and Its Relevance with Breast Tumor Subtyping. *Journal of Cancer*, 8, 3131-3141.

DAMGAARD, D., SENOLT, L. & NIELSEN, C. H. 2016. Increased levels of peptidylarginine deiminase 2 in synovial fluid from anti-CCP-positive rheumatoid arthritis patients: Association with disease activity and inflammatory markers. *Rheumatology*, 55, 918-927.

DANIELSON, K. M. & DAS, S. 2014. Extracellular Vesicles in Heart Disease: Excitement for the Future ? *Exosomes and microvesicles*, 2, 10.5772/58390.

DARRAH, E., ROSEN, A., GILES, J. T. & ANDRADE, F. 2012. Peptidylarginine deiminase 2, 3 and 4 have distinct specificities against cellular substrates: novel insights into autoantigen selection in rheumatoid arthritis. *Ann Rheum Dis*, 71, 92-8.

DAS, A. 2015. Anticancer Effect of AntiMalarial Artemisinin Compounds. *Ann Med Health Sci Res*, 5, 93-102.

DATTA, A., KIM, H., MCGEE, L., JOHNSON, A. E., TALWAR, S., MARUGAN, J.,

SOUTHALL, N., HU, X., LAL, M., MONDAL, D., FERRER, M. & ABDEL-MAGEED, A. B. 2018. High-throughput screening identified selective inhibitors of exosome biogenesis and secretion: A drug repurposing strategy for advanced cancer. *Scientific Reports*, 8, 8161.

DAUROS SINGORENKO, P., CHANG, V., WHITCOMBE, A., SIMONOV, D., HONG, J., PHILLIPS, A., SWIFT, S. & BLENKIRON, C. 2017. Isolation of membrane vesicles from prokaryotes: a technical and biological comparison reveals heterogeneity. *J Extracell Vesicles*, 6, 1324731.

DE VLEESCHOUWER, S. & BERGERS, G. 2017. Glioblastoma: To Target the Tumor Cell or the Microenvironment? *In: DE VLEESCHOUWER, S. (ed.) Glioblastoma*. Brisbane (AU): Codon Publications Copyright: The Authors.

DEVINSKY, O., CILIO, M. R., CROSS, H., FERNANDEZ-RUIZ, J., FRENCH, J., HILL, C., KATZ, R., DI MARZO, V., JUTRAS-ASWAD, D., NOTCUTT, W. G., MARTINEZ ORGADO, J., ROBSON, P. J., ROHRBACK, B. G., THIELE, E., WHALLEY, B. & FRIEDMAN, D. 2014. Cannabidiol: Pharmacology and potential therapeutic role in epilepsy and other neuropsychiatric disorders. *Epilepsia*, 55, 791-802.

DI VIZIO, D., KIM, J., HAGER, M. H., MORELLO, M., YANG, W., LAFARGUE, C. J., TRUE, L., RUBIN, M. A., ADAM, R. M., BEROUKHIM, R., DEMICHELIS, F. & FREEMAN, M. R. 2009. Oncosome formation in prostate cancer: Association with a region of frequent chromosomal deletion in metastatic disease. *Cancer Res*, 69, 5601-9.

DO VAL-DA SILVA, R. A., PEIXOTO-SANTOS, J. E., KANDRATAVICIUS, L., DE ROSS, J. B., ESTEVES, I., DE MARTINIS, B. S., ALVES, M. N. R., SCANDIUZZI, R. C., HALLAK, J. E. C., ZUARDI, A. W., CRIPPA, J. A. & LEITE, J. P. 2017. Protective Effects of Cannabidiol against Seizures and Neuronal Death in a Rat Model of Mesial Temporal Lobe Epilepsy. *Frontiers in Pharmacology*, 8.

DONATO, M. T., TOLOSA, L. & GOMEZ-LECHON, M. J. 2015. Culture and Functional Characterization of Human Hepatoma HepG2 Cells. *Methods Mol Biol*, 1250, 77-93.

DÖRSAM, B., REINERS, K. S. & VON STRANDMANN, E. P. 2018. Cancer-derived extracellular vesicles: friend and foe of tumour immunosurveillance. *Philosophical Transactions of the Royal Society B: Biological Sciences*, 373, 20160481.

DRAGOVIC, R. A., GARDINER, C., BROOKS, A. S., TANNETTA, D. S., FERGUSON, D. J., HOLE, P., CARR, B., REDMAN, C. W., HARRIS, A. L., DOBSON, P. J., HARRISON, P. & SARGENT, I. L. 2011. Sizing and phenotyping of cellular vesicles using Nanoparticle Tracking Analysis. *Nanomedicine*, 7, 780-8.

DREYTON, C. J., KNUCKLEY, B., JONES, J. E., LEWALLEN, D. M. & THOMPSON, P. R. 2014. Mechanistic Studies of Protein Arginine Deiminase 2: Evidence for a Substrate-Assisted Mechanism. *Biochemistry*, 53, 4426-4433.

DUMITRU, C. A., SANDALCIOGLU, I. E. & KARSAK, M. 2018. Cannabinoids in Glioblastoma Therapy: New Applications for Old Drugs. *Front Mol Neurosci*, 11, 159.

EL-ASSAAD, F., WHEWAY, J., HUNT, N. H., GRAU, G. E. R. & COMBES, V. 2014. Production, Fate and Pathogenicity of Plasma Microparticles in Murine Cerebral Malaria. *PLoS Pathogens*, 10, e1003839.

ELLIS, T. N. & KUEHN, M. J. 2010. Virulence and Immunomodulatory Roles of Bacterial Outer Membrane Vesicles. *Microbiology and Molecular Biology Reviews*, 74, 81-94.

ELLSWORTH, R. E., HOOKE, J. A., LOVE, B., KANE, J. L., PATNEY, H. L., ELLSWORTH,

D. L. & SHRIVER, C. D. 2008. Correlation of levels and patterns of genomic instability with histological grading of invasive breast tumors. *Breast Cancer Res Treat*, 107, 259-65.

ELLURI, S., ENOW, C., VDOVIKOVA, S., ROMPIKUNTAL, P. K., DONGRE, M., CARLSSON, S., PAL, A., UHLIN, B. E. & WAI, S. N. 2014. Outer membrane vesicles mediate transport of biologically active *Vibrio cholerae* cytolysin (VCC) from *V. cholerae* strains. *PLoS One*, 9, e106731.

ELMORE, S. 2007. Apoptosis: a review of programmed cell death. *Toxicol Pathol*, 35, 495-516.

EVANS-OSES, I., MOJOLI, A., MONGUIO-TORTAJADA, M., MARCILLA, A., ARAN, V., AMORIM, M., INAL, J., BORRAS, F. E. & RAMIREZ, M. I. 2017. Microvesicles released from *Giardia intestinalis* disturb host-pathogen response in vitro. *Eur J Cell Biol*, 96, 131-142.

FALAGAS, M. E., KASIAKOU, S. K. & SARAVOLATZ, L. D. 2005. Colistin: The Revival of Polymyxins for the Management of Multidrug-Resistant Gram-Negative Bacterial Infections. *Clinical Infectious Diseases*, 40, 1333-1341.

FERNANDEZ-RUIZ, J., MORENO-MARTET, M., RODRIGUEZ-CUETO, C., PALOMO GARO, C., GOMEZ-CANAS, M., VALDEOLIVAS, S., GUAZA, C., ROMERO, J., GUZMAN, M., MECHOULAM, R. & RAMOS, J. A. 2011. Prospects for cannabinoid therapies in basal ganglia disorders. *Br J Pharmacol*, 163, 1365-78.

FERT-BOBER, J., GILES, J. T., HOLEWINSKI, R. J., KIRK, J. A., UHRIGSHARDT, H., CROWGEY, E. L., ANDRADE, F., BINGHAM, I. I. I. C. O., PARK, J. K., HALUSHKA, M. K., KASS, D. A., BATHON, J. M. & VAN EYK, J. E. 2015. Citrullination of myofilament proteins in heart failure. *Cardiovascular Research*, 108, 232-242.

FRANCK, G., MAWSON, T. L., FOLCO, E. J., MOLINARO, R., RUVKUN, V.,

ENGELBERTSEN, D., LIU, X., TESMENITSKY, Y., SHVARTZ, E., SUKHOVA, G. K., MICHEL, J. B., NICOLETTI, A., LICHTMAN, A., WAGNER, D., CROCE, K. J. & LIBBY, P. 2018. Roles of PAD4 and NETosis in Experimental Atherosclerosis and Arterial Injury: Implications for Superficial Erosion. *Circ Res*, 123, 33-42.

FRIEDMAN, R. 2016. Drug resistance in cancer: molecular evolution and compensatory proliferation. *Oncotarget*, 7, 11746-11755.

FULSUNDAR, S., HARMS, K., FLATEN, G. E., JOHNSEN, P. J., CHOPADE, B. A. & NIELSEN, K. M. 2014a. Gene Transfer Potential of Outer Membrane Vesicles of *Acinetobacter baylyi* and Effects of Stress on Vesiculation. *Applied and Environmental Microbiology*, 80, 3469-3483.

FULSUNDAR, S., HARMS, K., FLATEN, G. E., JOHNSEN, P. J., CHOPADE, B. A. & NIELSEN, K. M. 2014b. Gene transfer potential of outer membrane vesicles of *Acinetobacter baylyi* and effects of stress on vesiculation. *Appl Environ Microbiol*, 80, 3469-83.

FUNAYAMA, R., TANIGUCHI, H., MIZUMA, M., FUJISHIMA, F., KOBAYASHI, M., OHNUMA, S., UNNO, M. & NAKAYAMA, K. 2017. Protein-arginine deiminase 2 suppresses proliferation of colon cancer cells through protein citrullination. *Cancer Science*, 108, 713-718.

GABARRINI, G., DE SMIT, M., WESTRA, J., BROUWER, E., VISSINK, A., ZHOU, K., A. ROSSEN, J. W., STOBERNACK, T., VAN DIJL, J. M. & JAN VAN WINKELHOFF, A. 2015. The peptidylarginine deiminase gene is a conserved feature of *Porphyromonas gingivalis*. *Scientific Reports*, 5, 13936.

GAILLARD, M. E., BOTTERO, D., ERREA, A., ORMAZÁBAL, M., ZURITA, M. E.,

MORENO, G., RUMBO, M., CASTUMA, C., BARTEL, E., FLORES, D., VAN DER LEY, P., VAN DER ARK, A. & F. HOZBOR, D. 2014. Acellular pertussis vaccine based on outer membrane vesicles capable of conferring both long-lasting immunity and protection against different strain genotypes. *Vaccine*, 32, 931-937.

GANGODA, L., BOUKOURIS, S., LIEM, M., KALRA, H. & MATHIVANAN, S. 2015. Extracellular vesicles including exosomes are mediators of signal transduction: Are they protective or pathogenic? *Proteomics*, 15, 260-271.

GAO, H., SENGUPTA, J., VALLE, M., KOROSTELEV, A., ESWAR, N., STAGG, S. M., VAN ROEY, P., AGRAWAL, R. K., HARVEY, S. C., SALI, A., CHAPMAN, M. S. & FRANK, J. 2003. Study of the structural dynamics of the E coli 70S ribosome using real-space refinement. *Cell*, 113, 789-801.

GARDINER, C. 2011. Update on Nanoparticle Tracking Analysis; Determination and Characterization of (Circulating) Microparticles; Part C : Novel Methodologies *ISTH Council's XXIII Congress*.

GERRITZEN, M. J. H., MARTENS, D. E., WIJFFELS, R. H., VAN DER POL, L. & STORK, M. 2017. Bioengineering bacterial outer membrane vesicles as vaccine platform. *Biotechnology Advances*, 35, 565-574.

GOLDSTEIN, E. J. C., CITRON, D. M., TYRRELL, K. L. & LEONCIO, E. 2018. In vitro stability of three oral vancomycin preparations stored at 2- 5 °C and ambient room temperature for up to 60 days against 100 Clostridioides (Clostridium) difficile and 25 Staphylococcus aureus strains. *Anaerobe*.

GONG, J., JAISWAL, R., MATHYS, J. M., COMBES, V., GRAU, G. E. & BEBAWY, M.

2012. Microparticles and their emerging role in cancer multidrug resistance. *Cancer Treat Rev*, 38, 226-34.

GÓRSKI, A., JOŃCZYK-MATYSIAK, E., ŁUSIAK-SZELACHOWSKA, M., MIĘDZYBRODZKI, R., WEBER-DĄBROWSKA, B. & BORYSOWSKI, J. 2017. The Potential of Phage Therapy in Sepsis. *Frontiers in Immunology*, 8, 1783.

GOTTESMAN, M. M. 2002. Mechanisms of cancer drug resistance. *Annu Rev Med*, 53, 615-27.

GRANT, R., ANSA-ADDO, E., STRATTON, D., ANTWI-BAFFOUR, S., JORFI, S., KHOLIA, S., KRIGE, L., LANGE, S. & INAL, J. 2011. A filtration-based protocol to isolate human plasma membrane-derived vesicles and exosomes from blood plasma. *J Immunol Methods*, 371, 143-51.

GRANUCCI, F., ZANONI, I., PAVELKA, N., VAN DOMMELEN, S. L. H., ANDONIOU, C. E., BELARDELLI, F., DEGLI ESPOSTI, M. A. & RICCIARDI-CASTAGNOLI, P. 2004. A Contribution of Mouse Dendritic Cell-Derived IL-2 for NK Cell Activation. *The Journal of Experimental Medicine*, 200, 287-295.

GRIFFIOEN, A. W. 2008. Anti-angiogenesis: making the tumor vulnerable to the immune system. *Cancer Immunology, Immunotherapy*, 57, 1553-1558.

GUJRATI, V., KIM, S., KIM, S. H., MIN, J. J., CHOY, H. E., KIM, S. C. & JON, S. 2014. Bioengineered bacterial outer membrane vesicles as cell-specific drug-delivery vehicles for cancer therapy. *ACS Nano*, 8, 1525-37.

GULLY, N., BRIGHT, R., MARINO, V., MARCHANT, C., CANTLEY, M., HAYNES, D., BUTLER, C., DASHPER, S., REYNOLDS, E. & BARTOLD, M. 2014a. *PLoS One*, 9.

GULLY, N., BRIGHT, R., MARINO, V., MARCHANT, C., CANTLEY, M., HAYNES, D.,

BUTLER, C., DASHPER, S., REYNOLDS, E. & BARTOLD, M. 2014b. Porphyromonas gingivalis Peptidylarginine Deiminase, a Key Contributor in the Pathogenesis of Experimental Periodontal Disease and Experimental Arthritis. *PLOS ONE*, 9, e100838.

GUO, Q., BEDFORD, M. T. & FAST, W. 2011. Discovery of Peptidylarginine Deiminase-4 Substrates by Protein Array: Antagonistic Citrullination and Methylation of Human Ribosomal Protein S2(). *Molecular bioSystems*, 7, 2286-2295.

GUO, S.-C., TAO, S.-C. & DAWN, H. 2018. Microfluidics-based on-a-chip systems for isolating and analysing extracellular vesicles. *Journal of Extracellular Vesicles*, 7, 1508271.

GURUNG, M., MOON, D. C., CHOI, C. W., LEE, J. H., BAE, Y. C., KIM, J., LEE, Y. C., SEOL, S. Y., CHO, D. T., KIM, S. I. & LEE, J. C. 2011. Staphylococcus aureus Produces Membrane-Derived Vesicles That Induce Host Cell Death. *PLoS ONE*, 6, e27958.

HANKINS, H. M., BALDRIDGE, R. D., XU, P. & GRAHAM, T. R. 2015. Role of flippases, scramblases and transfer proteins in phosphatidylserine subcellular distribution. *Traffic*, 16, 35-47.

HAPPOLD, C., ROTH, P., WICK, W., SCHMIDT, N., FLOREA, A. M., SILGINER, M., REIFENBERGER, G. & WELLER, M. 2012. Distinct molecular mechanisms of acquired resistance to temozolomide in glioblastoma cells. *J Neurochem*, 122, 444-55.

HARRIS, D. A., PATEL, S. H., GUCEK, M., HENDRIX, A., WESTBROEK, W. & TARASKA, J. W. 2015. Exosomes Released from Breast Cancer Carcinomas Stimulate Cell Movement. *PLoS ONE*, 10, e0117495.

HARRISON P., G. C., AND SARGENT I. 2014. *Extracellular vesicles in Health & Disease* 393-394, Taylor and Francis.

HASEGAWA, Y., FUTAMATA, H. & TASHIRO, Y. 2015. Complexities of cell-to-cell communication through membrane vesicles: implications for selective interaction of membrane vesicles with microbial cells. *Frontiers in Microbiology*, 6.

HAY, J. C. 2007. Calcium: a fundamental regulator of intracellular membrane fusion? *EMBO Reports*, 8, 236-240.

Hernández-Cervantes R, Méndez-Díaz M, Prospéro-García Ó, Morales-Montor J: Immunoregulatory Role of Cannabinoids during Infectious Disease. *Neuroimmunomodulation* 2017;24:183-199. doi: 10.1159/000481824

HIENTZ, K., MOHR, A., BHAKTA-GUHA, D. & EFFERTH, T. 2017. The role of p53 in cancer drug resistance and targeted chemotherapy. *Oncotarget*, 8, 8921-8946.

HILL, M. M., ADRAIN, C., DURIEZ, P. J., CREAGH, E. M. & MARTIN, S. J. 2004. Analysis of the composition, assembly kinetics and activity of native Apaf-1 apoptosomes. *Embo j*, 23, 2134-45.

HOLLIDAY, D. L. & SPEIRS, V. 2011. Choosing the right cell line for breast cancer research. *Breast Cancer Research*, 13, 215.

HOMOLYA, L., ORBÁN, T. I., CSANÁDY, L. & SARKADI, B. 2011. Mitoxantrone is expelled by the ABCG2 multidrug transporter directly from the plasma membrane. *Biochimica et Biophysica Acta (BBA) - Biomembranes*, 1808, 154-163.

HONG, X., CHEDID, K. & KALKANIS, S. N. 2012. Glioblastoma cell line-derived spheres in serum-containing medium versus serum-free medium: a comparison of cancer stem cell

properties. *Int J Oncol*, 41, 1693-700.

HORIBATA, S., ROGERS, K. E., SADEGH, D., ANGUISH, L. J., MCELWEE, J. L., SHAH, P., THOMPSON, P. R. & COONROD, S. A. 2017. Role of peptidylarginine deiminase 2 (PAD2) in mammary carcinoma cell migration. *BMC Cancer*, 17, 378.

HOUSMAN, G., BYLER, S., HEERBOTH, S., LAPINSKA, K., LONGACRE, M., SNYDER, N. & SARKAR, S. 2014. Drug Resistance in Cancer: An Overview. *Cancers*, 6, 1769-1792.

HUANG, W., WANG, S., YAO, Y., XIA, Y., YANG, X., LI, K., SUN, P., LIU, C., SUN, W., BAI, H., CHU, X., LI, Y. & MA, Y. 2016. Employing Escherichia coli-derived outer membrane vesicles as an antigen delivery platform elicits protective immunity against *Acinetobacter baumannii* infection. *Scientific Reports*, 6, 37242.

IBEAS BIH, C., CHEN, T., NUNN, A. V., BAZELOT, M., DALLAS, M. & WHALLEY, B. J. 2015. Molecular Targets of Cannabidiol in Neurological Disorders. *Neurotherapeutics*, 12, 699-730.

IFFLAND, K. & GROTENHERMEN, F. 2017. An Update on Safety and Side Effects of Cannabidiol: A Review of Clinical Data and Relevant Animal Studies. *Cannabis and Cannabinoid Research*, 2, 139-154.

INAL, J. M., ANSA-ADDO, E. A., STRATTON, D., KHOLIA, S., ANTWI-BAFFOUR, S. S., JORFI, S. & LANGE, S. 2012. Microvesicles in health and disease. *Arch Immunol Ther Exp (Warsz)*, 60, 107-21.

INAL, J. M., KOSGODAGE, U., AZAM, S., STRATTON, D., ANTWI-BAFFOUR, S. & LANGE, S. 2013. Blood/plasma secretome and microvesicles. *Biochim Biophys Acta*, 1834,

2317-25.

INDRAN, I. R., TUFO, G., PERVAIZ, S. & BRENNER, C. 2011. Recent advances in apoptosis, mitochondria and drug resistance in cancer cells. *Biochim Biophys Acta*, 1807, 735-45.

IVANOV, A. I. 2014. Pharmacological inhibitors of exocytosis and endocytosis: novel bullets for old targets. *Methods Mol Biol*, 1174, 3-18.

JACOB, J. T., LACOUR, O. J. & BURGOYNE, C. F. 2001. Slow release of the antimetabolite 5-fluorouracil (5-FU) from modified Baerveldt glaucoma drains to prolong drain function. *Biomaterials*, 22, 3329-35.

JAIN, S. & PILLAI, J. 2017. Bacterial membrane vesicles as novel nanosystems for drug delivery. *International Journal of Nanomedicine*, 12, 6329-6341.

JAN, A. T. 2017a. Outer Membrane Vesicles (OMVs) of Gram-negative Bacteria: A Perspective Update. *Frontiers in Microbiology*, 8, 1053.

JAN, A. T. 2017b. Outer Membrane Vesicles (OMVs) of Gram-negative Bacteria: A Perspective Update. *Front Microbiol*, 8.

JANG, B., ISHIGAMI, A., KIM, Y. S., & CHOI, E. K. (2017). The Peptidylarginine Deiminase Inhibitor Cl-Amidine Suppresses Inducible Nitric Oxide Synthase Expression in Dendritic Cells. *International journal of molecular sciences*, 18(11), 2258. doi:10.3390/ijms18112258

JENNING, M., MARKLEIN, B., YETTERBERG, J., BURMESTER, G. & SKRINER, K. 2017. AB0101 New mutated peptidylarginine deiminase from porphyromonas gingivalis a target in early ra citrullinates major ra-autoantigens. *Annals of the Rheumatic Diseases*, 76, 1081-1081.

JIANG, B., YIN, S., YOU, B., HUANG, G., YANG, Z., ZHANG, Y., CHEN, Y., CHEN, J.,

YUAN, Z., RAO, X., HU, X., GONG, Y. & PENG, Y. 2017. A 5-year Survey Reveals Increased Susceptibility to Glycopeptides for Methicillin-Resistant *Staphylococcus aureus* Isolates from *Staphylococcus aureus* Bacteremia Patients in a Chinese Burn Center. *Front Microbiol*, 8, 2531.

JORFI, S., ANSA-ADDO, E. A., KHOLIA, S., STRATTON, D., VALLEY, S., LANGE, S. & INAL, J. 2015. Inhibition of microvesiculation sensitizes prostate cancer cells to chemotherapy and reduces docetaxel dose required to limit tumor growth *in vivo*. *Scientific Reports*, 5, 13006.

KALRA, H., DRUMMEN, G. P. C. & MATHIVANAN, S. 2016. Focus on Extracellular Vesicles: Introducing the Next Small Big Thing. *International Journal of Molecular Sciences*, 17, 170.

KARASU, E., EISENHARDT, S. U., HARANT, J. & HUBER-LANG, M. 2018. Extracellular Vesicles: Packages Sent With Complement. *Frontiers in Immunology*, 9.

KARPMAN, D., STÅHL, A.-L. & ARVIDSSON, I. 2017. Extracellular vesicles in renal disease. *Nature Reviews Nephrology*, 13, 545.

KATSIR, L. & BAHAR, O. 2017. Bacterial outer membrane vesicles at the plant–pathogen interface. *PLoS Pathogens*, 13, e1006306.

KENNY, E. F., HERZIG, A., KRÜGER, R., MUTH, A., MONDAL, S., THOMPSON, P. R., BRINKMANN, V., VON BERNUTH, H. & ZYCHLINSKY, A. 2017. Diverse stimuli engage different neutrophil extracellular trap pathways. *eLife*, 6, e24437.

KERYER-BIBENS, C., PIOCHE-DURIEU, C., VILLEMANT, C., SOUQUÈRE, S., NISHI, N., HIRASHIMA, M., MIDDELDORP, J. & BUSSON, P. 2006. Exosomes released by EBV

infected nasopharyngeal carcinoma cells convey the viral Latent Membrane Protein 1 and the immunomodulatory protein galectin 9. *BMC Cancer*, 6, 283.

KHARINA, A., PODOLICH, O., FAIDIUK, I., ZAIKA, S., HAIDAK, A., KUKHARENKO, O., ZAETS, I., TOVKACH, F., REVA, O., KREMENSKOY, M. & KOZYROVSKA, N. 2015. Temperate bacteriophages collected by outer membrane vesicles in *Komagataeibacter intermedius*. *J Basic Microbiol*, 55, 509-13.

KHOLIA, S., JORFI, S., THOMPSON, P. R., CAUSEY, C. P., NICHOLAS, A. P., INAL, J. M. & LANGE, S. 2015. A novel role for peptidylarginine deiminases in microvesicle release reveals therapeutic potential of PAD inhibition in sensitizing prostate cancer cells to chemotherapy. *Journal of Extracellular Vesicles*, 4, 10.3402/jev.v4.26192.

KIM, R., EMI, M. & TANABE, K. 2007. Cancer immunoediting from immune surveillance to immune escape. *Immunology*, 121, 1-14.

KIM, S.-M. & KIM, H.-S. 2017. Engineering of extracellular vesicles as drug delivery vehicles. *Stem Cell Investigation*, 4.

KLEIN, K., GIGLER, ALEXANDER M., ASCHENBRENNER, T., MONETTI, R., BUNK, W., JAMITZKY, F., MORFILL, G., STARK, ROBERT W. & SCHLEGEL, J. 2012. Label-Free Live-Cell Imaging with Confocal Raman Microscopy. *Biophysical Journal*, 102, 360-368.

KLIMENTOVA, J. & STULIK, J. 2015. Methods of isolation and purification of outer membrane vesicles from gram-negative bacteria. *Microbiol Res*, 170, 1-9.

KLIMENTOVÁ, J. & STULÍK, J. 2015. Methods of isolation and purification of outer membrane vesicles from gram-negative bacteria. *Microbiological Research*, 170, 1-9.

KNIGHT, J.S., LUO W., O'DELL, A.A., YALAVARTHI, S., ZHAO, W., SUBRAMANIAN, V., GUO, C., GRENN, R.C., THOMPSON, P.R., EITZMAN, D.T. and KAPLAN, M.J. Peptidylarginine deiminase inhibition reduces vascular damage and modulates innate immuneresponses in murine models of atherosclerosis. *Circ Res.* 2014;114(6):947-56

KOCH, R., AUNG, T., VOGEL, D., CHAPUY, B., WENZEL, D., BECKER, S., SINZIG, U., VENKATARAMANI, V., VON MACH, T., JACOB, R., TRUEMPER, L. & WULF, G. G. 2016. Nuclear Trapping through Inhibition of Exosomal Export by Indomethacin Increases Cytostatic Efficacy of Doxorubicin and Pixantrone. *Clin Cancer Res*, 22, 395-404.

KONG, D., LI, Y., WANG, Z. & SARKAR, F. H. 2011. Cancer Stem Cells and Epithelial-to-Mesenchymal Transition (EMT)-Phenotypic Cells: Are They Cousins or Twins? *Cancers*, 3, 716-729.

KOSGODAGE, U. S., MOULD, R., HENLEY, A. B., NUNN, A. V., GUY, G. W., THOMAS, E. L., INAL, J. M., BELL, J. D. & LANGE, S. 2018. Cannabidiol (CBD) Is a Novel Inhibitor for Exosome and Microvesicle (EV) Release in Cancer. *Frontiers in Pharmacology*, 9.

KOSGODAGE, U.S., ONGANER, P.U., MACLATHCY, A., MOULD, R., NUNN, A.V., GUY G.W., KRAEV, N., CHATTERTON, N., THOMAS, E. L., INAL, J.M. BELL, J.D., and LANGE, S. (2019) Cannabidiol Affects Extracellular Vesicle Release, miR21 and miR126, and Reduces Prohibitin Protein in Glioblastoma Multiforme Cells. *Translational Oncology*, 12(3), 513-522

KOSGODAGE, U.S., ONGANER, P.U., MACLATHCY, A., KRAEV, N., CHATTERTON, N., NICHOLAS, A.P., INAL, J.M. and LANGE, S. (2018). Peptidylarginine Deiminases Post-Translationally Deiminate Prohibitin and Modulate Extracellular Vesicle Release and MicroRNAs in Glioblastoma Multiforme. *Int J Mol Sci.*, 28;20(1)

KOSGODAGE, U. S., TRINDADE, R. P., THOMPSON, P. R., INAL, J. M. & LANGE, S. 2017. Chloramidine/Bisindolylmaleimide-I-Mediated Inhibition of Exosome and Microvesicle

Release and Enhanced Efficacy of Cancer Chemotherapy. *Int J Mol Sci*, 18.

KOVAR, M., BOYMAN, O., SHEN, X., HWANG, I., KOHLER, R. & SPRENT, J. 2006.

Direct stimulation of T cells by membrane vesicles from antigen-presenting cells. *Proc Natl Acad Sci U S A*, 103, 11671-6.

KRUGER, P., SAFFARZADEH, M., WEBER, A. N., RIEBER, N., RADSAK, M., VON BERNUTH, H., BENARAFI, C., ROOS, D., SKOKOWA, J. & HARTL, D. 2015. Neutrophils: Between host defence, immune modulation, and tissue injury. *PLoS Pathog*, 11, e1004651.

KSHETRY, A. O., PANT, N. D., BHANDARI, R., KHATRI, S., SHRESTHA, K. L., UPADHAYA, S. K., POUDEL, A., LEKHAK, B. & RAGHUBANSHI, B. R. 2016. Minimum inhibitory concentration of vancomycin to methicillin resistant *Staphylococcus aureus* isolated from different clinical samples at a tertiary care hospital in Nepal. *Antimicrobial Resistance and Infection Control*, 5, 27.

KUEHN, M. J. & KESTY, N. C. 2005. Bacterial outer membrane vesicles and the host pathogen interaction. *Genes Dev*, 19, 2645-55.

KULKARNI, H. M., NAGARAJ, R. & JAGANNADHAM, M. V. 2015. Protective role of *E. coli* outer membrane vesicles against antibiotics. *Microbiological Research*, 181, 1-7.

KULP, A. & KUEHN, M. J. 2010. Biological functions and biogenesis of secreted bacterial outer membrane vesicles. *Annu Rev Microbiol*, 64, 163-84.

KUSACZUK, M., KRĘTOWSKI, R., STYPUŁKOWSKA, A. & CECHOWSKA-PASKO, M. 2016. Molecular and cellular effects of a novel hydroxamate-based HDAC inhibitor – belinostat – in glioblastoma cell lines: a preliminary report. *Investigational New Drugs*, 34, 552-564.

LANGE, S. 2016. Peptidylarginine Deiminases as Drug Targets in Neonatal Hypoxic–Ischemic Encephalopathy. *Frontiers in Neurology*, 7.

LANGE, S., GALLAGHER, M., KHOLIA, S., KOSGODAGE, U. S., HRISTOVA, M., HARDY, J. & INAL, J. M. 2017a. Peptidylarginine Deiminases-Roles in Cancer and Neurodegeneration and Possible Avenues for Therapeutic Intervention via Modulation of Exosome and Microvesicle (EV) Release? *Int J Mol Sci*, 18.

LANGE, S., GALLAGHER, M., KHOLIA, S., KOSGODAGE, U. S., HRISTOVA, M., HARDY, J. & INAL, J. M. 2017b. Peptidylarginine Deiminases—Roles in Cancer and Neurodegeneration and Possible Avenues for Therapeutic Intervention via Modulation of Exosome and Microvesicle (EV) Release? *International Journal of Molecular Sciences*, 18, 1196.

LANGE, S., GOGEL, S., LEUNG, K. Y., VERNAY, B., NICHOLAS, A. P., CAUSEY, C. P., THOMPSON, P. R., GREENE, N. D. & FERRETTI, P. 2011. Protein deiminases: new players in the developmentally regulated loss of neural regenerative ability. *Dev Biol*, 355, 205-14.

LANGE, S., ROCHA-FERREIRA, E., THEI, L., MAWJEE, P., BENNETT, K., THOMPSON, P. R., SUBRAMANIAN, V., NICHOLAS, A. P., PEEBLES, D., HRISTOVA, M. & RAIVICH, G. 2014. Peptidylarginine deiminases: novel drug targets for prevention of neuronal damage following hypoxic ischemic insult (HI) in neonates. *J Neurochem*, 130, 555-62.

LEE, S. Y. 2016. Temozolomide resistance in glioblastoma multiforme. *Genes & Diseases*, 3, 198-210.

LEONEL, C., FERREIRA, L., BORIN, T., GOBBE MOSCETTA, M., FREITAS, G., RAINERI HADDAD, M., ANTONIO DE CAMARGOS PINTO ROBLES, J., ZUCCARI, D.A.P.C. 2017.

Inhibition of Epithelial-mesenchymal Transition in Response to Treatment with Metformin and Y27632 in Breast Cancer Cell Lines. *Anti-cancer agents in medicinal chemistry*. 17.

10.2174/1871520617666170102153954.

LEPE, J. A., DOMINGUEZ-HERRERA, J., PACHON, J. & AZNAR, J. 2014. Determining accurate vancomycin MIC values for methicillin-resistant *Staphylococcus aureus* by the microdilution method. *J Antimicrob Chemother*, 69, 136-8.

LEWIS, H.D., LIDLLE, J., COOTE, J.E., ATKINSON, S.J., BARKER, M.D., BAX, B.D., BICKER, K.L., BINGHAM, R.P., CAMPBELL, M., CHEN, Y.H., CHUNG, C.W., CRAGGS, P.D., DAVIS, R.P., EBERHARD, D., JOBERTY, G., LIND, K.E., LOCKE, K., MALLER, C., MARTINOD, K., PATTEN, C., POLYAKOVA, O., RISE, C.E., RUDIGER, M., SHEPHEPPARD, R.J., SLADE, D.J., THOMAS, P., THORPE, J., YAO, G., DREWES, G., WAGNER, D.D., THOMPSON, P.R., PRINJHA, R.K., WILSON, D.M. Inhibition of PAD4 activity is sufficient to disrupt mouse and human NET formation. *Nat Chem Biol*. 2015;11(3):189-91.

LI, B., ANTONYAK, M. A., ZHANG, J. & CERIONE, R. A. 2012. RhoA triggers a specific signaling pathway that generates transforming microvesicles in cancer cells. *Oncogene*, 31, 4740-9.

LI, C. J., LIU, Y., CHEN, Y., YU, D., WILLIAMS, K. J. & LIU, M. L. 2013. Novel proteolytic microvesicles released from human macrophages after exposure to tobacco smoke. *Am J Pathol*, 182, 1552-62.

LI, P., WANG, D., YAO, H., DORET, P., HAO, G., SHEN, Q., QIU, H., ZHANG, X., WANG, Y., CHEN, G. & WANG, Y. 2010. Coordination of PAD4 and HDAC2 in the regulation of p53 target gene expression. *Oncogene*, 29, 3153-62.

LIN, D. M., KOSKELLA, B. & LIN, H. C. 2017. Phage therapy: An alternative to antibiotics in the age of multi-drug resistance. *World Journal of Gastrointestinal Pharmacology and*

Therapeutics, 8, 162-173.

LIU, J.-P., WANG, T.-T., WANG, D.-G., DONG, A.-J., LI, Y.-P. & YU, H.-J. 2016. Smart nanoparticles improve therapy for drug-resistant tumors by overcoming pathophysiological barriers. *Acta Pharmacologica Sinica*, 38, 1.

LIU, L., HAMMAR, K., SMITH, P. J., INOUE, S. & KEEFE, D. L. 2001. Mitochondrial modulation of calcium signaling at the initiation of development. *Cell Calcium*, 30, 423-33.

LIU, Z., DEIBLER, R. W., CHAN, H. S. & ZECHIEDRICH, L. 2009. The why and how of DNA unlinking. *Nucleic Acids Research*, 37, 661-671.

LIU, Y., DEFOURNY, K., SMID E., TJAKKO, A. Gram-Positive Bacterial Extracellular Vesicles and Their Impact on Health and Disease. *Frontiers in Microbiology* 9, 1502 (2018)

LIVERMORE, D. M., WARNER, M., MUSHTAQ, S., DOUMITH, M., ZHANG, J. & WOODFORD, N. 2011. What remains against carbapenem-resistant Enterobacteriaceae? Evaluation of chloramphenicol, ciprofloxacin, colistin, fosfomicin, minocycline, nitrofurantoin, temocillin and tigecycline. *International Journal of Antimicrobial Agents*, 37, 415-419.

LOCATELLI, M., MELUCCI, D., CARLUCCI, G. & LOCATELLI, C. 2012. RECENT HPLC STRATEGIES TO IMPROVE SENSITIVITY AND SELECTIVITY FOR THE ANALYSIS OF COMPLEX MATRICES. *Instrumentation Science & Technology*, 40, 112-137.

LUO, Y., KNUCKLEY, B., LEE, Y.H., STALLCUP, M.R., THOMPSON, P.R. J. A fluoroacetamide-based inactivator of protein arginine deiminase 4: design, synthesis, and in vitro and in vivo evaluation. *Am Chem Soc.* 2006;128(4):1092-3.

LYNAM-LENNON, N., MAHER, S. G., MAGUIRE, A., PHELAN, J., MULDOON, C., REYNOLDS, J. V. & O'SULLIVAN, J. 2014. Altered Mitochondrial Function and Energy Metabolism Is Associated with a Radioresistant Phenotype in Oesophageal Adenocarcinoma.

PLOS ONE, 9, e100738.

MAAS, S. L. N., BREAKFIELD, X. O. & WEAVER, A. M. 2017. Extracellular Vesicles: Unique Intercellular Delivery Vehicles. *Trends Cell Biol*, 27, 172-188.

MACDONALD, I. A. & KUEHN, M. J. 2012. Offense and defense: microbial membrane vesicles play both ways. *Research in microbiology*, 163, 607-618.

MACKENZIE, A., WILSON, H. L., KISS-TOTH, E., DOWER, S. K., NORTH, R. A. & SURPRENANT, A. 2001. Rapid secretion of interleukin-1beta by microvesicle shedding. *Immunity*, 15, 825-35.

MACLAYTON, D. O., SUDA, K. J., COVAL, K. A., YORK, C. B. & GAREY, K. W. 2006. Case-control study of the relationship between MRSA bacteremia with a vancomycin MIC of 2 µg/mL and risk factors, costs, and outcomes in inpatients undergoing hemodialysis. *Clinical Therapeutics*, 28, 1208-1216.

MAGNADÓTTIR, B., HAYES, P., HRISTOVA, M., BRAGASON, B. T., NICHOLAS, A. P., DODDS, A. W., GUÐMUNDSÓTTIR, S. & LANGE, S. 2018. Post-translational protein deimination in cod (*Gadus morhua* L.) ontogeny novel roles in tissue remodelling and mucosal immune defences? *Developmental & Comparative Immunology*, 87, 157-170.

MAGNADOTTIR, B., HAYES, P., HRISTOVA, M., BRAGASON, B. T., NICHOLAS, A. P., DODDS, A. W., GUETHMUNSDOTTIR, S. & LANGE, S. 2018. Post-translational protein deimination in cod (*Gadus morhua* L.) ontogeny novel roles in tissue remodelling and mucosal immune defences? *Dev Comp Immunol*, 87, 157-170.

MALHOTRA, V. 2013. Unconventional protein secretion: an evolving mechanism. *Embo j*, 32, 1660-4.

MALVERN. 2015 News Medical. Characterizing Exosomes and Microvesicles with Nanoparticle Tracking Analysis *News Medical*.

MANGAT, P., WEGNER, N., VENABLES, P. J. & POTEMPA, J. 2010. Bacterial and human peptidylarginine deiminases: targets for inhibiting the autoimmune response in rheumatoid arthritis? *Arthritis Res Ther*, 12, 209.

MANNING, A. J. & KUEHN, M. J. 2011. Contribution of bacterial outer membrane vesicles to innate bacterial defense. *BMC Microbiol*, 11, 258.

MANSOORI, B., MOHAMMADI, A., DAVUDIAN, S., SHIRJANG, S. & BARADARAN, B. 2017. The Different Mechanisms of Cancer Drug Resistance: A Brief Review. *Advanced Pharmaceutical Bulletin*, 7, 339-348.

MARESZ, K. J., HELLVARD, A., SROKA, A., ADAMOWICZ, K., BIELECKA, E., KOZIEL, J., GAWRON, K., MIZGALSKA, D., MARCINSKA, K. A., BENEDYK, M., PYRC, K., QUIRKE, A. M., JONSSON, R., ALZABIN, S., VENABLES, P. J., NGUYEN, K. A., MYDEL, P. & POTEMPA, J. 2013. Porphyromonas gingivalis facilitates the development and progression of destructive arthritis through its unique bacterial peptidylarginine deiminase (PAD). *PLoS Pathog*, 9, e1003627.

MAROON, J. & BOST, J. 2018. Review of the neurological benefits of phytocannabinoids. *Surgical Neurology International*, 9, 91.

MARTIN, S. K. & KYPRIANOU, N. 2015. Exploitation of the Androgen Receptor to Overcome Taxane Resistance in Advanced Prostate Cancer. *Adv Cancer Res*, 127, 123-58.

MASSI, P., SOLINAS, M., CINQUINA, V. & PAROLARO, D. 2013. Cannabidiol as potential anticancer drug. *Br J Clin Pharmacol*, 75, 303-12.

- MCALLISTER, S. D., CHAN, C., TAFT, R. J., LUU, T., ABOOD, M. E., MOORE, D. H., ALDAPE, K. & YOUNT, G. 2005. Cannabinoids selectively inhibit proliferation and induce death of cultured human glioblastoma multiforme cells. *J Neurooncol*, 74, 31-40.
- MCALLISTER, S. D., SOROCEANU, L. & DESPREZ, P. Y. 2015. The Antitumor Activity of Plant-Derived Non-Psychoactive Cannabinoids. *J Neuroimmune Pharmacol*, 10, 255-67.
- MCCAIG, W. D., KOLLER, A. & THANASSI, D. G. 2013. Production of outer membrane vesicles and outer membrane tubes by *Francisella novicida*. *J Bacteriol*, 195, 1120-32.
- MCGUIRE, P., ROBSON, P., CUBALA, W. J., VASILE, D., MORRISON, P. D., BARRON, R., TAYLOR, A. & WRIGHT, S. 2018. Cannabidiol (CBD) as an Adjunctive Therapy in Schizophrenia: A Multicenter Randomized Controlled Trial. *Am J Psychiatry*, 175, 225-231.
- MECKES, D. G., JR. & RAAB-TRAUB, N. 2011. Microvesicles and viral infection. *J Virol*, 85, 12844-54.
- MENCK, K., SÖNMEZER, C., WORST, T. S., SCHULZ, M., DIHAZI, G. H., STREIT, F., ERDMANN, G., KLING, S., BOUTROS, M., BINDER, C. & GROSS, J. C. 2017. Neutral sphingomyelinases control extracellular vesicles budding from the plasma membrane. *Journal of Extracellular Vesicles*, 6, 1378056.
- MERSCH-SUNDERMANN, V., KNASMULLER, S., WU, X. J., DARROUDI, F. & KASSIE, F. 2004. Use of a human-derived liver cell line for the detection of cytoprotective, antigenotoxic and cogenotoxic agents. *Toxicology*, 198, 329-40.
- MILLER, I. V. & GRUNEWALD, T. G. 2015. Tumour-derived exosomes: Tiny envelopes for big stories. *Biol Cell*, 107, 287-305.

MOHANAN, S., CHERRINGTON, B. D., HORIBATA, S., MCELWEE, J. L., THOMPSON, P. R. & COONROD, S. A. 2012. Potential Role of Peptidylarginine Deiminase Enzymes and Protein Citrullination in Cancer Pathogenesis. *Biochemistry Research International*, 2012, 895343.

MOISEENKO, F., VOLKOV, N., BOGDANOV, A., DUBINA, M. & MOISEYENKO, V. 2017. Resistance mechanisms to drug therapy in breast cancer and other solid tumors: An opinion. *F1000Research*, 6, 288.

MONTGOMERY, A. B., KOPEC, J., SHRESTHA, L., THEZENAS, M. L., BURGESS BROWN, N. A., FISCHER, R., YUE, W. W. & VENABLES, P. J. 2016. Crystal structure of *Porphyromonas gingivalis* peptidylarginine deiminase: implications for autoimmunity in rheumatoid arthritis. *Ann Rheum Dis*, 75, 1255-61.

MOORE, C., KOSGODAGE, U., LANGE, S. & INAL, J. M. 2017. The emerging role of exosome and microvesicle- (EV-) based cancer therapeutics and immunotherapy. *Int J Cancer*.

MORALES-KASTRESANA, A., TELFORD, B., MUSICH, T. A., MCKINNON, K., CLAYBORNE, C., BRAIG, Z., ROSNER, A., DEMBERG, T., WATSON, D. C., KARPOVA, T. S., FREEMAN, G. J., DEKRUYFF, R. H., PAVLAKIS, G. N., TERABE, M., ROBERT GUROFF, M., BERZOFISKY, J. A. & JONES, J. C. 2017. Labeling Extracellular Vesicles for Nanoscale Flow Cytometry. *Scientific Reports*, 7, 1878.

MOSCARELLO, M. A., LEI, H., MASTRONARDI, F. G., WINER, S., TSUI, H., LI, Z., ACKERLEY, C., ZHANG, L., RAIJMAKERS, R. & WOOD, D. D. 2013a. Inhibition of peptidyl-arginine deiminases reverses protein-hypercitrullination and disease in mouse models of multiple sclerosis. *Disease Models & Mechanisms*, 6, 467-478.

MOSCARELLO, M. A., LEI, H., MASTRONARDI, F. G., WINER, S., TSUI, H., LI, Z., ACKERLEY, C., ZHANG, L., RAIJMAKERS, R. & WOOD, D. D. 2013b. Inhibition of peptidyl-arginine deiminases reverses protein-hypercitrullination and disease in mouse models of multiple sclerosis. *Disease Models & Mechanisms*, 6, 467-478.

MOSKOWITZ, S. M., GARBER, E., CHEN, Y., CLOCK, S. A., TABIBI, S., MILLER, A. K., DOCTOR, M. & SAIMAN, L. 2010. Colistin susceptibility testing: evaluation of reliability for cystic fibrosis isolates of *Pseudomonas aeruginosa* and *Stenotrophomonas maltophilia*. *Journal of Antimicrobial Chemotherapy*, 65, 1416-1423.

MUTH A. & THOMPSON P.R. DEVELOPMENT OF THE PROTEIN ARGININE DEIMINASE (PAD) INHIBITORS. IN: NICHOLAS A., B. S., THOMPSON P. (EDS) 2017. Development of the Protein Arginine Deiminase (PAD) Inhibitors. In: Nicholas A., Bhattacharya S., Thompson P. (eds)

MUTHUSAMY, B.-P., NATARAJAN, P., ZHOU, X. & GRAHAM, T. R. 2009. Linking Phospholipid flippases to vesicle-mediated protein transport. *Biochimica et biophysica acta*, 1791, 612-619.

MUTH, A., SUBRAMANIAN, V., BEAUMONT, E., NAGAR, M., KERRY, P., MCEWAN, P., SRINATH, H., CLANCY, K., PARELKAR, S., THOMPSON, P.R. Development of a Selective Inhibitor of Protein Arginine Deiminase 2. *J Med Chem*. 2017 Apr 13;60(7):3198-3211. doi: 10.1021/acs.jmedchem.7b00274. Epub 2017 Mar 31.

NANBO, A., KAWANISHI, E., YOSHIDA, R. & YOSHIYAMA, H. 2013. Exosomes derived from Epstein-Barr virus-infected cells are internalized via caveola-dependent endocytosis and promote phenotypic modulation in target cells. *J Virol*, 87, 10334-47.

NG, K., MABASA, V. H., CHOW, I. & ENSOM, M. H. 2014. Systematic review of efficacy,

pharmacokinetics, and administration of intraventricular vancomycin in adults. *Neurocrit Care*, 20, 158-71.

NICHOLAS, A. P. & WHITAKER, J. N. 2002. Preparation of a monoclonal antibody to citrullinated epitopes: its characterization and some applications to immunohistochemistry in human brain. *Glia*, 37, 328-36.

NICKEL, W. 2005. Unconventional secretory routes: direct protein export across the plasma membrane of mammalian cells. *Traffic*, 6, 607-14.

NISHIDA-AOKI, N., TOMINAGA, N., TAKESHITA, F., SONODA, H., YOSHIOKA, Y. & OCHIYA, T. 2017. Disruption of Circulating Extracellular Vesicles as a Novel Therapeutic Strategy against Cancer Metastasis. *Molecular Therapy*, 25, 181-191.

NOLTE-'T HOEN, E., CREMER, T., GALLO, R. C. & MARGOLIS, L. B. 2016. Extracellular vesicles and viruses: Are they close relatives? *Proceedings of the National Academy of Sciences of the United States of America*, 113, 9155-9161.

NOWAK, M. & TRYNISZEWSKI, W., SAMIAK, A., WLODARCZYK, A., NOWAK J., NOWAK, P.,D. (2018). Light Emission from the Fe²⁺-EGTA-H₂O₂ System: Possible Application for the Determination of Antioxidant Activity of Plant Phenolics. *Molecules*. 23. 866. 10.3390/molecules23040866.

O'DONOGHUE, E. J. & KRACHLER, A. M. 2016. Mechanisms of outer membrane vesicle entry into host cells. *Cell Microbiol*, 18, 1508-1517.

OKOYE, F. I., BUSHAR, N. D. & FARBER, D. L. 2009. CHAPTER 8M - Signal Transduction. *In: HOCHBERG, M. C., SILMAN, A. J., SMOLEN, J. S., WEINBLATT, M. E. & WEISMAN,*

M. H. (eds.) *Rheumatoid Arthritis*. Philadelphia: Mosby.

OLSEN, I. & AMANO, A. 2015. Outer membrane vesicles – offensive weapons or good Samaritans? *Journal of Oral Microbiology*, 7, 27468.

OLSSON, M. & ZHIVOTOVSKY, B. 2011. Caspases and cancer. *Cell Death Differ*, 18, 1441-9.

PARK, A. J., SURETTE, M. D. & KHURSIGARA, C. M. 2014. Antimicrobial targets localize to the extracellular vesicle-associated proteome of *Pseudomonas aeruginosa* grown in a biofilm. *Front Microbiol*, 5, 464.

PASCUCCI, L., COCCE, V., BONOMI, A., AMI, D., CECCARELLI, P., CIUSANI, E., VIGANO, L., LOCATELLI, A., SISTO, F., DOGLIA, S. M., PARATI, E., BERNARDO, M. E., MURACA, M., ALESSANDRI, G., BONDIOLOTTI, G. & PESSINA, A. 2014. Paclitaxel is incorporated by mesenchymal stromal cells and released in exosomes that inhibit in vitro tumor growth: a new approach for drug delivery. *J Control Release*, 192, 262-70.

PASQUIER, J., MAGAL, P., BOULANGÉ-LECOMTE, C., WEBB, G. & LE FOLL, F. 2011. Consequences of cell-to-cell P-glycoprotein transfer on acquired multidrug resistance in breast cancer: a cell population dynamics model. *Biology Direct*, 6, 5-5.

PAVIA, S. C., PIERRE, A., NOWAKOWSKI, J. (2000). Antimicrobial activity of nicotine against a spectrum of bacterial and fungal pathogens. *Journal of medical microbiology*. 49. 675-6. 10.1099/0022-1317-49-7-675.

PERAZZOLI, G., PRADOS, J., ORTIZ, R., CABA, O., CABEZA, L., BERDASCO, M., GÓNZALEZ, B. & MELGUIZO, C. 2015. Temozolomide Resistance in Glioblastoma Cell Lines: Implication of MGMT, MMR, P-Glycoprotein and CD133 Expression. *PLOS ONE*, 10, e0140131.

PEREZ-CRUZ, C., CARRION, O., DELGADO, L., MARTINEZ, G., LOPEZ-IGLESIAS, C. & MERCADE, E. 2013. New type of outer membrane vesicle produced by the Gram-negative bacterium *Shewanella vesiculosa* M7T: implications for DNA content. *Appl Environ Microbiol*, 79, 1874-81.

PÉREZ-CRUZ, C., DELGADO, L., LÓPEZ-IGLESIAS, C. & MERCADE, E. 2015. Outer Inner Membrane Vesicles Naturally Secreted by Gram-Negative Pathogenic Bacteria. *PLoS ONE*, 10, e0116896.

PIKTEL, E., NIEMIROWICZ, K., WĄTEK, M., WOLLNY, T., DEPTUŁA, P. & BUCKI, R. 2016. Recent insights in nanotechnology-based drugs and formulations designed for effective anti-cancer therapy. *Journal of Nanobiotechnology*, 14, 39.

PIRBADIAN, S., BARCHINGER, S. E., LEUNG, K. M., BYUN, H. S., JANGIR, Y., BOUHENNI, R. A., REED, S. B., ROMINE, M. F., SAFFARINI, D. A., SHI, L., GORBY, Y. A., GOLBECK, J. H. & EL-NAGGAR, M. Y. 2014. *Shewanella oneidensis* MR-1 nanowires are outer membrane and periplasmic extensions of the extracellular electron transport components. *Proceedings of the National Academy of Sciences*, 111, 12883-12888.

PISANTI, S., MALFITANO, A. M., CIAGLIA, E., LAMBERTI, A., RANIERI, R., CUOMO, G., ABATE, M., FAGGIANA, G., PROTO, M. C., FIORE, D., LAEZZA, C. & BIFULCO, M. 2017. Cannabidiol: State of the art and new challenges for therapeutic applications. *Pharmacol Ther*, 175, 133-150.

PISTRITTO, G., TRISCIUOGLIO, D., CECI, C., GARUFI, A. & D'ORAZI, G. 2016.

Apoptosis as anticancer mechanism: function and dysfunction of its modulators and targeted therapeutic strategies. *Aging (Albany NY)*, 8, 603-619.

PLOTNIKOV, E. Y., SILACHEV, D. N., POPKOV, V. A., ZOROVA, L. D., PEVZNER, I. B., ZOROV, S. D., JANKAUSKAS, S. S., BABENKO, V. A., SUKHIKH, G. T. & ZOROV, D. B. 2017. Intercellular Signalling Cross-Talk: To Kill, To Heal and To Rejuvenate. *Heart Lung Circ*, 26, 648-659.

PLUCHINO, S., COSSETTI, C., SMITH, J., IRACI, N., LEONARDI, T. & ALFARO CERVELLO, C. 2012. Extracellular Membrane Vesicles and Immune Regulation in the Brain. *Frontiers in Physiology*, 3.

POGGE VON STRANDMANN, E., SIMHADRI, V. R., VON TRESCKOW, B., SASSE, S., REINERS, K. S., HANSEN, H. P., ROTHE, A., BOLL, B., SIMHADRI, V. L., BORCHMANN, P., MCKINNON, P. J., HALLEK, M. & ENGERT, A. 2007. Human leukocyte antigen-B associated transcript 3 is released from tumor cells and engages the NKp30 receptor on natural killer cells. *Immunity*, 27, 965-74.

POKHAREL, D., PADULA, M. P., LU, J. F., TACCHI, J. L., LUK, F., DJORDJEVIC, S. P. & BEBAWY, M. 2014. Proteome analysis of multidrug-resistant, breast cancer-derived microparticles. *J Extracell Vesicles*, 3.

POVEA-CABELLO, S., OROPESA-AVILA, M., DE LA CRUZ-OJEDA, P., VILLANUEVA PAZ, M., DE LA MATA, M., SUAREZ-RIVERO, J. M., ALVAREZ-CORDOBA, M., VILLALON-GARCIA, I., COTAN, D., YBOT-GONZALEZ, P. & SANCHEZ-ALCAZAR, J. A. 2017. Dynamic Reorganization of the Cytoskeleton during Apoptosis: The Two Coffins Hypothesis. *Int J Mol Sci*, 18.

PubChem- <https://pubchem.ncbi.nlm.nih.gov/compound/colistin> (ccessed Mar. 9,2019)

PubChem-National Center for Biotechnology Information. PubChem Compound Database;

CID=2396, <https://pubchem.ncbi.nlm.nih.gov/compound/2396> (accessed Mar. 12, 2019).

PubChem-National Center for Biotechnology Information. PubChem Compound Database;

CID=4677, <https://pubchem.ncbi.nlm.nih.gov/compound/4677> (accessed Mar. 12, 2019).

PubChem-National Center for Biotechnology Information. PubChem Compound Database;

CID=89594, <https://pubchem.ncbi.nlm.nih.gov/compound/89594> (accessed Mar. 12, 2019).

QI, S.-S., SUN, J.-H., YU, H.-H. & YU, S.-Q. 2017. Co-delivery nanoparticles of anti-cancer drugs for improving chemotherapy efficacy. *Drug Delivery*, 24, 1909-1926.

RABBANI, A., FINN, R. M. & AUSIO, J. 2005. The anthracycline antibiotics: antitumor drugs that alter chromatin structure. *Bioessays*, 27, 50-6.

RAEVEN, R. H. M., BRUMMELMAN, J., PENNING, J. L. A., VAN DER MAAS, L., TILSTRA, W., HELM, K., VAN RIET, E., JISKOOT, W., VAN ELS, C. A. C. M., HAN, W. G. H., KERSTEN, G. F. A. & METZ, B. 2016. Bordetella pertussis outer membrane vesicle vaccine confers equal efficacy in mice with milder inflammatory responses compared to a whole-cell vaccine. *Scientific Reports*, 6, 38240.

RAJAGOPALA, S. V., CASJENS, S. & UETZ, P. 2011. The protein interaction map of bacteriophage lambda. *BMC Microbiology*, 11, 213-213.

RAJEEVE, V., VENDRELL, I., WILKES, E., TORBETT, N. & CUTILLAS, P. R. 2014. Cross-species Proteomics Reveals Specific Modulation of Signaling in Cancer and Stromal Cells by Phosphoinositide 3-kinase (PI3K) Inhibitors. *Mol Cell Proteomics*, 13, 1457-70.

REÁTEGUI, E., VAN DER VOS, K. E., LAI, C. P., ZEINALI, M., ATAI, N. A., ALDIKACTI, B., FLOYD, F. P., H. KHANKHEL, A., THAPAR, V., HOCHBERG, F. H., SEQUIST, L. V., NAHED, B. V., S. CARTER, B., TONER, M., BALAJ, L., T. TING, D., BREAKFIELD, X. O. & STOTT, S. L. 2018. Engineered nanointerfaces for microfluidic isolation and molecular profiling of tumor-specific extracellular vesicles. *Nature Communications*, 9, 175.

REGGETI, F. & BIENZLE, D. 2011. Flow cytometry in veterinary oncology. *Vet Pathol*, 48, 223-35.

REN, Y., ZHOU, X., MEI, M., YUAN, X.-B., HAN, L., WANG, G.-X., JIA, Z.-F., XU, P., PU, P.-Y. & KANG, C.-S. 2010. MicroRNA-21 inhibitor sensitizes human glioblastoma cells U251 (PTEN-mutant) and LN229 (PTEN-wild type) to taxol. *BMC Cancer*, 10, 27.

RESCH-GENGER, U., HOFFMANN, K., NIETFELD, W., ENGEL, A., NEUKAMMER, J., NITSCHKE, R., EBERT, B. & MACDONALD, R. 2005. How to improve quality assurance in fluorometry: fluorescence-inherent sources of error and suited fluorescence standards. *J Fluoresc*, 15, 337-62.

REYES-ROBLES, T., DILLARD, R. S., CAIRNS, L. S., SILVA-VALENZUELA, C. A., HOUSMAN, M., ALI, A., WRIGHT, E. R. & CAMILLI, A. 2018a. *Vibrio cholerae* outer membrane vesicles inhibit bacteriophage infection. *Journal of Bacteriology*.

REYES-ROBLES, T., DILLARD, R. S., CAIRNS, L. S., SILVA-VALENZUELA, C. A., HOUSMAN, M., ALI, A., WRIGHT, E. R. & CAMILLI, A. 2018b. *Vibrio cholerae* outer membrane vesicles inhibit bacteriophage infection. *J Bacteriol*.

RIMMERMAN, N., BEN-HAIL, D., PORAT, Z., JUKNAT, A., KOZELA, E., DANIELS, M. P., CONNELLY, P. S., LEISHMAN, E., BRADSHAW, H. B., SHOSHAN-BARMATZ, V. & VOGEL, Z. 2013. Direct modulation of the outer mitochondrial membrane channel, voltage dependent anion channel 1 (VDAC1) by cannabidiol: a novel mechanism for cannabinoid induced cell death. *Cell Death & Disease*, 4, e949.

RIVERA, E. & GOMEZ, H. 2010. Chemotherapy resistance in metastatic breast cancer: the evolving role of ixabepilone. *Breast Cancer Research*, 12, S2.

ROBINET, A., HOIZEY, G. & MILLART, H. 2005. PI 3-kinase, protein kinase C, and protein kinase A are involved in the trigger phase of β 1-adrenergic preconditioning. *Cardiovascular Research*, 66, 530-542.

RODRIGUES, M., FAN, J., LYON, C., WAN, M. & HU, Y. 2018. Role of Extracellular Vesicles in Viral and Bacterial Infections: Pathogenesis, Diagnostics, and Therapeutics. *Theranostics*, 8, 2709-2721.

RODRIGUEZ, S. B., STITT, B. L. & ASH, D. E. 2009. Expression of peptidylarginine deiminase from *Porphyromonas gingivalis* in *Escherichia coli*: enzyme purification and characterization. *Arch Biochem Biophys*, 488, 14-22.

ROIER, S., ZINGL, F. G., CAKAR, F., DURAKOVIC, S., KOHL, P., EICHMANN, T. O., KLUG, L., GADERMAIER, B., WEINZERL, K., PRASSL, R., LASS, A., DAUM, G., REIDL, J., FELDMAN, M. F. & SCHILD, S. 2016a. A novel mechanism for the biogenesis of outer membrane vesicles in Gram-negative bacteria. *Nature Communications*, 7, 10515.

ROIER, S., ZINGL, F. G., CAKAR, F., DURAKOVIC, S., KOHL, P., EICHMANN, T. O., KLUG, L., GADERMAIER, B., WEINZERL, K., PRASSL, R., LASS, A., DAUM, G., REIDL,

- J., FELDMAN, M. F. & SCHILD, S. 2016b. A novel mechanism for the biogenesis of outer membrane vesicles in Gram-negative bacteria. *Nat Commun*, 7, 10515.
- ROJAS, L. J., SALIM, M., COBER, E., RICHTER, S. S., PEREZ, F., SALATA, R. A., KALAYJIAN, R. C., WATKINS, R. R., MARSHALL, S., RUDIN, S. D., DOMITROVIC, T. N., HUJER, A. M., HUJER, K. M., DOI, Y., KAYE, K. S., EVANS, S., FOWLER, J. V. G., BONOMO, R. A. & VAN DUIN, D. 2017. Colistin Resistance in Carbapenem-Resistant *Klebsiella pneumoniae*: Laboratory Detection and Impact on Mortality. *Clinical Infectious Diseases*, 64, 711-718.
- ROMPIKUNTAL, P. K., VDOVIKOVA, S., DUPERTHUY, M., JOHNSON, T. L., ÅHLUND, M., LUNDMARK, R., OSCARSSON, J., SANDKVIST, M., UHLIN, B. E. & WAI, S. N. 2015. Outer Membrane Vesicle-Mediated Export of Processed PrtV Protease from *Vibrio cholerae*. *PLoS One*, 10.
- ROSEBLADE, A., LUK, F., UNG, A. & BEBAWY, M. 2015. Targeting microparticle biogenesis: a novel approach to the circumvention of cancer multidrug resistance. *Curr Cancer Drug Targets*, 15, 205-14.
- RUISS, R., JOCHUM, S., MOCIKAT, R., HAMMERSCHMIDT, W. & ZEIDLER, R. 2011. EBV-gp350 Confers B-Cell Tropism to Tailored Exosomes and Is a Neo-Antigen in Normal and Malignant B Cells—A New Option for the Treatment of B-CLL. *PLOS ONE*, 6, e25294.
- RUPERT, D. L. M., CLAUDIO, V., LÄSSER, C. & BALLY, M. 2017. Methods for the physical characterization and quantification of extracellular vesicles in biological samples. *Biochimica et Biophysica Acta (BBA) - General Subjects*, 1861, 3164-3179.
- RYAN, D., DRYSDALE, A. J., LAFOURCADE, C., PERTWEE, R. G. & PLATT, B. 2009. Cannabidiol targets mitochondria to regulate intracellular Ca²⁺ levels. *J Neurosci*, 29, 2053-63.

- SAARI, H., LAZARO-IBANEZ, E., VIITALA, T., VUORIMAA-LAUKKANEN, E., SILJANDER, P. & YLIPERTTULA, M. 2015. Microvesicle- and exosome-mediated drug delivery enhances the cytotoxicity of Paclitaxel in autologous prostate cancer cells. *J Control Release*, 220, 727-37.
- SADOVSKA, L., EGLITIS, J. & LINE, A. 2015. Extracellular Vesicles as Biomarkers and Therapeutic Targets in Breast Cancer. *Anticancer Res*, 35, 6379-90.
- SALGIA, R. & KULKARNI, P. 2018. The Genetic/Non-genetic Duality of Drug 'Resistance' in Cancer. *Trends in Cancer*, 4, 110-118.
- SAMPATH, J., SUN, D., KIDD, V. J., GRENET, J., GANDHI, A., SHAPIRO, L. H., WANG, Q., ZAMBETTI, G. P. & SCHUETZ, J. D. 2001. Mutant p53 cooperates with ETS and selectively up-regulates human MDR1 not MRP1. *J Biol Chem*, 276, 39359-67.
- SANNER, T. & GRIMSRUD, T. K. 2015a. Nicotine: Carcinogenicity and Effects on Response to Cancer Treatment - A Review. *Front Oncol*, 5, 196.
- SANNER, T. & GRIMSRUD, T. K. 2015b. Nicotine: Carcinogenicity and Effects on Response to Cancer Treatment – A Review. *Frontiers in Oncology*, 5, 196.
- SANTIANA, M., GHOSH, S., HO, B. A., RAJASEKARAN, V., DU, W.-L., MUTSAFI, Y., DE JÉSUS-DIAZ, D. A., SOSNOVTSEV, S. V., LEVENSON, E. A., PARRA, G. I., TAKVORIAN, P. M., CALI, A., BLECK, C., VLASOVA, A. N., SAIF, L. J., PATTON, J. T., LOPALCO, P., CORCELLI, A., GREEN, K. Y. & ALTAN-BONNET, N. 2018. Vesicle Cloaked Virus Clusters Are Optimal Units for Inter-organismal Viral Transmission. *Cell Host & Microbe*, 24, 208-220.e8.

SCHER, J. U. & ABRAMSON, S. B. 2013. Periodontal disease, Porphyromonas gingivalis, and rheumatoid arthritis: what triggers autoimmunity and clinical disease? *Arthritis Research & Therapy*, 15, 122-122.

SCHIMMEL, P. 2008. Development of tRNA synthetases and connection to genetic code and disease. *Protein Science : A Publication of the Protein Society*, 17, 1643-1652.

SCHOLAR, E. 2007. Antimetabolites. In: ENNA, S. J. & BYLUND, D. B. (eds.) *xPharm: The Comprehensive Pharmacology Reference*. New York: Elsevier.

SCHREMPF, H., KOEBSCH, I., WALTER, S., ENGELHARDT, H. & MESCHKE, H. 2011. Extracellular Streptomyces vesicles: amphorae for survival and defence. *Microb Biotechnol*, 4, 286-99.

SCHWECHHEIMER, C. & KUEHN, M. J. 2013. Synthetic effect between envelope stress and lack of outer membrane vesicle production in Escherichia coli. *J Bacteriol*, 195, 4161-73.

SCHWECHHEIMER, C. & KUEHN, M. J. 2015. Outer-membrane vesicles from Gram negative bacteria: biogenesis and functions. *Nat Rev Micro*, 13, 605-619.

SEAMAN, A., DARRAH, E., INFANTINO, M., MEACCI, F., MANFREDI, M., BENUCCI, M. & MAHLER, M. 2016. Anti-peptidyl-arginine deaminase 3 (PAD3) antibodies as a promising marker to measure joint damage in patients with rheumatoid arthritis. *Autoimmun Rev*, 15, 776-80.

SEED, K. D. 2015. Battling Phages: How Bacteria Defend against Viral Attack. *PLOS Pathogens*, 11, e1004847.

SEGURA, E., NICCO, C., LOMBARD, B., VERON, P., RAPOSO, G., BATTEUX, F.,

- AMIGORENA, S. & THERY, C. 2005. ICAM-1 on exosomes from mature dendritic cells is critical for efficient naive T-cell priming. *Blood*, 106, 216-23.
- SESEN, J., DAHAN, P., SCOTLAND, S. J., SALAND, E., DANG, V.-T., LEMARIÉ, A., TYLER, B. M., BREM, H., TOULAS, C., COHEN-JONATHAN MOYAL, E., SARRY, J.-E. & SKULI, N. 2015. Metformin Inhibits Growth of Human Glioblastoma Cells and Enhances Therapeutic Response. *PLOS ONE*, 10, e0123721.
- SHABBIR, M. A. B., HAO, H., SHABBIR, M. Z., WU, Q., SATTAR, A. & YUAN, Z. 2016. Bacteria vs. Bacteriophages: Parallel Evolution of Immune Arsenals. *Frontiers in Microbiology*, 7.
- SHAH, A. B., REJNIAK, K. A. & GEVERTZ, J. L. 2016. Limiting the Development of Anti-Cancer Drug Resistance in a Spatial Model of Micrometastases.. *Mathematical biosciences and engineering : MBE*, 13, 1185-1206.
- SHAH, V., TARATULA, O., GARBUZENKO, O. B., TARATULA, O. R., RODRIGUEZ RODRIGUEZ, L. & MINKO, T. 2013. Targeted Nanomedicine for Suppression of CD44 and Simultaneous Cell Death Induction in Ovarian Cancer: An Optimal Delivery of siRNA and Anticancer Drug. *Clinical Cancer Research*, 19, 6193-6204.
- SHEN, L.-M., QUAN, L. & LIU, J. 2018. Tracking Exosomes in Vitro and *in Vivo* To Elucidate Their Physiological Functions: Implications for Diagnostic and Therapeutic Nanocarriers. *ACS Applied Nano Materials*, 1, 2438-2448.
- SIEVERS, F. & HIGGINS, D. G. 2018. Clustal Omega for making accurate alignments of many protein sequences. *Protein Sci*, 27, 135-145.
- SIGAL, A. & ROTTER, V. 2000. Oncogenic mutations of the p53 tumor suppressor: the demons of the guardian of the genome. *Cancer Res*, 60, 6788-93.

SIMMONS, M., DRESCHER, K., NADELL, C. D. & BUCCI, V. 2018. Phage mobility is a core determinant of phage–bacteria coexistence in biofilms. *The ISME Journal*, 12, 531-543.

SINGH, M. S., TAMMAM, S. N., SHETAB BOUSHEHRI, M. A. & LAMPRECHT, A. 2017. MDR in cancer: Addressing the underlying cellular alterations with the use of nanocarriers. *Pharmacol Res*, 126, 2-30.

SILVA, D., CACERES, M., ARANCIBIA, R., MARTINEZ, C., MARTINEZ, J., and SMITH, P.C. Effects of cigarette smoke and nicotine on cell viability, migration and myofibroblastic differentiation. *J Periodontal Res*. 2012 Oct;47(5):599-607

SLADE, D. J., FANG, P., DREYTON, C. J., ZHANG, Y., FUHRMANN, J., REMPEL, D., BAX, B. D., COONROD, S. A., LEWIS, H. D., GUO, M., GROSS, M. L., THOMPSON, P. R. (2015). Protein arginine deiminase 2 binds calcium in an ordered fashion: implications for inhibitor design. *ACS chemical biology*, 10(4), 1043-53.

SMITH, I. M. & HOSHI, N. 2011. ATP Competitive Protein Kinase C Inhibitors Demonstrate Distinct State-Dependent Inhibition. *PLoS ONE*, 6, e26338.

SOLINAS, M., MASSI, P., CINQUINA, V., VALENTI, M., BOLOGNINI, D., GARIBOLDI, M., MONTI, E., RUBINO, T. & PAROLARO, D. 2013. Cannabidiol, a non-psychoactive cannabinoid compound, inhibits proliferation and invasion in U87-MG and T98G glioma cells through a multitarget effect. *PLoS One*, 8, e76918.

STAMPANONI BASSI, M., SANCESARIO, A., MORACE, R., CENTONZE, D. & IEZZI, E. 2017. Cannabinoids in Parkinson's Disease. *Cannabis and Cannabinoid Research*, 2, 21-29.

STENTZ, R., HORN, N., CROSS, K., SALT, L., BREARLEY, C., LIVERMORE, D. M. & CARDING, S. R. 2015. Cephalosporinases associated with outer membrane vesicles released by

Bacteroides spp. protect gut pathogens and commensals against β -lactam antibiotics. *Journal of Antimicrobial Chemotherapy*, 70, 701-709.

STRATTON, D., MOORE, C., ANTWI-BAFFOUR, S., LANGE, S. & INAL, J. 2015.

Microvesicles released constitutively from prostate cancer cells differ biochemically and functionally to stimulated microvesicles released through sublytic C5b-9. *Biochem Biophys Res Commun*, 460, 589-95.

STREET, C. A. & BRYAN, B. A. 2011. Rho Kinase Proteins—Pleiotropic Modulators of Cell Survival and Apoptosis. *Anticancer research*, 31, 3645-3657.

SUBIK, K., LEE, J.-F., BAXTER, L., STRZEPEK, T., COSTELLO, D., CROWLEY, P., XING, L., HUNG, M.-C., BONFIGLIO, T., HICKS, D. G. & TANG, P. 2010. The Expression Patterns of ER, PR, HER2, CK5/6, EGFR, Ki-67 and AR by Immunohistochemical Analysis in Breast Cancer Cell Lines. *Breast Cancer : Basic and Clinical Research*, 4, 35-41.

SULAKVELIDZE, A., ALAVIDZE, Z. & MORRIS, J. G. 2001. Bacteriophage Therapy. *Antimicrobial Agents and Chemotherapy*, 45, 649-659.

SUN, X., BIZHANOVA, A., MATHESON, T. D., YU, J., ZHU, L. J. & KAUFMAN, P. D. 2017. Ki-67 Contributes to Normal Cell Cycle Progression and Inactive X Heterochromatin in p21 Checkpoint-Proficient Human Cells. *Molecular and Cellular Biology*, 37, e00569-16.

SUN, Y.-Z., RUAN, J.-S., JIANG, Z.-S., WANG, L. & WANG, S.-M. 2018. Extracellular Vesicles: A New Perspective in Tumor Therapy. *BioMed Research International*, 2018, 7.

SUZUKI, J., FUJII, T., IMAO, T., ISHIHARA, K., KUBA, H. & NAGATA, S. 2013. Calcium dependent Phospholipid Scramblase Activity of TMEM16 Protein Family Members. *The Journal of Biological Chemistry*, 288, 13305-13316.

SWANSON, G. P., FAULKNER, J., SMALLEY, S. R., NOBLE, M. J., STEPHENS, R. L., O'ROURKE, T. J., WEISS, G. R., QUICK, D. P., THOMPSON, I. M., JR. & CRAWFORD, E. D. 2006. Locally advanced prostate cancer treated with concomitant radiation and 5-fluorouracil: Southwest Oncology Group Study 9024. *J Urol*, 176, 548-53; discussion 553.

SYED, S., SCHOBBER, J., BLANCO, A. & ZUSTIAK, S. P. 2017. Morphological adaptations in breast cancer cells as a function of prolonged passaging on compliant substrates. *PLOS ONE*, 12, e0187853.

SZCZEPANSKI, M. J., SZAJNIK, M., WELSH, A., WHITESIDE, T. L. & BOYIADZIS, M. 2011. Blast-derived microvesicles in sera from patients with acute myeloid leukemia suppress natural killer cell function via membrane-associated transforming growth factor-beta1. *Haematologica*, 96, 1302-9.

TABIB-SALAZAR, A., LIU, B., BARKER, D., BURCHELL, L., QIMRON, U., MATTHEWS, S. J. & WIGNESHWERARAJ, S. 2018. T7 phage factor required for managing RpoS in *Escherichia coli*. *Proc Natl Acad Sci U S A*, 115, E5353-e5362.

TAI, S., SUN, Y., SQUIRES, J. M., ZHANG, H., OH, W. K., LIANG, C. Z. & HUANG, J. 2011. PC3 is a cell line characteristic of prostatic small cell carcinoma. *Prostate*, 71, 1668-79.

TAKEDA, M., YAMAGAMI, K. & TANAKA, K. 2014. Role of phosphatidylserine in phospholipid flippase-mediated vesicle transport in *Saccharomyces cerevisiae*. *Eukaryot Cell*, 13, 363-75.

TALHOUT, R., SCHULZ, T., FLOREK, E., VAN BENTHEM, J., WESTER, P. & OPPERHUIZEN, A. 2011. Hazardous compounds in tobacco smoke. *Int J Environ Res Public Health*, 8, 613-28.

TAMBARO, S. & BORTOLATO, M. 2012. Cannabinoid-related agents in the treatment of anxiety disorders: current knowledge and future perspectives. *Recent patents on CNS drug discovery*, 7, 25-40.

TANASE, C. P., OGREZEANU, I. & BADIU, C. 2012. 6 - Signal Transduction. *In: TANASE, C. P., OGREZEANU, I. & BADIU, C. (eds.) Molecular Pathology of Pituitary Adenomas.* London: Elsevier.

TANG, R. & FANG, F. 2017. Trial of Cannabidiol for Drug-Resistant Seizures in the Dravet Syndrome. *N Engl J Med*, 377, 699.

TEITZ, T., WEI, T., VALENTINE, M. B., VANIN, E. F., GRENET, J., VALENTINE, V. A., BEHM, F. G., LOOK, A. T., LAHTI, J. M. & KIDD, V. J. 2000. Caspase 8 is deleted or silenced preferentially in childhood neuroblastomas with amplification of MYCN. *Nat Med*, 6, 529-35.

TEOW, S.-Y., LIEW, K., KHOO, A. S.-B. & PEH, S.-C. 2017. Pathogenic Role of Exosomes in Epstein-Barr Virus (EBV)-Associated Cancers. *International Journal of Biological Sciences*, 13, 1276-1286.

TER-OVANESYAN, D., KOWAL, E. J. K., REGEV, A., CHURCH, G. M. & COCCUCCI, E. 2017. Imaging of Isolated Extracellular Vesicles Using Fluorescence Microscopy. *Methods Mol Biol*, 1660, 233-241.

THERY, C., OSTROWSKI, M. & SEGURA, E. 2009. Membrane vesicles as conveyors of immune responses. *Nat Rev Immunol*, 9, 581-93.

THERY, C., WITWER, K., AIKAWA, E., ALCARAZ, M., ANDERSON, J., ANDRIANTSITOHAINA, E. ET AL., (2018) Minimal information for studies of extracellular vesicles 2018 (MISEV2018): a position statement of the International Society for Extracellular Vesicles and update of the MISEV2014 guidelines, *Journal of Extracellular Vesicles*, 7:1, DOI: 10.1080/20013078.2018.1535750

TIAN, Y., LI, S., SONG, J., JI, T., ZHU, M., ANDERSON, G. J., WEI, J. & NIE, G. 2014. A doxorubicin delivery platform using engineered natural membrane vesicle exosomes for targeted tumor therapy. *Biomaterials*, 35, 2383-90.

TORRES, S., LORENTE, M., RODRIGUEZ-FORNES, F., HERNANDEZ-TIEDRA, S., SALAZAR, M., GARCIA-TABOADA, E., BARCIA, J., GUZMAN, M. & VELASCO, G. 2011. A combined preclinical therapy of cannabinoids and temozolomide against glioma. *Mol Cancer Ther*, 10, 90-103.

TOYOFUKU, M., MORINAGA, K., HASHIMOTO, Y., UHL, J., SHIMAMURA, H., INABA, H., SCHMITT-KOPPLIN, P., EBERL, L. & NOMURA, N. 2017. Membrane vesicle-mediated bacterial communication. *The Isme Journal*, 11, 1504.

TOYOFUKU, M., NOMURA, N., and EBERL, L. Types and origins of bacterial membrane vesicles. *Nature Reviews Microbiology* volume 17, pages13–24 (2019)

TU, R., GROVER, H. M. & KOTRA, L. P. 2016. Peptidyl Arginine Deiminases and Neurodegenerative Diseases. *Curr Med Chem*, 23, 104-14.

TURPIN, D., TRUCHETET, M. E., FAUSTIN, B., AUGUSTO, J. F., CONTIN-BORDES, C., BRISSON, A., BLANCO, P. & DUFFAU, P. 2016. Role of extracellular vesicles in autoimmune diseases. *Autoimmun Rev*, 15, 174-83.

TZIPILEVICH, E., HABUSHA, M. & BEN-YEHUDA, S. 2017. Acquisition of Phage Sensitivity by Bacteria through Exchange of Phage Receptors. *Cell*, 168, 186-199.e12.

ISTVAN, U. and LUMIR, H.(2016). Human Metabolites of Cannabidiol: A Review on Their Formation, Biological Activity, and Relevance in Therapy. *Cannabis and cannabinoid research*. 1. 90-101. 10.1089/can.2015.0012.

VADER, P., BREAKFIELD, X. O. & WOOD, M. J. A. 2014. Extracellular vesicles: Emerging targets for cancer therapy. *Trends in molecular medicine*, 20, 385-393.

VALENTI, R., HUBER, V., FILIPAZZI, P., PILLA, L., SOVENA, G., VILLA, A., CORBELLI, A., FAIS, S., PARMIANI, G. & RIVOLTINI, L. 2006. Human tumor-released microvesicles promote the differentiation of myeloid cells with transforming growth factor-beta mediated suppressive activity on T lymphocytes. *Cancer Res*, 66, 9290-8.

VALENZUELA, M. M. A., NEIDIGH, J. W. & WALL, N. R. 2014. Antimetabolite Treatment for Pancreatic Cancer. *Chemotherapy*, 3, 137.

VAN DER MEEL, R., FENS, M. H., VADER, P., VAN SOLINGE, W. W., ENIOLA ADEFESO, O. & SCHIFFELERS, R. M. 2014. Extracellular vesicles as drug delivery systems: lessons from the liposome field. *J Control Release*, 195, 72-85.

VAN DOORMAAL, F. F., KLEINJAN, A., DI NISIO, M., BULLER, H. R. & NIEUWLAND, R. 2009. Cell-derived microvesicles and cancer. *Neth J Med*, 67, 266-73.

VAN NIEL, G., D'ANGELO, G. & RAPOSO, G. 2018. Shedding light on the cell biology of extracellular vesicles. *Nature Reviews Molecular Cell Biology*, 19, 213.

VEJPONGSA, P. & YEH, E. T. H. 2014. Prevention of Anthracycline-Induced Cardiotoxicity:

Challenges and Opportunities. *Journal of the American College of Cardiology*, 64, 938-945.

VELASCO, G., HERNANDEZ-TIEDRA, S., DAVILA, D. & LORENTE, M. 2016. The use of cannabinoids as anticancer agents. *Prog Neuropsychopharmacol Biol Psychiatry*, 64, 259-66.

VELASCO, G., HERNANDEZ-TIEDRA, S., DAVILA, D. & LORENTE, M. 2017.

Corrigendum to "The use of cannabinoids as anticancer agents" [Prog. Neuro-Psychopharmacol. Biol. Psychiatry 64 (2016) 259-266]. *Prog Neuropsychopharmacol Biol Psychiatry*, 74, 57.

VIAUD, S., TERME, M., FLAMENT, C., TAIEB, J., ANDRE, F., NOVAULT, S., ESCUDIER, B., ROBERT, C., CAILLAT-ZUCMAN, S., TURSZ, T., ZITVOGEL, L. & CHAPUT, N. 2009. Dendritic cell-derived exosomes promote natural killer cell activation and proliferation: a role for NKG2D ligands and IL-15Ralpha. *PLoS One*, 4, e4942.

VOLKOVA, M. & RUSSELL, R. 2011. Anthracycline Cardiotoxicity: Prevalence, Pathogenesis and Treatment. *Current Cardiology Reviews*, 7, 214-220.

VYAS, S., ZAGANJOR, E. & HAIGIS, M. C. 2016. Mitochondria and Cancer. *Cell*, 166, 555-566.

WAGNER, B. A., EVIG, C. B., RESZKA, K. J., BUETTNER, G. R. & BURNS, C. P. 2005. Doxorubicin increases intracellular hydrogen peroxide in PC3 prostate cancer cells. *Archives of biochemistry and biophysics*, 440, 181-190.

WANG, F., CHEN, Y., ZHANG, D., ZHANG, Q., ZHENG, D., HAO, L., LIU, Y., DUAN, C., JIA, L. & LIU, G. 2012. Folate-mediated targeted and intracellular delivery of paclitaxel using a novel deoxycholic acid-O-carboxymethylated chitosan-folic acid micelles. *Int J Nanomedicine*, 7.

WANG, H., VO, T., HAJAR, A., LI, S., CHEN, X., PARISENTI, A. M., BRINDLEY, D. N. & WANG, Z. 2014. Multiple mechanisms underlying acquired resistance to taxanes in selected docetaxel-resistant MCF-7 breast cancer cells. *BMC Cancer*, 14, 37-37.

WANG, H., YAN, H. M., TANG, M. X., WANG, Z. H., ZHONG, M., ZHANG, Y., DENG, J. T. & ZHANG, W. 2010. Increased serum levels of microvesicles in nonvalvular atrial fibrillation determined by ELISA using a specific monoclonal antibody AD-1. *Clin Chim Acta*, 411, 1700-4.

WANG, J., HU, B., XU, M., YAN, Q., LIU, S., ZHU, X., SUN, Z., REED, E., DING, L., GONG, J., LI, Q. Q. & HU, J. 2006. Use of bacteriophage in the treatment of experimental animal bacteremia from imipenem-resistant *Pseudomonas aeruginosa*. *Int J Mol Med*, 17, 309-317.

WANG, L., HU, C. & SHAO, L. 2017. The antimicrobial activity of nanoparticles: present situation and prospects for the future. *International Journal of Nanomedicine*, 12, 1227-1249.

WANG, X., THOMPSON, C. D., WEIDENMAIER, C. & LEE, J. C. 2018. Release of *Staphylococcus aureus* extracellular vesicles and their application as a vaccine platform. *Nature Communications*, 9, 1379.

WATANABE, K., UENO, M., KAMIYA, D., NISHIYAMA, A., MATSUMURA, M., WATAYA, T., TAKAHASHI, J. B., NISHIKAWA, S., NISHIKAWA, S.-I., MUGURUMA, K. & SASAI, Y. 2007. A ROCK inhibitor permits survival of dissociated human embryonic stem cells. *Nat Biotech*, 25, 681-686.

WATANAKUNAKORN, C. 1984. Mode of action and in-vitro activity of vancomycin. *J Antimicrob Chemother*, 14 Suppl D, 7-18.

WHITMORE, S. E. & LAMONT, R. J. 2012. Tyrosine phosphorylation and bacterial virulence. *International Journal Of Oral Science*, 4, 1.

WIESER, A., STORZ, E., LIEGL, G., PETER, A., PRITSCH, M., SHOCK, J., WAI, S. N. & SCHUBERT, S. 2014. Efficient quantification and characterization of bacterial outer membrane derived nano-particles with flow cytometric analysis. *Int J Med Microbiol*, 304, 1032-7.

WITALISON, E. E., CUI, X., CAUSEY, C. P., THOMPSON, P. R. & HOFSETH, L. J. 2015. Molecular targeting of protein arginine deiminases to suppress colitis and prevent colon cancer. *Oncotarget*, 6, 36053-36062.

WOLF, P. 1967. The nature and significance of platelet products in human plasma. *Br J Haematol*, 13, 269-88.

WONG, S. L. & WAGNER, D. D. 2018. Peptidylarginine deiminase 4: a nuclear button triggering neutrophil extracellular traps in inflammatory diseases and aging. *Faseb j*, fj201800691R.

WÜRSTLE, S., SCHNEIDER, F., RINGEL, F., GEMPT, J., LÄMMER, F., DELBRIDGE, C., WU, W. & SCHLEGEL, J. 2017. Temozolomide induces autophagy in primary and established glioblastoma cells in an EGFR independent manner. *Oncology Letters*, 14, 322-328.

WYBRANSKA, I., POLUS, A., MIKOLAJCZYK, M., KNAPP, A., SLIWA, A., ZAPALA, B., STASZEL, T. & DEMBINSKA-KIEC, A. 2013. Apoptosis-related gene expression in glioblastoma (LN-18) and medulloblastoma (Daoy) cell lines. *Human Cell*, 26, 137-148.

XIBILLE-FRIEDMANN, D., MARTINEZ-RIVERA, J.-I., DE LA GARZA-RAMOS, M., RODRIGUEZ-AMADO, J., BUSTOSRIVERA-BAHENA, C., SANDOVAL-RIOS, M. & MONTIEL-HERNANDEZ, J.-L. 2014. AB0117 Peptidyl-Arginine Deiminase (PAD) Activity

and the Citrullination of Soluble Blood Proteins in Relation with Periodontal Activity, P. Gingivitis and Clinical Activity of Rheumatoid Arthritis Patients. Preliminary Study. *Annals of the Rheumatic Diseases*, 73, 842-843.

XIE, S., QIN, J., LIU, S., ZHANG, Y., WANG, J., SHI, X., LI, D., ZHOU, J. & LIU, M. 2016. Cep70 overexpression stimulates pancreatic cancer by inducing centrosome abnormality and microtubule disorganization. *Scientific Reports*, 6, 21263.

XIONG, J., MILLER, V. M., LI, Y. & JAYACHANDRAN, M. 2012. Microvesicles at the crossroads between infection and cardiovascular diseases. *Journal of Cardiovascular Pharmacology*, 59, 124-132.

YAHAV, D., FARBMAN, L., LEIBOVICI, L. & PAUL, M. 2012. Colistin: new lessons on an old antibiotic. *Clinical Microbiology and Infection*, 18, 18-29.

YAMAGISHI, T., SAHNI, S., SHARP, D. M., ARVIND, A., JANSSON, P. J. & RICHARDSON, D. R. 2013. P-glycoprotein mediates drug resistance via a novel mechanism involving lysosomal sequestration. *J Biol Chem*, 288, 31761-71.

YU, Z., ZHANG, L., QIN, W., YIN, J. & QIU, J. 2017. Exogenous Catalase Stimulates the Polymyxin E-Induced Rapid Killing of *Paenibacillus polymyxa*. *International Journal of Peptide Research and Therapeutics*.

ZAIDI, M.I., WATTOO, F.H., WATTOO, M.H., TIRMIZI, S.A. and SALMAN, S. 2012. Antibacterial activities of nicotine and its zinc complex. *African Journal of Microbiology Research* Vol. 6(24), pp.5134-5137

ZARGARIAN, S., SHLOMOVITZ, I., ERLICH, Z., HOURIZADEH, A., OFIR-BIRIN, Y., CROKER, B. A., REGEV-RUDZKI, N., EDRY-BOTZER, L. & GERLIC, M. 2017.

Phosphatidylserine externalization, “necroptotic bodies” release, and phagocytosis during necroptosis. *PLOS Biology*, 15, e2002711.

ZHANG, J., STEVENS, M. F. & BRADSHAW, T. D. 2012. Temozolomide: mechanisms of action, repair and resistance. *Curr Mol Pharmacol*, 5, 102-14.

ZHAO, X., CHEN, Q., LI, Y., TANG, H., LIU, W. & YANG, X. 2015. Doxorubicin and curcumin co-delivery by lipid nanoparticles for enhanced treatment of diethylnitrosamine induced hepatocellular carcinoma in mice. *Eur J Pharm Biopharm*, 93.

ZHOU, A., KANG, T. M., YUAN, J., BEPLER, C., NGUYEN, C., MAO, Z., NGUYEN, M. Q., YEH, P. & MILLER, J. H. 2015. Synergistic Interactions of Vancomycin with Different Antibiotics against *Escherichia coli*: Trimethoprim and Nitrofurantoin Display Strong Synergies with Vancomycin against Wild-Type *E. coli*. *Antimicrobial Agents and Chemotherapy*, 59, 276-281.

ZONG, H., VERHAAK, R. G. W. & CANOLL, P. 2012. The cellular origin for malignant glioma and prospects for clinical advancements. *Expert Review of Molecular Diagnostics*, 12, 383-394.

ZUARDI, A. W., CRIPPA, J. A., HALLAK, J. E., BHATTACHARYYA, S., ATAKAN, Z., MARTIN-SANTOS, R., MCGUIRE, P. K. & GUIMARAES, F. S. 2012. A critical review of the antipsychotic effects of cannabidiol: 30 years of a translational investigation. *Curr Pharm Des*, 18, 5131-40.